NOVA SCHOOL OF SCIENCE & TECHNOLOGY

DEPARTAMENT OF LIFE SCIENCES

NANOHEATERS – LOCALIZED HYPERTHERMIA FOR PRECISE GENE DELIVERY

DANIELA FILIPA CARDOSO FERREIRA

Master in Biochemistry

DOCTORATE IN BIOLOGY, SPECIALTY IN BIOTECHNOLOGY

NOVA University Lisbon

March, 2025

NOVA SCHOOL OF SCIENCE & TECHNOLOGY

DEPARTAMENT OF LIFE SCIENCES

NANOHEATERS – LOCALIZED HYPERTHERMIA FOR PRECISE GENE DELIVERY

DANIELA FILIPA CARDOSO FERREIRA

Master in Biochemistry, Faculty of Science and Technology of the University of Coimbra

Adviser: Pedro Miguel Ribeiro Viana Baptista
Full Professor, NOVA School of Science and Technology, NOVA University Lisbon

Co-adviser: Maria Alexandra Núncio de Carvalho Ramos Fernandes
Full Professor, NOVA School of Science and Technology, NOVA University Lisbon

Examination Committee:

Chair: João Paulo Miranda Ribeiro Borges
Full Professor, NOVA School of Science and Technology, NOVA University Lisbon

Rapporteurs: Frederico Castelo Alves Ferreira
Associate Professor, Instituto Superior Técnico, University of Lisbon

Ana Catarina Beco Pinto Reis
Assistant Professor with Habilitation, Faculty of Pharmacy, University of Lisbon

Adviser: Pedro Miguel Ribeiro Viana Baptista
Full Professor, NOVA School of Science and Technology, NOVA University Lisbon

Members: João Paulo Miranda Ribeiro Borges
Full Professor, NOVA School of Science and Technology, NOVA University Lisbon

DOCTORATE IN BIOLOGY, SPECIALTY IN BIOTECHNOLOGY

NOVA University Lisbon
March, 2025

Nanoheaters – Localized hyperthermia for precise gene delivery

A quem me faz sorrir e voar.

ACKNOWLEDGMENTS

Gostaria de agradecer à FCT – Fundação para a Ciência e a Tecnologia, I.P. pelo financiamento a esta tese no âmbito da Bolsa de Doutoramento 2020.06599.BD (https://doi.org/10.54499/2020.06599.BD), e às instituições de acolhimento do Programa Doutoral em Biologia que providenciaram os meios necessários para a realização da tese, ao Departamento de Ciências da Vida, à Faculdade de Ciências e Tecnologia e à unidade de investigação Unidade de Ciências Biomoleculares Aplicadas - UCIBIO da Universidade NOVA de Lisboa. Este trabalho foi também financiado por fundos nacionais através da FCT I.P., no âmbito do projeto UIDP/04378/2020 (https://doi.org/10.54499/UIDP/04378/2020) e UIDB/04378/2020 (https://doi.org/10.54499/UIDB/04378/2020) da UCIBIO, do projeto LA/P/0140/2020 do Laboratório Associado Instituto para a Saúde e a Bioeconomia - i4HB, projeto NANOHEAT – 2022.04315.PTDC (https://doi.org/10.54499/2022.04315.PTDC), e do projeto MagicCELLGene – M-ERA-NET/2/0008/2016 da Associação para a Inovação de Desenvolvimento da FCT - NOVA.ID.FCT.

Ao meu orientador Professor Doutor Pedro Viana Baptista, obrigada por acreditar em mim, pela motivação e pelas palavras objetivas e claras, por nunca me deixar contentar com pouco e puxar sempre por mim para ir mais além do meu conhecimento. À minha orientadora Professora Doutora Alexandra Fernandes, obrigada não só por acreditar em mim, mas pela sua disponibilidade e ajuda sempre que precisava, e por toda a confiança que depositou no meu trabalho. O meu sincero obrigada por me acolherem nos vossos laboratórios em Setembro de 2018 e fazerem grande parte do meu desenvolvimento profissional e académico.

A todos os colegas e alunos que passaram pelos laboratórios Nanomedicine e Human Genetics and Cancer Therapeutics com os quais tive oportunidade não só de aprender e de ajudar, como também tive a possibilidade de partilhar bons e maus momentos. Um especial agradecimento à Catarina Rodrigues, Luís Raposo e Bruno Veigas por toda ajuda no início da minha jornada como investigadora. Muito obrigada aos meus colegas Inês Martins aka Jeová, Margarida Silva, Cinthia Barroco, Sandra Cordeiro, Daniela Alexandre, André Luz, mas especialmente ao meu Ruben e à minha Bia. Ruben, obrigada por teres aparecido na minha vida ainda tu eras um aluno da licenciatura, e que bom é ver-te crescer e tornares-te num excelente investigador. E a ti Bia, nem sei onde começar, mas sei que a nossa amizade vai mais além que os géis de agarose que partilhávamos nos primeiros dias. Obrigada por seres minha amiga,

pelos sorrisos e pelas lágrimas, tenho orgulho do caminho que construímos ao longo dos nossos Doutoramentos.

Obrigada aos meus amigos de sempre, especialmente à Rute, Joana, Rafael, Cila, Jessica, Carolina e Afonso, por me fazerem rir. Às minhas meninas de Biologia que permanecem até hoje, Tamara, Marina, Diana e Catarina, pela amizade e partilha.

À minha família, aos meus avós, tios e primos, o meu obrigada por todo o apoio, amor e carinho - "A primeira neta e sobrinha será Doutora um dia".

O melhor fica para o fim... obrigada aos meus três grandes pilares, Mãe, Pai e mana Ritinha. Obrigada pelo amor, por me fazerem voar e acreditar que o saber não ocupa lugar. Obrigada por tudo!!!

"Nothing in life is to be feared, it is only to be understood. Now is the time to understand more, so that we may fear less." (Marie Curie).

ABSTRACT

Gene therapy relies on the precise transfection of nucleic acid effectors into cancer cells, such as small interfering RNA (siRNA) and antisense oligonucleotides (ASO). Therefore, novel therapeutic approaches are widely needed to deliver silencing moieties with maximal transfection efficiency and minimal toxicity. This thesis explored the use of mild hyperthermia mediated by gold nanoparticles (AuNPs) or magnetic nanoparticles (MNPs) to enhance nucleic acids delivery with spatiotemporal control over laser irradiation or magnetic modulation, respectively.

First, the photothermal effect of AuNPs under visible light irradiation was verified, leading to enhanced cellular uptake. The potential of mild photothermy via AuNPs was demonstrated by effectively silencing the *GFP* gene in colorectal carcinoma cell line (HCT116) and breast adenocarcinoma cell line (MCF-7), with comparable gene silencing efficiency to commercial transfection reagent, but without cytotoxicity. Improving gene silencing strategies in 3D cell cultures is important since it provides *in vitro* models that closely resemble the *in vivo* tumor microenvironment (TME). Then, it was shown that mild photothermy mediated by AuNPs functionalized with ASO decreases *c-MYC* oncogene expression in HCT116 cells and 7-day spheroids, respectively.

Localized magnetic hyperthermia mediated by immobilized MNPs on the cell membrane through bioorthogonal chemistry improves the transfection of *anti-GFP* in MCF-7 cells, with similar efficacy and less cytotoxicity compared to standard transfection reagent. Taking advantage of this approach, an effective *IDO1* gene silencing was obtained through the transfection of siRNA in dendritic cells derived from an acute monocytic leukemia cell line (THP-1). Moreover, the upregulation of pro-inflammatory cytokines *IL6*, *TNFA*, and *IL12* genes and the downregulation of anti-inflammatory *IL10* gene might contribute to a more immunogenic state in a TME context.

In summary, this thesis highlights nanoparticle-mediated mild hyperthermia as a promising strategy for controlled and efficient nucleic acids delivery that might pave the way for improved gene therapy applications in more complex cancer models.

Keywords: cancer therapy, nucleic acids transfection, gene silencing, mild hyperthermia, gold nanoparticles, magnetic nanoparticles

RESUMO

A terapia genética depende da transfeção precisa de ácidos nucleicos nas células cancerígenas, como *small interfering RNA* (siRNA) e oligonucleotidos *antisense* (ASO). Novas abordagens terapêuticas são extremamente necessárias para uma transfeção eficiente com toxicidade reduzida. Esta tese explorou o uso de hipertermia leve mediada por nanopartículas de ouro (AuNPs) ou nanopartículas magnéticas (MNPs) para melhorar a entrega de ácidos nucleicos com controlo espácio-temporal sob irradiação laser ou modulação magnética, respetivamente.

Foi primeiro verificado o efeito fototermal de AuNPs sob irradiação de luz visível, que levou ao aumento do *uptake* celular. O potencial da fototermia leve via AuNPs foi demonstrado ao silenciar o gene *GFP* nas linhas de carcinoma colorretal (HCT116) e adenocarcinoma da mama (MCF-7), com eficiência de silenciamento comparável ao reagente comercial para transfeção, mas sem citotoxicidade. Melhorar as estratégias de silenciamento genético em culturas celulares 3D é importante, uma vez que são modelos *in vitro* que melhor se assemelham ao microambiente tumoral (TME) *in vivo*. Assim sendo, foi observado que a fototermia leve mediada por AuNPs funcionalizadas com ASO diminuiu a expressão do oncogene *c-MYC* em células HCT116 e esferoides de 7 dias, respetivamente.

Hipertermia magnética localizada mediada por MNPs imobilizadas na membrana celular através de química bio-ortogonal melhorou a transfeção de *anti-GFP* nas células MCF-7 com eficiência e menos citotoxicidade que o reagente comercial. Através desta estratégia, foi obtido o silenciamento do gene *IDO1* após a entrega de siRNA em células dendríticas derivadas de uma linha celular de leucemia monocítica aguda (THP-1). Além disso, o aumento da expressão genética das citocinas pró-inflamatórias *IL6*, *TNFA* e *IL12* e a diminuição da anti-inflamatória *IL10* podem contribuir para um estado mais imunogénico no contexto do TME.

Em resumo, esta tese destaca a hipertermia leve mediada por nanopartículas como uma estratégia promissora para a entrega controlada e eficiente de ácidos nucleicos, o que pode abrir caminho para novas aplicações de terapia genética em modelos de cancro mais complexos.

Palavras chave: terapia do cancro, transfeção de ácidos nucleicos, silenciamento genético, hipertermia leve, nanopartículas de ouro, nanopartículas magnéticas

CONTENTS

LIST OF FIGURES

LIST OF TABLES

LIST OF EQUATIONS

ACRONYMS AND ABBREVIATIONS

2D	Two-dimensional
3D	Three-dimensional
AA-AuNP	Amino acid-functionalized gold nanoparticles
AAVs	Adeno-associated viruses
Ac_4ManNAz	Tetraacetylated *N*-azidoacetylmannosamine
AcGFP1	*Aequorea coerulescens* green fluorescent protein 1 gene
ADCs	Antibody-drug conjugates
AdVs	Adenoviruses
AMF	Alternating magnetic field
ASO	Antisense oligonucleotides
ATCC	American Type Culture Collection
AuNPs	Gold nanoparticles
AuNP@*c-MYC*	Gold nanoparticles functionalized with PEG and ASO against *c-MYC*
AuNP@Citrate	Citrate-capped gold nanoparticles
AuNP@PEG	Gold nanoparticles functionalized with PEG
AuNP@*scramble*	Gold nanoparticles functionalized with PEG and scramble ASO
B-CLL	B-chronic lymphocytic leukemia
BAG3	Bcl-2 associated athanogene domain 3 gene
BAX	B-cell lymphoma protein 2 associated protein X
BCL-2	B-cell lymphoma protein 2
BCR-ABL1	Breakpoint cluster region-Abelson murine leukemia 1 fusion gene

BRAF	B-Raf oncogene/v-Raf murine sarcoma viral oncogene homolog B
BRCA1/2	Breast cancer gene 1 and 2
BSA	Bovine serum albumin
c-MYC	Cellular myelocytomatosis oncogene
CAFs	Cancer-associated fibroblasts
CAR-T	Chimeric antigen receptor T
CCL	Chemokine ligand
CCR	Chemokine receptor
CD	Cluster of differentiation
CDK4/6	Cyclin-dependent kinase 4 and 6
CMV	Human cytomegalovirus
CO	Cyclooctyne derivates
copGFP	Green fluorescent protein gene for reporter stable cell lines
CRC	Colorectal cancer
CRISPR	Clustered regularly interspaced short palindromic repeats
CT	Computerized tomography
CTAB	Cetyltrimethylammonium bromide
CTCF	Corrected total cell fluorescence
CTLA-4	Cytotoxic T lymphocyte-associated protein 4
CW	Continuous wave
DBCO	Dibenzocyclooctyne derivatives
DCs	Dendritic cells
DEPC	Diethylpyrocarbonate
DLS	Dynamic light scattering
DMEM	Dulbecco's Modified Eagle Medium
DMSO	Dimethyl sulfoxide
DPBS	Phosphate buffer saline solution with extra Ca^{2+} and Mg^{2+}
DPSS	Diode-pumped solid-state laser
DSB	Double-strand break
dsRNA	Double-stranded RNA

DTNB	5,5-Dithiobis(2-nitrobenzoic acid)
DTT	Dithiothreitol
ECM	Extracellular matrix
EDC.HCL	N-(3-dimethylaminopropyl)-N′-ethylcarbodiimide hydrochloride
EGFP	Enhanced green fluorescent protein gene
EPR	Enhanced permeability and retention
ER	Estrogen receptor
EthD-1	Ethidium homodimer-1
FBS	Fetal bovine serum
FDA	Food and Drug Administration
FITC	Fluorescein isothiocyanate
GADPH	Glyceraldehyde-3-phosphate dehydrogenase gene
Gal-3	Galectin-3
GFP	Green fluorescent protein
GSH	Glutathione
HDAC	Histone deacetylase
HER-2	Human epidermal growth factor receptor 2
HGF	Hepatocyte growth factor
HIF-1α	Hypoxia-inducible factor 1 alpha
HSPs	Heat shock proteins
IARC	International Agency for Research on Cancer
ICP-AES	Inductively coupled plasma atomic emission spectroscopy
iDCs	Immature dendritic cells
IDO1	Indoleamine 2,3-dioxygenase 1
IL	Interleukin
IR	Infrared irradiation
KRAS	Kirsten ras oncogene/Kirsten rat sarcoma viral oncogene homolog
LbL-AuNP	Layer-by-layer-fabricated gold nanoparticles
LDH	Lactate hydrogenase
LDI	Laser diode intensity

LLC	Lewis lung carcinoma
LPS	Lipopolysaccharides from *Escherichia coli* O111:B4
LSPR	Localized surface plasmon resonance
mAb	Monoclonal antibodies
ManNAz	N-α-azidoacetylmannosamine
mDCs	Mature dendritic cells
MDM2	Mouse double minute 2 homolog
MDSCs	Myeloid-derived suppressor cells
MEM	Minimum essential medium
mGLuR5	Metabotropic glutamate receptor 5 gene
MHC	Major histocompatibility complex
miRNA	microRNA
MM-AuNP	Mixed-monolayer-protected gold nanoparticles
MNPs	Magnetic nanoparticles
MNPs@PMAO@PEG @CO	Magnetic nanoparticles coated with PMAO modified with a fluorescent dye, and functionalized PEG-NH_2 and CO derivate
MNPs@PMAO@PEG @DBCO	Magnetic nanoparticles coated with PMAO modified with a fluorescent dye, and functionalized with PEG-NH_2 and DBCO derivate
MRI	Magnetic resonance imaging
mRNA	Messenger RNA
mTOR	Mechanistic target of rapamycin
MTS	3-(4,5-dimethylthiazol-2-yl)-5-(3-carboxymethoxyphenyl)-2-(4-sulfophenyl)-2H-tetrazolium
MUC1	Mucin-1 gene
NAD^+	Nicotinamide adenine dinucleotide
NIR	Near-infrared irradiation
NK cells	Natural killer cells
NLS	Nuclear localization signal
NOTCH3	Notch receptor 3 gene
NSCLC	Non-small cell lung cancer

p53	Tumor protein P53
PAM	Protospacer adjacent motif
PARP	Poly (adenosine diphosphate-ribose) polymerase
PBS	Phosphate buffer saline solution
PBST	Phosphate buffer saline solution with 0.1% Tween 20 reagent
PD-1	Programmed cell death protein 1
PD-L1	Programmed cell death ligand 1
PDI	Polydispersity index
PDT	Photodynamic therapy
PE	Phycoerythrin
PEG	Polyethylene glycol
PEI	Polyethyleneimine
pGFP	pAcGFP1 Nuc Vector
PI3K	Phosphoinositide 3-kinase
PKM2	Pyruvate kinase isoenzyme type M2 gene
Plk1	Polo-like kinase 1 gene
PMAO	Poly(maleic anhydride-*alt*-1-octadecene)
PR	Progesterone receptor
PTT	Photothermal therapy
rh GM-CSF	Recombinant human granulocyte macrophage colony-stimulating factor
rh IL-4	Recombinant human interleukin 4
rh TNF-α	Recombinant human tumor necrosis factor α
RISC	RNA-induced silencing complex
RNAi	RNA interference
ROS	Reactive oxygen species
RPMI	Roswell Park Memorial Institute 1640 medium
RT	Room temperature
RT-qPCR	Real-time quantitative polymerase chain reaction
SAR	Specific Absorption Rate

SDS	Sodium dodecyl sulfate
sgRNA	Single-stranded guide RNA
shRNA	Short hairpin RNA
siRNA	Small interfering RNA
SLP	Specific Loss Power
SPAAC	Strain-promoted click azide-alkyne cycloaddition reaction
SPR	Surface plasmon resonance
SSB	Sodium Tetraborate Buffer
T cells	T lymphocytes
TALENs	Transcription activator-like effector nucleases
TBE	Tris-Borate-EDTA
TEM	Transmission electron microscopy
TGF-β	Transforming growth factor β
Th1 cells	Type 1 T helper cells
THP-1-derived DCs	Acute monocytic leukemia cell line differentiated in dendritic cells
TIL	Tumor-infiltrating lymphocytes
TMA-DPH	(1-(4-Trimethylammoniumphenyl)-6-Phenyl-1,3,5-Hexatriene p-Toluenesulfonate) hydrophobic fluorescent membrane probe
TMARA	Tetramethylrhodamine 5-(6)-carboxamide
TME	Tumor microenvironment
TNAs	Therapeutic nucleic acids
TNBC	Triple-negative breast cancer
TNF-α	Tumor necrosis factor alpha
Treg cells	Regulatory T cells
UV	Ultraviolet irradiation
UV-Vis	Ultraviolet-visible absorption spectroscopy
VEGF	Vascular endothelial growth factor
WHO	World Health Organization
ZFNs	Zinc finger nucleases

LIST OF PUBLICATIONS

Included in this thesis:

Ferreira, D., Fontinha, D., Martins, C., Pires, D., Fernandes, A. R., & Baptista, P. V. (2020). Gold Nanoparticles for Vectorization of Nucleic Acids for Cancer Therapeutics. *Molecules (Basel, Switzerland)*, *25*(15), 3489. https://doi.org/10.3390/molecules25153489

Ferreira, D., Fernandes, A.R. & Baptista, P.V. Mild hyperthermia via gold nanoparticles and visible light irradiation for enhanced siRNA and ASO delivery in 2D and 3D tumour spheroids. *Cancer Nano* 15, 19 (2024). https://doi.org/10.1186/s12645-024-00256-4.

Oliveira, B. B., **Ferreira, D.**, Fernandes, A. R., & Baptista, P. V. (2023). Engineering gold nanoparticles for molecular diagnostics and biosensing. *Wiley interdisciplinary reviews. Nanomedicine and nanobiotechnology*, *15*(1), e1836. https://doi.org/10.1002/wnan.1836

Idiago-López, J., **Ferreira, D.**, Asín, L., Moros, M., Armenia, I., Grazú, V., Fernandes, A. R., de la Fuente, J. M., Baptista, P. V., & Fratila, R. M. Membrane-localized magnetic hyperthermia promotes intracellular delivery of cell-impermeant probes. *Nanoscale*, *16*(32), 15176–15195 (2024). https://doi.org/10.1039/d4nr01955e

Cordeiro, S., Oliveira, B.B., Valente, R., **Ferreira, D.**, Luz, A., Baptista, P. V. & Fernandes, A. R. (2024). Breaking the mold: 3D cell cultures reshaping the future of cancer research. *Front. Cell Dev. Biol.* 12:1507388. https://doi.org/10.3389/fcell.2024.1507388

Not included in this thesis:

Susnik, E., Bazzoni, A., Taladriz-Blanco, P., Balog, S., Moreno-Echeverri, A. M., Glaubitz, C., Oliveira, B. B., **Ferreira, D.**, Baptista, P. V., Petri-Fink, A., & Rothen-Rutishauser, B. (2023). Epidermal growth factor alters silica nanoparticle uptake and improves gold-nanoparticle-mediated gene silencing in A549 cells. *Frontiers in nanotechnology*, *5*, 1220514. https://doi.org/10.3389/fnano.2023.1220514

Kordestani, N., Rudbari, H. A., Fernandes, A. R., Raposo, L. R., Baptista, P. V., **Ferreira, D.**, Bruno, G., Bella, G., Scopelliti, R., Braun, J. D., Herbert, D. E., & Blacque, O. (2020). Antiproliferative Activities of Diimine-Based Mixed Ligand Copper(II) Complexes. *ACS combinatorial science*, *22*(2), 89–99. https://doi.org/10.1021/acscombsci.9b00202

1

INTRODUCTION

The literature review presented in this chapter provides a general contextualization of the thesis, in which part of the information presented has previously been published in the following manuscripts (I reviewed and critically discussed the references in the text).

Ferreira, D., Fontinha, D., Martins, C., Pires, D., Fernandes, A. R., & Baptista, P. V. (2020). Gold Nanoparticles for Vectorization of Nucleic Acids for Cancer Therapeutics. *Molecules (Basel, Switzerland)*, *25*(15), 3489. https://doi.org/10.3390/molecules25153489

Oliveira, B. B., **Ferreira, D.**, Fernandes, A. R., & Baptista, P. V. (2023). Engineering gold nanoparticles for molecular diagnostics and biosensing. *Wiley interdisciplinary reviews. Nanomedicine and nanobiotechnology*, *15*(1), e1836. https://doi.org/10.1002/wnan.1836

Cordeiro, S., Oliveira, B.B., Valente, R., **Ferreira, D.**, Luz, A., Baptista, P. V. & Fernandes, A. R. (2024). Breaking the mold: 3D cell cultures reshaping the future of cancer research. *Front. Cell Dev. Biol.* 12:1507388. https://doi.org/10.3389/fcell.2024.1507388

1.1 Cancer: definition and incidence

Cancer comprises a group of diseases arising from the uncontrolled growth and proliferation of abnormal cells, which hijack the molecular mechanisms of cell regulation and promote invasion of tissues. At later stages, the alteration of local metabolic and physiologic conditions may be capable of dissemination throughout the whole organism and colonization of different tissues and organs, known as metastasis [1]. It is essential to understand cancer biology and underlying cell and molecular mechanisms, which is the basis to improve the development of novel therapeutic systems [2,3].

The World Health Organization (WHO) estimates cancer, trachea, bronchus, and lung cancers, as the sixth leading cause of death worldwide, resulting in approximately 10 million deaths in 2020 [4]. Recently, the WHO's cancer agency, the International Agency for Research on Cancer (IARC), released the latest estimates of the global burden of cancer. In 2022, there were an estimated 20 million new cancer cases and 9.7 million deaths. The new estimates available on IARC's Global Cancer Observatory show that 10 types of cancer collectively comprised around two-thirds of new cases and deaths globally in 2022, and the three major cancer types are lung, breast, and colorectal cancers (Figure 1.1). Lung cancer is the most prevalent cancer in men (15.2%), followed by prostate (14.2%) and colorectal (10.4%) cancers. Breast cancer accounts for nearly a quarter of new cases in women (23.8%), followed by lung (9.4%) and colorectal (8.9%) cancers [3,5,6].

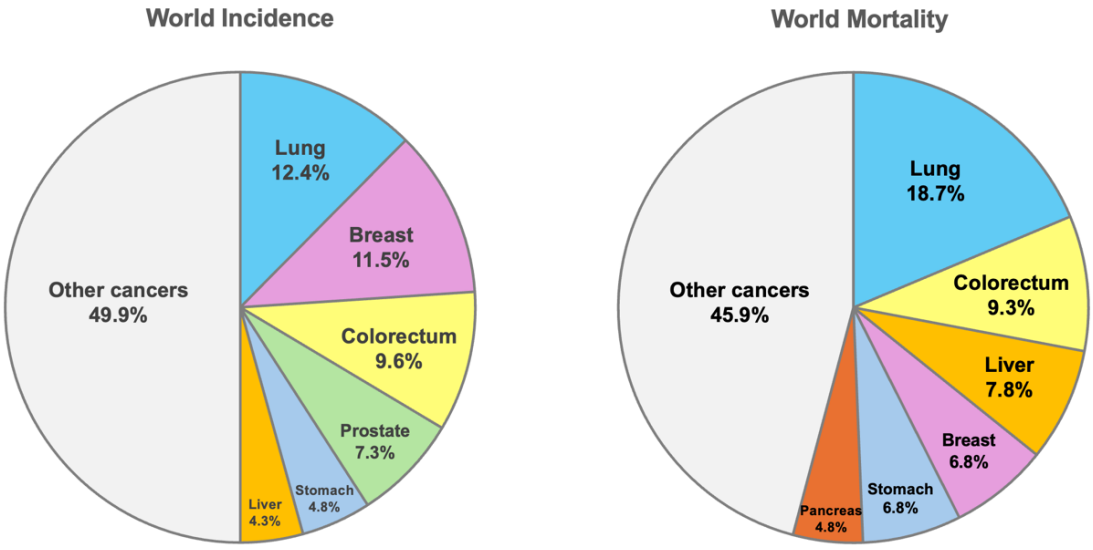

Figure 1.1 - Cancer Worldwide: incidence and mortality rates for both sexes and all ages (Adapted from IARC, 2022[3,5]).

1.2 Cancer progression and metastasis

The initiation and progression of a tumor involve a series of molecular alterations that deregulate canonical pathways of cell development, significantly reducing the regulatory control imposed by the body on the individual cell. One of the most critical characteristics of cancer cells is their resistance to cell cycle control. These random molecular deviations affect not only the foundation of the tumor but also the stage of differentiation and the invasive potential of cancer cells [1,7].

The Hallmarks of Cancer were introduced as a set of functional capabilities that human cells acquire during their transition from a normal state to neoplastic growth, particularly those crucial for malignant tumor development. This framework offers a conceptual foundation that enables the understanding of the complex phenotypes observed in various human tumor types and their variants through a common set of fundamental cellular characteristics [7]. These hallmarks include the acquired capabilities for supporting proliferative signaling, evading growth suppressors, resisting cell death, enabling replicative immortality, inducing/accessing vasculature, activating invasion and metastasis, reprogramming cellular metabolism, and avoiding immune destruction. Recently, Hanahan reported that deregulating cellular metabolism and avoiding immune destruction, can be considered core hallmarks, and proposed nonmutational epigenetic reprogramming, senescent cells, unlocking phenotypic plasticity and polymorphic microbiomes as emerging hallmarks and enabling characteristics [7,8]. Several of these hallmarks highlight the significance of tumor-surrounding cells and the key role of cell communication in cancer development. The cellular and molecular environment surrounding tumor cells, the tumor microenvironment (TME), plays a leading role in the Hallmarks of Cancer, and consequently in the cancer progression and metastasis.

1.3 Tumor microenvironment in cancer

Hannah and Weinberg recognized that TME comprises heterogeneous and interactive populations of cancer cells and cancer stem cells, along with various recruited stromal cell types. It is already widely recognized that this transformed parenchyma and its associated stroma plays a crucial role in tumorigenesis and malignant progression [7]. Cancer cells are surrounded by different cellular and non-cellular components, such as stromal and immune cells, extracellular matrix (ECM), and extracellular vesicles, which together constitute the TME (Figure 1.2) [2,9]. The cellular components of TME include cancer-associated fibroblasts (CAFs), pericytes, endothelial cells from the blood and lymphatic vasculature, adipocytes, lymphocytes, natural killer (NK) cells, tumor-associated macrophages and dendritic cells (DCs). The principal non-cellular component of TME is the ECM, a complex structure composed of several macromolecules, such as fibrous proteins (e.g., collagen, fibronectin, and elastin), glycoproteins, proteoglycans, cytokines, chemokines and growth factors[9–11]. The main functions of

ECM include supporting the tumor structure, maintaining tissue homeostasis, and modulation of cell-to-cell and cell-matrix interactions. These functions significantly influence cell proliferation, differentiation, and survival [10,11]. Besides the ECM, biochemical factors (e.g., diffusion gradients of molecules, signaling factors, oxygen, and nutrients) as well as biophysical factors (e.g., shear stress and interstitial flow), also play an important role in TME [12,13].

DCs are a heterogeneous group of immune cells and specific antigen-presenting cells that play a significant role in the modulation of T cell-dependent immunity in the adaptive and innate responses [14–17]. Recently, DCs expressing indoleamine 2,3-dioxygenase 1 (IDO1) have been described as an acquired mechanism of immune tolerance due to the ability to suppress the function of effector T and NK cells, and to induce the expansion of regulatory T cells (Treg cells), tolerogenic DCs and myeloid-derived suppressor cells (MDSCs), promoting neovascularization of solid tumors [15,18–20]. IDO1 is a cytosolic heme-containing enzyme involved in the degradation of tryptophan to kynurenine and the modulation of innate immune responses [21–23]. The overexpression of this enzyme has been reported in cancer cells and the stroma surrounding the TME (e.g., endothelial cells, fibroblasts, immune cells, and mesenchymal cells), as well in peripheral blood mononuclear cells of cancer patients [21,24–26]. However, IDO1 expression patterns and the exact mechanism of function are still unclear [27–29]. Currently, IDO1 is an important immunotherapy target in cancer due to the induction of anticancer responses, hereafter IDO inhibitors (e.g., indoximod and epacadostat) are being evaluated in clinical trials in combination with chemotherapy and immune checkpoint antibodies [18,30–34].

Overall, TME is responsible for the regulation of tumor growth, invasion, metastasis, immune responses, and drug resistance processes [11]. Cancer is now recognized as a complex disease dependent on the interaction of cancer cells with TME and it is essential to establish cancer models (e.g. 3D spheroids) capable of mimicking those interactions to provide more insights about the mechanisms of cancer progression and enhance the predictiveness of novel therapeutic screening [2,35,36].

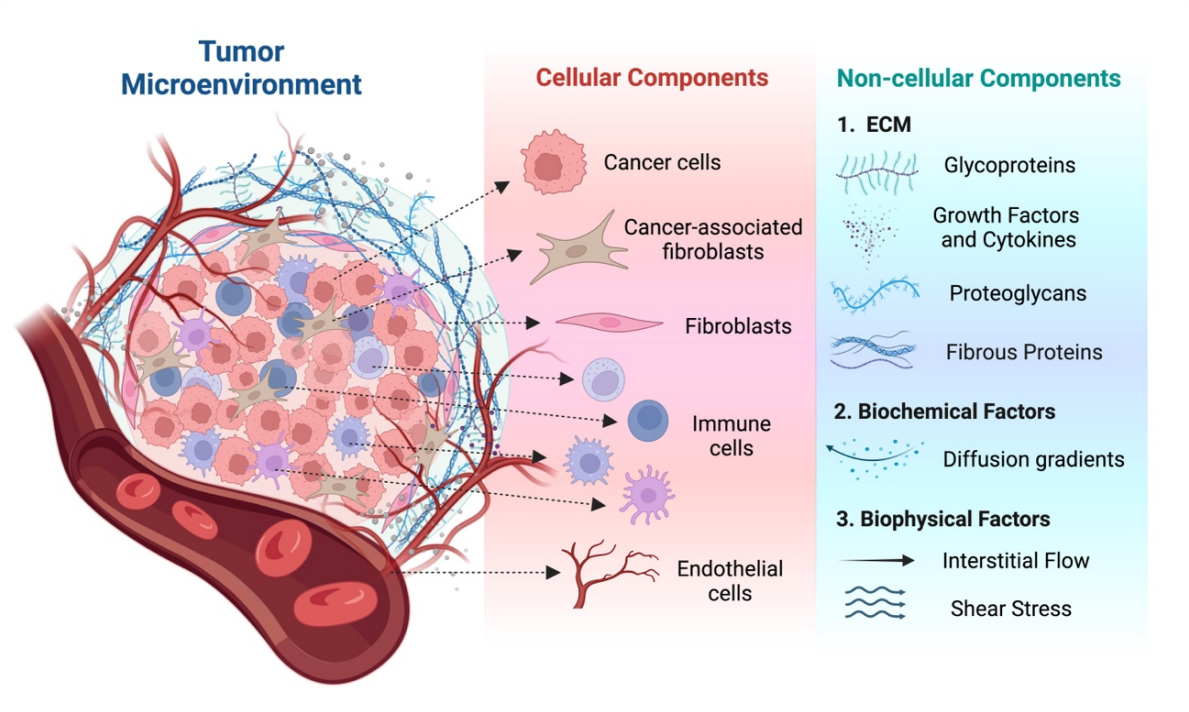

Figure 1.2 - Representation of the TME cellular and non-cellular components and their organization within the tumor mass. Established cancers are typically surrounded by stromal cells (fibroblasts, immune and endothelial cells) and non-cellular components such as ECM and biochemical and biophysical factors, which form a complex network that supports tumor growth, immune evasion, and metastasis (Adapted from Cordeiro *et al.*[2]). (Created with BioRender.com)

1.4 Different types of cancer

The different types of cancer are classified based on the specific cells or tissues from which it forms. For instance, carcinoma arises from epithelial cells, adenocarcinoma in gland cells, sarcoma in mesenchymal cells (bone and soft tissues), leukemia in blood cells (bone marrow), and lymphoma in B or T lymphocytes [37].

The following sections will focus on colorectal and breast cancers, as they serve as the cancer models used in this dissertation. Moreover, these two types of cancer show high incidence and mortality, making them suitable for further developments and novel targeted strategies.

1.4.1 Colorectal cancer (CRC)

Colorectal cancer (CRC), which includes colon and/or rectum cancer, is the second most deadly and the third most frequent cancer worldwide and represents a significant public health issue [3,38]. CRC is a genetically heterogeneous disorder, involving multiple molecular pathways that drive tumor development and metastasis [34,39]. CRC is caused by abnormal growth and proliferation of glandular epithelial cells from a normal epithelium (colon polyps

and adenoma), which only affects the colon or rectum through the adenoma-carcinoma sequence [38].

Sporadic, hereditary, and colitis-associated are the three main forms of CRC. Both genetic and environmental factors influence the risk of developing CRC. Several studies have shown that family history, chronic inflammation, and diet and lifestyle (e.g., reduced physical activity and increasing consumption of fatty foods) are risk factors for CRC progression [40,41]. Patients with an inflammatory colon are more likely to develop CRC, which is typically caused by genetic mutations and inflammatory immunological events, thus key factors in the tumor development include host immune system, epigenetic events, and somatic mutation [42,43]. For instance, the CRC progression in patients with Crohn's disease and long-standing ulcerative colitis increases with age [44]. A polyp typically takes 10 to 15 years to develop into a malignant tumor. Therefore, CRC might be prevented by routine screening, to identify and remove polyps at the early stage. Still, only 40% of CRC cases can be detected earlier and CRC can potentially recur even after surgery and post-surgery treatment [38].

The most important prognostic factors include the stage of cancer, site and number of metastasis, and host immunological characteristics. The early diagnosis of CRC can reduce metastasis and increase the survival rate, using different diagnostic techniques (e.g., colonoscopy, liquid biopsy, sigmoidoscopy, and fecal occult blood tests) [45]. However, most CRC patients experience metastases despite improvements in diagnosis and treatment (5-year survival rate of less than 12%) [34,42]. Surgery is the primary treatment for CRC and might be usually combined with chemotherapy and radiotherapy, as part of the clinical approach proceedings [45,46]. Most CRC patients developed resistance to modern chemotherapies, which reduced the effectiveness of anticancer therapeutics and resulted in chemotherapy failure [38]. The development of innovative and more precise approaches (e.g., targeted therapy) are required for CRC treatment.

1.4.2 Breast cancer

Breast cancer is the most frequently diagnosed cancer in women worldwide (1% of all cases are in men [47]), with an estimated 2.3 million new cases and over 685,000 deaths in 2020 [48,49]. The incidence of breast cancer is influenced by genetic and non-genetic features, where some can also be supported by genetic predisposition, including germline mutations of high-penetrance genes such as breast cancer 1/2 (*BRCA1/2*), and markers of the immune microenvironment which includes programmed death-ligand (PD-L1) and tumor-infiltrating lymphocyte (TIL) [50,51]. Non-genetic factors include lifestyle factors (e.g., excess body weight and alcohol consumption), radiation exposure, high mammographic density, age, reproductive risk factors (e.g., early menarche and late menopause), exogenous female hormones, and the presence of histologic lesions (e.g., atypical hyperplasia) [52,53]. Multiple biological entities involved in breast cancer heterogeneity (pathology, gene expression, and genomic alterations) impact treatment response and clinical behavior. Currently, the standard criteria of main

characteristics (tumor size and grade, nodal involvement, histopathology, and marker expression) are insufficient to guide important treatment decisions, especially in advanced tumors [48].

Breast cancers are highly heterogeneous, with comparable morphological features that can have diverse clinical courses owing to their distinct gene profile [50,54]. Five molecular subtypes of breast cancer were determined: luminal A, luminal B, Human Epidermal Growth Factor Receptor 2 (HER-2) positive non-"luminal", basal-like, and special histological types; each subtype corresponds to the immunophenotypes of cancer cells that are determined based on pathological criteria. High expression of genes associated with estrogen receptor (ER) activity and HER2 receptor expression, and low expression of genes associated with proliferation are characteristics of luminal type A. Luminal type B features encompass a positive ER status with low gene expression, and an increased expression of genes related to proliferation compared to luminal type A [55]. Basal-like breast cancer is similar to triple-negative breast cancer (TNBC), with the lack of HER2 receptor expression and the estrogen and progesterone receptors (PR). Nevertheless, some basal-like breast cancer expresses HER2 [48]. The overexpression of the *HER2* gene combined with the lack of ER and PR is what defines the molecular subtype of breast cancer known as HER2-positive [54].

Mammography screening and adjuvant therapy have been largely responsible for improved outcomes in breast cancer [56]. The treatment of breast cancer varies depending on the molecular features and subtype, which includes local-regional therapy (surgery and radiation therapy) and systemic therapy. Systemic therapies consist of hormone therapy with targeted agents (e.g., CDK4/6 inhibitors and phosphoinositide 3-kinase (PI3K) inhibitors) for hormone receptor-positive types, chemotherapy, anti-HER2 therapy for HER2-positive types, poly adenosine (ADP)-ribose polymerase (PARP) inhibitors for *BRCA1/2* mutation carriers and immunotherapy for part of TNBC [50,54]. For instance, early-stage TNBC and HER2-positive are treated with preoperative or neoadjuvant therapy (e.g., targeted drugs and immune checkpoint inhibitors) [50]. More than 15-20% of all breast cancers are TNBC and it is of particular interest due to its highly invasive nature and poor responsiveness to treatment [23]. Individualized therapy and treatment escalation and de-escalation based on cancer biology and early response to therapy are the ultimate objectives of future therapeutic approaches for breast cancer [48,50].

1.5 Cancer therapy

Cancer therapy relies on the selective destruction of malignant cells while preserving healthy tissue. Cancer treatments have been developed over the past 170 years, highlighting novel therapies that have improved clinical outcomes and patient's quality of life [57]. From the usage of general anesthesia in surgeries in the middle of the 1800s to the invention of X-rays by Wilhelm Conrad Röntgen in the late 19th century [58], to the advances in chemotherapy during World War II [59] and the recent developments in immunotherapy and gene therapy, each milestone has played a crucial role in the breakthrough of cancer therapy [57]. Recently,

considerable progress has been developed to identify and characterize oncological biomarkers, leading to innovative approaches for detecting cancer cells and providing tools for molecular staging of cancer progression. These advances have been essential for the molecular detection and early diagnosis of cancer, as well as for the establishment of new and more precise and targeted treatment strategies [1,57,60]. Among the plethora of molecular biomarkers in cancer, those capable of identifying germline or somatic mutations, transcriptional changes, and post-translational modifications have been pivotal in advancing innovative cancer diagnostics and therapeutics [61]. Still, the main treatment options upon diagnosis include surgery, radiotherapy, chemotherapy, immunotherapy, or a combination of these therapies, and gene therapy. Below, I shall briefly discuss the diverse types of cancer treatments and their recent advancements.

1.5.1 Surgery

Surgery is the oldest method of cancer therapy and the primary intervention, which offers a high possibility of treating solid non-metastatic tumors, especially when diagnosed early and combined with other treatments (e.g., radiotherapy and chemotherapy). Furthermore, additional evaluation of the malignant tissue (tumor imaging and biopsy) is necessary to determine whether surgery can be conducted to remove the tumor [62,63]. The development of cancer surgery began in the early 20th century with significant procedures, including the first abdominoperineal resection [64], lobectomy [65], and radical hysterectomy [66]. Modern advancements include non-invasive techniques such as laparoscopic colectomy [67], videothoracoscopy, radiofrequency ablation, and radiosurgery (e.g., Cyberknife®) [68]. Breast-conserving surgery with sentinel-node removal [69], laryngoscopic laser surgery [70], and the Da Vinci® robotic system [71] represent the latest innovations in oncological surgery [72].

For local primary tumors, whole surgical resection is the most effective and preferred method in cancer treatment, but surgery as monotherapy is associated with an elevated risk of cancer recurrence and the formation of metastasis [63]. The surgical trauma can cause systemic and localized inflammatory responses, which clinical studies have associated with the growth of micrometastases [73]. To address this challenge, it is crucial to combine surgery with radiotherapy and chemotherapy to reduce the risk of metastasis and cancer recurrence [63].

1.5.2 Radiotherapy

Radiotherapy is one of the most effective cancer treatments based on the use of radiation beams (e.g., X-rays or protons) to destroy or prevent the growth of tumor cells [62,74]. There are three main types of radiotherapy: teletherapy (external), brachytherapy (internal), and radiosurgery (stereotactic radiotherapy) [74]. Radiation therapy aims to target cancer cells with maximum precision while minimizing damage to nearby normal cells [75]. Nevertheless, toxicity in normal tissues has been observed (e.g., local radio-inflammatory responses) of some cancer patients [76,77]. Radical radiotherapy is a viable alternative to surgery, which offers

effective long-term tumor control for several cancer types (e.g., lung, and head and neck cancer). Clinical data suggests it often leads to longer survival and improved disease control compared to other cancer treatments [78].

The effectiveness of radiotherapy as a standalone treatment for advanced cancer remains a topic of debate. For example, thoracic radiotherapy is an important treatment for inoperable stage III non-small cell lung cancer (NSCLC), but the use of standard radiotherapy (e.g., prophylactic cranial irradiation) only increases survival by around 5%. Despite technological advances and chemotherapy progress, the potential of radiotherapy in cancer treatment remains low due to its poor efficiency and toxic side effects [79]. Radiation therapy can be combined with surgery, chemotherapy, or immunotherapy. It is primarily used as neoadjuvant therapy to shrink tumors before surgery and as adjuvant therapy to eliminate any remaining microscopic tumor cells after surgery [80]. Advancements in computerized tomography (CT) imaging technology and other technological tools have evolved radiotherapy from 2D to 3D and four-dimensional methods, with significant improvements in dose distribution, intensity, and accuracy [81].

1.5.3 Chemotherapy

Chemotherapy is one of the most common treatments currently available to treat cancer, which involves the use of chemotherapeutic agents (alone or in combination) to treat local or metastatic solid tumors and malignant neoplasms of the hematopoietic system [82,83]. In cancer therapy, it is important to reduce the tumors' size to increase their susceptibility to chemotherapy due to the higher division of cancer cells and proliferation rate, compared to normal cells [82,83]. Clinical chemotherapy is classified into three main categories: preoperative (before surgery), intraoperative (during surgery), and postoperative (after surgery). It can also be combined with pre-radiotherapy for enhanced treatment efficacy [62,84]. Over the years, the toxic side effects of chemotherapeutic agents have been well-documented, including nausea, vomiting, diarrhea, hair loss, and loss of appetite. Moreover, patients have experienced some drug-resistant cancer, bone marrow suppression, and kidney and liver failure [84,85].

Still, chemotherapy is the first-line treatment for various cancers, even with the emergence of novel treatments such as immunotherapies (e.g., immune checkpoint inhibitors) and oncogene-targeted therapies (e.g., tyrosine kinase inhibitors), which combined with conventional chemotherapy have shown promising results [86,87]. Chemoradiotherapy for esophageal cancer [88] and adjuvant chemotherapy for colon cancer [89] are two examples of how chemotherapy before or after surgery and/or in combination with radiotherapy can provide long-term survival of several patients, in localized cancers [86]. PARP inhibitors, angiogenesis inhibitors, histone deacetylase (HDAC) inhibitors, mechanistic target of rapamycin (mTOR) inhibitors, hedgehog pathway blockers, tyrosine kinase inhibitors, proteasome inhibitors, and p53/mouse double minute 2 homolog (MDM2) inhibitors are a few of the promising inhibitor therapies that have been used to treat solid cancers [90,91].

1.5.4 Immunotherapy

The era of cytotoxic drug therapy has paved the way to the new era of precise immunotherapy based on the immune system for cancer treatment [62,92]. Improved knowledge of the immune surveillance mechanism led to the next revolutionary wave in cancer immunotherapy [93]. Immunotherapy incorporates the use of constituents of the immune system (e.g., cytokines, antibodies, lymphocytes, DCs, and other immune cells) to identify and destroy cancer cells, offering a targeted therapy with higher efficiency, specificity, less toxicity, and capable of prolonging patients' survival [72]. Cancer immunotherapy was recognized as the most significant scientific breakthrough of 2013 owing to its remarkable innovation and efficacy. James Allison and Tasuku Honjo were awarded the 2018 Nobel Prize in Physiology or Medicine for their research on cytotoxic T lymphocyte-associated protein 4 (CTLA-4) and programmed cell death protein 1 (PD-1) in cancer treatment [62].

The development of immunotherapies has been reported (e.g., adoptive cellular therapy, immune checkpoint blockade, and cancer vaccinology), which highlighted the capacity of T cells against cancer [92,94,95]. Prostate cancer, kidney cancer, NSCLC, melanoma, and other solid tumors have all been successfully treated with cancer immunotherapy [62,96]. The majority of the 11 cancer immunotherapies approved by the US Food and Drug Administration (FDA) in 2020 are monoclonal antibodies (mAb) immune checkpoint inhibitors, including PD-1/PD-L1 mAb, and CTLA-4 mAb, and cell therapy based on chimeric antigen receptor T (CAR-T) cells [97]. Regarding the limitations and toxicity of traditional cancer therapies, clinicians and scientists have explored novel approaches with more efficacy and fewer negative side effects [62]. However, cancer immunotherapies can cause side effects such as allergic reactions, vomiting, diarrhea, loss of appetite, cardiotoxicity, liver, kidney, and lung damage [74,98].

1.5.5 Combinatorial therapy

Recent advancements in cancer therapy have significantly improved the understanding of key pathways involved in tumor progression, paving the way for more precise and effective treatment strategies. Targeted therapy has emerged as a less toxic alternative to conventional chemotherapy; however, its standalone use remains insufficient for cancer treatment due to tumor complexity [74,99]. Combinatorial therapies, including targeted therapies (e.g., immune checkpoint inhibitors, small molecule inhibitors) and chemotherapeutic agents (e.g., taxanes and platinum compounds), have demonstrated synergistic effects that enhance treatment efficacy, overcome drug resistance, and improve the overall survival rate of cancer patients [99,100].

Cetuximab is an EGFR inhibitor that plays a crucial role in treating CRC and is frequently combined with chemotherapeutic drugs such as oxaliplatin, irinotecan, and fluorouracil. Other targeted therapies for CRC include panitumumab (EGFR inhibitor) and bevacizumab (VEGF inhibitor), which are combined with anticancer drugs to enhance therapeutic

efficiency and improve patient outcomes [74]. For instance, the efficacy of Avastin (bevacizumab) combined with 5-fluorouracil prolonged the survival of patients with advanced CRC [99,101]. Ipilimumab (CTLA-4 inhibitor) combined with chemotherapy is the first-line treatment for TNBC [57], and HER2 inhibitors, such as pertuzumab and trastuzumab, are mostly used combined and/or in combination with chemotherapeutic agents (e.g., docetaxel, paclitaxel) for the treatment of breast cancer [57,74]. Recently, Liu *et al.* revised that the US FDA has approved 90 combination therapies between 2006 and March 20, 2024. Still, the patient selection criteria are strict since only specific subgroups of cancer patients are eligible for these treatments. There is an increased demand for predictive biomarkers, drug selection, drug dosages, treatment duration, and further *in vivo* studies and clinical trials for combined cancer therapies [57].

1.5.6 Gene therapy

Gene therapy has proven to be a promising targeted approach against cancer. Extensive research has been conducted based on the concept of introducing therapeutic nucleic acids (TNAs) into target cells in a controlled manner to block the expression of specific genes that have been promoting cancer progression (e.g., gene silencing of proto-oncogenes) or restoring the expression of tumor suppressor genes (e.g., *p53*), which have lost their function [1]. Various gene therapy strategies rely on the capability of vectorizing TNAs and/or a combination of tools for gene editing into the desired target cells, which aim to correct molecular events that contribute to cancer development [102]. These platforms include gene and genome editing tools that provide the capacity to regulate gene expression, reconfigure chromatin structure, and manipulate DNA. Gene and genome editing tools are capable of inducing and modulating mechanisms of endogenous RNA interference (RNAi), and those able to target specific molecular markers, decrease oncogenes expression, and reprogram cell phenotypes [103–105]. Gene therapy tools have the purpose of regulating gene expression and the genome, which is important for tracking tumor development and cancer cell survival. Major limitations can be solved by the upgrade of delivery strategies and the use of proper probe designs, which should be proficient in carrying high payloads of the desired TNAs for gene therapy. Strong efforts have emerged for precise delivery of the cargo, such as protection against degradation by endonucleases and an increase in circulation half-life [1,106]. Furthermore, inefficient targeting of the desired cell may be solved by employing vectorization of TNAs with nanoparticles, which can enhance off-target effects (e.g., disruption of gene function and erroneous integration) [107].

Gene therapy can target DNA, using genome editing tools such as clustered regularly interspaced short palindromic repeats (CRISPR) and CRISPR-associated (Cas) proteins, meganucleases, transcription activator-like effector nucleases (TALENs) and zinc finger nucleases (ZFNs); or RNA, using RNAi mechanisms, antisense oligonucleotides (ASO), ribozymes and riboswitches [1,108]. Herein, I shall briefly discuss some of the most promising tools, either conceptual or already translated to the clinics.

1.5.6.1 Genome editing tools

1.5.6.1.1 CRISPR/Cas9

One of the most promising, efficient, and precise methods applied to gene therapy is CRISPR and CRISPR-associated (Cas) proteins. This genome editing system allows for targeted genomic modifications, and there are three main execution strategies: direct delivery of Cas9 protein and single-stranded guide RNA (sgRNA); direct delivery of messenger RNA (mRNA) and sgRNA; and plasmid-based CRISPR/Cas9 strategy. CRISPR/Cas9 facilitates efficient multiplex genome editing, with the possibility of simultaneous deletion or insertion of multiple DNA sequences [109,110]. CRISPRs were discovered in bacteria due to their mechanism of inducing RNA-guided DNA cleavage, essential for bacteria's adaptive defense against exogenous DNA. The structure of the Cas genes is important for the way that CRISPR-Cas systems were organized into two major classes [111,112]: class 1 includes multiprotein complexes, though class 2 systems comprise one effector protein, including a subtype that is the most used CRISPR/ Cas9 system [113,114]. sgRNA was designed to bind and complement the target DNA site in a specific sequence and to ensure compatibility with Cas9 endonuclease and Cas9 protein, followed by a protospacer adjacent motif (PAM), that specifically cleaves the DNA to create a double-strand break (DSB) [115]. Still, the development of effective delivery systems for CRISPR/Cas9 elements for specific targets remains a challenge for clinical therapeutics.

CRISPR/Cas9 is fast to develop, simple, and cost-saving in comparison with other gene editing tools [116]. The potential for simultaneous multiple loci editing, cost-effectiveness, and flexibility are advantages of the usage of this platform [107,116]. Additionally, the use for insertion, editing, and knockdown in genomes provides a major benefit. However, limitations, such as the high frequency of random integration and activation of the non-homologous end-joining DNA repair pathway, which may lead to microdeletions at the DSB site, have been reported [110,115,117]. CRISPR/Cas9 has been applied in a variety of *in vivo* and *in vitro* research for cancer therapy. Recently, their application in T cell cancer therapy has been reported [118,119].

1.5.6.1.2 ZNFs - Zinc Fingers

ZNFs are the first DNA-binding domain used for many years for gene editing [120]. In 1985, Klug laboratory discovered a protein that contained 7-11 zinc ions with a linear arrangement of independent domains that could bind DNA. Resulting from the fusion of a cleavage domain that is not sequence-specific to a site-specific DNA-binding domain, ZNFs can bind with highly affinity DNA and are capable of recognizing RNA or even DNA-RNA fusions [121]. *FokI* type II restriction endonuclease formed DNA cleaving domain, and those domains can be dimerized to precisely target genomic sequences [122].

ZNFs can join short and extremely conserved linkers to form multiple ZNFs proteins. The Cys2His2 family is organized by two cysteine and two histidine folded into one α-helix and two antiparallel β-strands. Also, these domains are comprised of 28-30 amino acids belonging to a superfamily with around 700 ZNFs in the human proteome [121]. The optimization of functional domains is significant to enable the development of different modules for

genome editing. The ZNFs interaction and specificity to the target are defined by the number of fingers and each finger's amino acid sequence [123]. DNA-binding domains recognize trinucleotide DNA sequences, but longer DNA sequences may also be targeted by them. ZNFs may be designed to include a variety of effector domains to recognize virtually any DNA sequence. However, this genome editing tool has its drawbacks, including high off-target effects, as well as being expensive and difficult to use. As so, clinical application in HIV treatment has been reported [123,124].

1.5.6.1.3 TALENs - Transcription activator-like effector nucleases

DBSs are produced by a nonspecific DNA cleavage domain united to a custom-made sequence-specific binding domain, known as TALENs. The transcription activator-like effector (TALE) is a highly conserved repeat sequence, which the DNA-binding domain derives [121]. *FokI* is a functional endonuclease responsible for the stimulation of site-specific DSBs for DNA recombination to modify the target gene sequence. The endonuclease cleavage domain should be dimerized to cut the two DNA strands, such as TALEN modules that are designed in pairs to bind the two specific sites of the target. Site-specific recombinases, transcriptional modulators and activators, and nuclease activity are modifications needed when multiple effector domains are added to effort TALEN functionality [125,126]. The major limitation for cloning repeat TALE arrays is the large-scale assembly of matching repeat sequences. To overcome restrictions of this technique, several strategies such as "Golden Gate" cloning, connection-independent cloning, and high-throughput assembly using solid phases have been proposed [127,128].

DNA targeting specificity comes from the fused bacterial TALE proteins. TALEN arrays recognize only a single nucleotide (as opposed to ZFNs), and it has no impact on the binding specificity. TALEN-engineered nucleases demonstrate better specificity and efficiency than ZNFs, although the major constraint is cloning of the large modules in series and joining these modules in designated order by ligase in an efficient way. Along with several *in vitro* and *in vivo* studies, TALEN applications in cervical intraepithelial neoplasia and hematological malignancies are in clinical trial evaluation [104,124,129].

1.5.6.1.4 Meganucleases

Meganucleases are grouped into five main families: His-Cys box, H-N-H, GIY-YIG, LAGLIDADG, and PD-(D/E)XK. The LAGLIDADG family shows a wide range of gene editing tools that are principally toward the modulation of splicing and maturation of RNA. These endodeoxyribonucleases are characterized by large motifs capable of targeting specific nucleotide sequences for the replacement, modification, or elimination of those nucleotide sequences [113,130]. DmoCre and E-Drel are protein variants that combined with meganucleases provide enhanced capability in targeted cleavage, representing an example of genome editing. Some advantages of their usage are low cytotoxicity but still require further studies due to the impact of the side effects on the organism [131].

Meganucleases technology involves re-engineering the DNA-binding specificity that naturally occurs in the family of homing endonucleases. Meganucleases are the smallest class of engineered nucleases, making them potentially amenable to all standard gene delivery methods since they offer fewer off-target effects. Despite their potential, meganucleases are difficult to construct, time-consuming, and high-cost, which restricts their application as gene editing tools [124,130].

1.5.6.1.5 Ribozymes and Riboswitches

Ribozymes are catalytic RNAs in an autonomous manner, participating in cellular processes. RNA hydrolysis and RNA ligation reactors are catalyzed by ribozymes, and they are categorized according to their major function in two categories: splicing and cleaving ribozymes. Splicing ribozymes can be used to control gene expression through mRNA splicing [113,132]. The riboswitch term is applied to "metabolite sensing RNA switches" and can interact with small molecules such as ions and other regulatory RNAs. Responding to internal and external triggers, RNA-based sensors like riboswitches upon modification of RNA conformation may be related to gene expression regulation [132].

1.5.6.2 Gene silencing: RNAi mechanism and ASO

Gene silencing involves the intracellular delivery of TNAs, typically employing RNAi mechanisms to modulate gene expression. This includes approaches like small interfering RNA (siRNA), microRNA (miRNA), and short hairpin RNA (shRNA). Most gene silencing targets are associated with oncogenes (e.g., *c-MYC*, *KRAS*, *BCR-ABL1*), which trigger abnormal cell proliferation by increasing gene expression or enhancing the activity of oncoproteins. Gene silencing may also inhibit tumor suppressor genes (e.g., *p53*), which normally prevent cell proliferation and tumor formation, or affect other genes involved in tumor survival, such as those regulating angiogenesis (e.g., *VEGF*) [133,134].

RNAi technology has emerged as a promising therapeutic strategy, particularly in cancer treatment. RNAi is facilitated by double-stranded RNA (dsRNA), which plays a role in regulating gene expression (e.g., shRNA and siRNA). Also, miRNA interacts with the cytoplasmic RNA-induced silencing complex (RISC), leading to either mRNA degradation or translational repression [135]. Antisense DNA technology allows for the inhibition or downregulation of protein production by utilizing ASO that are complementary to the target sequence. Antisense DNA technology using ASO is a valuable approach for gene expression regulation, which has already been used with chemotherapy agents for combined therapy in cancer. The most used in gene silencing is RNAi technology, specifically siRNA [136]. Figure 1.3 represents an overview of the mechanism of action of RNAi technology (e.g., siRNA) and Antisense DNA technology with ASO for gene silencing applications.

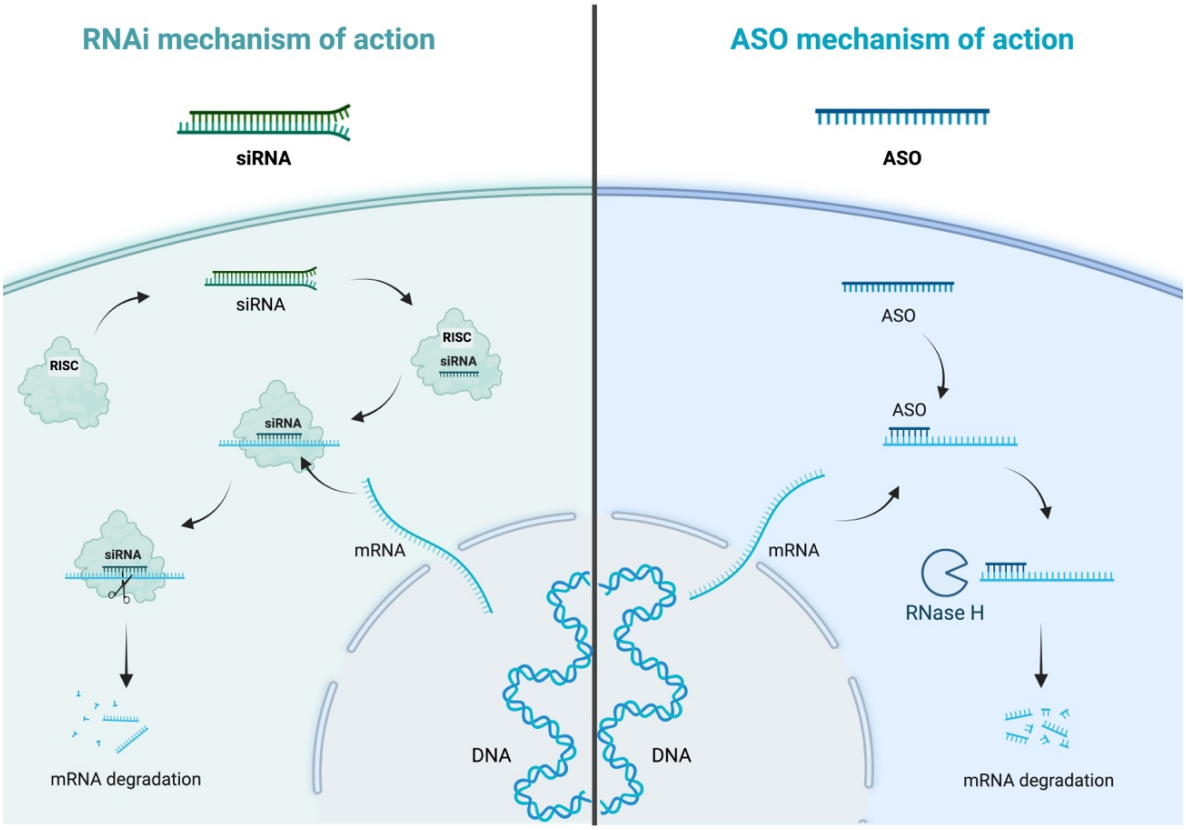

Figure 1.3 - Mechanism of action of siRNA (left) and ASO (right) for gene silencing or modulation of gene expression. The siRNA is incorporated into RISC, where the guide strand (antisense strand) is retained, while the passenger strand (sense strand) is degraded. Then, siRNA binds to a complementary sequence on the target mRNA, and the catalytic component of RISC (Ago2) cleaves the mRNA, leading to mRNA degradation. On the other hand, ASO binds to target mRNA, and RNAse H is recruited to mediate mRNA degradation (or steric hindrance, where the ASO blocks the binding of ribosomes to the mRNA).

Currently have been introduced novel targeting strategies, such as RNAi mechanisms, which have a special interest in cancer therapy and gene silencing [137–139]. RNAi technology relies on the use of short interfering RNA molecules, potent regulatory agents that are employed to downregulate gene expression. The cytoplasmic RISC participates in these mechanisms for RNAi technology, in which RNAi is typically used to manipulate gene expression. RNA fragments can bind RISC, which possesses enzymatic activity, then when activated with an incorporated single strand of miRNA or siRNA, can recognize target mRNA that is destroyed by Ago2, a protein present in RISC. siRNA and shRNA are the most TNAs used for gene silencing, based on RNA-based therapeutic platforms [140–142]. The involvement of miRNAs in cancer was firstly studied in B-chronic lymphocytic leukemia (B-CLL), where miRNA genes *miR-15* and *miR-16* proved to be downregulated in the majority of B-CLL cases [143]. For example, miRNA can activate mRNA degradation or suppression of translation. RNAi technology has been used in CRC for targeting genes involved in signaling pathways (e.g., *c-MYC* and *KRAS*), which are responsible for the survival, proliferation, and metastasis of malignant cells [144–146]. Some of the limitations are short half-lives due to RNases, low biochemical stability, and prohibitive costs. This approach has been applied for *in vitro* and *in vivo* studies, which are important for the advances in cancer clinical trials, including silencing oncogenes that are

implicated in TME [147]. Additionally, nanocarriers as vectors to deliver RNA cargo are used to improve cellular uptake and reduce off-target effects. An example is Patisiran, the first siRNA drug loaded in lipid nanoparticles approved by the US FDA in 2018 [148].

Antisense DNA technology using ASO is a valuable approach for gene expression regulation and can be applied for combined therapy along with chemotherapy agents to improve cancer treatment. These synthetic oligonucleotides were first reported in 1978 by Stephenson and Zamecnik, showing to be specific for the regulation of gene expression. They were called ASO due to their complementary to RNA sense strand, consisting of 15-20 nucleic acid length [136,149]. The usage of ASO that are complementary to specific-site sequences permits downregulating the production of amino acids essential for cancer cell development and survival. The creation of different molecules is considerable important for advances in antisense DNA technology to enhance target delivery, efficacy, and safety for clinical trials [139,150].

ASO are small DNA or RNA molecules complementary to their target mRNA, and binding to their target result in mRNA splicing or degradation of target transcripts. Also, ASO can be used to modulate the ratio of splicing variants or correct some splicing defects, by induction of exon-inclusion or exon-skipping [151]. Splice switching oligonucleotides are alternative pre-mRNA splicing manipulated, and simple to design and vectorize inside the cell. There are some obstacles to *in vivo* delivery (e.g., immunogenic) that may cause side effects and short half-lives due to RNase activity. Second-generation ASO were developed to overcome non-sequence specific side effects of the first generation, to enhance target-binding affinity, hybridization affinities, and nuclease resistance [152]. Recently, third-generation ASO have been provided to improve their delivery to the specific site, which can bind covalently to a ligand or nanocarriers (e.g., lipid and metal nanoparticles, protein, liposomes) [152,153]. Single and double-stranded ASO are briefly filtered by the kidney and exhibit low serum protein binding and limited tissue distribution, which due to rapid clearance several nanocarriers have been developed to enhance cellular uptake [154,155]. Fomivirsen is the first ASO drug approved in 1998 by the US FDA for cytomegalovirus retinitis [156]. Mipomersen and lomitapide are two ASO drugs approved by the US FDA in 2013 for familial hypercholesterolemia, acting on the expression of apolipoprotein-β for cholesterol level reduction [157]. Lately, ASO technology started in clinical trials for Duchenne muscular dystrophy treatment and their clinical application has been reported in thalassemia [149].

Although these cancer treatments have made significant contributions to the ongoing fight against cancer, they are often invasive techniques and/or usually lack selectivity for cancer cells, leading to a range of adverse side effects that can impede the success of therapy, which contribute to relapse and lack of quality of life for cancer patients. Therefore, there is an increasing demand for alternative, non-invasive, and selective targeted therapies to address these challenges. These precise approaches often involve directing/targeting drugs, oligonucleotides, or other (bio)molecules directly to cancer cells – the case of Nanomedicine [1,106].

1.6 Nanomedicine

Nanotechnology has brought the opportunity to combine different therapeutic systems, including dendrimers, liposomes, metallic nanoparticles, micelles, polymeric nanoparticles, and silica nanoparticles. These approaches exhibit a wide range of unique physical-chemical characteristics and can be synthesized easily for vectorization of the cargo, with the capability to visualize their distribution and accumulation at the specific target site in real time [1]. Furthermore, nanotechnology has paved the way for nanotheranostics, combining therapy and diagnostics into a single platform [158–160].

Nanomedicines in cancer therapy encompass a wide range of nanoparticles and nanotechnologies that have gained attention upon the approval of the first nanomedicine Doxil by the US FDA in 1995 [161]. Nanomedicine leverages nanotechnology to improve stability, bioavailability and biocompatibility of druggable elements while allowing for targeting and imaging, thus optimizing delivery and therapeutic efficacy [1]. These nanomedicines are nanocarriers on the nanoscale which can include drugs, proteins, peptides, nucleic acids, and other (bio)molecules. Lipid-based nanocarriers, inorganic-based nanoparticles, and polymer-based nanocarriers are the most used, and viral vectors and ADCs (Antibody-Drug conjugates) can be considered nanomedicines [1,57] (Figure 1.4). Novel cancer therapies based on gene therapy, such as the delivery of TNAs vectorized with a variety of nanoplatforms (e.g., organic and inorganic nanoparticles), have been developed in the past years [148,162,163].

Approaches can be designed to selectively target specific cells or tissues by incorporating (bio)molecules that enhance the uptake of therapeutic agents by cancer cells. Both active and passive targeting strategies are employed to direct therapeutic agents to the desired cells. Passive targeting leverages the body's pathophysiological changes, such as altered fluid and solute dynamics, while active targeting involves the use of specific biomolecules (e.g., antibodies, peptides, or small molecules) that are recognized by the target cells, improving selectivity and uptake [158,164–166]. Also, nanomedicines allow the precise delivery of several (bio)chemotherapeutics to multiple tumor markers, mediating stimuli-response drug release, which may result in a synergistic methodology to tackle cancer resistance and heterogeneity [167,168]. These nanomedicines have the advantage of extending the circulation time of therapeutic agents and enabling stimuli-responsive drug release and uptake by cells [169].

Advances in imaging techniques, such as electron microscopy, super-resolution fluorescence microscopy, and single particle tracking, have been essential for a better understanding of the nanoparticles' intracellular pathways and trafficking. Nanomedicine applications highlight the impact of barriers to efficient cellular uptake of nanoparticles and their developments and strategies deployed to overcome these barriers (glycocalyx and macromolecular crowding) [106,167,170]. Still, novel strategies to enhance the targeting and delivery of the nanocarriers to tumor cells are required.

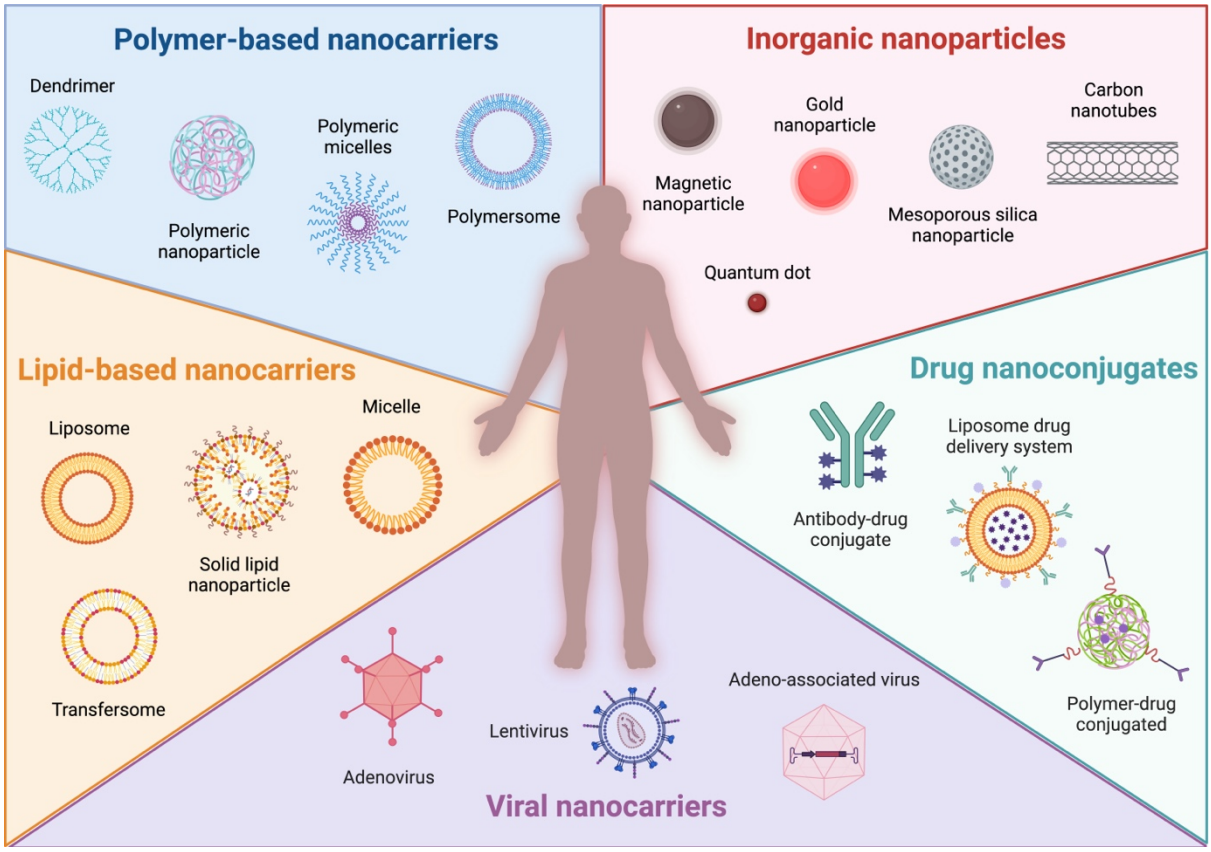

Figure 1.4 - Schematic illustration of different nanoplatforms (polymer-based, lipid-based, inorganic nanoparticles, drug-conjugated, and viral nanocarriers) used for cancer therapy. (Created with BioRender.com)

1.7 Nanoplatforms for delivery of therapeutic nucleic acids

Transfection allows the selective introduction of TNAs into living cells for enhancement or inhibition of protein synthesis. However, efficient nanocarriers are necessary to overcome transfection issues (e.g., TNAs degradation by nucleases). Various nanosized vehicles have been developed for the delivery of TNAs, including polymeric particles, dendrimers, semiconductor quantum dots, amino acids, liposomes, carbon-based nanostructures, viral vectors, silica, and metallic nanoparticles [106,162,163,171]. These carriers are crucial for targeting cancer cells with TNAs, but their efficacy in carrying to malignant cells remains a challenge to the clinics [171–173]. Viral and non-viral carriers, such as organic and inorganic nanoparticles, are particularly suitable for this purpose and can be prepared in many ways. Viral vectors often exhibit higher transfection efficiency compared to non-viral vectors, but they frequently induce strong immune responses and exhibit significant cytotoxicity [174]. In contrast, non-viral vectors are favored due to their ease of production, lower costs, and reduced immunotoxicity [175]. Among these, lipid nanoparticles are the most used approach for TNAs delivery [176,177].

Adenoviruses (AdVs), retroviruses, lentiviruses, herpes simplex virus, and adeno-associated viruses (AAVs) are the most common viral vectors used for gene therapy [178]. Gendicine

was the first gene therapy tool approved in 2003 by the Chinese FDA. This approach is a recombinant AdVs engineered to express tumor suppressor gene *p53* for the treatment of head and neck squamous cell carcinoma. Gendicine enhances treatment efficacy when combined with radiotherapy and chemotherapy and also demonstrates the improvement of therapeutic radiation effects in pancreatic cancer cells, although more clinical trials are necessary [179]. One of the major concerns of the employment of gene therapy approaches is the long-term risk. Clinical trials have been evaluated based on the integration of a vector that improves the delivery of TNAs to the specific target site to overcome the uncertain long-term risk [105]. Liposomes, cationic lipids, inorganic nanoparticles, dendrimers, polymers, and exosomes are some examples of non-viral vectors used for non-invasive administration (e.g., through skin and eyes). For example, lipid nanoparticles formulations have been used in several *in vitro* and *in vivo* studies, improving the delivery of TNAs to target cells or tissues [1,180].

RNAi and antisense technology are promising tools for the efficient delivery of therapeutic siRNA, miRNA, shRNA, or ASO, although the *in vivo* systemic delivery remains a challenge due to several limitations (e.g., degradation by nucleases, low cellular uptake, and instant renal clearance). Furthermore, the development of effective and safe nanocarriers to highlight the systemic administration of silencing moieties for gene therapy is necessary. To overcome this limitation, RNA or DNA molecules should be nuclease-resistant chemically to avoid degradation and combined with viral and non-viral nanocarriers [181,182]. Hence, non-viral nanocarriers such as liposomes, polymers, or inorganic nanoparticles have been developed to deliver RNA silencers effectively. Cationic lipids (e.g., Lipofectamine™ reagent) can form complexes with negatively charged siRNA/ASO to improve *in vitro* transfection efficiency, but with some cytotoxicity [183]. For instance, metal nanoparticles, such as gold (AuNPs) and magnetic (MNPs) have gained attention as excellent alternatives for TNAs vectorization and delivery [1].

1.8 Metal nanoparticles in gene silencing – general concepts

Metallic nanoparticles have been extensively utilized in various biomedical applications due to their unique physical and chemical properties, which are highly influenced by factors such as size, shape, surface-area-to-volume ratio, biocompatibility, and amphiphilicity. These nanoparticles are usually synthesized through straightforward methods and can be easily functionalized with a wide range of biomolecules, such as drugs, nucleic acids, proteins, or antigens, using simple chemical techniques to enhance their biological functionality and activity [106,184,185].

Several types of metal nanoparticles can be functionalized with nucleic acids, and their chemical nature can be modified to improve their uptake by endocytosis. For an efficient uptake and short-term cellular interaction, the maximum size of nanoparticles must be around 100 nm, and their surface must be functionalized to ensure biocompatibility. Also, the nanoparticle core is important (chemical composition) for long-term biocompatibility and

biodegradability [186–188]. For gene silencing, nanoparticles can deliver the cargo into the cytoplasm, while the transfer of nanoparticles into the nucleus is necessary for DNA transfection (e.g., plasmid vector transfection) [189]. Efficient nanocarriers are required for high transfection, ensuring biocompatibility, long-term biodegradation, and site-selective application. Some of the advantages of metallic nanoparticles are their easy finetune, size, surface functionalization, nucleic acid protection, and biocompatibility. The selection of surface chemistry is pivotal for optimizing loading capacity and addressing limitations, such as nanoparticles' instability in biological environments [106,190]. It plays a fundamental role in passively targeting the carriers to the desired site, regulating circulation half-life, modulating cellular uptake, and either evading or activating the immune response. Therefore, surface chemistry is essential in controlled-release systems, enabling precise and spatiotemporal control for the specific delivery of the cargo in a "smart" controlled manner [1].

A better knowledge of interactions between nanoparticles and cells is required to design delivery systems suitable for clinical applications [186,191]. Cell surface engineering has emerged to promote targeting and delivery based on the chemical modification of biomolecules of cell membranes (e.g., glycoproteins) and their interaction with nanomaterials [170,192,193]. The main approaches for the conjugation of nanoparticles with cells involve ligand-receptor recognition and covalent binding. Ligand-receptor recognition requires the functionalization of the nanoparticles with biomolecules (e.g., peptides, aptamer, antibodies, carbohydrates, among others), which recognize and bind to specific receptors on the cell membrane through non-covalent bonds [194]. On the other hand, covalent bonding is based on the formation of stable bonds between nanoparticles and chemical groups on the cell membrane (e.g., amine and thiol groups) [195]. Nevertheless, both approaches have significant limitations of selectivity and efficiency [196–198]. To address those challenges, bioorthogonal click chemistry reactions arise as a powerful alternative for coupling nanoparticles with cells owing to their ability to occur within living systems with specificity and minimal interference with native biological processes [170,199]. One of the most notable reactions is the strain-promoted click azide-alkyne cycloaddition reaction (SPAAC) [200].

Additionally, nanoscale structures can be directed toward cancer sites by leveraging physiological changes within the tumor for passive targeting. The enhanced permeability and retention (EPR) effect is a paradigm that possibly facilitates the extravasation of nanoparticles through the endothelial cells of surrounding blood vessels into tumors. This occurs due to the leaky nature of tumor vasculature, which arises from the rapid and disorganized growth of new blood vessels (e.g., angiogenesis) that supply the tumor with essential nutrients. These vessels develop rapidly, lacking the structural maturity needed for stability [1,201]. In the case of triggered targeting, nanoparticles can release their cargo in response to external stimuli, such as magnetic field (e.g., magnetic hyperthermia using MNPs), electric field (e.g., electroporation, ultrasound, radiofrequency), or light (e.g., photothermal therapy using AuNPs) [202,203]. For instance, metal nanoparticles have emerged as effective carriers for the delivery of silencing moieties, with AuNPs playing a prominent role.

This thesis focuses on the potential of AuNPs and MNPs as "nanoheaters" to promote cell uptake, improving gene silencing for cancer therapy. Herein, I shall discuss the general

concepts of these nanoparticles, such as surface modification, targeting and delivery, as well as their important role as therapeutic agents in gene therapy applications.

1.8.1 Gold Nanoparticles (AuNPs)

The synthesis of gold nanoparticles (AuNPs) was first reported in the early 19th century by Michael Faraday, who produced a red color solution of colloidal AuNPs using chloroauric acid and phosphorus as the reducing agent [204]. Later, Turkevich simplified the process by using a citrate reduction method, which became a foundational technique for AuNP synthesis [205]. Over the years, many other synthesis methods were developed to create AuNPs with varied sizes and shapes, depending on the synthesis procedure, pH, and passivating agents [206,207]. Two main approaches for large-scale AuNPs synthesis are top-down and bottom-up. The top-down approach involves breaking down bulk material into the nanoparticle using techniques such as laser ablation, ultraviolet (UV) and infrared (IR) irradiation, ion sputtering, and aerosol technology [159]. The bottom-up methodology consists of building nanoparticles from precursor molecules, which are ionized when energy is given to the system. Turkevich method is an example of a bottom-up strategy since Au^{3+} is reduced to Au^{0} by the action of citrate (reducing agent) [159]. For instance, other chemical synthesis options based on a bottom-up system are the Brust Method [208], Seed-Mediated Growth [209], and Digestive Ripening [210]. Bottom-up approaches are preferred for producing low-size dispersion and uniform AuNPs and are widely used in biomedical applications due to their simplicity and lower cost [211,212].

The advantageous features of AuNPs derive from their morphology (e.g., size, shape, core charge, surface ligands, solvent) which can be adjusted to optimize their properties. AuNPs can be functionalized with a variety of (bio)molecules (e.g., drugs, proteins, oligonucleotides) to change their physicochemical behavior, such as the surface charge. Therefore, the functionalization of AuNPs allows for enhanced selectivity and specific targeting and delivery, which is valuable for cancer therapy applications (Figure 1.5) [159,213,214]. Key properties include their optical properties associated to the localized surface plasmon resonance (LSPR), optoelectronic characteristics related to size and shape, and a high surface-to-volume ratio [159,215]. However, challenges arise in controlling these properties during large-scale production, as factors affecting synthesis and functionalization that are not fully understood. Surface Plasmon Resonance (SPR) is defined by matching the oscillation cycle (resonance) between the electrons on the surface of a conductive metal (plasmons) with photons irradiated by a light source with a specific wavelength [159]. SPR effect causes light to be absorbed or scattered, which is the fundamental principle used in color-based biosensors. AuNPs between 5 and 100 nm exhibit LSPR in the visible spectrum, while changes in size, shape, and surface can shift the LSPR to near-infrared (NIR) or UV regions [216]. For example, Au-nanorods and Au-nanoshells absorb NIR light, making them particularly useful for *in vivo* imaging (e.g., deeper tissue penetration) compared to spherical AuNPs. Due to their high density, AuNPs are also effective as contrast agents in CT SCAN, X-ray imaging, photoacoustic tomography, and fluorescence quenching, making them versatile for *in vivo* and *in vitro* assays [217–219].

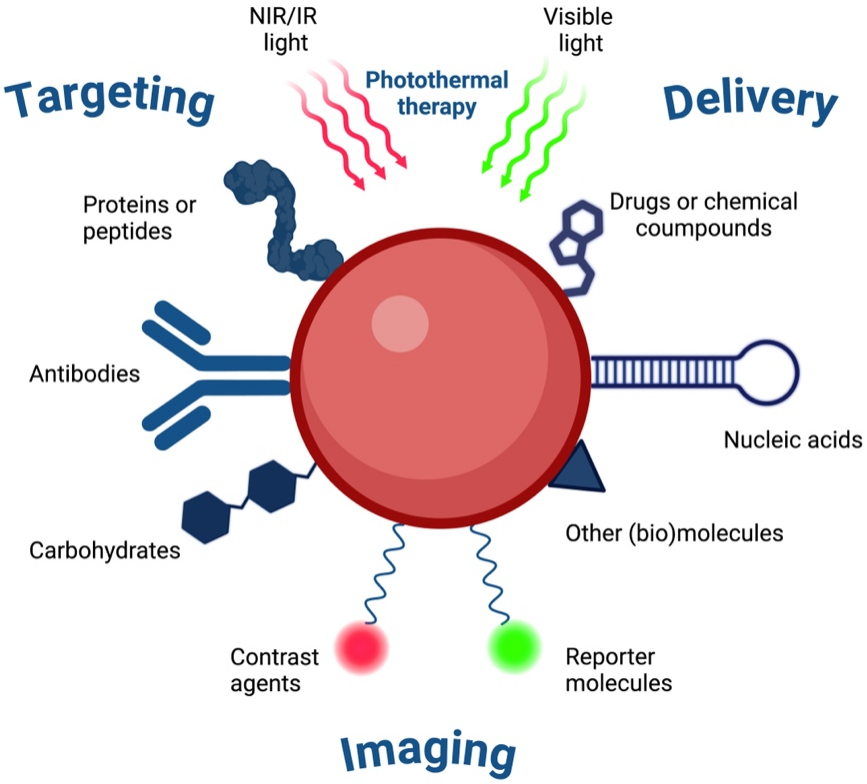

Figure 1.5 - Design of a multifunctional AuNP functionalized with different (bio)molecules for cancer therapy applications. (Created with BioRender.com)

1.8.1.1 Surface modification

The AuNPs are ideal scaffolds for functionalization with various molecules due to their high surface-to-volume ratio and surface chemistry. The colloidal solution of AuNPs can be stabilized using agents (e.g., sodium borohydride, sodium citrate, or ascorbic acid) that maintain repulsive forces, preventing agglomeration [220]. The most common method for AuNPs synthesis involves citrate reduction of a gold salt, where citrate simultaneously acts as a reducing and stabilizing agent, preventing aggregation through electrostatic repulsion in neutral pH solutions. However, changes in pH solutions can lead to aggregation and nonspecific molecule absorption (e.g., protein corona) [159]. The formation of a protein corona depends on the size, surface chemistry, and morphology of the Au-nanoconjugates. This interaction can influence cellular recognition, potentially affecting colloidal stability, cellular uptake, and immune response activation. Therefore, in addition to the therapeutic cargo and targeting moieties functionalization, it is often necessary to functionalize the AuNP with biocompatible and hydrophilic molecules to minimize or prevent the formation of protein corona [221].

Currently, the functionalization methods of AuNPs include either one or a combination of functional groups, such as surfactants and polymers, polypeptides, bovine serum albumin (BSA), amino acids, antibodies, oligonucleotides, receptors, among others [159].

Polyethylene glycol (PEG) functionalization is widely used to enhance the stability of AuNPs in complex media, improving biocompatibility and circulation time *in vivo* by preventing opsonization [222]. Heavier PEG chains offer more stability while reducing cellular absorption owing to negative immune responses and clearance by macrophages. Conversely, lighter PEG chains provide less stability while improving circulation time and responsiveness to media changes [223]. Other stabilizing agents have been explored such as polyethyleneimine (PEI), silica, BSA, and lipoic acid, though addressing more drawbacks such as rapid renal clearance, uncontrolled binding, and adverse immune responses. Therefore, considerations of long-term side effects and lack of specific biodistribution are required when selecting a stabilizing agent [159].

Surface functionalization strategies are divided into covalent methods (e.g., thiol-gold bonds) and non-covalent methods (e.g., electrostatic interactions and physisorption of ionized ligands). Thiol moieties have been reported as passivating agents that offer higher stability compared with others (e.g., acyl group and coupling molecules containing amine groups) [212]. Overall, surface modifications of AuNPs are designed to enhance stability and biocompatibility, strengthen interactions with biological molecules, and improve their ability to carry the cargo with specificity for the required target.

1.8.1.2 Targeting and delivery

Functionalization of AuNPs for (bio)molecular targeting often involves attaching antibodies, peptides, amino acids, oligonucleotides, proteins, or specific ligands to the nanoparticle surface. Au-nanoconjugates provide increased stability, sensitivity, and specificity for cell targeting, but the increase in their hydrodynamic size could reduce cellular uptake. In addition, the rapid diffusion rate and potential immunogenicity are some of the limitations concerning Au-nanoconjugates [224]. Optimal functionalization strategies should be tailored to the specific application since several types of functionalization agents show limitations, such as non-specific binding, instability, and toxicity [159].

Various strategies have been developed to functionalize spherical AuNPs for gene silencing applications. Owing to their surface properties and ease of functionalization, AuNPs used for gene silencing are typically conjugated with different molecules to enhance delivery and uptake by target cells, protect against enzymatic degradation, and avoid triggering an immune response that could eliminate these Au-nanoconjugates from the body. To increase stability, some of these molecules are attached to the nanoparticle surface either through covalent bonds, with thiol-gold bonding (S-Au) being the most common, or via electrostatic interactions [225]. Stabilization techniques include the use of nucleotide monolayers, which enhance the resistance of TNAs to nuclease degradation while reducing toxicity using synthetic polymer or other stabilizers. For example, cationic polymers such as PEI, are often employed for their improved stability in physiological environments and higher transfection efficiency [226,227]. Cationic lipids are another excellent example of a stabilizer agent owing to the formation of lipoplexes to enhance the stability of lipid-DNA complexes [228,229]. Among stabilizers, PEG

is widely used due to its ability to provide greater stability against enzymatic and non-enzymatic hydrolysis, reduced acute cytotoxicity, and improved circulation time [230,231].

Functionalization with polymeric stabilizers like PEG, PEI, and polyglycerol imparts a neutral surface charge, enhancing solubility, biocompatibility, and circulation time in biological systems. Moreover, negatively charged nucleic acids may bind to cationic AuNPs via ionic interactions, and the neutralization of their charge minimizes adsorption to plasma proteins such as opsonins, thus preventing Au-nanoconjugates clearance by phagocytosis [106,232]. AuNPs can also be functionalized with thiolated oligonucleotides, alkythiol-terminated oligonucleotides, amine-terminated siRNAs, or cysteamine-terminated miRNAs [171]. The strong affinity of AuNPs for binding oligonucleotides and other (bio)molecules containing thiol groups makes them ideal carriers for the delivery of silencing moieties, such as ASO and siRNA. These functionalized systems have been applied in a wide range of gene silencing applications and for tracking specific target genes in nanotheranostics. The delivery of TNAs mediated by AuNPs is significantly influenced by the assembly and design of the nucleic acids into functional Au-nanoconjugates. Among the various conjugation strategies, covalent attachment and supramolecular assembly of TNAs are preferred for gene silencing applications. This preference is due to the straightforward interaction between the sulfur in thiolated (modified) TNAs and the AuNP surface (S-Au bonding). Non-covalent conjugates are also attractive since supramolecular assembly allows the use of unmodified nucleic acids while maintaining efficacy in gene therapy applications [233–235]. Other methods for TNAs loading include amino acid-functionalized AuNPs (AA-AuNPs) [236], mixed-monolayer-protected AuNPs (MM-AuNPs) [237], layer-by-layer-fabricated AuNPs (LbL-AuNPs) [238], among others.

1.8.1.3 Therapeutic agents

AuNPs have been recognized as efficient and specific carriers for targeted delivery of RNAi and antisense molecules (e.g., siRNA and ASO), either alone or in combination with antibodies or drugs [239,240]. AuNPs have also gained attention as theranostic agents in cancer due to their unique physico-chemical characteristics and biocompatibility, such as their optical behavior from LSPR. For instance, spherical AuNPs are effective vectors for gene therapy due to their ease of synthesis and functionalization via thiol-based chemistry, biocompatibility, large specific surface area, high cellular uptake, rapid endosomal escape, and usually present low cytotoxicity [106,134,241]. An important advantage of Au-nanoconjugates is their ability to selectively deliver TNAs into cancer cells for gene silencing while protecting them from nucleases degradation (Figure 1.6) [106,242].

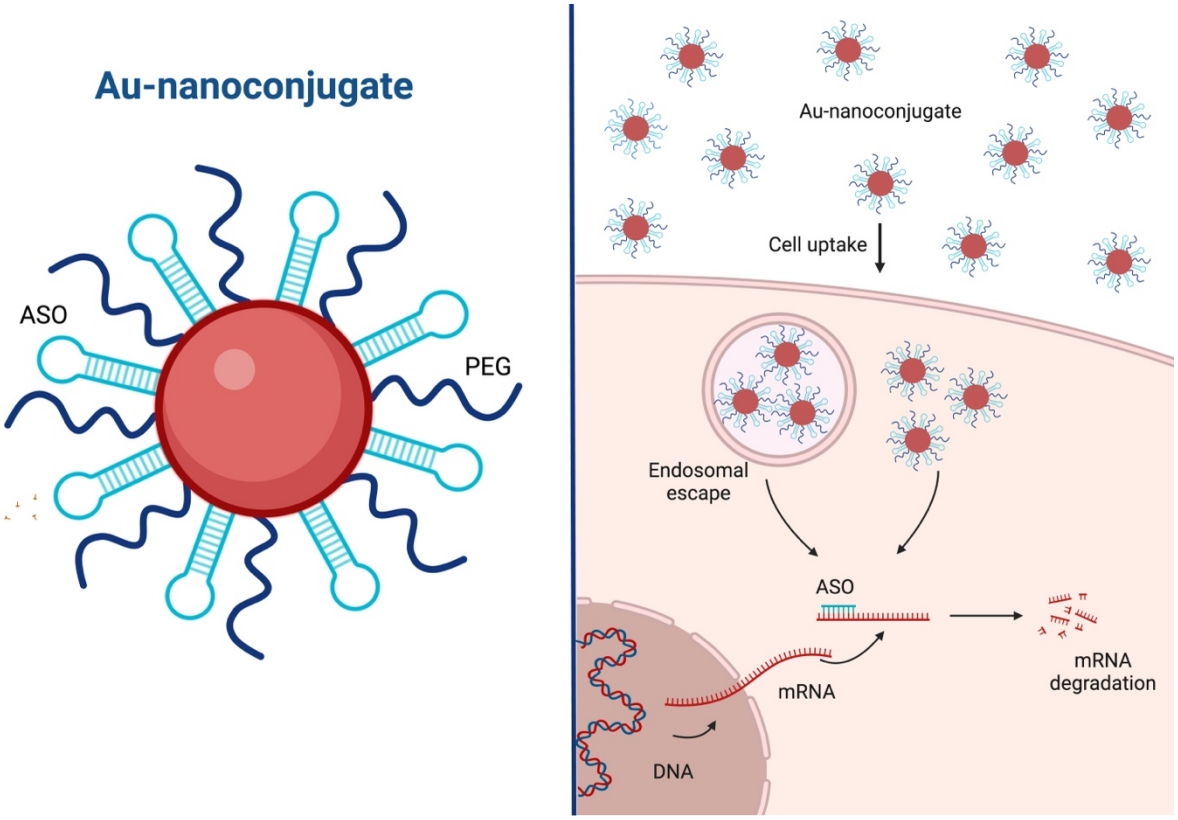

Figure 1.6 - Overview of the general concept for intracellular delivery of Au-nanoconjugates (AuNPs functionalized with PEG and silencing moieties – ASO) for effective gene silencing in cancer cells. (Created with BioRender.com)

The properties of these nanoparticles, such as surface charge and polarity, facilitate cellular uptake through active transport, primarily via endocytosis. This can occur through various pathways, including clathrin-mediated, caveolae-mediated, or clathrin- and caveolae-independent endocytosis [243]. Endosomal escape is a significant challenge in nanoparticle-based gene delivery, as it directly impacts transfection efficiency. Several mechanisms for AuNPs to escape the endosome have been described, either before or after releasing their

cargo, and vary depending on the nanoparticle type and surface functionalization. However, in most cases, this escape is considered to occur through the "proton sponge" effect [233,244]. Controlled and stimuli-responsive release of TNAs can be achieved through various mechanisms and processes. Many strategies depend on ECM conditions, such as temperature, pH, enzymatic activity, or ionic strength, as well as intracellular processes, such as the reduction of thiol bonds by glutathione (GSH). GSH-based release strategy depends on the Au-nanoconjugate design (e.g., different densities of PEG) and intracellular GSH levels [245]. External stimuli, such as light irradiation or ultrasound, can be used for spatiotemporal control of TNAs release. The release of TNAs can be triggered by applying high-intensity laser pulses, while mild photothermy increases cell membrane fluidity, promoting cellular uptake and endosomal escape of Au-nanoconjugates. Synergistic strategies have been developed to enhance the effectiveness of cancer therapies. Nevertheless, these promising approaches still require extensive long-term toxicological studies to evaluate their safety and impact on biological systems [1].

The use of spherical AuNPs for the delivery of TNAs into cancer cells has been reported in the literature, not only for targeting or destroying malignant cells but also for modulating the TME [9,240]. Previous studies *in vitro* and *in vivo* of our group highlight the powerful capacity of delivery of silencing moieties using AuNPs. For instance, Conde *et al.* employed an antisense Au-nanobeacon for gene silencing, which demonstrated the efficiency and non-toxicity of the silencer in the HCT116, a CRC cell line transiently transfected with an enhanced green fluorescent protein (EGFP) plasmid [239]. Another study reported engineered Au-nanoconjugates to deliver siRNA specifically to malignant cells using a mouse lung cancer model, which results demonstrate the efficiency of this approach on the downregulation of the *c-MYC* gene [246]. Vinhas *et al.* described effective gene silencing using ASO targeting the *BCR-ABL1* gene vectorized by AuNP in the K562 chronic myeloid leukemia cell line [247]. The most common types of AuNP used for TNAs vectorization for cancer therapy applications are described in Table 1.1.

Table 1.1 - The most common types of AuNPs used in cancer therapy (Adapted from Ferreira *et al.*, 2020[1]).

AuNPs	Characteristics	Advantages	Limitations	Applications	TNAs	*In vivo* distribution
Au-nanorods	Elongated nanoparticle, showing longitudinal plasmon wavelength with nearly linear dependence on their aspect ratio.	Tunable properties, including SPR.	Low drug loading capacity. Poor control over size distribution.	Tunable optical resonance in the NIR for *in vivo* applications, such as imaging and photothermy.	siRNA DNA aptamers ASO RNA decoys	Accumulation in the liver, long circulation time, and high accumulation in the tumors.
Au-nanocubes	Hollow with ultrathin and porous walls. Easy to synthesize (scale up).	Tunable sizes and scalability.	Few data about toxicity, biodistribution, and physiological response.	Theranostics (SPR can be tuned between 600-1200 nm). Hollow interiors allow encapsulation. Porous walls for ease drug release.	siRNA miRNA	Medium level accumulation in the liver, kidneys and spleen. Rapidly excreted.
Au-nanoshells	Spherical with a dielectric core covered by a thin gold shell.	Improve *in vivo* bioavailability and controlled drug release.	Lack of targeting efficacy. Limited tracking/monitoring *in vivo*.	Controlled/triggered drug delivery via irradiation (NIR).	siRNA ASO	Short circulation times, accumulation in liver and spleen. No induction of tissue damage (necrosis, inflammatory infiltrate or fibrosis) liver, spleen, kidney or bone marrow.
Au-nanospheres	Spherical solid.	Ease of functionalization. Enhanced cellular uptake.	Prone to aggregation. Multitude of possible cell uptake routes render difficult to control.	Extremely versatile for photothermy, and combined therapy.	ASO siRNA miRNA	Short circulation time and accumulation in the liver with low accumulation in the tumors.

1.8.2 Magnetic Nanoparticles (MNPs)

The synthesis of MNPs involves various techniques tailored to control their size, shape, morphology, stability, and magnetic properties for specific applications. The past decade has witnessed extensive research in the development of different approaches for the synthesis of MNPs [248,249]. Currently, the most used are chemical methods: co-precipitation, thermal decomposition, micro-emulsion, hydrothermal, and sol-gel synthesis [248]. Eco-friendly alternatives are provided by biological methods, including biomimetic synthesis using microorganisms or plant extracts [250], while physical methods (e.g., ball milling method) often require specialized equipment and a controlled environment for precise control over the size and shape of MNPs [251].

MNPs are nanomaterials typically ranging from 1 to 100 nm and exhibit unique magnetic features that set them apart from their bulk counterparts [252]. Physical characteristics, such as the size and shape of MNPs, have a direct impact on nanoparticle's behavior and functionality, which might influence their magnetic response, biocompatibility, and cellular uptake [252]. MNPs belong to a distinct category of nanoparticles characterized by their ability to interact with external magnetic fields due to their superparamagnetic, ferrimagnetic, or ferromagnetic properties. Due to their advantageous properties, MNPs have been employed as contrast agents for magnetic resonance imaging (MRI) [253] and used as "nanoheaters" for magnetic fluid hyperthermia [254], and as nanocarriers for controlled drug delivery [255], and magnetofection [256,257]. Furthermore, MNPs can be specifically designed for a therapeutic application, such as hyperthermia combined with drug delivery [258,259], or to combine therapeutics with diagnostics, known as theranostics [260–262] (Figure 1.7). Current studies focus on innovative methods using MNPs have been reported in biomedical applications, including in the field of advancing tissue repair and regeneration [263,264].

MNPs (especially iron oxide nanoparticles) have gained attention for biomedical applications upon their approval by the US Food and Drug Administration [265]. Generally, MNPs comprise materials such as iron oxide, magnetite, and maghemite and can include other materials (e.g., cobalt, nickel, or alloys). These compositions are usually coated with silica, surfactants, or biocompatible materials (e.g., polymers) which provide functionality, stability, and biocompatibility [266]. Their surface properties are highly dependent on the surface area, which influences the surface charge, interactions, oxidation state, and heating efficiency of MNPs [266,267]. The physical properties of nanoparticles, including their size, shape, coating, and chemical compositions, are important to address safety and biocompatibility. Moreover, the understanding of the reactivity and interactions between nanoparticles or with biological barriers (e.g., cell membranes) are of critical importance in biomedical applications [252,268].

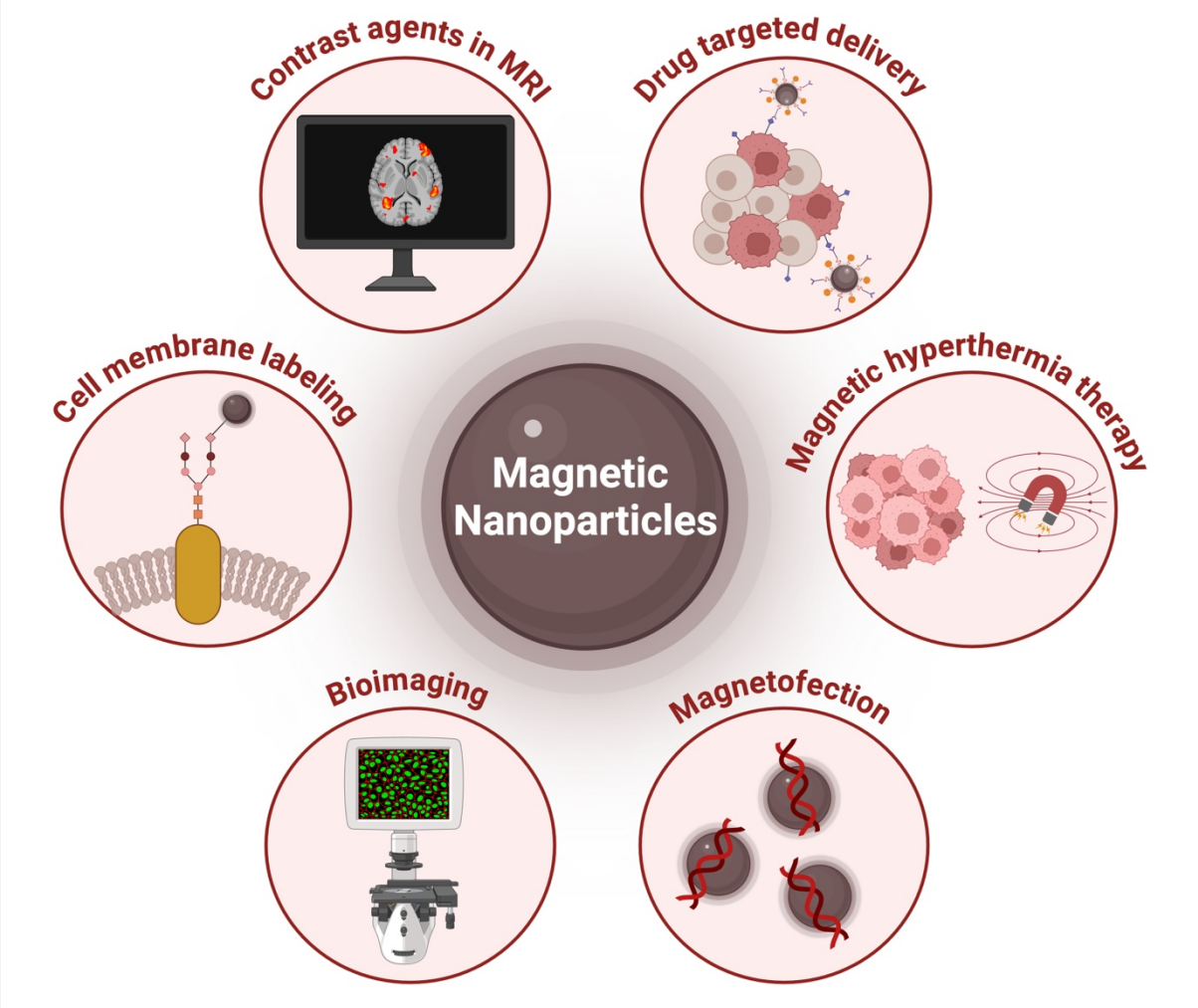

Figure 1.7 - Various biomedical applications using MNP for cancer therapy. (Created with BioRender.com)

1.8.2.1 Surface modification

Coating of MNPs is a crucial step to improve their functionality, stability, and biocompatibility for biomedical applications. MNPs can be stabilized during the synthesis process with surfactants or polymers or after the synthesis process with materials such as monolayer ligands, polymer mixtures, (bio)molecules, and inorganic compounds [269]. The post-synthesis procedure provides a broader range of options for the functionalization of MNPs, which requires the binding of biomolecules to the nanoparticle surface (e.g., peptides, antibodies, nucleic acids, among others) for cancer therapy [252]. MNPs can be coated with a variety of different molecules, including polymeric coating and silica-based coating. Natural (e.g., gelatin, dextran, and hyaluronic acid [270]) and synthetic polymers (e.g., Poly(maleic anhydride-alt-1-octadecene), poly(vinyl alcohol), and poly(lactic acid) [192,271]) are frequently utilized for MNPs coating, where the latter are the most used due to their capacity to prevent nanoparticle aggregation while improving their biocompatibility in a biological environment.

MNPs can be functionalized with specific biomolecules (e.g., peptides, antibodies, aptamers, carbohydrates, among others) to enhance their ability to penetrate biological barriers

[170] and specifically target cell surface receptors by active targeting [272,273], while passive targeting involves the accumulation of nanoparticles in solid tumors via the EPR effect [201]. The employment of multifunctionalized magnetic nanoconjugates with high-density display of (bio)molecules in nanoparticles' surface for targeted application can be particularly advantageous in the biomedical field [274,275]. MNPs, more specifically iron oxide nanoparticles, are known to be efficient nanocarriers for gene silencing applications. The internalization of iron oxide nanoparticles into cells is mainly through endocytosis and is highly dependent on their coating [276] and size [277,278]. These types of MNPs can be prepared in smaller sizes using chemical methods with their surface modified with a wide range of polymers, that are covalently or non-covalently attached to silencing moieties to protect them from degradation [279–281]. MNPs are frequently coated with surface polymer layers to improve the intracellular delivery of TNAs. PEG [282], PEI [283,284] and chitosan [285,286] are examples of polymers that have been applied as stabilizers through the improvement of electrostatic repulsion between iron oxide nanoparticles in the colloidal solution [287,288]. For instance, PEI can be used to coat iron oxide nanoparticles, conferring a positive surface charge that facilitates electrostatic interaction with TNAs [289,290]. Still, surface modification strategies to enhance the efficacy of gene delivery (e.g., cation density, high molecular weight, and ratio of polymer to nucleic acid) often increase the toxicity of the nanocarrier and off-target gene silencing effect [288,291,292].

1.8.2.2 Targeting and delivery

The functionalization of MNPs has been widely explored in the past years for effective targeting and delivery of (bio)molecules, including proteins, antibodies, drugs, TNAs, ligands, and compounds. Due to their unique physicochemical properties, MNPs have gained significant attention for the development of innovative therapeutic and diagnostic applications based on cell surface engineering, such as metabolic glycoengineering and SPAAC reaction [193]. The combination of SPAAC chemistry and metabolic glycoengineering has introduced a novel strategy for active cell targeting with nanoparticles, which might overcome the challenges of receptors heterogeneity between different cell types or their limited density in conventional approaches [293]. The metabolic machinery of the cells can be used to incorporate *ad hoc* azide bioorthogonal reporters on the cell membrane glycocalyx. Nanoparticles functionalized with complementary strained alkyne probes (e.g., cyclooctyne) have been reported to react with these artificial chemical receptors present on cell membranes [199,294,295]. Bioorthogonal click chemistry has been reported as a potential strategy to bind nanoparticles to cell surfaces, although their successful applicability depends on the click reactivity of the partners and on a variety of other factors that usually control the interaction of nanoparticles with cell surfaces [170,193].

The physicochemical properties of the nanoparticles (e.g., size, shape, and surface charge) have a significant impact on their interaction with cells [296]. The functionalization of nanoparticles with multiple targeting ligands depends on their size and is essential to promote a multivalent binding to cell surface receptors, which might command the uptake and subcellular localization of the nanoparticles [297]. In addition, the unspecific adsorption of

biomolecules (mostly proteins) in the nanoparticles' surface is triggered by their exposition to biological environments. The formation of protein corona may adversely affect the bioorthogonal reactivity of nanoparticles owing to steric hindrance [298]. Overall, the appropriate surface engineering of the nanoparticles depends on all these factors to ensure high performance in terms of bioorthogonal reactivity for biomedical applications, and it would be desirable to assess the reactivity in different media that could resemble the cellular environment [170,192,193]. A recent work conducted by Idiago-López *et al.* reported the use of SPAAC reaction for the covalent attachment of MNPs functionalized with a cyclooctyne (CO) derivative or a dibenzocyclooctyne (DBCO) derivative on living cell membranes engineering to express azide artificial reporters, by incubating the cancer cell lines with tetraacetylated *N*-azidoacetylmannosamine (Ac_4ManNAz) – Figure 1.8 [193]. This study offers valuable insights into the suitable surface engineering of MNPs to ensure high bioorthogonal click chemistry for gene silencing applications, including for intracellular delivery of TNAs mediated by transient changes in cell membranes through localized magnetic hyperthermia.

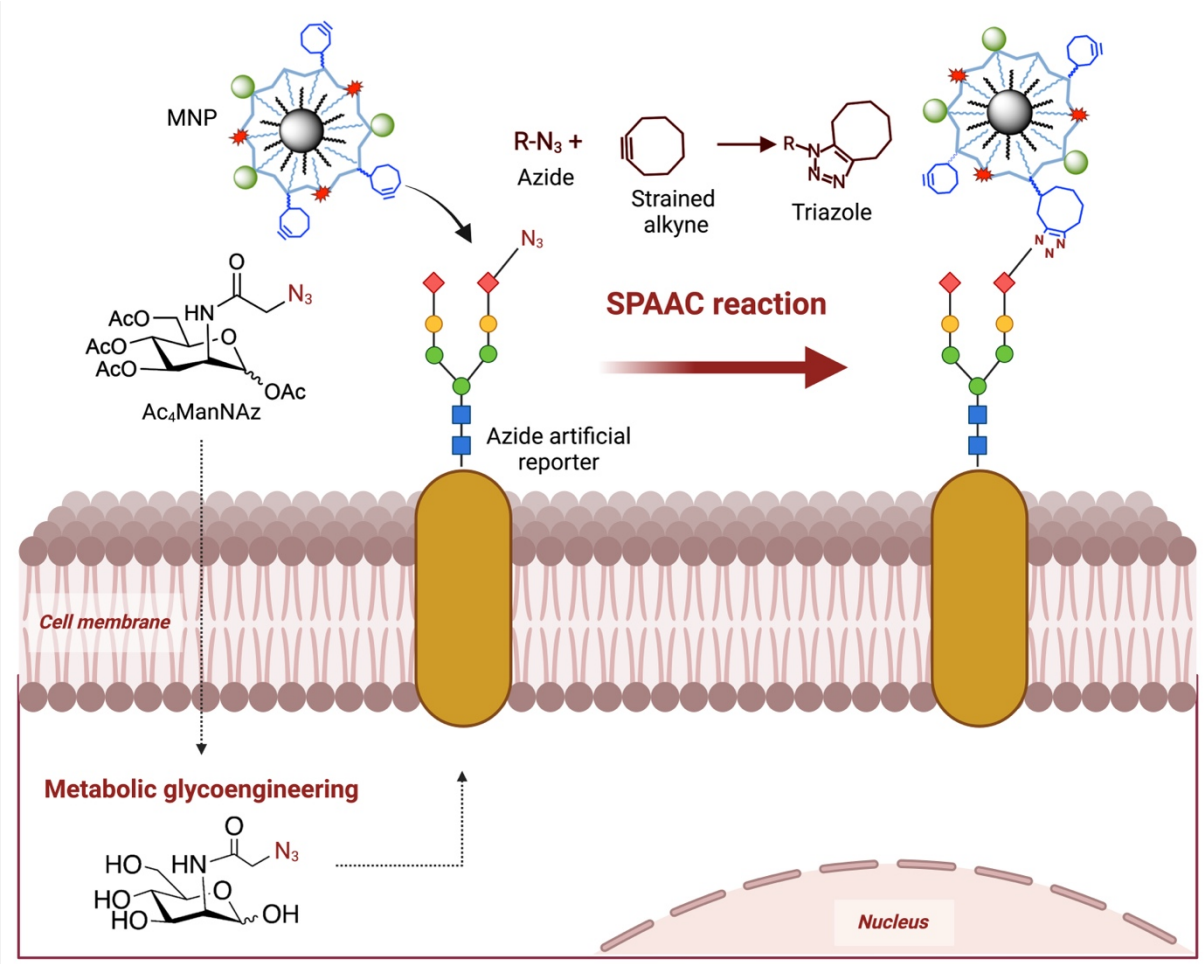

Figure 1.8 - General concept of SPAAC bioorthogonal chemistry using MNPs described by Idiago-López *et al.*, 2022 [193]. These MNPs were functionalized with strained alkynes and immobilized on the cell membrane previously subjected to metabolic glycoengineering to express unnatural azide reporters. (Created with BioRender.com)

1.8.2.3 Therapeutic agents

Iron oxide nanoparticles exhibit superparamagnetism in response to an external magnetic field, which enables the targeted image-guided delivery of TNAs, also known as magnetofection [279]. Magnetofection is an advanced technique that enhances conventional transfection methods by incorporating MNPs to deliver (therapeutic) nucleic acids (e.g., siRNA, ASO, or DNA/RNA) into target cells. Regarding the magnetic properties of these nanoparticles, this approach aims to improve the precision and efficiency of gene transfection. In fact, magnetofection has been applied to transport (therapeutic) nucleic acids into cells for gene delivery [299]. MNPs attached to nucleic acid molecules can be introduced into the body and guided to the target site (e.g., cells or tissues) by using an external magnetic field [300]. This method offers a valuable tool for gene therapy due to the enhancement of the efficiency of gene transfection. Nucleic acid molecules can be linked to the surface of MNPs either indirectly through chemical linkers [301] or directly via electrostatic interactions, particularly using PEI coatings [302,303]. For instance, superparamagnetic nanoparticles coated with PEI have been shown to transfect DNA *in vitro* and *in vivo* using an external magnetic field [304]. The ability of magnetofection to introduce siRNA into HeLa cells was described later by Schillinger *et al*. [256]. Boyer *et al.* showed the efficiency of transfection of siRNA in human neuroblastoma SHEP cells using iron oxide nanoparticles modified with two different polymers in either the presence or absence of a magnetic field [305,306]. A study based on iron oxide nanoparticles coated with PEI and loaded with gene vectors presented high transfection efficiency and antitumor effect in oral squamous cell [307]. PEI functionalized-MNPs loaded with siRNA were used for intracellular gene silencing and imaging to improve the therapeutic efficiency through apoptosis and autophagy in glioblastoma cells [308]. Cruz-Acuña *et al.* demonstrated the use of PEI-functionalized iron oxide nanoparticles loaded with RNA sequences for RNA delivery leads to an efficient protein knockdown in breast cancer [309].

Magnetofection offers significant advantages (e.g., targeting and reduced cytotoxicity) over traditional transfection methods, such as cationic lipids [310–312]. Recently, Chung *et al.* revealed that using iron oxide nanoparticles functionalized with peptides (NP-CTX-R10) to deliver siRNA to silence O6-methylguanine-DNA methyltransferase, efficiently improves the exposition of tumor cells to temozolomide, an alkylating drug [313]. Another study demonstrated that MNPs loaded with siRNA were able to effectively knockdown the expression of *GAPDH* in human endothelial cells and *NOTCH3* in human vascular smooth muscle cells, which siRNA and CD31 conjugated with MNP precisely targeted and delivered siRNA into endothelial cells in a co-culture system under shear stress to simulate blood flow [314].

1.9 Hyperthermia

The use of heat for therapeutic purposes has increased since Dr. William Cooley first noted in the 1890s that fever caused by a bacterial infection in cancer patients is associated

with a strong antitumor effect [315,316]. Heat shock responses triggered by hyperthermia may potentiate cancer cells death compared to normal cells [317]. Hyperthermia has been classified into three categories based on temperature ranges: thermal ablation (≥ 45ºC), mild hyperthermia (40-42ºC), or moderate hyperthermia (42-45ºC) [318,319].

Heat is often employed to destroy cancer cells through a process known as thermal ablation. Thermal ablation involves the exposition of tissues to high temperatures (≥ 45°C), which causes irreversible damage to proteins and other molecules and induces necrotic cell death. Protein denaturation and aggregation, DNA damage, and lipid membrane disruption, followed by cell cycle arrest, mitochondrial damage, oxidative stress, and apoptosis, are the main processes that cause cell death induced by hyperthermia above 43ºC [319,320]. On the other hand, hyperthermia < 43ºC does not directly kill cancer cells and may reduce damage to surrounding healthy tissues while increasing cell membrane permeability and cell uptake [315,321]. Mild to moderate hyperthermia causes reversible alterations in tissue physiology, which depends on the thermal dose of the treatment. These alterations include reoxygenation and increased blood flow, immune activation, changes in protein structures, altered metabolic pathways, and inhibited DNA repair [317,322–325]. Hyperthermia acts as a chemosensitizer (e.g., improved drug accumulation and toxicity) [326,327] and as a catalyst for antitumor immunotherapies [328] and enhanced tumor oxygenation, which improves radiotherapy through reactive oxygen species (ROS) production [329]. Hyperthermia is classified based on the application area into local (applicators for treatment of superficial or localized small tumors within a body cavity), regional (collected heated patient's blood to increase the temperature of a body part), and whole-body treatment (temperature raises to 43ºC by thermal baths) [318,330]. Even though several studies have evidenced the potential of hyperthermia treatment in cancer therapy, it is required to address challenges such as off-target toxicity, heterogeneous tumor heating, and limited overall efficiency [324].

Recent efforts have been focused on hyperthermia as a solution to enhance cancer treatments, driven by the development of nanoparticles that passively accumulate at the tumor site and can generate heat in response to external stimuli (e.g., light or magnetic field) [319,331–333]. The design of functional metallic nanoparticles, such as AuNPs and MNPs, has been spurred by the need for more precise and efficient cancer therapeutics with fewer negative side effects while minimizing exposure in surrounding healthy cells. The combination of AuNPs or MNPs with hyperthermia is being widely studied as an adjuvant therapy for cancer treatment (e.g., combined with chemotherapy) [319,320]. Photothermal therapy (PTT) and magnetic hyperthermia are two nanoparticle-mediated hyperthermia treatments, shown as selective and noninvasive approaches for cancer therapy [319]. Advancements in nanomedicine have enabled the development of a wide range of nanoparticles with heating capacities for PTT and magnetic hyperthermia, with AuNPs and iron oxide nanoparticles playing a lead role for heat generation upon light irradiation and magnetic field modulation, respectively [334,335]. The unique optical features of AuNPs to convert light to heat are applied in PTT, whereas in magnetic hyperthermia application, the MNPs generate heat in response to an external alternating magnetic field (AMF) [319,332]. Still, only three hyperthermia-based nanoparticles have advanced

to the clinical trial phase: Magnablate® and Nanotherm® for magnetic hyperthermia and AuroShell® (gold-based formulation from AuroLase®) for laser-induced hyperthermia [319].

Nanoparticles-mediated hyperthermia for delivery of TNAs is an emerging area of interest due to its potential to enhance cellular uptake and mediate their therapeutic efficiency. It is expected that the silencing moiety can be released or triggered only in the desired location using specific stimuli [1,320]. Here, I shall briefly introduce PTT and magnetic hyperthermia as powerful tools for mild hyperthermia-based gene silencing in cancer therapy (Figure 1.9).

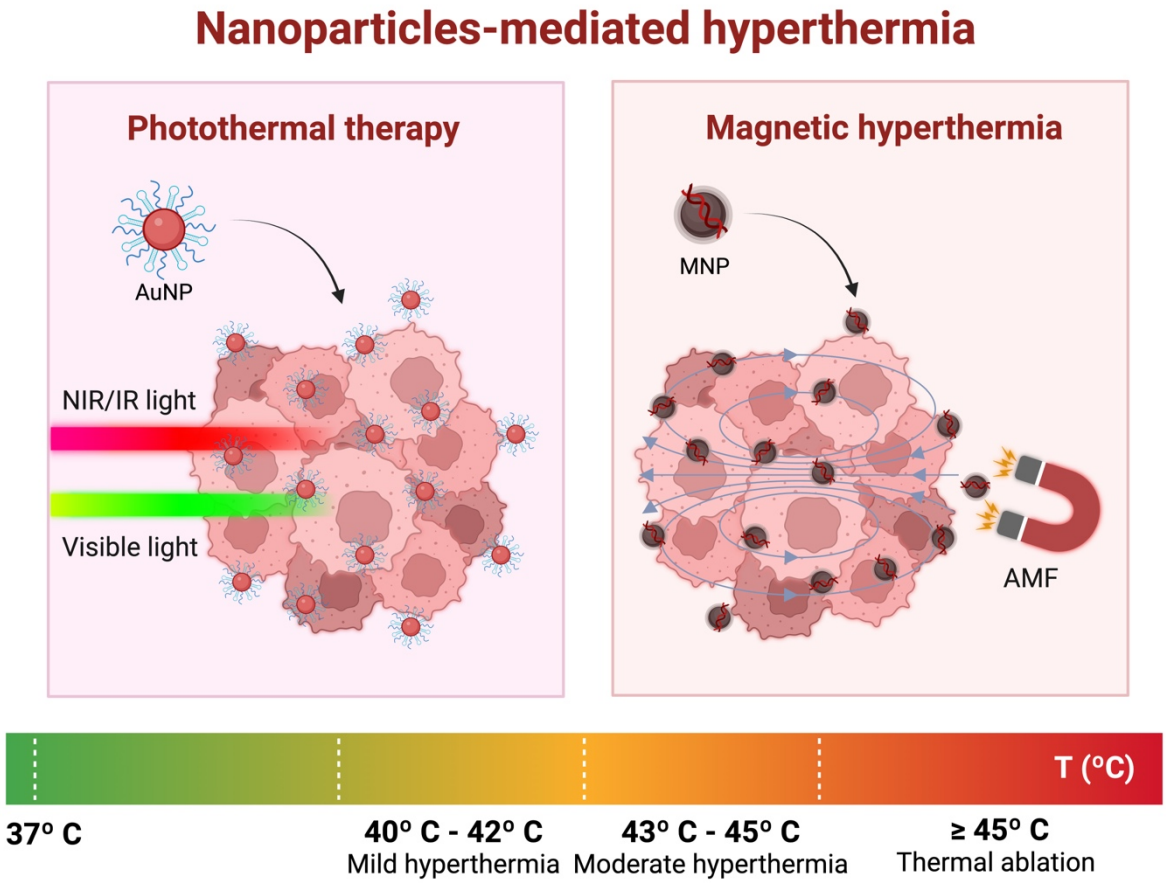

Figure 1.9 - Overview of nanoparticles-mediated approaches for hyperthermia application to promote the intracellular delivery of silencing moieties in cancer cells. (Created with BioRender.com)

1.9.1 Photothermal therapy

PTT and photodynamic therapy (PDT) are based on the use of photosensitized materials combined with light radiation to target tumor cells, improving therapeutic outcomes in cancer research [336]. The photothermal and photodynamic agents, upon reaching the tumor site and irradiated, can convert light energy into heat (PTT) or chemical energy (PDT) to effectively destroy malignant cells. For instance, PTT enables precise control of temperature-induced cell death by modulating light intensity [337] while PDT induces ROS [338], which subsequently triggers the release of inflammatory mediators and activates an immune response

[339,340]. Metallic nanoparticles (e.g. AuNPs), carbon-based nanoparticles (e.g., carbon nanotubes), hybrid nanoparticles, silica nanoparticles, polymeric nanoparticles, semiconducting nanocrystals, and rare earth ion-doped nanocrystals have been used in PTT [341]. Several *in vitro* and *in vivo* studies have been focused on the targeting ability, photothermal conversional efficiency, concentration, and physicochemical properties of nanoparticles in the optimization of light exposure parameters (e.g., exposure time, power density, and light wavelength) [319,321]. AuNPs have gained significant attention in the medical field due to their unique physicochemical characteristics. Their tunable optical properties (e.g., LSPR) in the visible and NIR regions make them valuable tools for a wide range of applications, such as *in vitro* diagnostics, *in vivo* imaging, and therapeutics [342]. AuNPs have been explored in PTT as strong visible and NIR light-absorption agents and can generate intense thermal energy upon light exposure which enables cancer treatments based on hyperthermia [343–345]. AuNPs use lower laser energy doses to achieve a therapeutic effect which facilitate targeted heating in specific areas while minimizing damage to surrounding tissues [346,347]. Still, using laser sources with emission wavelengths that overlap with the SPR peak of AuNPs is expected to enhance light-to-heat conversion. Au-nanorods and Au-nanoshells have been widely reported in PTT since their LSPR are in the NIR and IR region, owing to the negligible absorption of physiological fluids and tissues which allow for deeper light penetration into tissues [241,348].

Compared to Au-nanorods and Au-nanoshells, spherical AuNPs offer unique features that could be advantageous for PTT research. Au-nanospheres mediated-PTT offer simpler synthesis processes, easy bioconjugation, and the ability to improve specificity, enhanced biocompatibility, cellular uptake, and show lower cytotoxicity compared to cetyltrimethylammonium bromide surfactant, typically used to stabilize Au-nanorods [345]. However, spherical AuNPs do not have broad tunable light absorption peak in NIR region since their absorption peak is in the visible region (around 500-600 nm). An early study conducted by El-Sayed *et al.* demonstrated the effectiveness of Au-nanospheres with an LSPR around 530 nm as photothermal agents when irradiated oral squamous carcinoma cell lines, using a continuous wave (CW) visible argon ion laser at 514 nm [349]. Enhanced gene delivery has also been demonstrated using AuNPs functionalized with oligonucleotides. When exposed to an intense laser pulse, the bonds between the oligonucleotides and nanoparticles are disrupted, triggering cytoplasmic release of the oligonucleotides [350]. Table 1.2 shows some examples of PTT combined with AuNPs for gene silencing in cancer therapy.

Table 1.2 - Examples of PTT combined with AuNPs for gene silencing in cancer cells.

AuNPs type	TNAs	Laser settings	Description	Ref
Au-nanorods	siRNA	CW 808 nm, 0.5 W for 5 or 7 minutes	Two different studies denoted the combination of *PKM2* gene silencing and PTT for the effective inhibition of cell proliferation in breast cancer cell lines.	351,352
Au-nanorods	siRNA	CW 810 nm, 3.3 W/cm² for 3 minutes	Au-nanoconjugates demonstrated the ability to deliver siRNA against *BAG3* gene and improve PPT efficiency in an oral squamous cell carcinoma cell line and *in vivo* tumor xenograft.	353
Au-nanoprisms	siRNA	CW 633 nm, 0.8 W/cm² for 3 minutes	The Au-nanoconjugates functioned as nanocarriers for siRNA delivery to downregulate *PD-L1* expression and as photothermal agents for PTT in lung cancer cells line and lung cancer cells-derived tumors.	354
Au-nanostars	siRNA	CW 808 nm, 1.2 W/cm² for 300 seconds	Effective delivery siRNA targeting *VEGF* into glioblastoma cell line with PTT improved cells death and showed the potential of Au-nanoconjugates for tumor CT imaging and thermal imaging *in vivo* xenografted tumor model.	355
Au-nanoflowers	DNA	CW 808 nm, 1 W/cm², for various time exposures	Controlled gene silencing of *c-MYC* in MCF-7 breast cancer cell line using Au-nanoflowers (self-assembly of ultrasmall AuNP with triplex-forming oligonucleotide sequence and its complementary strand) combined with NIR irradiation.	356
Au-nanocages	miRNA	CW 808 nm, 1.25 W/cm², for 10 minutes	Hepatocellular carcinoma cell models experiment showed the efficacy of Au-nanoconjugates for the delivery of *anti-miR-181b* to suppress tumor growth and decrease tumor volumes *in vivo* under NIR irradiation.	357
Au-nanoshells	ASO siRNA	CW 800 nm, 2.5 W/cm², for 2 minutes	Light-triggered delivery of Au-nanoconjugates functionalized with ASO or siRNA resulted in an effective downregulation of targeted *GFP* expression in human lung cancer cell line with lower cytotoxicity.	358
Au-nanorods	siRNA	CW 808 nm, 2 W/cm², for 5 minutes	The gene silencing efficiency of Au-nanoconjugates downregulates the gene expression of *HSPA1A*, leading to a reduced protein expression of HSP70 for improved cell uptake and PTT in murine colorectal carcinoma cells line.	359
Au-nanospheres	siRNA	CW 655 nm, 50 W for different time exposures	The *in vitro* and *in vivo* studies described the potential of RNAi-AuNP nanoconstructs for *VEGF* gene silencing, then combined with PTT demonstrated tumor growth inhibition and tumor ablation in PC-3 tumor bearing mice model.	360
Au-nanorods	siRNA	CW 808 nm, 2 or 1 W/cm² for 5 minutes	A multifunctional Au-nanoconjugate can enhanced antitumor immunity owing to the effective *IDO* gene silencing and the synergistic anti-neoplastic effects via PTT using *in vitro* and *in vivo* Lewis lung carcinoma cell models.	29
Au-nanospheres	siRNA	Pulsed 532 nm, 850 picoseconds at a repetition rate of 20.25 kHz.	Gene knockdown of *EGFP* upon an efficient transfection of a fluorescent labeled siRNA by AuNP mediated (GNOME) laser transfection with high cell viability in canine pleomorphic adenoma cells stably transfected with pd2-EGFP-N1.	361

1.9.2 Magnetic hyperthermia

One major advantage of MNPs is their high surface area-to-volume ratio, which allows for a variety of functionalization and modifications for biomedical applications. This feature enables the development of MNPs with unique magnetic properties and biocompatibility [252], that are appropriate for a wide range of applications for cancer therapy in an *in vivo* scenario (e.g., MRI, targeted drug administration [203,362,363], and magnetic hyperthermia [364]). The versatility of MNPs stems from their capacity to respond to external magnetic fields, which enables precise control for manipulation within biological systems. The magnetic properties of MNPs are particularly advantageous for targeted therapies due to the possibility of delivering therapeutic agents (e.g., TNAs) directly to specific sites while reducing the side effects [365].

MNPs have also been used as nanocarriers, where the use of an external magnetic field might result in their accumulation in a particular site in the organism. Furthermore, MNPs may act as "heat-converters" owing to the generated heat via magnetic energy loss upon exposure to an external magnetic field, assisting strategies relying on mild hyperthermia (40–42ºC), mainly used for enhanced cell membrane permeability and fluidity, or more severe hyperthermia (> 43ºC), which could destroy cancer cells. Magnetic hyperthermia has been shown to improve the delivery of (bio)molecules through the cell compartments, which might be possibly due to the creation of "hotspots" in the cell membrane [366–369]. This approach has been applied for cancer therapy since the 1950s and offers precise targeting while reducing damage to healthy cells for drug delivery compared to chemotherapy [370–372].

The control of gene expression in tumors in a spatiotemporal manner presents a promising strategy for gene therapy. Magnetic hyperthermia is a minimally invasive technique based on the use of AMF that allows for deep penetration into tissues and can regulate gene expression [373]. The specific absorption rate values of MNPs are measured to evaluate the rate at which energy is absorbed when tissues or cells are exposed to a radio frequency electromagnetic field [374]. For instance, the application of AMF to improve transfection efficiency can be applied in polymeric MNPs-nucleic acid complexes *in vitro* and for the targeted delivery of TNAs *in vivo* studies. Once MNPs reach the tumor site, TNAs are released by either pH-dependent reactions, enzymatic cleavage of the crosslinking polymers, or polymer matrix relapse. At the same time, the overexpression of heat shock proteins (HSPs) can be induced due to the slight increase in temperature [375–377]. Therefore, magnetic hyperthermia can induce gene expression of therapeutic genes, such as tumor necrosis factor alpha (TNF-α), based on the use of expression vectors with heat-responsive promoters (e.g., HSPs promoter), which either directly destroy tumor cells or work synergistically to enhance the antitumor effects of hyperthermia [378–381]. Table 1.3 shows some examples of magnetic hyperthermia combined with MNPs for gene silencing in cancer therapy.

Table 1.3 - Examples of magnetic hyperthermia combined with MNPs for gene silencing in cancer cells.

MNPs type	TNAs	AMF settings	Description	Ref
Iron oxide nanoparticles	shRNA	AMF 3 kW, for 30 minutes	Development of multifunctional MNPs for effective gene silencing of *MUC1* and for magnetic hyperthermia effect using AMF showed high therapeutical potential *in vitro* and *in vivo* TNBC cell models.	382
Iron oxide-nanocages	siRNA	AMF 335 kHz, for 5 minutes	Iron oxide-nanocages loaded with siRNA silence luciferase when an AMF is applied and can enhanced the delivery of siRNA of the nanoparticles undergo Brownian motion in luciferase expressing reporter B16-F10 melanoma cells.	383
Iron oxide-nanocages	siRNA	AMF 445 kHz, for 5 minutes	The release and delivery of siRNA against *mGLuR5* gene was enhanced by an AMF applied in the iron oxide-nanoconjugates with a effectively gene silencing in osteosarcoma cell lines.	384
Zinc-doped iron oxide nanooctahedral	siRNA	AMF 250 kHz, for 5 minutes	Efficient gene silencing of *HSP70* and *HSP90* due to the cellular uptake and the tumor specific accumulation of the nanoconjugates by magnetic hyperthermia in breast cancer cell line and 4T1 subcutaneous tumor model.	385
Graphite coated iron cobalt nanoparticles	siRNA	AMF 334 kHz, for 5 minutes	The combination of *EGFRvIII* gene silencing with magnetic hyperthermia using multifunctional MNPs inhibited cell proliferation and induced cell death in U87–EGFRvIII glioblastoma cell line.	386
Bacterial magnetosomes	shRNA	AMF 54 kHz, for 30 minutes	The nanosystem co-delivers with efficiency doxorubicin and a recombinant plasmid HSP70 with a shRNA against *Plk1* gene under a AMF in osteosarcoma cell line.	387
Polycation-based magnetic nanoclusters	shRNA	AMF 357 kHz, for 10 minutes	These nanoplatform demonstrated anticancer effect by combination therapy of immune checkpoint *PD-L1* gene silencing with magnetic hyperthermia using *in vitro* and *in vivo* mouse melanoma models	388

1.10 Scope of thesis

Gene therapy relies on the precise transfection of nucleic acid effectors into cells, usually based on RNAi tools (e.g., siRNA) and antisense DNA technology (e.g., ASO) for modulation of gene expression. Ideally, these effectors should be vectorized into cells with maximal transfection efficiency in selected target cells and with minimal toxicity. The use of metallic nanoparticles to vectorize and deliver TNAs into cells constitutes a "smart" alternative to conventional transfection agents, such as cationic lipid vesicles or virus-like particles.

In this thesis, I propose the use of AuNPs or MNPs to promote the delivery of nucleic acids, whose cell uptake occurs by mild hyperthermia triggered by photothermy or magnetic modulation, respectively. The hypothesis is that, under controlled parameters, irradiation with visible light on AuNPs and the use of an AMF for MNPs - "nanoheaters" - might trigger localized heating upon adsorption at the cell membrane. This will modulate the permeability of the cell membrane, allowing for intracellular delivery with improved efficiency and tremendous spatiotemporal control suitable for gene therapy applications. The main goal of this thesis is to develop a novel, universal, and highly efficient methodology for the introduction of TNAs into cells triggered by mild hyperthermia.

This dissertation is structured into seven chapters. **Chapter 1** provides a literature review on the main topic of the thesis. **Chapter 2** presents a detailed description of the materials and methods used in the experimental work. **Chapters 3 to 6** focus on the use of "nanoheaters" for precise nucleic acid delivery:

Mild hyperthermia for nucleic acid transfection via AuNPs and visible light irradiation - in this **chapter 3**, AuNPs were synthesized and functionalized for the generation of "hotspots" on the cell membrane triggered by a green laser. The application of mild hyperthermia in different 2D cancer cell line models was attempted and the uptake of TNAs, cells response, cytotoxicity and transfection efficiency analyzed. Comparison with a commercial cationic lipid reagent was done.

Mild photothermy triggered ASO delivery for gene silencing of *c-MYC* oncogene - in this **chapter 4** enhanced silencing of a crucial oncogene, *c-MYC,* was assessed in 2D and in more complex 3D tumor spheroid models using mild photothermy via Au-nanoconjugates functionalized with ASO, combined with visible light irradiation.

Membrane-localized magnetic hyperthermia for transfection of nucleic acids - in this **chapter 5** magnetic hyperthermia and MNPs were used to achieve localized heating of the cell membrane through SPAAC bioorthogonal chemistry. Gene silencing efficacy and cytotoxicity were compared to a commercial cationic lipid reagent.

Transfection of siRNA against *IDO1* gene via magnetic hyperthermia in THP-1-derived DCs - in this Chapter 6, **i**mmobilization of MNPs on the cell membrane (via SPAAC reaction) was used to enhance siRNA transfection against an immunomodulatory gene (*IDO1*) frequently overexpressed in the TME, using hard-to-transfect DCs as a model.

Chapter 7 presents the final conclusions and future perspectives.

2

Materials and Methods

2.1 Materials

2.1.1 Reagents and materials

All chemicals and materials used are presented in Table 2.1 and all equipment in Table 2.2 (except for the synthesis and characterization of MNPs provided by Javier Idiago-López from Instituto de Nanociencia y Materiales de Aragón, INMA (CSIC-Universidad de Zaragoza) and Centro de Investigación Biomédica en Red de Bioingeniería, Biomateriales y Nanomedicina (CIBER-BBN), Spain). All chemicals were of molecular biology grade. Ultrapure water used in these processes came from a Millipore water purification system (Merck Millipore, USA).

Table 2.1 - List of reagents and materials.

Name (CAS Number)	Cat. No.	Company
1 cm path Quartz Spectrophotometer Cuvettes (Quartz Suprasil®)	105-202-15-40	Hellma-Analytics, Germany
12 mm coverslips	20012	SPL Life Sciences, South Korea
5,5-Dithiobis(2-nitrobenzoic acid), DTNB (69-78-3)	D8130	Sigma-Aldrich, USA
24-Well Cell Culture Plate	SPL30024	SPL Life Sciences, South Korea
96-Well Cell Culture Plate	SPL30096	SPL Life Sciences, South Korea
Acrodisc syringe filters 32 mm, 0.2 μm	4652	Pall corporation, USA
Anti-rabbit c-MYC antibody	ab32072	Abcam, UK
Bovine Serum Albumin, BSA (9048-46-8)	MB04602	NZYTech, Portugal
Calcium chloride (10043-52-4)	C1016	Sigma-Aldrich, USA
Cell culture 25 cm^3 T-Flask	SPL70025	SPL Life Sciences, South Korea
Cell culture 75 cm^3 T-Flask	SPL70075	SPL Life Sciences, South Korea
CellTiter 96® AQueous One Solution Cell Proliferation Assay Kit	G3580	Promega, USA
Chloroform (67-66-3)	438581	CARLO ERBA Reagents, Italy
CytoTox 96® Non-Radioactive Cytotoxicity Assay	G1780	Promega, USA
Dibenzylcyclooctyne-PEG_4-5/6-Sulforhodamine B, DBCO	CLK-A132-1	Jena Bioscience, Germany

Dibenzylcyclooctyne-PEG_4-5/6-TAMRA, DBCO	CLK-A131-1	Jena Bioscience, Germany
Diethylpyrocarbonate, DEPC (1609-47-8)	159220	Sigma-Aldrich, USA
Dimethyl sulfoxide, DMSO (67-68-5)	D5879	Sigma-Aldrich, USA
Dithiothreitol, DTT (3483-12-3)	D0632	Sigma-Aldrich, USA
Dulbecco's Modified Eagle Medium, DMEM	41965062	Gibco™ Thermo Fisher Scientific, USA
Dulbecco's Modified Eagle Medium, DMEM (without phenol red)	21063029	Gibco™ Thermo Fisher Scientific, USA
Ethanol (64-17-5)	32221	Honeywell, Fluka, USA
Ethyl Acetate (141-78-6)	109623	Merck Millipore, USA
Fetal Bovine Serum, FBS	10500064	Gibco™ Thermo Fisher Scientific, USA
Fluorescein isothiocyanate/FITC-conjugated anti-rabbit antibody	ab6717	Abcam UK
Neubauer chamber	8100204	Hirschmann™, Germany
Hoechst 33258 (23491-45-4)	H3569	Invitrogen™, Thermo Fisher Scientific, USA
Hydrochloric acid (7647-01-0)	30721	Honeywell, Fluka, USA
Illustra™ NAP-5™ Columns, Sephadex™ G-25 DNA Grade	17-0853-02	GE Healthcare, USA
Ionomycin (56092-82-1)	I0634	Sigma-Aldrich, USA
Isopropyl Alcohol (67-63-0)	CL00.0906	Chem-Lab NV, Belgium
Lipofectamine™ LTX Plus Reagent	15338030	Invitrogen™, Thermo Fisher Scientific, USA
Lipofectamine™ RNAiMAX	13778030	Invitrogen™, Thermo Fisher Scientific, USA
Lipopolysaccharides from *Escherichia coli* O111:B4, LPS	L5293	Sigma-Aldrich, USA
LIVE/DEAD™ Viability/Cytotoxicity Kit	L3224	Invitrogen™, Thermo Fisher Scientific, USA
Magnesium chloride (7786-30-3)	208337	Sigma-Aldrich, USA
MEM nonessential amino acid	11140050	Gibco™ Thermo Fisher Scientific, USA
Nitric Acid (7697-37-2)	30709	Honeywell, Fluka, USA

Nunclon™ Sphera™ 96-Well, Nunclon Sphera-Treated, U-Shaped-Bottom Microplate	174925	Thermo Fisher Scientific, USA
NZY M-MuLV First-Strand cDNA Synthesis Kit	MB17202	NZYTech, Portugal
NZYol	MB18501	NZYTech, Portugal
NZYSupreme qPCR Green Master Mix (2x)	MB41902	NZYTech, Portugal
O-(2-Mercaptoethyl)-O′-methyl-hexa(ethylene glycol), PEG (M_W:356 Da) (651042-82-9)	672572	Sigma-Aldrich, USA
One-step NZY RT-qPCR Green kit	MB34302	NZYTech, Portugal
pAcGFP1-Nuc Vector 4.8 kb	632431	Takara Bio Company, Japan
Paraformaldehyde (30525-89-4)	P6148	Sigma-Aldrich, USA
Penicillin/Streptomycin	15140122	Gibco™ ThermoFisher Scientific, USA
Phycoerythrin/PE-conjugated anti-mouse IgG1 antibody	ab91357	Abcam, UK
Phycoerythrin/PE-conjugated anti-mouse CD80 antibody	ab69778	Abcam, UK
Phycoerythrin/PE-conjugated anti-mouse CD83 antibody	ab234242	Abcam, UK
Phycoerythrin/PE-conjugated anti-mouse CD86 antibody	ab77226	Abcam, UK
Plastic cuvettes	67.742	Sarstedt, Germany
Poly-L-lysine solution 0.01% (25988-63-0)	A-005-C	Merck Millipore, USA
Potassium chloride (7447-40-7)	104936	Merck Millipore, USA
Potassium dihydrogen phosphate (7778-77-0)	104873	Merck Millipore, USA
ProLong™ Glass Antifade Mountant	P36982	Invitrogen™, Thermo Fisher Scientific, USA
Recombinant human Granulocyte Macrophage Colony-Stimulating Factor, rh GM-CSF (83869-56-1)	H5666	Sigma-Aldrich, USA
Recombinant human Interleukin 4, rh IL-4 (207137-56-2)	H7291	Sigma-Aldrich, USA

Recombinant human Tumor Necrosis Factor α, rh TNF-α (94948-59-1)	H8916	Sigma-Aldrich, USA
Roswell Park Memorial Institute 1640 medium, RPMI	61870044	Gibco™ Thermo Fisher Scientific, USA
Roswell Park Memorial Institute 1640 medium, RPMI (without phenol red)	11835030	Gibco™ Thermo Fisher Scientific, USA
Sodium Chloride (7647-14-5)	71379	Sigma-Aldrich, USA
Sodium Dodecyl Sulfate, SDS (151-21-3)	L5750	Sigma-Aldrich, USA
Sodium Phosphate Dibasic (7558-79-4)	71642	Sigma-Aldrich, USA
Sodium Phosphate Monobasic Monohydrate (10049-21-5)	S3522	Sigma-Aldrich, USA
Tetraacetylated *N*-azidoacetylmannosamine, Ac_4ManNAz (361154-30-5)	CLK-1084	Jena Bioscience, Germany
Tetrachloroauric (III) acid trihydrate (16961-25-4)	G4022	Sigma-Aldrich, USA
Trisodium Citrate dihydrate (68-04-2)	S4641	Sigma-Aldrich, USA
TRIsure™	BIO-38032	Bioline, UK
Triton™ X-100 (9002-93-1)	93420	Sigma-Aldrich, USA
Trypan Blue Solution, 0.4%	15250061	Gibco™ ThermoFisher Scientific
TrypLE™ Express	12604021	Gibco™ Thermo Fisher Scientific
Tween® 20 (9005-64-5)	P1379	Sigma-Aldrich, USA
Versene Solution	15040066	Gibco™ Thermo Fisher Scientific

2.1.2 Equipment

Table 2.2 - List of equipment.

Name	Company
Attune® Acoustic Focusing Flow Cytometer	Attune®, Life Technologies, USA
D5 Series device (magnetic hyperthermia applicator) DM100 Series device (magnetic hyperthermia applicator)	nB nanoscale Biomagnetics, Spain
Centrifuge (Sigma 1-14)	Sigma-Aldrich, USA
Centrifuge (Sigma 3-16K)	Sartorius, Sigma-Aldrich
Confocal Microscope Zeiss LSM 710	Zeiss, Germany
Continuous wave 532 nm green diode-pumped solid-state laser coupled to optical fiber	Changchun New Industries, Optoelectronics Tech Co., LTD, China
Laminar flow chamber	Faster S.r.l., Italy
Infinite M200 Microplate reader	Tecan, Switzerland
Malvern Zetasizer Nano ZS	Malvern Panalytical, UK
Nikon TMS Inverted Microscope	Nikon, Tokyo, Japan
Nanodrop spectrophotometer (ND-1000)	NanoDrop Technologies, USA
Omega Thermocouple HH806AU	Omega engineering, USA
Open-access software platform FIJI - ImageJ	National Institutes of Health, USA
Qiagen Rotor-Gene Q cycler	Qiagen, Germany
Sanyo CO_2 Incubator	Electric Biomedical Co., Japan
Ti-U Eclipse model inverted microscope equipped with DS- Qi1Mc digital camera	Nikon, Japan
Ultrasonic Cleaner S30H	Elma, Switzerland
UV mini-1240 spectrophotometer	Shimadzu, Japan

2.2 Methods

All the methods common to more than one chapter will be presented in this section to avoid repetition and improve readability.

2.2.1 Synthesis and characterization of AuNPs

2.2.1.1 Synthesis of AuNPs

AuNPs were synthesized resorting to the citrate reduction method described by Lee and Meisel [389]. A heated aqueous solution of trisodium citrate (25 mL; 38.8 mM) was added to a boiling aqueous solution of tetrachloroauric acid (225 mL; 1 mM) under stirring reflux resulting in a deep red colloidal solution, indicating the formation of AuNPs. This solution was kept under heat and stirred for 25 minutes and later cooled down to room temperature (RT). Citrate-capped AuNPs (AuNP@Citrate) were sterilized using a 0.2 μm syringe filter and stored protected from light at RT until further use [390]. The nanoparticles' concentration was characterized by Beer-Lambert law. The AuNPs should present a typical Surface Plasmon Resonance peak at around 520 nm with a corresponding extinction coefficient of ≈ 2.33×10^{8} $M^{-1}.cm^{-1}$ [391,392].

2.2.1.2 Characterization of AuNPs

AuNPs and Au-nanoconjugates were assessed by ultraviolet-visible absorption spectroscopy (UV-Vis), dynamic light scattering (DLS), zeta (ζ) potential, and transmission electron microscopy (TEM). UV-Vis spectra were acquired on a UV-Vis spectrophotometer in the range 400-800 nm using a 1 cm path quartz cuvette at RT. The hydrodynamic diameter, polydispersity index (PDI), and ζ-potential were measured by DLS resorting to a Malvern Zetasizer Nano ZS at 25°C, scattering angle 173° and laser wavelength 633 nm. TEM analysis was provided as a service at Instituto Gulbenkian de Ciência (IGC) and the core diameters were calculated using the open-access software platform FIJI - ImageJ.

2.2.1.3 Functionalization of AuNPs with PEG (AuNP@PEG)

AuNPs were functionalized with polyethylene glycol (PEG) for improved stability in biological media as previously reported [390]. Briefly, to achieve 100% or 30% coverage of the AuNPs' surface, 10 nM of AuNP@citrate were incubated with 0.028% SDS (w/v) and 0.01 mg/mL or 0.003 mg/mL of thiolated PEG, respectively, for 16 h under agitation at RT. The

excess PEG was removed by centrifugation at 14000 g for 30 minutes at 4°C (three times), and the free thiol-PEG was quantified in the supernatants via the Ellman's Assay.
A standard curve in the range of 0.0002-0.035 mg/mL of PEG was performed by mixing the appropriate amount of dilute solution of PEG for each concentration with 300 μL of phosphate buffer 0.5 M (pH=7) and Milli-Q water until 900 μL (final volume). Also, 600 μL of the supernatants recovered were mixed with 300 μL of phosphate buffer 0.5 M (pH=7). 21 μL of 5,5'-dithio-bis-(2-nitrobenzoic acid) (DTNB) solution was added to each sample and incubated for 15 minutes. Triplicates of each sample were measured, and the spectra were analyzed by measuring the sum of the absorbance between 400 and 500 nm. A 100% coverage was considered when the supernatant showed no traces of free thiol, which indicated that all thiol-PEG had been bonded to the AuNPs surface.

2.2.2 MNPs synthesis and characterization

2.2.2.1 MNPs synthesis

Monodisperse spherical iron oxide nanoparticles with a core diameter of 13 nm were obtained in organic phase and transferred to aqueous phase according to the protocol optimized by Fratila *et al.* and Moros *et al.* [192,193,393]. The concentrations of MNPs indicated represent the concentrations of iron and were determined as indicated in MNPs characterization (section 2.2.2.3).

2.2.2.2 Functionalization of the MNPs with PEG and cyclooctyne or dibenzylcyclooctyne derivatives [192]

MNPs@PMAO@PEG were obtained by incubating 1 mg of MNPs@PMAO with 22.26 μmoles of α-methoxy-ω-amino poly(ethylene glycol) (MW= 750 Da) in 420 μL of sodium tetraborate buffer (SSB) pH 9 (50 mM of boric acid and 50 mM of sodium borate). A solution containing 6.25 mg of N-(3-dimethylaminopropyl)-N'-ethylcarbodiimide hydrochloride (EDC·HCl) dissolved in 20 μL of SSB buffer (50 mM, pH 9), was prepared 2 times and one volume of solution was added to the previous mixture and shaken in a rotator disk during 30 minutes in the absence of light. Then, a second addition of EDC·HCl solution was done and the reaction mixture was incubated for another 3 h in the rotator disk. Finally, the excess of ligand was removed by washing the MNPs with Milli-Q water in a centrifugal filter with a 100 kDa molecular weight cut-off membrane at 8497xg for 15 minutes (each wash and repeated for a total of six washing steps).

MNPs@PMAO@PEG@CO and MNPs@PMAO@PEG@DBCO were obtained by incubating 0.5 mg of MNPs@PMAO@PEG with 273 μL of cyclooctynylamine (11-(cyclooct-2-yn-1-yloxy)-3,6,9-trioxaundecylamine) or dibenzocyclooctynylamine (DBCO-PEG_4-NH_2)

derivatives (5 mM), respectively, in 1.2 mL of SSB (50 mM, pH 9). Two additions of 3.125 mg of EDC dissolved in 10 μL of SSB (50 mM, pH 9) were done in the same incubation conditions previously described. Finally, the ligand excess was removed by washing the MNPs as previously described for the MNPs@PMAO@PEG. The cyclooctyne derivative used for the functionalization was prepared following the procedure described by Fratila *et al.* [192].

2.2.2.3 MNPs characterization

2.2.2.3.1 Iron concentration

The iron concentrations of the nanoparticles suspensions were determined using a standard colorimetric method. Three replicas of samples of 5 μL and 45 μL of solvent (hexane or water) were incubated with 100 μL of aqua regia solution (HCl/HNO_3; 3/1) at 60°C for 15 minutes, after which Milli-Q water was added until a final volume of 500 μL. 50 μL of the final total volume of each solution were transferred to a 96-well plate. Then, 60 μL of a solution consisting of 50 μL of 4 N KOH and 10 μL of 0.25 M Tiron (1,2-dihidroxybenzen-3,5-disulfonic acid), and 100 μL of 0.2 M Na_3PO_4 (pH = 9.7) were added. The measurement of the sample absorbance at 480 nm was carried out on a Thermo Scientific Multiskan™ GO or a Biotek Synergy H1 UV/Vis microplate spectrophotometer. A similar protocol was followed using iron standard solutions (100 – 800 μg/mL) to obtain a calibration curve.

2.2.2.3.2 DLS and ζ-potential measurements

DLS and ζ-potential measurements were performed on a Malvern Zetasizer Nano ZS at 25°C and pH 7, considering a refractive index of 2.0 and an absorption index of 1.0 for Fe_3O_4. Samples were prepared at a concentration of 0.05 mg Fe/mL in Milli-Q water. Each sample was measured five times, combining 10 runs per measurement. Results were treated using the Malvern software Zetasizer Nano 7.13.

2.2.2.3.3 Agarose gel electrophoresis

For the agarose gel electrophoresis, a solution of 1% agar in 0.5x Tris-Borate-EDTA (TBE) was prepared. MNPs samples mixed with 20% glycerol: 0.5x TBE were loaded in the gel and an electric field of 90 V was applied for 45 minutes.

2.2.2.3.4 TEM analysis

TEM imaging and size analysis of the MNPs were performed on an FEI Tecnai T20 instrument operating at an accelerating voltage of 80-200 kV (Laboratorio de Microscopias

Avanzadas LMA, University of Zaragoza). Samples were prepared on carbon-coated copper grids by depositing a drop of a diluted MNPs suspension; TEM grids were allowed to dry at RT for 24 h before visualization. MNPs size and size distribution were determined using the Digital Micrograph software or ImageJ software by measuring the diameter of at least 200 MNPs per image.

2.2.2.3.5 Characterization of the heating properties of MNPs

The specific absorption rate (SAR) was calculated using a DM100 Series AMF applicator. Samples were measured at a concentration of 1 mg Fe/mL in Milli-Q Water. The AMF was applied for 3 minutes using a field amplitude of 23.9 kA/m and a frequency of 418 kHz while the temperature was recorded using an optic fiber sensor incorporated in the equipment. The SAR value was calculated according to the temperature slope obtained at the beginning of the measurement. Specific loss power (SLP) measurements were carried out using a D5 Series AMF applicator with a coil (CAL2) connected to a vacuum pump to achieve thermal isolation of the sample and using a capacitor (120 nF) to evaluate different frequency ranges. MNPs samples were prepared at a concentration of 1 mg Fe/mL in water and/or supplemented cell culture medium. For each measurement, the temperature variation was recorded for 5 minutes and the SLP was calculated by linear curve fitting at the initial instants (30-60 seconds) using the ZAR application provided by the equipment software (MANIAC) and indicating the value of the sample concentration (mg Fe/mL).

2.2.2.3.6 Thermogravimetric analysis

Thermogravimetric analysis was performed on lyophilized MNPs samples using a TA STD 2960 simultaneous DTA-DTGA instrument in air, at a heating rate of 10ºC/minutes.

2.2.3 Cell culture maintenance

HCT116 colorectal carcinoma (ATCC® CCL-247™) and MCF-7 breast adenocarcinoma (ATCC® HTB-22™) were purchased from the American Type Culture Collection (ATCC, Manassas, VA, USA). MCF-7/GFP breast adenocarcinoma expressing constitutively an optimized version of GFP - copGFP (Cat# AKR-211) was purchased from Cell Biolabs (Cell Biolabs Inc, San Diego, CA, USA). Cells were grown in Dulbecco's modified Eagle's medium (DMEM) supplemented with 10% (v/v) fetal bovine serum (FBS) and 1% (v/v) penicillin/streptomycin (100 U/mL). MCF-7 and MCF-7/GFP were also supplemented with 1% (v/v) of MEM nonessential amino acid. THP-1 acute monocytic leukemia cells (ATCC® TIB-202™) were grown in RPMI 1640 medium (Roswell Park Memorial Institute 1640) supplemented with 10%

(v/v) FBS, 1% (v/v), 1% (v/v) penicillin/streptomycin (100 U/mL) and 1% (v/v) MEM non-essential amino acids.

Cells were maintained in 75 cm^2 or 25 cm^2 culture flasks at 37°C in a 5% CO_2 atmosphere and 99% relative humidity. Upon attaining confluency, adherent cells were trypsinized with TrypLE™ Express, stained with 0.4% Trypan Blue solution, counted using a Neubauer chamber, and cultured into fresh medium and culture flasks. THP-1 cells were further differentiated in THP-1-derived DCs and HCT116 cells were used to obtain 3D tumor spheroids.

2.2.4 Plasmid Transfection with Lipofectamine™ LTX with Plus Reagent

HCT116 and MCF-7 cells were placed at a density of $2x10^4$ cells/well in a 96-well plate and $1.5x10^5$ cells/well in a 24-well plate, respectively, and cultured in DMEM for 24 h at 37°C, under standard cell culture conditions. A plasmid that encodes a GFP (λ_{ex} 475 nm/λ_{em} 505 nm) optimized for high expression in mammalian cells (pAcGFP1 Nuc Vector), was added (0.1, 0.25, and 0.5 μg/well in HCT116 cells; 0.25, 0.5 and 1 μg/well in MCF-7 cells) to cells using a 1:2 (plasmid: Lipofectamine) ratio and incubated in DMEM (0% FBS and without antibiotics) for approximately 4 h at 37°C, according to the Lipofectamine™ LTX with Plus Reagent manufacturer's recommendation. After 4 h of incubation, the medium was replaced with fresh DMEM. AcGFP1 expression was confirmed after 24 h by fluorescence microscopy (Ti-U Eclipse inverted microscope; FITC filter (excitation at 480/30 nm and emission at 535/40 nm)) and images were analyzed using ImageJ software.

2.2.5 Cells transfection with Lipofectamine™ RNAiMAX Reagent

For laser irradiation experiments, HCT116 and MCF7/GFP cells were seeded at a density of $2x10^4$ cells/well and $1x10^4$ cells/well respectively, in a 96-well plate and incubated for 24 h at 37°C under standard cell culture conditions. After 24 h, 20 nM of oligonucleotide was mixed with the cationic lipid reagent Lipofectamine™ RNAiMAX in DMEM without phenol red (0% FBS and without antibiotics) and incubated for 5 minutes in a microcentrifuge tube according to the manufacturer's recommendation. Next, this mixture was added to cells in DMEM without phenol red (Final 8% FBS) for 24 h in HCT116 cells; and 6 h and 24 h in MCF-7/GFP cells.

For magnetic hyperthermia experiments, MCF-7 cells, MCF7/GFP cells, and THP-1-derived DCs were seeded at a density of $1.5x10^5$ cells/well, $2.5x10^4$ cells/well, and $3x10^5$ cells/well respectively, in a 24-well plate and incubated for 24 h for MCF-7 and MCF-7/GFP cells and 48 h for THP-1-derived DCs, at 37°C under standard cell culture conditions. At 24 h,

MCF-7 cells were transfected transiently with pAcGFP1 Nuc Vector (carried out as described in section 2.2.4), then the cell culture medium of MCF-7 and MCF7/GFP cells was replaced with fresh DMEM. After 48 h, 20 nM of oligonucleotide or siRNA was mixed as described above. Next, this mixture was added to cells with the respective cell culture medium (Final 8% FBS) and incubated for 48 h in MCF-7 and MCF-7/GFP cells; for 24 h in THP-1-derived DCs.

Post-transfection incubation, total RNA was extracted, and the efficiency of transfection for *AcGFP1*, *copGFP* and *IDO1* silencing was evaluated by RT-qPCR and fluorescence microscopy for copGFP protein expression.

2.2.6 Cell viability and cytotoxicity

2.2.6.1 MTS Assay

Cell viability (irradiated and non-irradiated cells, with or without Au-nanoconjugates) was evaluated upon the stimuli via the 3-(4,5-dimethylthiazol-2-yl)-5-(3-carboxymethoxyphenyl)-2-(4-sulfophenyl)-2H-tetrazolium (MTS) assay -CellTiter 96® AQueous One Solution Cell Proliferation Assay. This assay is a colorimetric method to estimate the number of viable cells and relies on the dehydrogenation by metabolically active cells, which convert the MTS tetrazolium compound into formazan, a soluble colored product.

For laser experiments, HCT116 and MCF-7/GFP cells were incubated with the MTS solution (1:5 v/v in DMEM) for 1 h, at 37°C under standard cell culture conditions. For magnetic hyperthermia experiments, post-transfection THP-1-derived DCs and MCF-7 cells were placed at density of $5x10^4$ cells/well; MCF-7/GFP cells were plated $2.5x10^4$ cells/well, in a 96-well plate and MCF-7 and MCF-7/GFP (adherent cells) were incubated for 24 h while THP-1-derived DCs were immediately incubated with MTS solution (1:5 v/v RPMI) for 2 h, at 37ºC under 5% CO_2 and 99% relative humidity. At 24 h post-transfection for MCF-7 and MCF-7/GFP cells, the MTS solution was added to the cells and incubated for 1 h, under standard cell culture conditions. At 24 h post-transfection the cell culture medium of MCF-7 and MCF-7/GFP was removed, MTS solution was added to the cells (1:5 v/v DMEM) and incubated for 1 h, at 37°C under standard cell culture conditions.

To determine the viability of THP-1 and THP-1-derived DCs incubated with Ac_4ManNAz and MNPs, cells were seeded at a density of $6x10^4$ cells/well in a 96-well plate and incubated with 100 μM of Ac_4ManNAz at 37°C, under standard cell culture conditions. After 48 h of Ac_4ManNAz treatment, cells were washed twice with PBS and incubated for 30 minutes with 100 μg_{Fe}/mL of MNPs in RPMI without FBS at 37ºC, under 5% CO_2 and 99% relative humidity. Cells were then washed twice with PBS and the MTS solution (1:5 v/v in RPMI) was added to the cells and incubated for 1 h and 30 minutes at 37°C under standard cell culture conditions.

The absorbance was measured at 490 nm using a microplate reader Infinite M200. Cell viability was normalized to control cells (cells with culture medium). At least three independent biological assays with two technical replicates were performed (Equation 2.1).

$$Cell\ Viability\ (\%) = \frac{mean\ Abs.\ of\ treatment\ group}{mean\ Abs.\ of\ control\ group} \times 100 \quad \text{(Equation 2.1)}$$

2.2.6.2 LDH Assay

The membrane integrity of HCT116 2D cells/3D spheroids (irradiated or not, in the presence or absence of Au-nanoconjugates) was also evaluated by resorting to the release of intracellular lactate dehydrogenase (LDH) in cells supernatant by LDH assay - CytoTox 96 Non-Radioactive Cytotoxicity Assay. As a positive control for membrane rupture, the LDH lysis solution (1:10 v/v in DMEM) was prepared 1 h before the procedure and incubated in cells or spheroids. Following the HCT116 2D cells irradiation or 9 h of 3D spheroids challenge with Au-nanoconjugates, 50 µL of cells or spheroids supernatant are incubated with 50 µL of CytoTox 96 Reagent (1:1 ratio) in a 96-well plate for 30 minutes at RT, protected from light. Next, 50 µL of Stop Solution is added to the wells and incubated for 1 h at RT, in the dark. The absorbance was measured at 490 nm, on a microplate reader and cell membrane integrity was normalized to Control (untreated cells). For 3D spheroids, a fold change (ratio) to Control was performed to evaluate LDH activity. At least three independent biological assays with two technical replicates were performed (Equation 2.2).

$$Cell\ membrane\ integrity\ (\%) = 100 - \frac{mean\ Abs.\ of\ treatment\ group}{mean\ Abs.\ of\ control\ group} \quad \text{(Equation 2.2)}$$

2.2.7 Gene expression analysis

Total RNA was extracted from samples using the NZYol reagent or TRIsure™ reagent, according to the manufacturer's guidelines. The quality of RNA was assessed using the Nanodrop ND-1000 Spectrophotometer. RNA extracted from 2D cells was reverse transcribed to cDNA using the NZY M-MuLV First-Strand cDNA Synthesis kit followed by real-time quantitative polymerase chain reaction (RT-qPCR). RT-qPCR was performed using NZYSupreme qPCR Green Master Mix (2x) according to the manufacturer's protocol in a Qiagen Rotor-Gene Q cycler. The following conditions were used for the *AcGFP1* gene: initial denaturation at 95°C for 5 min; 30 cycles of 95°C 30 s, Tm 52°C for 30 s, 72°C for 45 s; and a final extension step at 72°C for 7 min; for *copGFP* gene: initial denaturation at 95°C for 5 min; 30 cycles of 95°C for 30 s, Tm 53°C for 30 s, 72°C for 30 s; and a final extension step at 72°C for 5

min; for *IDO1* gene: initial denaturation at 95°C for 5 min; 35 cycles of 95°C for 30 s, Tm 58°C for 30 s, 72°C for 15 s; for *IL6*, *IL10*, *TNFA* and *IL12A* genes: initial denaturation at 95°C for 5 min; 40 cycles of 95°C for 30 s, Tm 53°C for 30 s, 72°C for 30 s.

Total RNA was also extracted from HCT116 2D cells and six 3D spheroids, and RT-qPCR was performed using a One-step NZY RT-qPCR Green kit for the analysis of *c-MYC* gene expression. The set conditions for reverse transcription were 50°C for 20 min; and qPCR with initial denaturation at 95°C; 30 cycles of 95°C 15 s, Tm, and extension of 60°C for 15 s.

Gene expression was evaluated according to the $2^{-\Delta\Delta Ct}$ method [394], using the *18S* ribosomal gene as a reference. All primers and antisense oligonucleotides were purchased from STAB VIDA, Lda (Portugal), except siRNA against *IDO1* (Dharmacon™, Germany); all sequences and the sequence target of siRNA-*IDO1* can be found in Table 2.3 and Table 2.4.

Table 2.3 - Primers sequences Forward (Fwr) and Reverse (Rev) primers.

Gene	Sequence 5′-3′	Amplicon Size (bp)
AcGFP1	Fwr: ATGGTGAGCAAGGGCGAGGA Rev: CTTGTACAGCTCGTCCATGC	717
copGFP	Fwr: TTCTACCACTTCGGCACCTA Rev: TCCACCACGAAGCTGTAGTA	335
IDO1 (NM_002164.6)	Fwr: ACTGTGTCTTGGCAAACTGGAAG Rev: CAGCTGCTATTTCCACCAATAGAG	141
IL6 (NM_000600.5)	Fwr: GGT ACA TCC TCG ACG GCA TCT Rev: TCT TTG CTG CTT TCA CAC AT	76
IL10 (NM_000572.3)	Fwr: GGT TGC CAA GCC TTG TCT GA Rev: CCC CCA GGG AGT TCA CAT G	106
TNFA (NM_000594.4)	Fwr: CCA GGC AGT CAG ATC ATC TTC TC Rev: TAT CTC TCA GCT CCA CGC CA	143
IL12A (NM_001397992.1)	Fwr: GAATTTTACCCTTGCACTTCTGA Rev: CAGGCAACTCCCATTAGTTATGA	156
c-MYC (NM_002467.5)	Fwr: GCTCATTTCTGAAGAGGACTTGT Rev: AGGCAGTTTACATTATGGCTAAATC	229
18S (NR_003286.4)	Fwr: GTAACCCGTTGAACCCCATT Rev: CCATCCAATCGGTAGTAGCG	151

Table 2.4 - ASO and siRNA sequences used for gene silencing.

Gene	Sequence 5'-3'	Type
AcGFP1	GCAAGCUGACCCUGAAGUUC	Antisense RNA
copGFP	CACCCGCAUCGAGAAGUACG	Antisense RNA
IDO1	AGAAAGAGUUGAGAAGUUA	siRNA
c-MYC	5'-Mod Thiol C6 GCGCCCATTTCTTCCAGATATCCTCGCTGGGCGC	Antisense DNA
Scramble	5'-Mod Thiol C6 TTTCGGGTTGACGTTAGCCGGATCTACCGAAA	Antisense DNA

2.2.8 Statistical analysis

The data were analyzed using GraphPad Prism 8.0 (GraphPad Software, San Diego, USA). All experiments generally represented the average of at least three independent biological assays with two technical replicates and the corresponding errors, except when stated otherwise. The appropriate statistical test was used according to each case and was considered statistically significant at p-value < 0.05.

3

MILD HYPERTHERMIA FOR NUCLEIC ACIDS TRANSFECTION VIA AUNPS AND VISIBLE LIGHT IRRADIATION

Data enclosed in this chapter 3 were originally published in the following issue, where I was responsible for AuNPs and Au-nanoconjugates synthesis and characterization, for the photothermal characterization of Au-nanoconjugates, 2D cells challenge with Au-nanoconjugates, nucleic acids transfection efficiency, cell viability assessment, and for all the statistical analysis.

Ferreira, D., Fernandes, A.R. & Baptista, P.V. Mild hyperthermia via gold nanoparticles and visible light irradiation for enhanced siRNA and ASO delivery in 2D and 3D tumour spheroids. *Cancer Nano* 15, 19 (2024). https://doi.org/10.1186/s12645-024-00256-4.

This publication also includes additional data on AuNPs functionalized with ASO for silencing of *c-MYC* oncogene using mild photothermy in 2D cells and 3D tumor spheroids that will be described in chapter 4.

3.1 Introduction

PTT is an emerging technique for inducing hyperthermia to destroy cancer cells effectively and holds significant interest due to its simplicity, short treatment duration, and fast recovery [395]. Since the TME characteristics (e.g., acidic, hypoxic, loss of nutrients) tend to increase the sensitivity of tumor cells to heat, therapeutic approaches based on the conversion of light irradiation to heat by photothermal agents are required [396,397]. Currently, a wide range of external laser light sources, including visible and NIR light, have been described in PTT [398]. PTT is a highly effective and noninvasive approach to treat various types of cancer but has limitations such as lack of spatial selectivity in heating tumors while avoiding thermal injury to surrounding healthy tissues. To address collateral damage, photothermal agents have been introduced to enhance the selectivity of PTT in cancer therapy [395,399].

AuNPs have already demonstrated their potential to be used as photothermal agents due to their unique optical properties (e.g., SPR), using incident laser light sources (e.g., visible and NIR light) [159,398,400]. SPR depends on the interaction between an electromagnetic wave and free conduction electrons at the AuNPs' surface, due to their oscillation coherently in resonance with the frequency of light, producing strong electromagnetic fields. This effect significantly increases the AuNPs' ability to scatter and absorb light efficiently, making it appropriate for a variety of biomedical applications (e.g., biosensing and imaging). The electromagnetic energy transformed into heat because of electron excitation and relaxation by AuNPs is one of their unique physicochemical properties [159,342,347,401].

Localized hyperthermia is a well-known result of the increase of temperature specifically in target cells responding to photothermal agents. Three types of localized hyperthermia can be applied in tumor cells: mild hyperthermia (37 - 42°C), moderate hyperthermia (43 - 45°C), and thermal ablation (> 45°C) [321,402]. Mild hyperthermia could modulate the cell membrane behavior (e.g., fluidity and permeability) and increase the susceptibility of cancer cells to alternative therapeutic approaches, such as transfection of nucleic acids or drugs, and the delivery of AuNPs functionalized with (bio)molecules (e.g., drugs, antibodies, ASO) [361,403,404]. AuNPs are optimal for vectorization since they protect oligonucleotides against nucleases and degradation while providing the possibility to track internalization without significant cytotoxicity [405–407]. Due to their optical properties, AuNPs offer the possibility to use external actuators (e.g., light, radiofrequency) to trigger cell uptake [321,397,402,408–410]. The efficacy of combining spherical functionalized AuNPs with visible laser irradiation to enhance therapeutic outcomes *in vitro* and *in vivo* models has been reported [361,396,403,404,411].

This chapter presents a controlled mild hyperthermia system using visible green laser irradiation combined with spherical AuNPs as photothermal agents. The efficacy of this mild photothermal approach to improve the internalization of Au-nanoconjugates without cytotoxicity in the HCT116 colorectal carcinoma cell line was assessed. As a proof-of-concept, mild hyperthermia was used to enhance the transfection of nucleic acids in two different cancer cell lines, HCT116 cells and MCF-7/GFP breast adenocarcinoma cell line.

3.2 Materials and Methods

3.2.1 AuNPs and Au-nanoconjugates synthesis and characterization

AuNPs and Au-nanoconjugates were synthesized, functionalized, and characterized as described in section 2.2.1 (Chapter 2).

3.2.2 Irradiation and photothermal characterization

To determine the photothermal capability of the Au-nanoconjugates, these were irradiated at different concentrations (0.25 nM, 0.5 nM, 0.75 nM, and 1 nM) in water in a 96-well plate. For temperature measurements, a thermocouple was inserted in the wells before and immediately after visible light laser irradiation, as previously optimized in our group [396,411]. Irradiation was performed with a continuous wave (CW) 532 nm green diode-pumped solid-state laser (DPSS) coupled to an optical fiber under a laser diode intensity (LDI) 1.71 W/cm^2 or LDI 2.37 W/cm^2, for different exposure times (30 s, 60 s, 90 s, and 120 s) [396].

3.2.3 Stability assays of Au-nanoconjugates

To assess the effect of different media conditions on the stability of the Au-nanoconjugates before biological experiments, these were subjected to increasing ionic strength solutions to analyze if Au-nanoconjugates could sustain higher ionic strengths without aggregation. The stability assays were assessed via UV-Vis spectroscopy in different solutions using 10 nM of Au-nanoconjugates: DMEM without phenol red and FBS to avoid the formation of protein corona, PBS from 0 to 240 minutes to simulate the osmolarity and ion concentrations of the human body (isotonic conditions), and NaCl at concentrations ranging from 0 to 3.5 M to evaluate the ionic strength.

3.2.4 Cells challenge with Au-nanoconjugates

3.2.4.1 Laser irradiation in HCT116 cells

HCT116 cells were seeded at a density of 2x10^4 cells/well in a 96-well plate and incubated for 24 h at 37°C in a 99% humidified atmosphere and 5% (v/v) CO_2. Following 24 h, cells were challenged (or not) with 10 nM of AuNP@PEG 100% for 4 h, and then the cell culture medium was replaced with DMEM without phenol red (at 37°C). Cells were then irradiated

with a CW 532 nm green DPSS laser coupled to an optical fiber (LDI 1.71 W/cm^2 or 2.37 W/cm^2) for 90 s and 60 s, respectively. Controls without irradiation, with or without AuNPs, were also prepared. For temperature measurements, a thermocouple was inserted in the wells (in contact with the cell culture medium) before and immediately after visible light irradiation.

3.2.4.2 Cell viability and cytotoxicity

Cell viability and cytotoxicity assessment via MTS assay and LDH assay were performed as described in section 2.2.6 (Chapter 2). HCT116 cells membrane integrity was evaluated by Trypan Blue exclusion assay. Briefly, irradiated and non-irradiated cells, previously incubated (or not) for 4 h with 10 nM of AuNP@PEG 100%, were immediately incubated with Trypan Blue dye for 10 minutes, and washed three times with PBS to remove the excess of the dye. Several images were acquired with a bright field inverted microscope for the analysis of membrane integrity of irradiated and non-irradiated cells, with or without AuNPs.

3.2.4.3 Quantification of AuNPs internalization into cells

The internalization of the AuNP@PEG 100% in irradiated and non-irradiated HCT116 cells was analyzed via ICP-AES. For this experiment, HCT116 cells were washed with PBS, trypsinized with TrypLE™ Express, and centrifuged at 750 g for 5 minutes. The supernatant was removed and stored at 4°C, whereas the cell pellet was stored at −20°C. One day before analysis, 1 mL of freshly prepared aqua regia (HCl: HNO_3= 3:1) was added to the samples. A standard curve for gold was recorded to quantify the amount of intracellular gold (LAQV/REQUIMTE, Laboratório de Análises).

3.2.5 Mild photothermy via Au-nanoconjugates and visible laser irradiation for nucleic acid transfection

3.2.5.1 Plasmid transfection with Lipofectamine™ LTX with Plus Reagent

The plasmid transfection in HCT116 cells was performed as described in section 2.2.4 (Chapter 2).

3.2.5.2 Plasmid transfection with laser irradiation

HCT116 cells were seeded at a density of 2x10^4 cells/well in a 96-well plate and incubated for 24 h at 37°C in a 99% humidified atmosphere and 5% (v/v) CO_2. Following 24 h, cells

were challenged (or not) with 10 nM of AuNP@PEG 100% for 4 h, and then cell culture medium was replaced with DMEM without phenol red (at 37°C). Before laser irradiation, 0.1 μg or 0.25 μg of pAcGFP1 Nuc Vector was added to the respective well for cell transfection. Cells with AuNPs were irradiated with a CW 532 nm green DPSS laser coupled to an optical fiber under (LDI 2.37 W/cm^2) for 60 seconds to achieve mild hyperthermia. Controls without irradiation, with or without AuNPs, were also prepared. The effect of visible laser irradiation on the transfection of pGFP was evaluated with fluorescence microscopy images using ImageJ software (Ti-U Eclipse inverted microscope; FITC filter (excitation at 480/30 nm and emission at 535/40 nm)) for 24 h and 48 h after transfection and compared to Lipofectamine LTX™ and Plus reagent.

3.2.5.3 Laser irradiation in HCT116 and MCF-7/GFP cells

HCT116 and MCF-7/GFP cells were seeded at a density of $2x10^4$ cells/well and $1x10^4$ cells/well respectively, in a 96-well plate and incubated for 24 h at 37°C in a 99% humidified atmosphere and 5% (v/v) CO_2. After 24 h, HCT116 cells were transfected with 0.1 μg of pAcGFP1 Nuc Vector using Lipofectamine™ LTX with Plus Reagent. After 4 h of incubation with Lipo+pGFP complexes, the culture medium was replaced with DMEM without phenol red, and cells were challenged (or not) with 10 nM of AuNP@PEG 100% for 4 h. Next, the cell culture medium was replaced with DMEM without phenol red (at 37°C) containing 20 nM of *anti-AcGFP1*. For MCF-7/GFP: following 24 h, cells were challenged (or not) with 10 nM of AuNP@PEG 100% for 4 h, and then cell culture medium was replaced with DMEM without phenol red (at 37°C) containing 20 nM of *anti-copGFP*. Cells with AuNPs were then irradiated as described in section 3.2.5.2. Controls without irradiation, with or without AuNPs, were also prepared. After 6 h and 24 h for copGFP and 24 h for AcGFP1, GFP expression was confirmed by fluorescence microscopy and images were analyzed using ImageJ software. For fluorescence quantification, corrected total cell fluorescence (CTCF) was determined using Equation 3.1 [412].

$$CTCF = Integrated\ density\ of\ cell - (Area\ of\ cell \times Background\ mean\ fluorescence)$$
(Equation 3.1)

Also, MTS assay was performed and total RNA was extracted from irradiated and non-irradiated cells, and the effect of visible irradiation on the transfection of *anti-AcGFP1* and *anti-copGFP* silencing was evaluated by RT-qPCR and compared to a commercial transfection reagent, Lipofectamine™ RNAiMAX reagent, using the manufacturer's instructions.

3.2.5.4 Cells transfection with Lipofectamine™ RNAiMAX Reagent

The transfection of *anti-AcGFP1* and *anti-copGFP* in HCT116 and MCF-7/GFP cells, respectively, was performed as described in section 2.2.5 (Chapter 2).

3.2.5.5 Cell viability

Cell viability assessment via MTS assay was performed as described in section 2.2.6 (Chapter 2).

3.2.5.6 Gene expression analysis

The analysis of gene expression of *AcGFP1* and *copGFP* via RT-qPCR was performed as described in section 2.2.7 (Chapter 2).

3.2.6 Statistical analysis

Data were analyzed using GraphPad Prism 8.0 (GraphPad Software, San Diego, USA). One-way and two-way ANOVA with Tukey's multiple comparison, and unpaired parametric t-test with Welch's correction was used to evaluate the differences between groups. They were considered statistically significant at p-value < 0.05. Data are the mean value of at least three independent assays with at least two technical replicates, and the errors are calculated by the standard error of the mean.

3.3 Results and Discussion

3.3.1 Synthesis and characterization of Au-nanoconjugates

Spherical AuNPs with an average diameter of 12-14 nm were synthesized resorting to the citrate reduction method as described in section 2.2.1 (Chapter 2). Characterization of citrate-capped AuNPs (AuNP@Citrate) by UV-Vis, DLS, and TEM shows a maximum LSPR peak at 519 nm (Figure 3.1), a hydrodynamic diameter of 16.4 (± 0.1) nm, and an average spherical shape of 12.1 (± 1.5) nm (Figure 3.2). The concentration of AuNP@Citrate colloidal solution

was estimated by Beer-Lambert law using the molar extinction coefficient of gold for spherical AuNPs ($\varepsilon = 2.33\times10^{-8}M^{-1}\cdot cm^{-1}$) [391,392].

AuNP@Citrate were further functionalized with thiolated-PEG for 30% and 100% of coverage and characterized by UV-Vis, DLS, and TEM. PEG is frequently attached to the surface of AuNPs to enhance stability and biocompatibility, owing to the high affinity of thiol groups to gold [390,413]. We calculated the amount of PEG in AuNPs' surface by the quantification of free thiol-PEG in the supernatant via Ellman's assay, measuring the sum of the absorbance between 400 to 500 nm using a PEG standard curve (Figure 3.2). The 100% PEG coverage is represented by a concentration of 0.01 mg/mL, and 30% PEG coverage is represented by a concentration of 0.003 mg/mL. AuNP@PEG showed a slight red shift of the LSPR peak to 520 nm (Figure 3.1) and a slight increase in the hydrodynamic diameter 21.1 (± 0.3) and 18.5 (± 0.1) nm for 30% and 100% PEG coverage, respectively (Figure 3.2). Table 3.1 represents the physicochemical characteristics of AuNPs and Au-nanoconjugates in water measured via DLS and ζ-potential.

Table 3.1 - Physicochemical characteristics of AuNPs and Au-nanoconjugates measured by DLS, ζ-potential (at pH=6), and their polydispersity index (PDI).

AuNPs	Hydrodynamic diameter (nm)	ζ-potential	PDI
AuNP@Citrate	16.4 ± 0.1	-37.1 ± 0.5	0.170
AuNP@PEG 30%	21.1 ± 0.3	-70.7 ± 3.1	0.282
AuNP@PEG 100%	18.5 ± 0.1	-29.6 ± 2.7	0.171

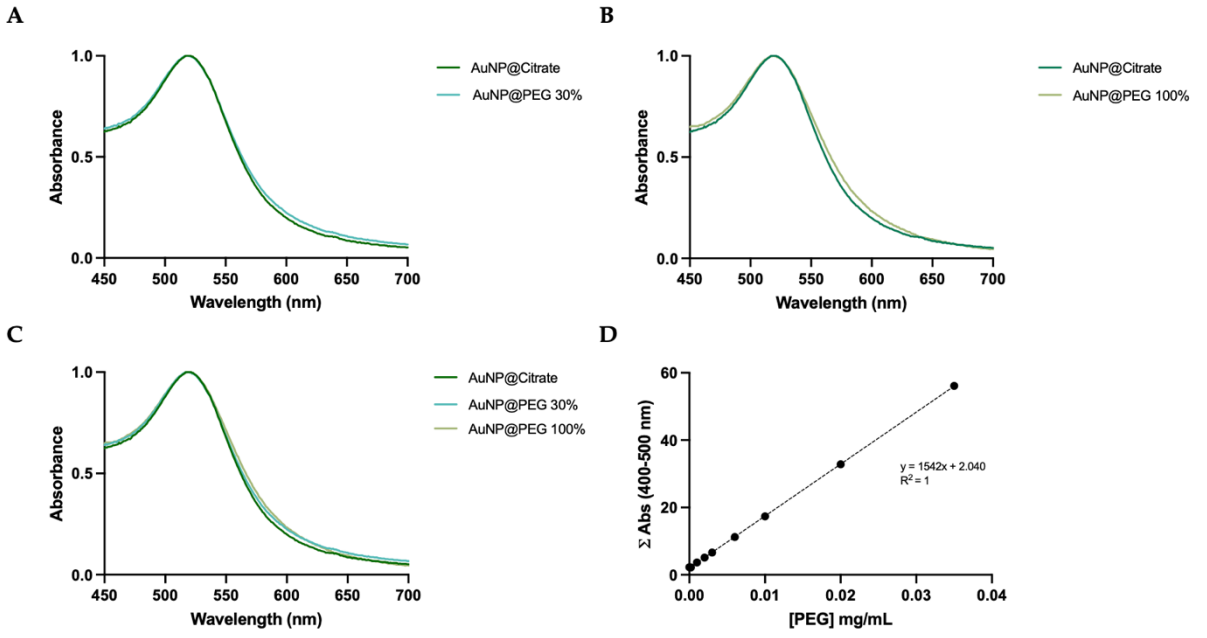

Figure 3.1 - Normalized absorbance UV-Vis spectra of Au-nanoconjugates and PEG standard curve. (A) UV-Vis spectra of AuNP@Citrate and AuNP@PEG 30%; (B) UV-Vis spectra of AuNP@Citrate and AuNP@PEG 100%. (C)

UV-Vis spectra of Au-nanoconjugates. (D) A standard curve with increasing concentrations of PEG via Ellman's Assay.

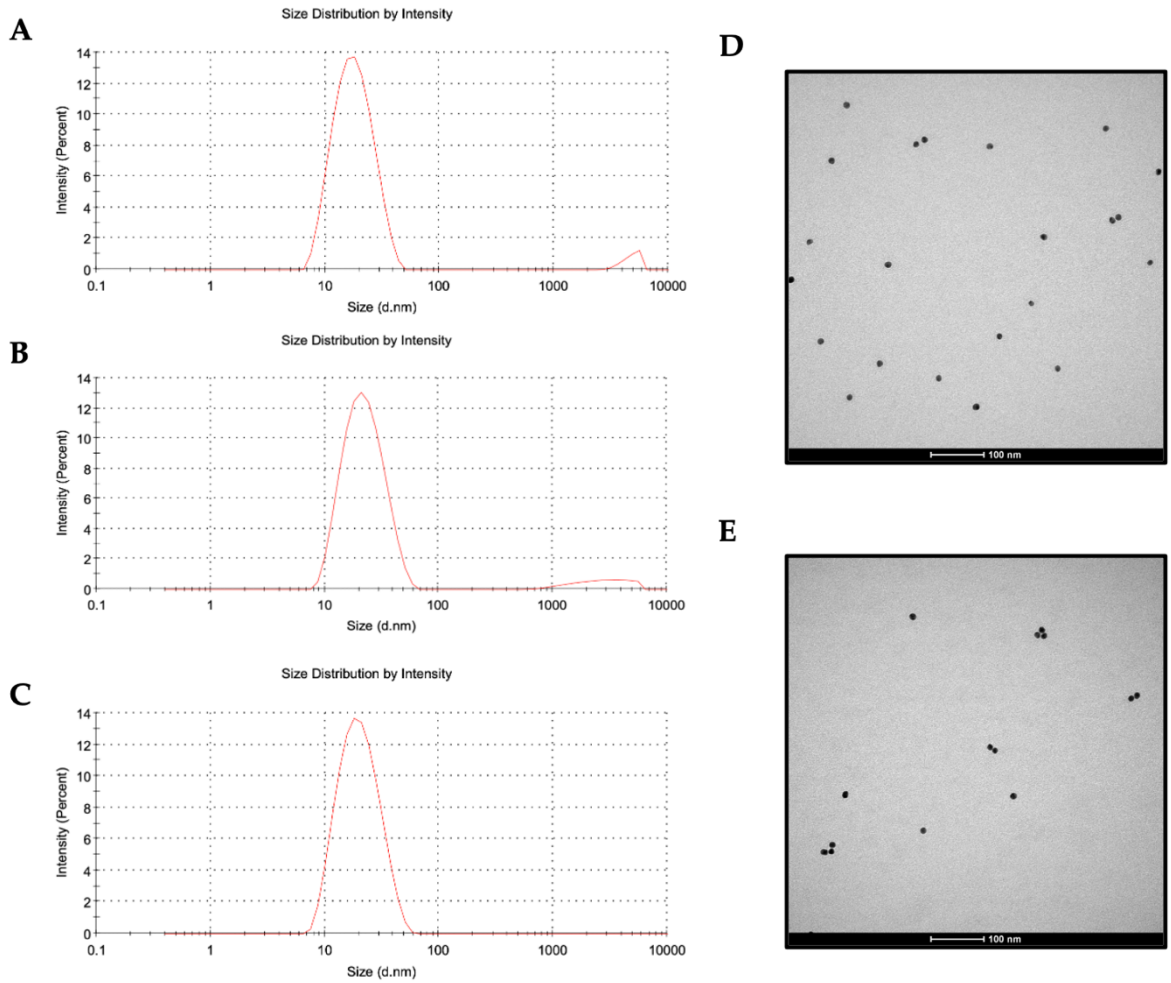

Figure 3.2 - Hydrodynamic size distribution of Au-nanoconjugates measured via DLS in water and TEM images to evaluate the diameter size of the AuNPs core. Hydrodynamic size distribution of (A) AuNP@Citrate, (B) AuNP@PEG 30%, and (C) AuNP@PEG 100% by DLS. The peak observed in each data set indicates the monodispersity of the colloidal AuNPs. TEM image of (D) AuNP@Citrate and (E) AuNP@PEG 100%. The average diameter of the AuNPs core is 12.1 (± 1.5) nm. Scale bars correspond to 100 nm.

3.3.2 Laser irradiation

The laser source performance was characterized previously by actinometry in our group [396,414]. The AuNP@PEG 30% and AuNP@PEG 100% were irradiated with a CW 532 nm green DPSS laser coupled to an optical fiber under a LDI 1.71 W/cm² or LDI 2.37 W/cm². The photothermal effect of the Au-nanoconjugates was assessed by irradiating a range of concentrations of pegylated AuNPs: 0.25 nM, 0.5 nM, 0.75 nM, and 1 nM; at different exposure times: 30 s, 60 s, 90 s and 120 s. The temperature variation (ΔT) was calculated by subtracting the

final temperature from the initial temperature in each AuNPs assay, excluding the temperature of the irradiated water. The thermal capacity of water 4.18 $J.g^{-1}.K^{-1}$ (q) and the irradiated mass (m) of 0.1 g were used to estimate the heat via Equation 3.2 [415,416], where we calculate Q, the heat energy transferred in joules (J) - Figure 3.3.

$$Q = q \times \Delta T \times m \quad \text{(Equation 3.2)}$$

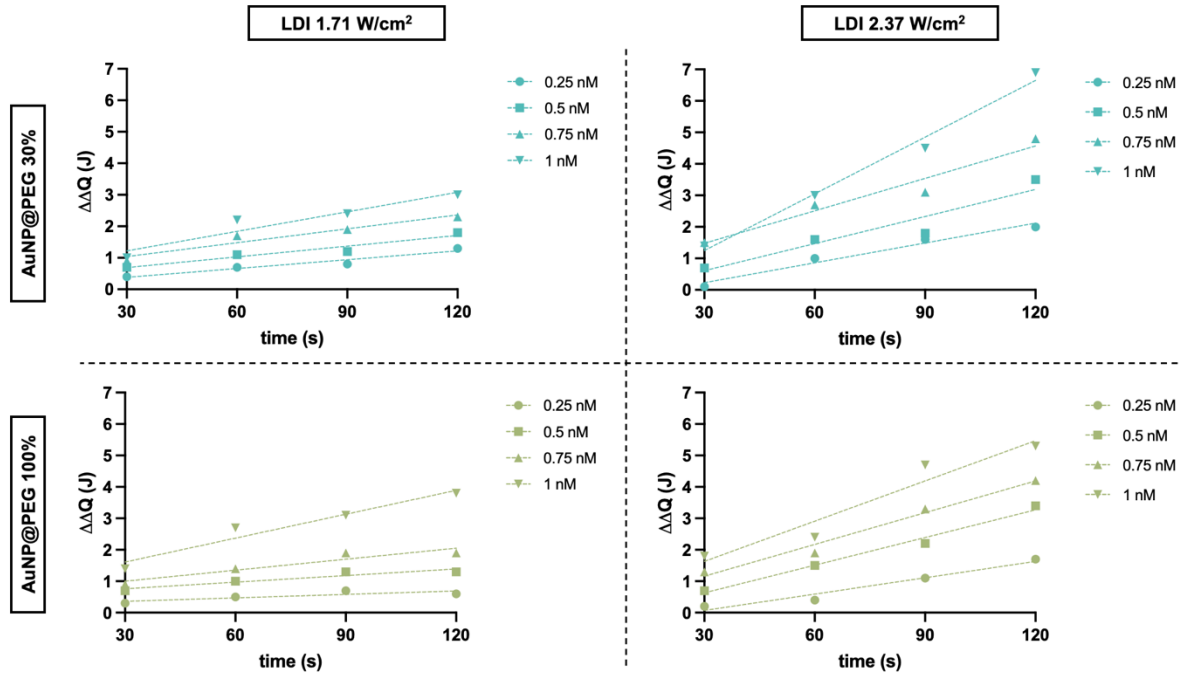

Figure 3.3 - Heat capacity of Au-nanoconjugates. The heat generated by the AuNP@PEG 30% and AuNP@PEG 100% was measured for different exposure times and concentrations of Au-nanoconjugates in water irradiated with LDI 1.71 W/cm² or LDI 2.37 W/cm².

Pegylated AuNPs have comparable photothermal effect when irradiated by the same LDI. Comparing the different conditions tested, LDI 2.37 W/cm² potentiates the heat generated by the Au-nanoconjugates compared to LDI 1.71 W/cm². Nonetheless, when Au-nanoconjugates were irradiated for 60 s with LDI 2.37 W/cm² and for 90 s with LDI 1.71 W/cm², the heat capacity of the Au-nanoconjugates was quite similar. We further used these setting conditions to calculate the heat generated per second by the Au-nanoconjugates, which was determined by dividing the total heat generated per assay by the number of nanoparticles, and then by the irradiation time selected: 90 s for LDI 1.71 W/cm² and 60 s for 2.37 W/cm² – Figure 3.4. The number of nanoparticles was estimated using the Avogadro number and the Beer-Lambert law [396,417].

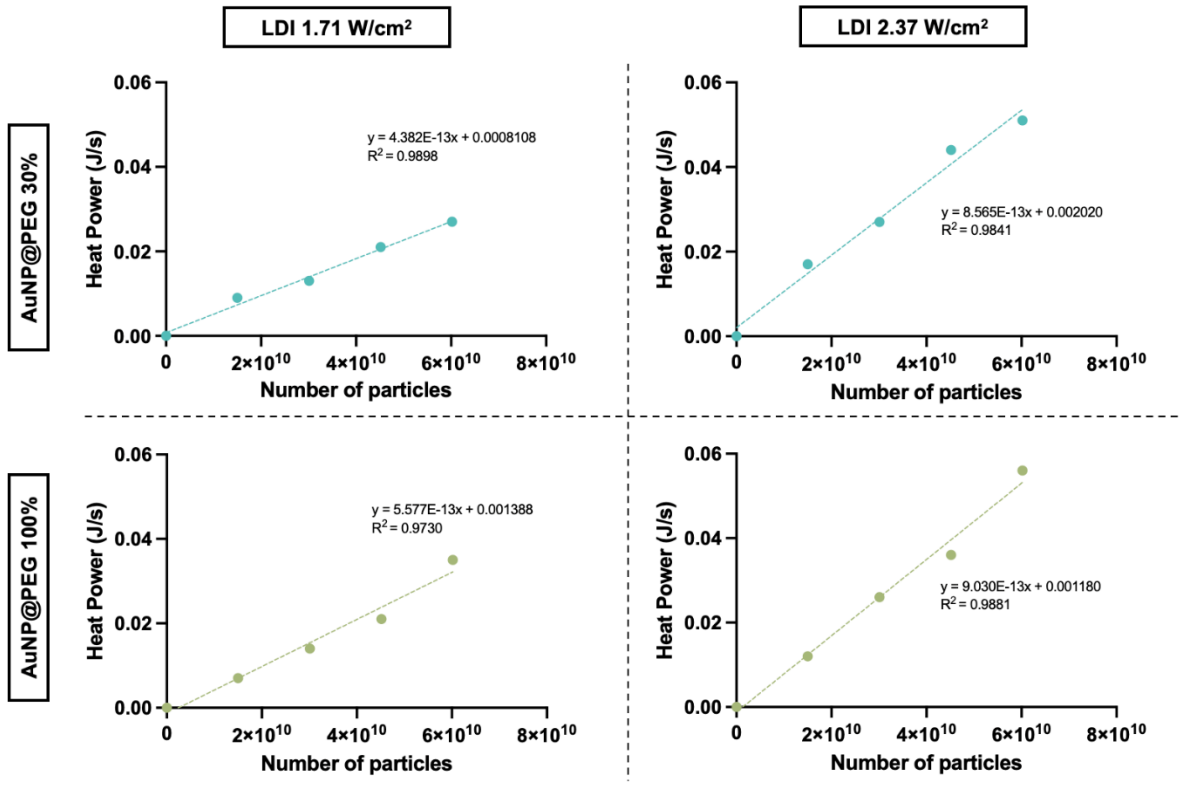

Figure 3.4 - The heat generated per second of Au-nanoconjugates. Four concentrations of AuNP@PEG 30% and AuNP@PEG 100% were irradiated at 1.71 W/cm² for 90 seconds or 2.37 W/cm² for 60 seconds in water. The temperature variation was measured to calculate heat generated per second as a function of the number of particles irradiated. The slope of the curve gives the heat generated per nanoparticle per second.

Under these conditions, the photothermal effect for LDI 1.71 W/cm² and LDI 2.37 W/cm² was determined to be 4.4 x 10^{-13} W and 8.9 x 10^{-13} W per particle for AuNP@PEG 30%, and 5.6 x 10^{-13} W and 9.0 x 10^{-13} W per particle for AuNP@PEG 100%, respectively. For mild hyperthermia, a target temperature of 41 - 42°C is desirable [396], corresponding to the ΔT values of 4 - 5°C attained for both types of pegylated AuNPs upon 60 s laser irradiation with 2.37 W/cm² (total energy of 47 J). Nevertheless, this value depends on irradiation power settings and is not comparable with other laser intensities or photothermal capacitates. Factors such as the extinction coefficient and the photothermal conversion efficiency of the photothermal agents, as well as the properties of laser light (e.g., different wavelengths), must be considered for the success of photothermal therapy [410,418–420]. Also, we observed that these settings conditions do not affect the optical properties of Au-nanoconjugates, since their LSPR was maintained after irradiation (Figure 3.5). Altogether, these settings were considered to achieve mild hyperthermia effect in cells and shall be used in further biological studies.

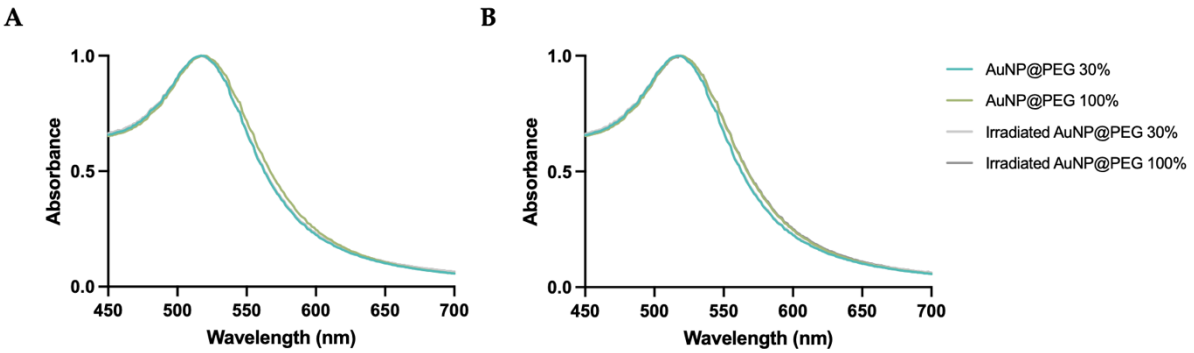

Figure 3.5 - Normalized absorbance UV-Vis spectra of irradiated and non-irradiated Au-nanoconjugates. Au-nanoconjugates were irradiated at (A) LDI 1.71 W/cm² for 90 s and (B) LDI 2.37 W/cm² for 60 s in water.

3.3.3 Stability assays

The stability of AuNPs is important for therapeutic applications, particularly to better understanding the nanoparticles' behavior *in vivo* conditions. AuNPs are prone to aggregation when not coated with a capping agent (e.g., citrate) or not functionalized with a surface polymer (e.g., PEG), which induces electrostatic stabilization of the AuNPs. In biological systems, nanoparticles must have to resist the ionic strength of diverse media conditions, to preserve their physical-chemical properties, especially SPR [421]. SPR is a unique optical property of noble metal nanoparticles and is highly sensitive to factors, such as size, shape, solvent environment, surface ligands and charge, temperature, pH, and ionic strength of the media [159]. Hence, it is essential to maintain stable SPR optical properties to enable effective photoconversion when irradiated with visible light irradiation. First, the stability of Au-nanoconjugates was studied in DMEM without phenol red and without FBS, to avoid the formation of protein corona. In Figure 3.6A we observed a slight LSPR deviation to 522 nm in AuNP@PEG 100% while AuNP@PEG 30% are prone to aggregation, with a red shift to 550 nm. AuNPs tend to be less stable in DMEM without FBS due to the absence of serum proteins and the presence of positive divalent ions (e.g., Ca^{2+} and Mg^{2+}) which can cause AuNPs aggregation by reducing the electrostatic repulsion between nanoparticles. AuNP@PEG 100% is more stable than AuNP@PEG 30% owing to the large amount of PEG chains present on the AuNPs' surface that ensure AuNPs stability. Nevertheless, DMEM supplemented with 10% FBS is recommended for biological applications with functionalized AuNPs since it increases the stability of AuNPs due to protein corona formation, providing steric hindrance and preventing nanoparticles aggregation [422].

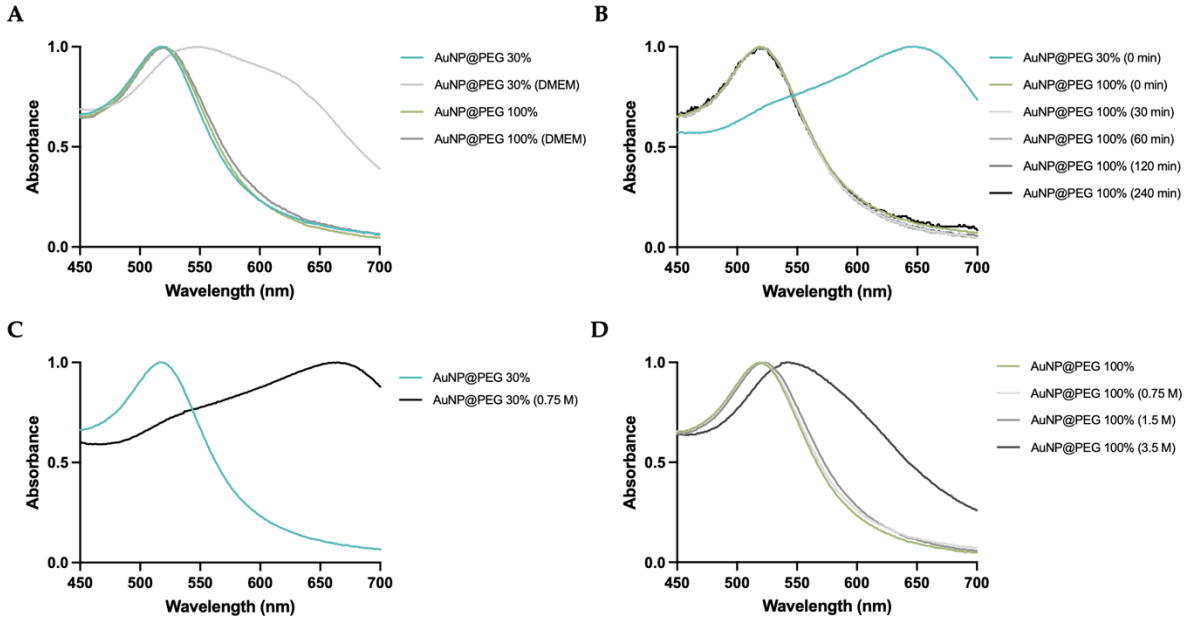

Figure 3.6 - Normalized UV-Vis spectra of Au-nanoconjugates in different media conditions. (A) UV-Vis spectra of Au-nanoconjugates in DMEM without FBS and respective Control (B) UV-Vis spectra of Au-nanoconjugates in PBS until 240 minutes. (C) UV-Vis spectra of AuNP@PEG 30% in NaCl 0.75 M and respective Control. (D) UV-Vis spectra of AuNP@PEG 100% with different concentrations of NaCl and respective Control.

The stability of the Au-nanoconjugates was also studied with PBS or different concentrations of NaCl (0-3.5 M) to simulate the osmolarity and ion concentration of biological systems. Figure 3.6B shows an LSPR red shift to 646 nm in AuNP@PEG 30% exposed to PBS (0 min), indicating the increase in AuNPs size. AuNP@PEG 30% were not entirely covered by PEG which led to a slight resistance to ionic strength and prone to aggregation. On the other hand, the LSPR of AuNP@PEG 100% is maintained for 240 minutes, which suggests that AuNPs coverage with 100% PEG are the most stable in PBS. AuNP@PEG 30% exposed to 0.75 M NaCl solution present a red shift of LSPR to 665 nm (Figure 3.6C), while AuNP@PEG 100% present higher resistance to the osmolarity and variation of the ionic strength (Figure 3.6D). AuNP@PEG 100% only present an LSPR red shift to 543 nm when exposed to 3.5 M NaCl solution. These results demonstrate that AuNPs' surface covered 100% with PEG are more suitable for biological applications. Herein, we shall use AuNP@PEG 100% to study the impact of visible laser irradiation combined with Au-nanoconjugates on cell viability, and cell uptake.

3.3.4 Cytotoxic and viability assays of HCT116 cells

To assess the effect of the selected conditions for mild hyperthermia in cells, HCT116 colorectal carcinoma cells were incubated for 4 h with 10 nM AuNP@PEG 100%, with or

without irradiation. We measured the initial and final temperature of irradiation exposure, which confirms the temperature variation (ΔT) around 5°C in sample AuNP@PEG+Laser (Table 3.2).

Table 3.2 - Temperature measurements of the DMEM without phenol red before and after irradiation in HCT116 cells.

	ΔT (°C)	
LDI	**Control+Laser**	**AuNP@PEG+Laser**
1.71 W/cm², 90 s	1.9 ± 0.5	5.1 ± 1.1
2.37 W/cm², 60 s	2.1 ± 0.6	5.4 ± 1.5

Some reports described that cancer cells may exhibit thermosensitive above 40°C, potentially leading to alterations in the permeability of their membranes [418,423]. Considering that, irradiated and non-irradiated cells were incubated with Trypan Blue 0.4% (m/v) solution and the images were acquired in a bright field inverted microscope. Trypan Blue is a dye impermeable to live cells that can penetrate necrotic cells or cells with permeable compromised membranes [424]. Our data show that HCT116 cells did not stain with Trypan Blue dye (Figure 3.7), proving that the integrity of the cell membrane was not compromised by these setting conditions, despite the slight increase in the temperature. For instance, our group previously reported that 52°C (thermal ablation) is the minimum final temperature necessary to impact cell membrane integrity and subsequently stained the cells with Trypan Blue dye [396].

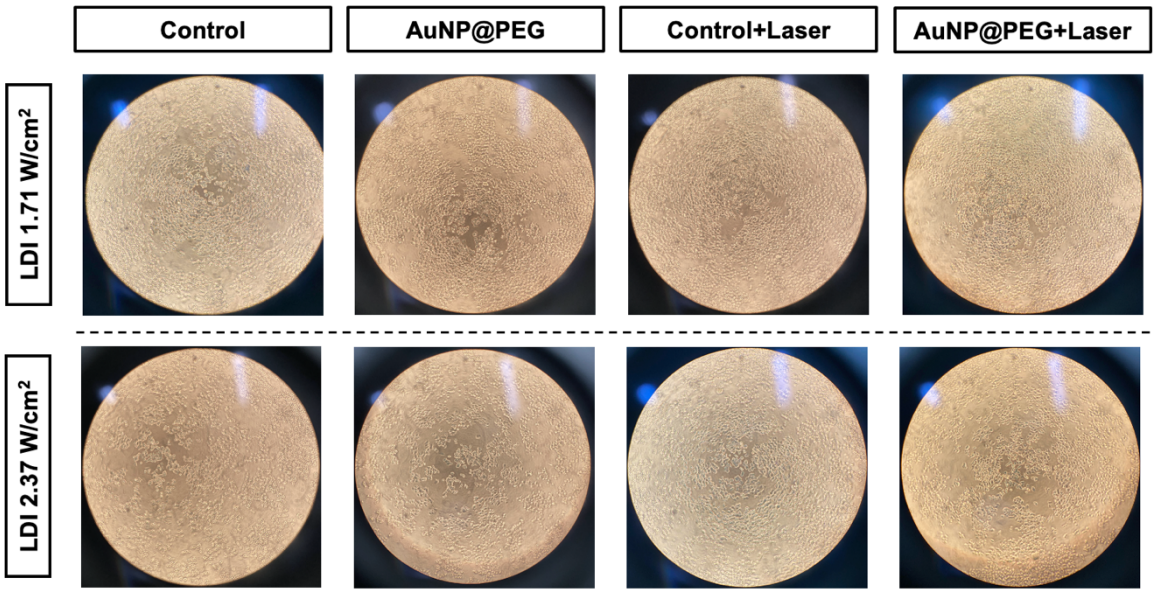

Figure 3.7 - Trypan Blue exclusion assay of HCT116 cells. Images of non-irradiated and irradiated HCT116 cells, with and without previous incubation for 4 h of 10 nM of AuNP@PEG 100%. Cells were irradiated under LDI 1.71

W/cm² for 90 s and 2.37 W/cm² for 60 s, upon Au-nanoconjugates incubation. Then, cells were incubated with Trypan Blue dye for 10 minutes in all sample conditions, and images were taken immediately after in a bright field using an inverted microscope.

HCT116 cell viability was further assessed by the MTS assay following 4 h of incubation with 10 nM of AuNP@PEG 100%, with or without irradiation. The MTS assay specifically relies on the activity of mitochondrial enzymes, such as dehydrogenases, which indicate functional and metabolically active cells [425,426]. The MTS data indicate that pegylated AuNPs, with or without laser irradiation, do not have an impact on cell viability (Figure 3.8).

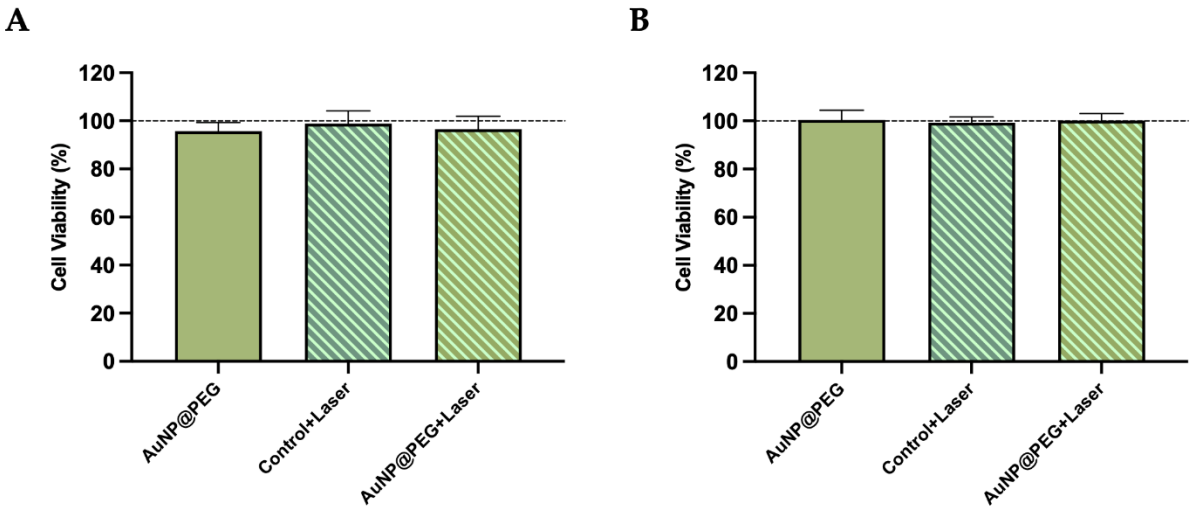

Figure 3.8 - Cell viability assay of HCT116 cells. Cell viability analysis of the irradiated and non-irradiated cells incubated for 4 h with AuNP@PEG 100% via MTS assay using (A) LDI 1.71 W/cm² for 90 s and (B) LDI 2.37 W/cm² for 60 s. The conditions tested were normalized to Control (untreated cells). Statistical differences were not observed between all the samples tested with the Control. Data represent the mean value ± the standard error of the mean of at least three biologically independent experiments with two technical replicates for each.

To complete the cell viability assessment, we used the LDH assay to evaluate simultaneously the cell's membrane permeability and integrity. This assay measures cytotoxicity by quantifying the LDH release in the cell culture medium and could indicate permeability and/or cell membrane damage [426,427]. Results show that AuNP@PEG 100% combined with laser irradiation might increase cells' membrane permeability using LDI 2.37 W/cm² for 60 s, but without compromising membrane integrity as corroborated by the Trypan Blue exclusion assay (Figure 3.9). Considering all the experiments, we select LDI 2.37 W/cm² for 60 s for future mild hyperthermia experiments.

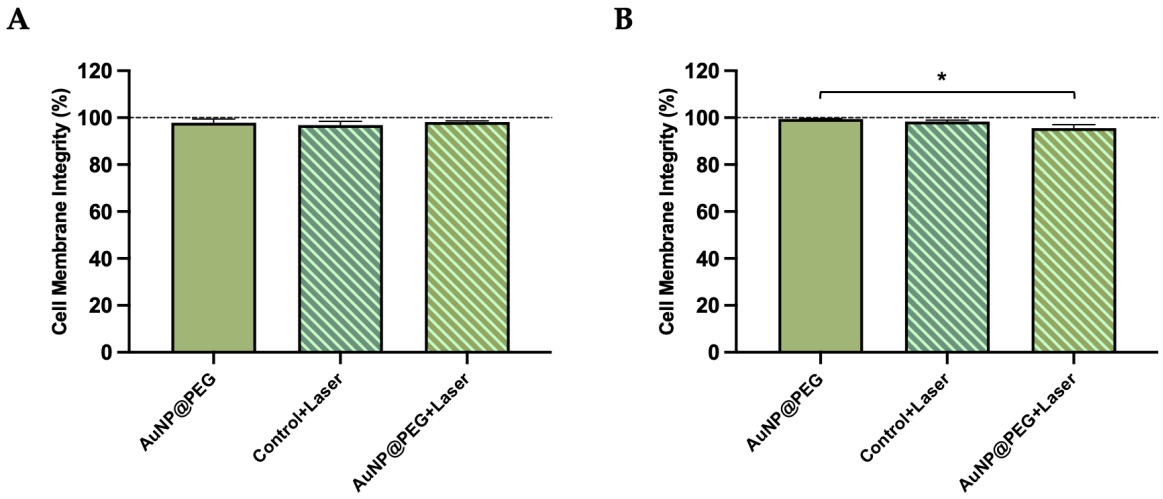

Figure 3.9 - Cell membrane integrity of HCT116 cells via LDH assay. Cell membrane integrity analysis of the irradiated cells with (A) LDI 1.71 W/cm² for 90 s and (B) LDI 2.37 W/cm² for 60 s, and non-irradiated cells incubated with AuNP@PEG 100% for 4 h. Statistical differences were observed between AuNP@PEG+Laser with the Control (untreated cells) and AuNP@PEG sample with LDI 2.37 W/cm² for 60 s (*$p < 0.05$; Unpaired parametric t-test with Welch's correction). Data represent the mean value ± the standard error of the mean of at least three biologically independent experiments with two technical replicates each.

3.3.5 Laser irradiation-induced Au-nanoconjugates uptake

TEM and ICP-AES were used to assess the uptake of Au-nanoconjugates by cells. TEM images of HCT116 cells incubated for 4 h with AuNP@PEG 100% show internalization of AuNPs in small clusters (Figure 3.10). This clustering is commonly observed for the internalization of the AuNPs [428,429].

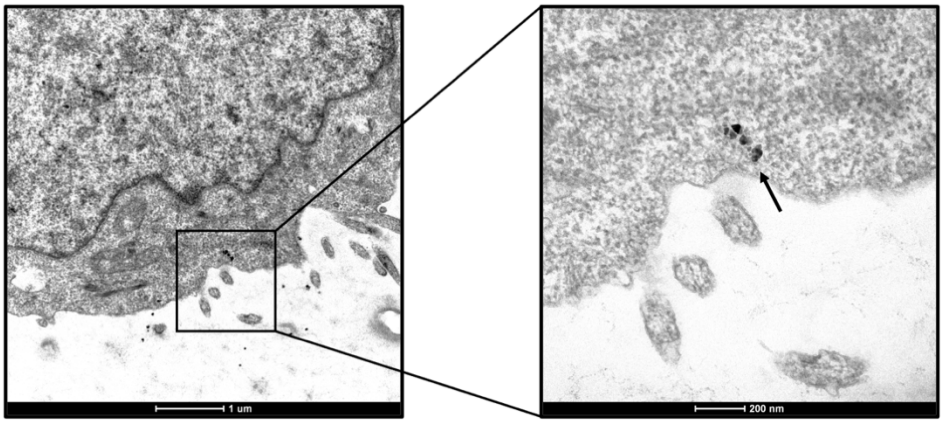

Figure 3.10 - TEM images of Au-nanoconjugate internalization at 4 h in HCT116 cells. Images of AuNP@PEG 100% clusters (indicated with a black arrow) inside HCT116 cells, observing more than four small dark clusters near the

cell membrane are visible due to the high electronic density of gold. Scale bars correspond to 1 μm and 200 nm, respectively.

Then, we determined the amount of gold inside the cells by ICP-AES in cells that were exposed to 10 nM of AuNP@PEG 100% for 2 h and 4 h either irradiated or non-irradiated. Data show that irradiated cells (AuNP@PEG+Laser) internalized approximately 1.4-fold more Au when compared to non-irradiated cells (AuNP@PEG) for 4 h of incubation (Figure 3.11). We hypothesize that the localized heat produced by irradiated AuNP@PEG somehow destabilizes the lipid bilayer, increasing fluidity and permeability, which allows an increase in the uptake of pegylated-AuNPs by cells. The creation of hotspots on the cell membrane has been observed since that influences the permeability of the membrane [430–432].

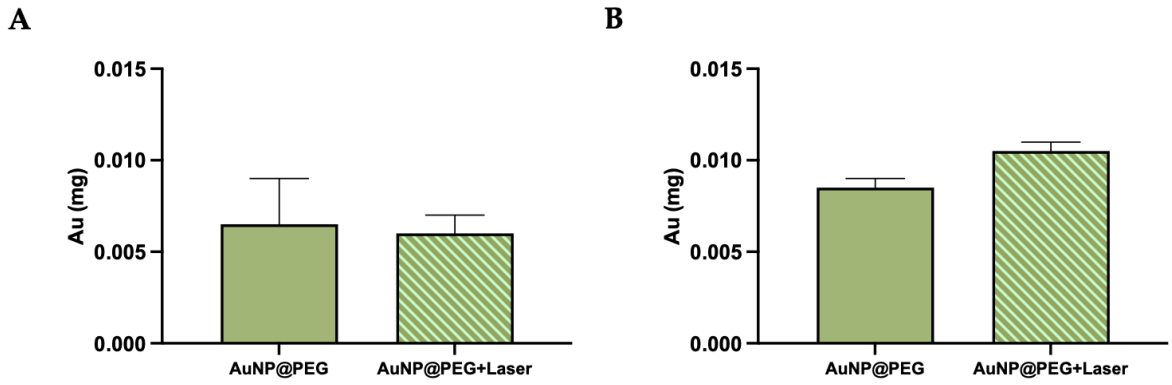

Figure 3.11 - Au uptake in irradiated and non-irradiated HCT116 cells at 2 h and 4 h. (A) ICP-AES analysis shows comparable Au uptake at 2 h between non-irradiated and irradiated cells, (B) and an increase of Au uptake in irradiated cells at 4 h exposed to 10 nM of AuNP@PEG 100%. Statistical differences were not observed between AuNP@PEG and AuNP@PEG+Laser samples. Data represent the mean value ± the standard error of the mean of an independent experiment with three technical replicates for each.

3.3.6 Proof-of-concept: transfection of nucleic acids via mild photothermy

3.3.6.1 Mild photothermy for pAcGFP1 Nuc Vector transfection in HCT116 cells

Initially, to determine that mild photothermy may be used to transfect nucleic acids, we used a plasmid that encodes an AcGFP1 optimized for high expression in mammalian cells (Cat. No 632431, Takara Bio Company). The protein expression can be easily monitored by fluorescence microscopy upon the accumulation of the AcGFP1 inside the nuclei of the cells. An efficient plasmid transfection and expression of the encoded protein are crucial to ensure a suitable and robust starting point to analyze the effect of mild photothermy via Au-nano-conjugates and visible laser irradiation for transfection.

In this regard, three main parameters play a key role in the optimization of the transfection of cells with the selected plasmid: cell confluency, pGFP quantity, and AcGFP1 expression post-transfection [189]. First, these parameters were optimized for an efficient plasmid transfection based on the use of Lipofectamine™ LTX with Plus Reagent, a standard commercial reagent for nucleic acid transfection [183]. First, cell confluency was adapted to be between 60% to 70%, as lower confluency percentages (< 50%) compromise cell transfection due to Lipofectamine™ LTX with Plus Reagent toxicity, and higher confluency (> 80%) reduces the surface area for an efficient transfection [189]. Once the cell confluency was optimized, the quantity of plasmid (0.25 and 0.5 μg/well) was evaluated. A standard protocol was followed, based on DMEM without FBS to avoid the interference of the cationic lipids with the serum proteins, and without antibiotics to minimize cytotoxicity effects derived from the increase of cell permeability provided by the cationic lipids. After 4 h or 24 h of cells incubation with Lipo+pGFP complexes, the cell culture medium was replaced with fresh supplemented DMEM and the analysis of AcGFP1 expression was performed by fluorescence microscopy at 24 h and 48 h post-transfection (Figure 3.12).

The impact of plasmid quantity and Lipo+pGFP complexes incubation in HCT116 cells morphology was also verified. We observed that incubation with Lipo+pGFP complexes for 4 h is adequate to obtain an optimal AcGFP1 expression at 24 h post-transfection, using 0.25 μg or 0.5 μg of pGFP quantity. Based on these results, we selected 0.25 μg (or less) plasmid quantity for subsequent mild photothermy experiments, using Lipofectamine™ LTX with Plus Reagent as a positive control for transfection.

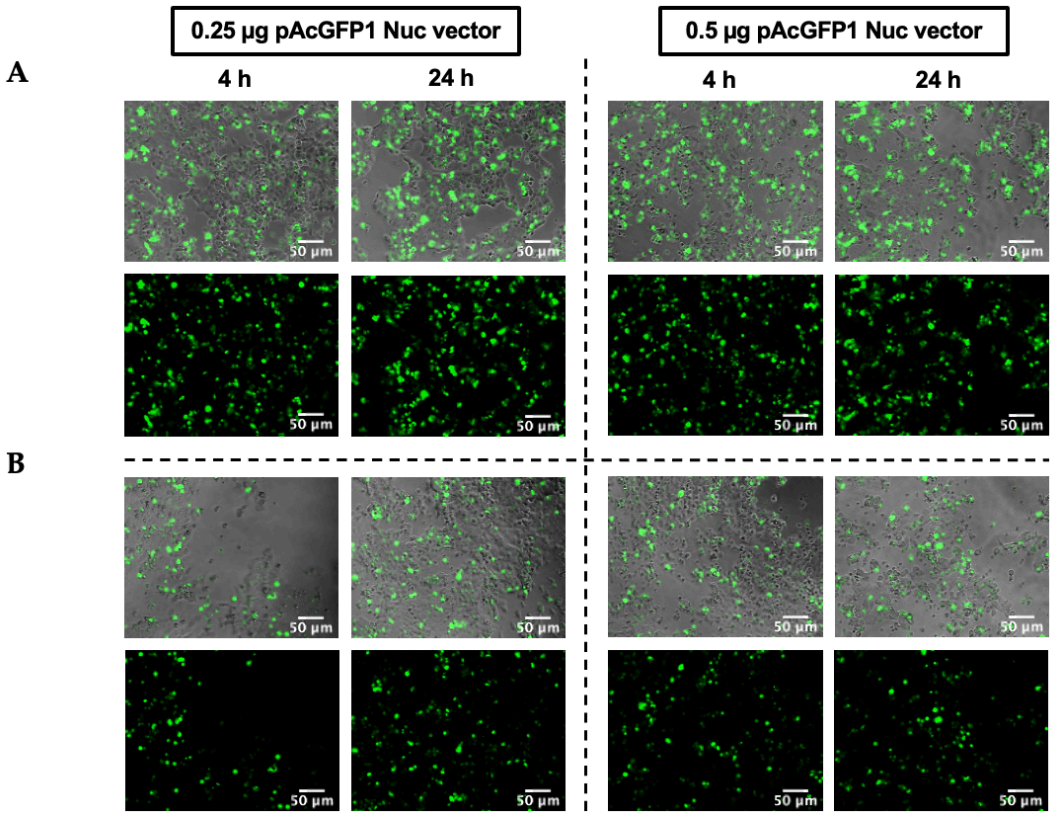

Figure 3.12 - Optimization of the quantity of pGFP for transfection with Lipofectamine LTX™ Plus Reagent. Fluorescence microscopy images were obtained for each amount of pGFP at (A) 24 h and (B) 48 h post-transfection in HCT116 cells. The Lipo+pGFP complexes were incubated for 4 h and 24 h in DMEM without FBS and antibiotics. Scale bars correspond to 50 µm.

Our previous experiments demonstrated that mild photothermy system is non-cytotoxic (Figure 3.8 and Figure 3.9) and has a slight effect on cells' membrane verified by the increase of AuNP@PEG uptake into HCT116 cells at 4 h of incubation (Figure 3.11), which might improve the permeabilization of the lipid bilayer for plasmid internalization. To transfect pGFP in HCT116 via mild photothermy, AuNP@PEG combined with laser irradiation were used. Cells were challenged with 10 nM of AuNP@PEG for 4 h at 37ºC. Later, the cell culture medium was replaced with DMEM without phenol red (37ºC) and 0.1 μg or 0.25 μg of pGFP was added for transfection before laser irradiation at 2.37 W/cm^2 for 60 seconds. The effect of mild photothermy for transfection of pGFP was evaluated by fluorescence microscopy at 24 h and 48 h, and compared to Lipofectamine™ LTX with Plus Reagent. Controls of irradiated cells and non-irradiated cells with or without AuNP@PEG were also performed. Figure 3.13 shows the efficient transfection of pGFP using Lipofectamine™ compared to other conditions tested (without AcGFP1 expression).

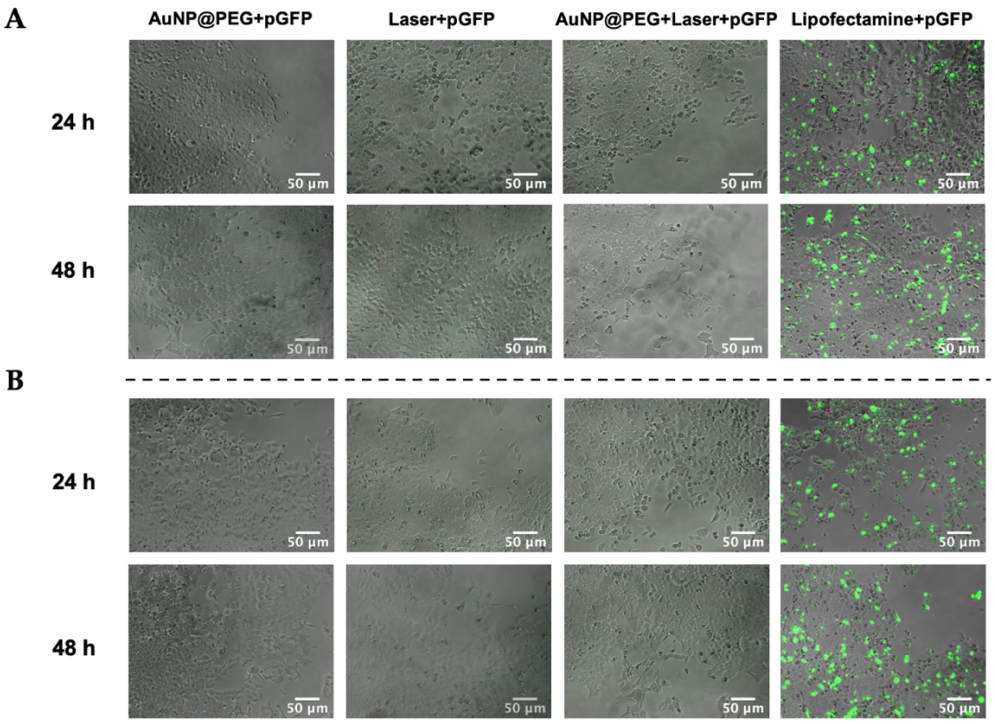

Figure 3.13 - Mild photothermy via Au-nanoconjugates combined with laser irradiation for pGFP transfection. Fluorescence microscopy images of HCT116 cells transfected with (A) 0.1 μg and (B) 0.25 μg of pGFP at 24 h and 48 h post-transfection. AcGFP1 expression was observed using Lipofectamine™. Scale bars correspond to 50 µm.

pGFP has an NLS sequence that significantly increases the efficacy of translocation of AcGFP1 into the nucleus of cells when transfection is well-succeeded. However, this mild photothermy strategy failed to transfect pGFP efficiently. Transfection of plasmid vectors using mild photothermy is a challenge owing to several factors, such as plasmid integrity and endosomal escape [433,434]. Primarily, pGFP needs to be near to cell membrane when irradiated AuNPs could mediate transient membrane disruptions. The effect of mild photothermy might not be enough to allow large plasmid molecules to pass through the lipid bilayer due to their negatively charged and high molecular weight [435]. On the other hand, a lack of endosomal escape might occur because pGFP failed to reach the nucleus (absence of AcGFP1 expression). For example, Vermeulen *et al.* revealed that using a yellow-green (561 nm) low-energy laser irradiation or higher-energy pulses and 10 nm spherical AuNPs were not able to induce efficient plasmid transfection in HeLa cervical adenocarcinoma cell line. One of the main reasons for transfection failure is plasmid integrity, and they also hypothesize that the pores formed in the endosomal membrane after heat generation are not large enough to allow the endosomal escape of plasmid molecules [435,436].

Despite these challenges, AuNPs have been already used to induce light-triggered endosomal escape and cytosolic delivery of several biomolecules (e.g., proteins, oligonucleotides) [358,437,438]. Based on these previous data, we considered mild photothermy via Au-nanoconjugates combined with visible light irradiation to enhance transfection of silencing

moieties, such as ASO. Silencing moieties are often designed to target mRNA in the cytoplasm and are significantly simpler in structure, which leads to a more effective delivery in the cells compared to plasmid vectors.

3.3.6.2 Mild photothermy for *AcGFP1* silencing in HCT116 cells

To demonstrate that mild photothermy may be used to improve the internalization of silencing moieties in HCT116 cells, AuNP@PEG and an *anti-GFP* were used (Figure 3.14). Firstly, a transient transfection model of HCT116 cells harboring a pAcGFP1 Nuc Vector was used as described in section 2.2.4. After 4 h of Lipo+pGFP complexes incubation, the cell culture medium was replaced by DMEM without phenol red, with or without 10 nM of AuNP@PEG for another 4 h at 37°C. Then, the cell medium was replaced with DMEM without phenol red at (37°C), and 20 nM of *anti-AcGFP1* was added before laser irradiation at 2.37 W/cm², for 60 seconds. The silencing efficiency between the commercially available Lipofectamine™ RNAiMAX and the mild photothermy mediated by the Au-nanoconjugates was compared for irradiated and non-irradiated cells, by assessing *AcGFP1* expression via RT-qPCR and fluorescence microscopy. A control with non-irradiated cells incubated with AuNP@PEG and the *anti-AcGFP1* (AuNP@PEG+ASO) was used to verify if the presence of AuNP@PEG could promote the intracellular delivery of ASO.

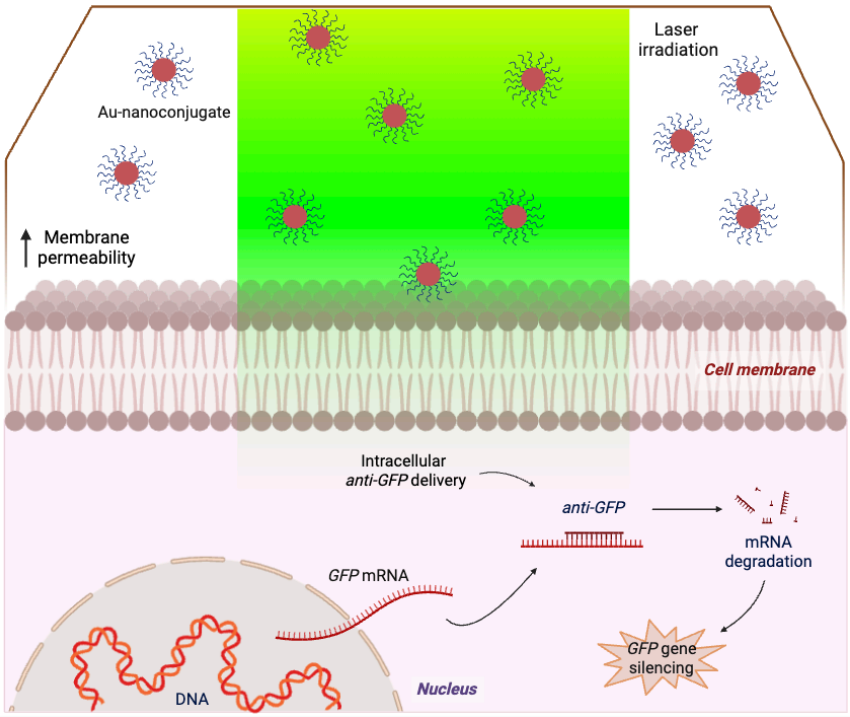

Figure 3.14 - Overall concept of the transfection of anti-*GFP* mediated by mild photothermy - AuNP@PEG+Laser+ASO. (Created with BioRender.com)

HCT116 cells transiently expressing AcGFP1 protein were observed in a fluorescence microscope after 24 h (Figure 3.15A). Due to the high levels of AcGFP1 protein expression induced by the human cytomegalovirus (CMV) promoter encoded in the pAcGFP1 Nuc Vector, the silencing effect of the *anti-AcGFP1* was masked from a protein fluorescence perspective. For this reason, the quantification of the silencing effect was performed at mRNA levels by RT-qPCR, which allows a higher sensitivity and accuracy. RT-qPCR data confirmed the silencing of *AcGFP1* for all conditions tested (Figure 3.15B). Irradiated cells with prior incubation with AuNP@PEG (AuNP@PEG+Laser+ASO), showed 70% lower *AcGFP1* expression compared to Control (cells without ASO, $2^{\Delta\Delta Ct} = 1$). This silencing effect was slightly more pronounced than that obtained for the Lipofectamine™ RNAiMAX reagent (approximately 65%). This might be due to irradiation causing the increased uptake of AuNPs, which in turn allows for a "dragging" effect of the oligonucleotide into the cell [439,440]. Additionally, non-irradiated cells with prior incubation of AuNP@PEG (AuNP@PEG+ASO) also showed a significant decrease (approximately 45%) of *AcGFP1* expression compared to control. Still, laser irradiation has proven a critical trigger for uptake of the silencing moiety since laser irradiation with AuNP@PEG (AuNP@PEG+Laser+ASO) reduces expression of *AcGFP1* 1.8-fold more than AuNP@PEG alone (AuNP@PEG+ASO).

None of these conditions showed any impact on cell viability as analyzed by the MTS assay (Figure 3.15C).

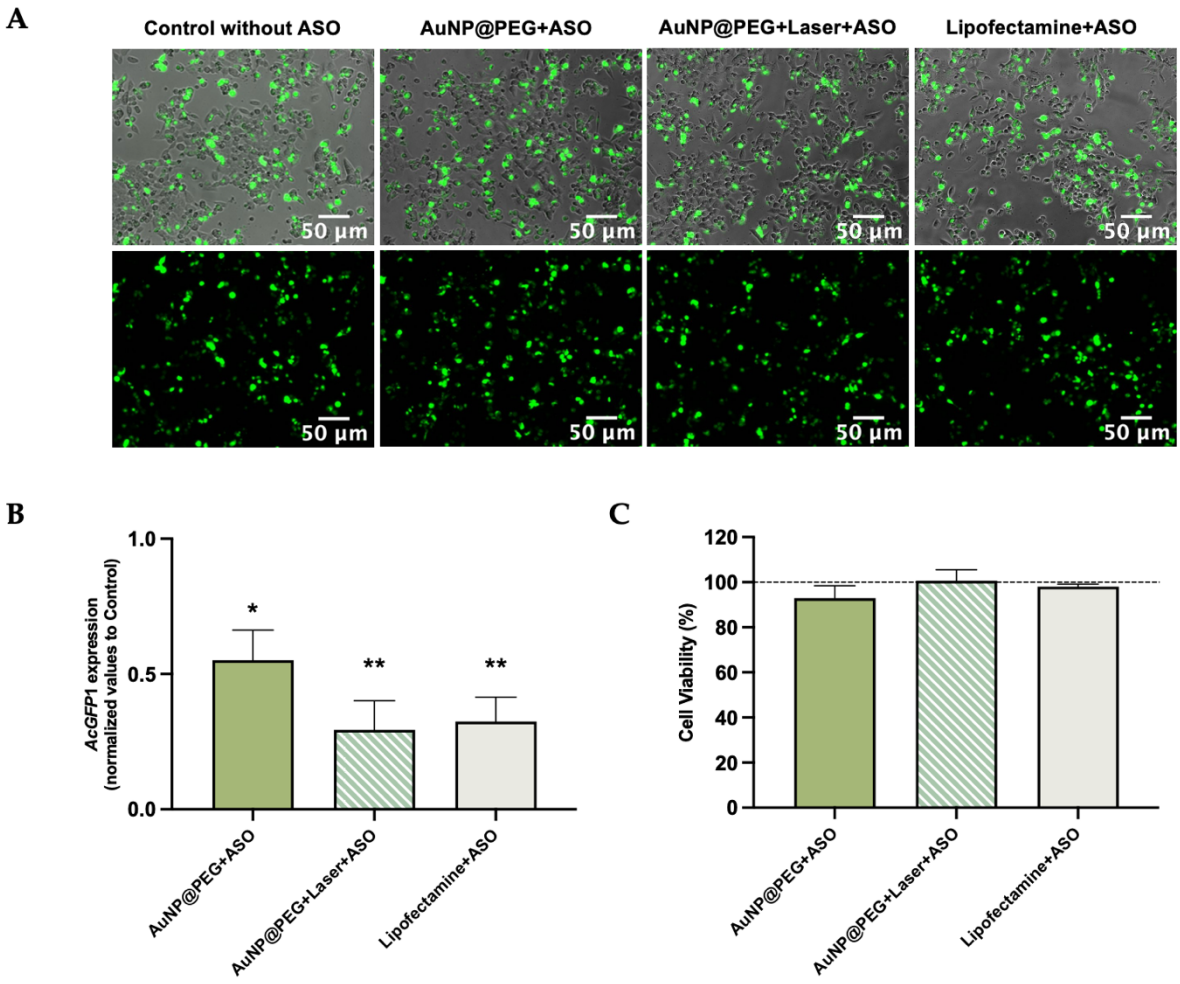

Figure 3.15 - Fluorescence microscopy images of HCT116 cells, RT-qPCR analysis, and cell viability assay. (A) Fluorescence microscopy images of HCT116 cells transiently expressing AcGFP1 protein 24 h after silencing experiment in the different conditions tested. Scale bars correspond to 50 µm. (B) *AcGFP1* gene expression in different conditions tested. Gene expression levels were normalized to the cells without *anti-AcGFP1* (Control, $2^{-\Delta\Delta Ct}=1$). Black asterisks indicate statistical differences between samples and Control (*$p < 0.05$; **$p < 0.01$; Unpaired parametric t-test with Welch's correction). Data represent the mean value ± the standard error of the mean of at least three biologically independent experiments with two technical replicates for each. (C) Cell viability analysis of the different samples tested after 24 h of *AcGFP1* silencing via MTS assay. The three conditions tested were normalized to Control. Statistical differences were not observed between all the samples tested with cell control without *anti-AcGFP1* (Control). Data represent the mean value ± the standard error of the mean of two biologically independent experiments with two technical replicates for each.

3.3.6.3 Mild photothermy for *copGFP* silencing in MCF-7/GFP cells

We then confirmed the robustness of our approach by using a constitutively expressed GFP model in the MCF-7 breast adenocarcinoma cell line, which has been reported to be more difficult to transfect with silencing moieties than the colorectal model cell line HCT116 [441,442]. The MCF-7 cell line is derived from a pleural effusion acquired from metastatic breast cancer

and is frequently used as a model of estrogen-positive breast cancer. Besides that, MCF-7 cells can be addressed as an interesting model for the development of novel therapies against breast cancer due to their remarkable genetic characteristics, such as chromosomal instability and clonal heterogeneity [443,444]. Several commercial viral and non-viral transfection reagents have been reported as suitable for the transfection of nucleic acids in MCF-7 cells [189]. However, MCF-7 cells typically grow in clumps or clusters, which difficult the transfection and the uptake of the therapeutic cargo due to a lower exposure of the cell's membrane surface.

Cells were incubated with 10 nM of AuNP@PEG for 4 h at 37°C before irradiation (AuNP@PEG+Laser+ASO). The cells' culture medium was replaced with DMEM without phenol red at (37°C) containing 20 nM of *anti-copGFP* and irradiated at 2.37 W / cm^2 for 60 seconds. Irradiated and non-irradiated cells were subsequently incubated for 6 h or 24 h, and *copGFP* expression was analyzed by RT-qPCR and fluorescence microscopy at each time-point (Figure 3.16).

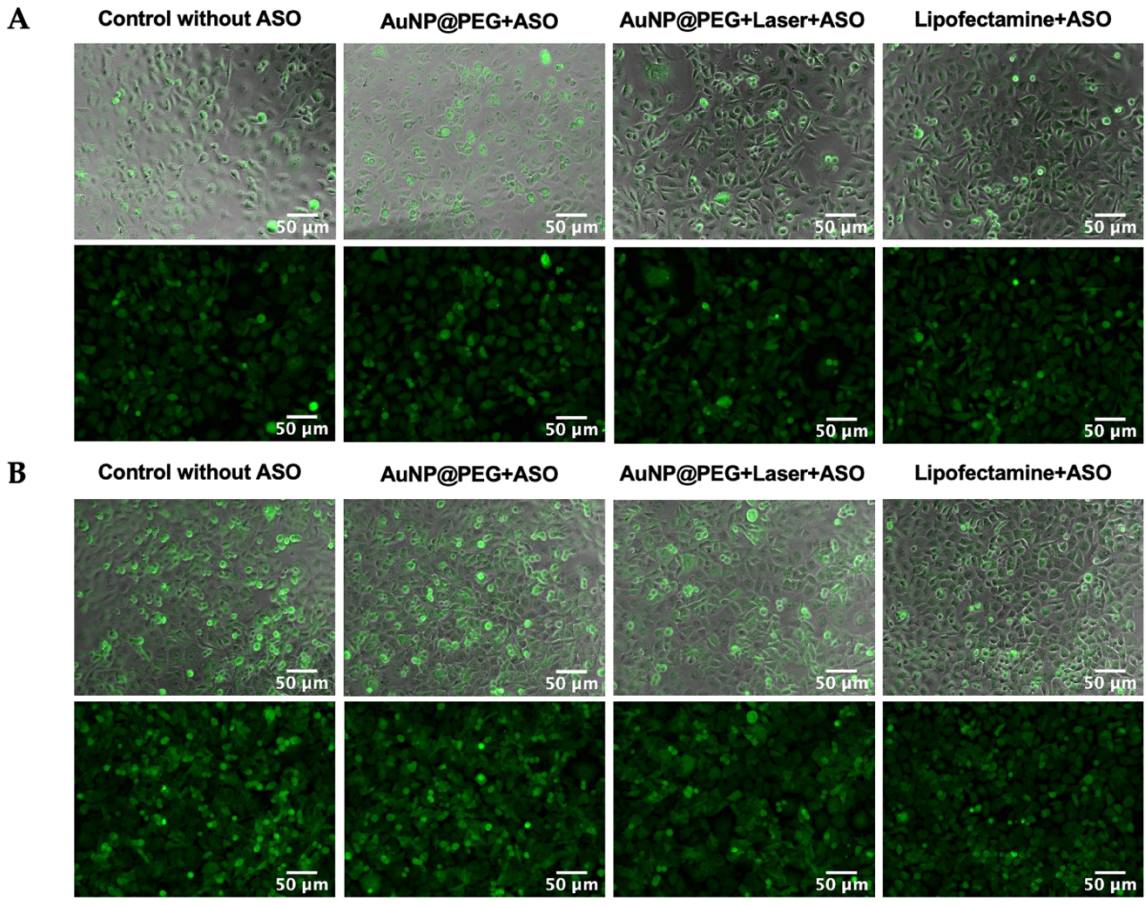

Figure 3.16 - Fluorescence microscopy images of MCF-7 cells constitutively expressing *copGFP* gene. The different conditions were tested at (A) 6 h and (B) 24 h after the silencing experiment. Scale bars correspond to 50 µm.

Mild photothermy via Au-nanoconjugates (AuNP@PEG+Laser+ASO) significantly reduced *copGFP* expression by 50% at 6 h and 24 h - see Figure 3.17A. This silencing efficacy is

comparable to that attained for the commercial Lipofectamine™ reagent (Lipofectamine+ASO). The quantitative analysis of CTCF of microscopy images at 6 h and 24 h post-transfection corroborates the silencing of gene expression. A similar reduction of copGFP protein expression can be observed at 6 h and 24 h for AuNP@PEG+Laser+ASO and Lipofectamine+ASO - Figure 3.17B. Several reports describe the cytotoxicity of cationic lipid reagents [445,446]. In fact, our mild photothermy approach for oligonucleotide transfection does not have an impact on the cells' viability contrary to Lipofectamine™ reagent – see Figure 3.17C.

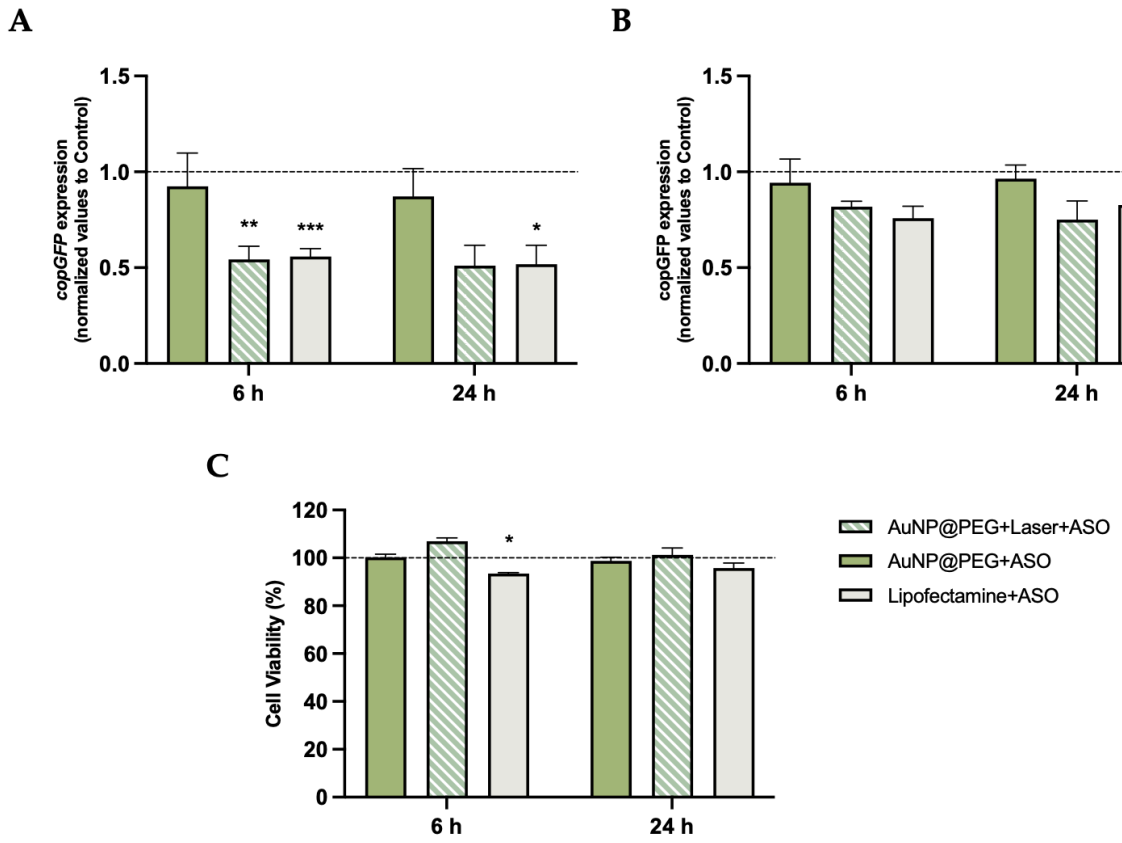

Figure 3.17 - RT-qPCR analysis, CTCF evaluation of the fluorescence microscopy images of MCF-7/GFP cells, and cell viability assay. (A) *copGFP* gene expression in different conditions tested at 6 h and 24 h. Gene expression levels were normalized to the cells without *anti-copGFP* (Control). Black asterisks denote statistical differences between samples and the Control, $2^{-\Delta\Delta Ct}=1$ (*$p < 0.05$; **$p < 0.01$; ***$p < 0.001$; two-way ANOVA - Mixed-effects analysis with Tukey's multiple comparison test). Data represent the mean value ± the standard error of the mean of at least three biologically independent experiments with two technical replicates for each. (B) CTCF analysis to evaluate copGFP protein expression at 6 h and 24 h post-ASO transfection. Statistical differences were not observed between all the samples tested with cells without *anti-copGFP* (Control). Data represent the mean value ± the standard error of the mean of two biologically independent experiments with three technical replicates each. (C) Cell viability analysis of the different samples tested after 6 h and 24 h of *copGFP* silencing via MTS assay. The three conditions tested were normalized to control. Statistical differences were observed between the cells treated with Lipofectamine™ (Lipofectamine+ASO) and cells without *anti-copGFP* (Control) (*$p < 0.05$; **$p < 0.01$; ***$p < 0.001$; two-way ANOVA - Mixed-effects analysis with Tukey's multiple comparison test). Data represent the mean value ± the standard error of the mean of at least three biologically independent experiments with two technical replicates each.

Overall, mild photothermy might trigger modification of the fluidity and permeability of the cell membrane, potentiating the uptake of ASO against *GFP*. PTT via visible light irradiation and AuNPs as photothermal agents to improve internalization of (bio)molecules are supported by previous reports of our group [396,403,404,411]. Nevertheless, the usage of this approach was only based on photothermal ablation to enhance the cytotoxic effect of doxorubicin [396,403], metallic compound [411], and anti-angiogenic peptide [404]. Using photothermal ablation increases cell death by cell membrane disruption and protein denaturation, while using mild photothermy might improve transfection of nucleic acids, without cytotoxicity. The increase in cell membrane fluidity enhances cellular uptake and promotes endosomal escape for nucleic acids release, which altogether potentiate the gene delivery efficacy [241]. Heinemann *et al.* demonstrated a transfection efficiency of 88% of a fluorescent-labeled *anti-GFP* siRNA, using a 532 nm Nd:YAG microchip laser emitting 850 ps pulses at a repetition rate of 20.25 kHz in ZMTH3 canine pleomorphic adenoma cells stably transfected with pd2-EGFP-N1, while maintaining a high cell viability [361] . This study reported that the effect of 200 nm AuNPs nonspecifically attached to the cell membrane combined with single laser pulses allows for membrane permeabilization. Compared to other laser types used for photoporation (e.g., femtosecond pulsed laser and nanosecond pulsed laser), CW lasers have been described as creating pores on the cell membrane based on localized heating. The increase in the temperature that changes the membrane dynamics can induce cell membrane permeability, leading to the transfection of exogenous molecules [447–450].

We consider that our mild photothermy strategy could lead to the development of a universal methodology to enhance the delivery of (therapeutic) nucleic acids (vectorized or not with AuNPs), whereas further studies of the thermal adaption of cellular membrane and the exact cellular mechanisms of internalization are required.

3.4 Conclusions

In this chapter, we synthesized and characterized spherical AuNPs with a core diameter of 12 nm, successfully functionalized with PEG for enhanced stability and biocompatibility. Photothermal experiments demonstrate that AuNPs are remarkable photothermal agents that can efficiently generate heat under green laser irradiation. These Au-nanoconjugates display similar heat generation, but AuNP@PEG 100% exhibits greater stability across different ionic strengths and media conditions. Cytotoxicity and viability assays reveal that AuNP@PEG with or without irradiation do not affect cell viability and cell membrane integrity. Still, a slight increase in membrane permeability is observed using LDI 2.37 W/cm² for 60 seconds, which might indicate a mild hyperthermia effect in HCT116 cells. Additionally, AuNP@PEG show higher cellular uptake in irradiated cells compared to non-irradiated cells after 4 hours, possibly due to the localized heating effect that might enhance membrane permeability.

Later on, we have shown that mild hyperthermia via Au-nanoconjugates and green laser irradiation continues to be a challenge for transfection of plasmid vectors, but it might be a safer and non-cytotoxic alternative to conventional transfection methods, for the delivery of (therapeutic) nucleic acids, enabling precise spatiotemporal control over laser irradiation. Herein, we presented two refined methods as proof-of-concept, demonstrating that our mild photothermy approach achieved comparable gene silencing to that of a commercial Lipofectamine™ reagent but with less cytotoxic effect on the MCF-7/GFP cells. Given that spherical AuNPs are recognized as effective vectors for delivering silencing moieties (e.g., ASO, siRNA, miRNA), we will further explore the internalization of ASO-functionalized AuNPs via mild photothermy in 2D models and their application in more complex 3D tumor models (spheroids) for *c-MYC* oncogene silencing (Chapter 4).

4

MILD PHOTOTHERMY TRIGGERED ASO DELIVERY FOR GENE SILENCING OF *C-MYC* ONCOGENE

Data enclosed in this chapter were originally published in the following issue and I was responsible for AuNPs and Au-nanoconjugates synthesis and characterization, laser irradiation and gene silencing experiments, immunofluorescence assays, cell cytotoxicity assessment, gene expression assays and statistical analysis.

Ferreira, D., Fernandes, A.R. & Baptista, P.V. Mild hyperthermia via gold nanoparticles and visible light irradiation for enhanced siRNA and ASO delivery in 2D and 3D tumour spheroids. *Cancer Nano* 15, 19 (2024). https://doi.org/10.1186/s12645-024-00256-4

4.1 Introduction

Gene therapy holds great potential to silence genes involved in tumor development and metastasis, such as *c-MYC* proto-oncogene. In fact, the literature reported that some pivotal oncogenes drive the uncontrolled growth and proliferation of cancer cells [146,241,451]. Gene silencing has been proposed as a powerful tool to silence target oncogenes, relying on TNAs (e.g., siRNA or ASO) to improve cancer therapeutics. However, its widespread application has limitations based on the delivery of naked nucleic acids (e.g., poor selectivity, off-target effects, and low circulation time due to the actuation of nucleases) [1,452]. Ideally, these agents should be vectorized into target cells with maximal transfection efficiency and minimal toxicity, preferably with spatiotemporal control over the uptake [453–455].

Nanomedicines have emerged as cutting-edge tools to tackle cancer cells, where promising strategies for gene silencing involve nanoparticles to effectively deliver nucleic acids that might enable precise control over gene expression through RNAi and ASO mechanisms. AuNPs have paved the way for an efficient delivery of silencing moieties due to their ease of functionalization with ASO while minimizing off-target effects and immune responses, and their ability to fine-tune their size, shape, and surface properties [1,452]. Moreover, AuNPs offer the possibility of spatiotemporal triggering of cell uptake through light irradiation due to their unique optical properties. For instance, Braun *et al.* reported that hollow gold nanoshells conjugated with siRNA and Tat peptides for cellular uptake were trapped within endosomes, which could escape upon exposure to a pulsed NIR laser, allowing the release of siRNA into the cytosol [456].

Although widely used in cancer research, 2D models fail to fully replicate the complexity of the in vivo environment, driving the demand for novel targeted therapies. To bridge the gap between experimental assays and patient tumor responses, more advanced and physiologically relevant models have been developed [2,457,458]. 3D models recapitulate the *in vivo* TME to closely resemble tumor growth and progression, which are necessary to better evaluate therapeutic responses [459,460]. The formation of cell-to-cell and cell-matrix interactions in 3D cell cultures (e.g., multicellular tumor spheroids and organoids) is a pivotal link between 2D cultures and animal models [461,462]. Spheroids are excellent *in vitro* 3D models that can mimic the structure of tumors owing to the formation of a gradient of nutrients, oxygen, pH, and metabolism products, and can also recreate some of their mechanisms, such as hypoxia and acidosis [459,463,464]. Recent studies reported that 3D tumor models exhibit similar spatial organization, gene and protein expression patterns, signaling pathways activation status, and drug resistance mechanisms to those observed *in vivo* [2,465,466].

Herein, we used visible light irradiation to enhance the internalization of ASO-functionalized AuNPs, enabling controlled and increased oligonucleotide delivery into 2D cell cultures and 3D tumor spheroids for targeted *c-MYC* gene silencing (Figure 4.1).

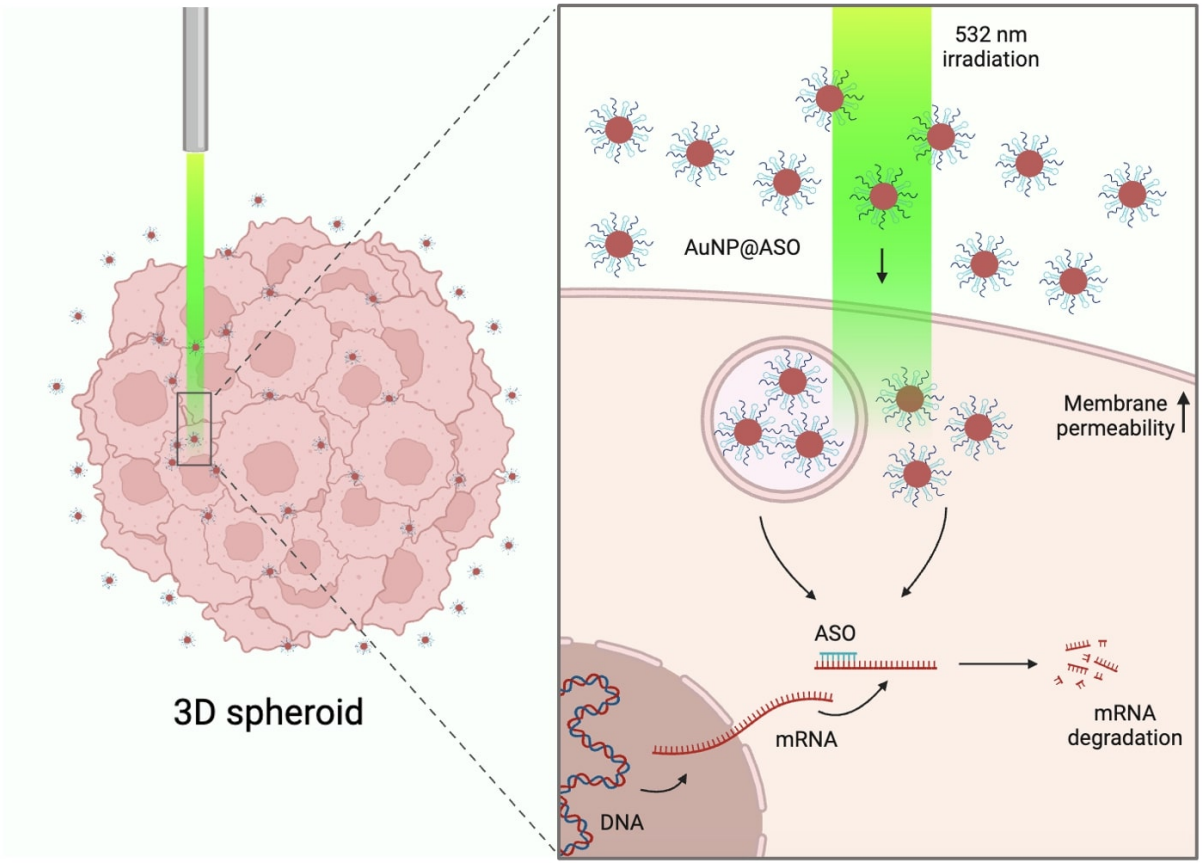

Figure 4.1 - Overview of the general concept for intracellular delivery of silencing nucleic acids in 3D tumor spheroid. The localized irradiation promotes nanoparticle uptake and effective delivery of ASO for gene silencing - triggered by mild hyperthermia. (Created with BioRender.com)

4.2 Materials and Methods

4.2.1 AuNP and Au-nanoconjugates synthesis and characterization

AuNP and Au-nanoconjugates were synthesized, functionalized, and characterized as described in section 2.2.1 (Chapter 2).

AuNPs with a 30% coverage of PEG (AuNP@PEG 30%) were prepared and subsequently functionalized with a thiolated stem-looped ASO complementary to the *c-MYC* transcript (GenBank NM_002467.5; AuNP@*c-MYC*) and a *scramble* oligonucleotide (AuNP@*scramble*) as a control, as previously described by our group [390,452]. ASO were added at a 1:150 AuNP: oligonucleotide proportion (as optimized by Oliveira *et al.*) after thiol reduction with 0.1 M of DTT and subsequent purification using a NAP-5 desalting column, according to the manufacturer's instructions [452]. First, the ionic strength of the solution of AuNPs with the purified oligonucleotides was gradually increased. The Au-nanoconjugates were incubated for 20 minutes with 10 mM phosphate buffer pH = 8, 2% SDS (AGE I), to a final concentration of

10 mM phosphate buffer (pH = 8) and 0.01% (w/v) SDS. Then, 10 mM phosphate buffer pH = 8, 1.5 M NaCl, 0.01% SDS (AGE II) was added in appropriate volumes to a final concentration of 10 mM phosphate buffer (pH = 8), 0.05 M NaCl and 0.01% (w/v) SDS. Serial additions of AGE II were performed to attain final concentrations of 0.1, 0.2, and 0.3 M of NaCl. After each AGE addition, a step of 10 seconds of ultrasounds and 20 minutes of incubation under agitation were performed. At last, the final solution was incubated for 16 h at RT under agitation, and the excess oligonucleotides were removed by two centrifugations at 15500 g for 1 h at 4°C and washed twice with diethylpyrocarbonate (DEPC)-treated water. The number of ASO functionalized to the nanoparticles' surface was inferred from the quantification of single-stranded DNA in the supernatants using a Nanodrop spectrophotometer, considering the initial amount of ASO added. The stability of the AuNP@PEG 30% and AuNP@ASO were measured by using 1 nM of the Au-nanoconjugates incubated in DMEM without phenol red for 24 h at 37ºC.

4.2.2 Laser irradiation in HCT116 2D cells

HCT116 2D cells were plated at a density of $2x10^4$ cells/well in a 96-well plate and incubated for 24 h at 37°C in a 99% humidified atmosphere and 5% (v/v) CO_2. After 24 h, the cells were challenged with AuNP@ASO and AuNP@PEG in DMEM without phenol red to evaluate *c-MYC* expression at different time points: 6 h, 9 h, 12 h, and 24 h. The concentration of ASO was 50 nM (0.39 nM of AuNP@*c-MYC* and 0.45 nM of AuNP@*scramble*), using 0.39 nM and 0.45 nM of AuNP@PEG 30% as controls - AuNP@PEG M and AuNP@PEG S, respectively, as previous selected and optimized by Oliveira *et al.* [452]. Following the initial assessment, the 9 h incubation period was selected for further experiments. Then, cells were irradiated after 4 h of Au-nanoconjugates incubation with a CW 532 nm green DPSS laser coupled to an optical fiber under (LDI 2.37 W/cm^2) for 60 seconds. Controls without irradiation, with or without AuNPs, were also prepared. Total RNA was extracted, and an MTS assay was performed. The effect of visible irradiation in the internalization of AuNP@ASO for *c-MYC* silencing was evaluated via RT-qPCR and Immunofluorescence assay.

4.2.3 Laser irradiation in HCT116 3D spheroids

For 3D colorectal tumor spheroids, HCT116 2D cells were seeded at a density of $5x10^3$ cells/well in an ultra-low attachment 96-well plate. HCT116 3D spheroids were grown for 3- and 7- days in DMEM at 37°C, under standard culture conditions, and monitored with Ti-U Eclipse inverted microscope, and Feret's diameter was analyzed using ImageJ software [459,467]. To determine the cell number, spheroids were dissociated through a 30 minute incubation

with TrypLE™ Express, followed by centrifugation at 500 g for 5 minutes. Cells were counted via the Trypan Blue exclusion method [403,459]. According to the same ratio of ASO per cell, the 3- and 7-days 3D spheroids were challenged with 25 nM and 60 nM of ASO, respectively (0.19 nM and 0.47 nM of AuNP@*c-MYC*; as controls, 0.23 nM and 0.54 nM of AuNP@*scramble*, respectively) in DMEM without phenol red. AuNP@PEG 30% was used for control of AuNP@*c-MYC* (0.19 nM and 0.47 nM - AuNP@PEG M) and AuNP@*scramble* (0.23 nM and 0.54 nM - AuNP@PEG S). Upon 4 h, HCT116 3D spheroids were irradiated as described above for HCT116 2D cells. Following 9 h of AuNP@ASO and AuNP@PEG incubation, total RNA was extracted, and LDH assay and LIVE/DEAD Viability/Cytotoxicity assay were performed. The effect of visible irradiation in the internalization of AuNP@ASO for *c-MYC* silencing was evaluated with RT-qPCR and Immunofluorescence assay.

4.2.4 Immunofluorescence assay in HCT116 2D cells/3D spheroids

HCT116 2D cells were fixed with 4% paraformaldehyde for 20 minutes, then washed three times with PBS and permeabilized with 0.1% Triton™-X 100 in PBS for 5 minutes. HCT116 3D spheroids were fixed with 4% paraformaldehyde for 1 h, then washed three times with PBS and subsequently permeabilized using 0.1% Triton-X™ 100 in PBS for 30 minutes. Cells were incubated with 7.5 μg/mL of Hoechst 33258 for 15 minutes and the spheroids were incubated for 45 minutes, then washed three times with PBS and the blocking was performed with 1% BSA in PBS with 0.1% Tween® 20 (PBST) for 1 h. Next, cells and spheroids were incubated overnight at 4°C with the primary antibody - anti-rabbit c-MYC antibody (1:200 dilution). After incubation, cells and spheroids were washed three times with PBST, cells were incubated for 1 h at RT with the secondary antibody - FITC-conjugated anti-rabbit antibody (1:500 dilution), whereas the spheroids were incubated for 3 h. The cells and spheroids were subsequently washed three times with PBST and visualized in PBST using a Ti-U Eclipse inverted microscope. Images were acquired using the DAPI emission filter (excitation at 360/40 nm and emission at 460/50 nm) and FITC emission filter (excitation at 480/30 nm and emission at 535/40 nm). Fluorescence microscopy images were analyzed using ImageJ software [459,467]. For fluorescence quantification, CTCF was determined using the Equation 3.1 (Chapter 3) for 2D cells, and the Equation 4.1 for spheroids [412,459].

$$CTCF = Integrated\ density\ of\ spheroid - (Area\ of\ spheroid \times Background\ mean\ fluorescence)$$ (Equation 4.1)

4.2.5 Cell cytotoxicity

Cell cytotoxicity assessment via MTS and LDH assays were performed as described in section 2.2.6 (Chapter 2).

LIVE/DEAD Viability/Cytotoxicity assay was performed to assess the impact of visible irradiation after the *c-MYC* silencing experiment in HCT116 3D spheroids. Following the 9 h of silencing, the irradiated and non-irradiated spheroids were washed with PBS and incubated with 1 μM of Calcein AM and 2 μM of Ethidium homodimer-1 (EthD-1) in PBS for approximately 45 minutes, at 37°C in a 99% humidified atmosphere and 5% (v/v) CO_2. Fluorescence microscopy images were acquired by a Ti-U Eclipse inverted microscope using a FITC emission filter (excitation at 480/30 nm and emission at 535/40 nm) and G2A emission filter (excitation at 535/50 nm and emission >590 nm). Fluorescence microscopy images were analyzed using ImageJ software, and for fluorescence quantification, CTCF was determined using Equation 4.1. The ratio between Calcein AM and EthD-1 was performed to evaluate viability/cytotoxicity.

4.2.6 Gene expression analysis

The analysis of *c-MYC* gene expression was performed via RT-qPCR as described in section 2.2.7 (Chapter 2).

4.2.7 Statistical analysis

Data were analyzed using GraphPad Prism 8.0 (GraphPad Software, San Diego, USA). One-way ANOVA with Tukey's multiple comparison test, and unpaired parametric t-test with Welch's correction were used to evaluate differences between groups. They were considered statistically significant at p-value < 0.05. Data are the mean value of at least three independent assays with at least two technical replicates, and the errors are calculated by the standard error of the mean.

4.3 Results and discussion

4.3.1 Synthesis and characterization of Au-nanoconjugates

AuNPs with 30% of PEG coverage were functionalized with ASO complementary to the *c-MYC* transcript (AuNP@*c-MYC*) and with scramble control, with a sequence without any target on the human genome (AuNP@*scramble)*. Characterization of AuNP@Citrate and AuNP@PEG 30% by UV-Vis shows a maximum LSPR peak at 519 nm and 520 nm, respectively, and functionalization with ASO resulted in an additional slight red shift of the LSPR peak to 522 nm (Figure 4.2). It was denoted an increase in the average hydrodynamic diameters of Au-nanoconjugates upon functionalization with ASO, 35.7 (± 0.2) nm for AuNP@*c-MYC* and 35 (± 0.2) nm for AuNP@*scramble* (Table 4.1).

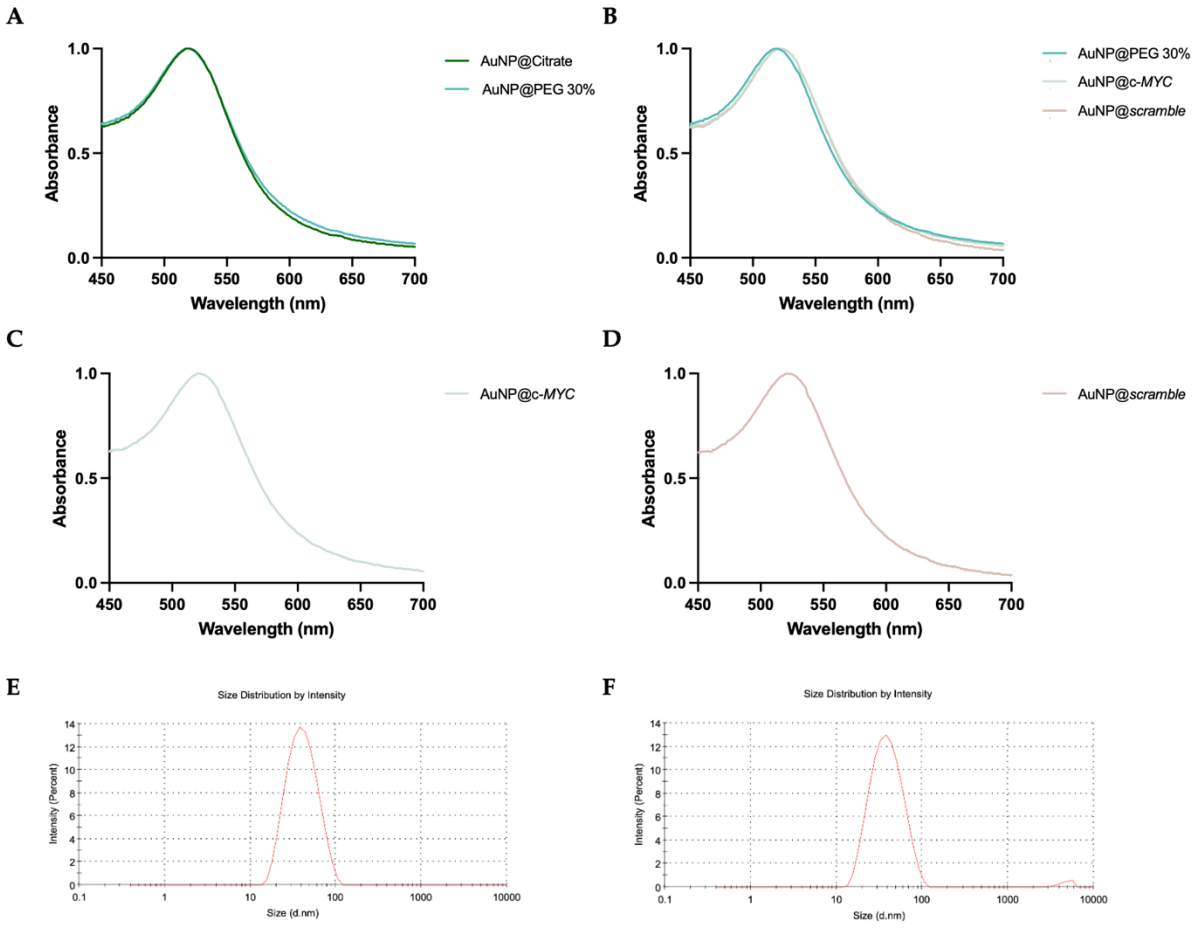

Figure 4.2 - Normalized absorbance UV-Vis spectra of AuNP and Au-nanoconjugates, and the hydrodynamic size distribution of AuNP@ASO measured via DLS in water. (A) UV-Vis spectra of AuNP@Citrate and AuNP@PEG 30%. (B) UV-Vis spectra of AuNP@PEG 30%, AuNP@*c-MYC* and AuNP@*scramble*. (C) UV-Vis spectra of AuNP@*c-*

MYC. (D) UV-Vis spectra of AuNP@*scramble*. Hydrodynamic size distribution of (E) AuNP@*c-MYC* and (D) AuNP@*scramble* by DLS. The peak observed in each data set indicates the monodispersity of the colloidal AuNP.

Table 4.1 - Physicochemical characteristics of AuNP and Au-nanoconjugates measured by DLS, ζ-potential (at pH=6), and their PDI and ratio AuNP/ASO functionalized.

AuNP	**Hydrodynamic diameter**	**ζ-potential**	**PDI**	**Ratio AuNP/ASO (1:150)**
AuNP@Citrate	16.4 ± 0.1	-37.1 ± 0.5	0.170	-
AuNP@PEG 30%	21.1 ± 0.3	-70.7 ± 3.1	0.282	-
AuNP@*c-MYC*	35.7 ± 0.2	-74.1 ± 2.3	0.199	1:129
AuNP@*scramble*	35.0 ± 0.2	-78.2 ± 5.4	0.237	1:111

A stability assay in DMEM was performed to verify the stability of the Au-nanoconjugates in a supplemented cell culture medium. AuNP@PEG 30% and AuNP@ASO were incubated in DMEM without phenol red for 24 h at 37ºC (Figure 4.3). The UV-Vis spectra show a LSPR peak at 520 nm for AuNP@PEG 30% and 522 nm for AuNP@*c-MYC* and AuNP@*scramble* at 0 h. After 24 h of incubation, it was denoted a slight red shift of the LSPR peak to 525 nm of the Au-nanoconjugates, which does not compromise the optical features of AuNP as photothermal agents. This slight shift of the LSPR peak might be derived from the formation of protein corona on the nanoparticles surface, owing to the presence of FBS in DMEM.

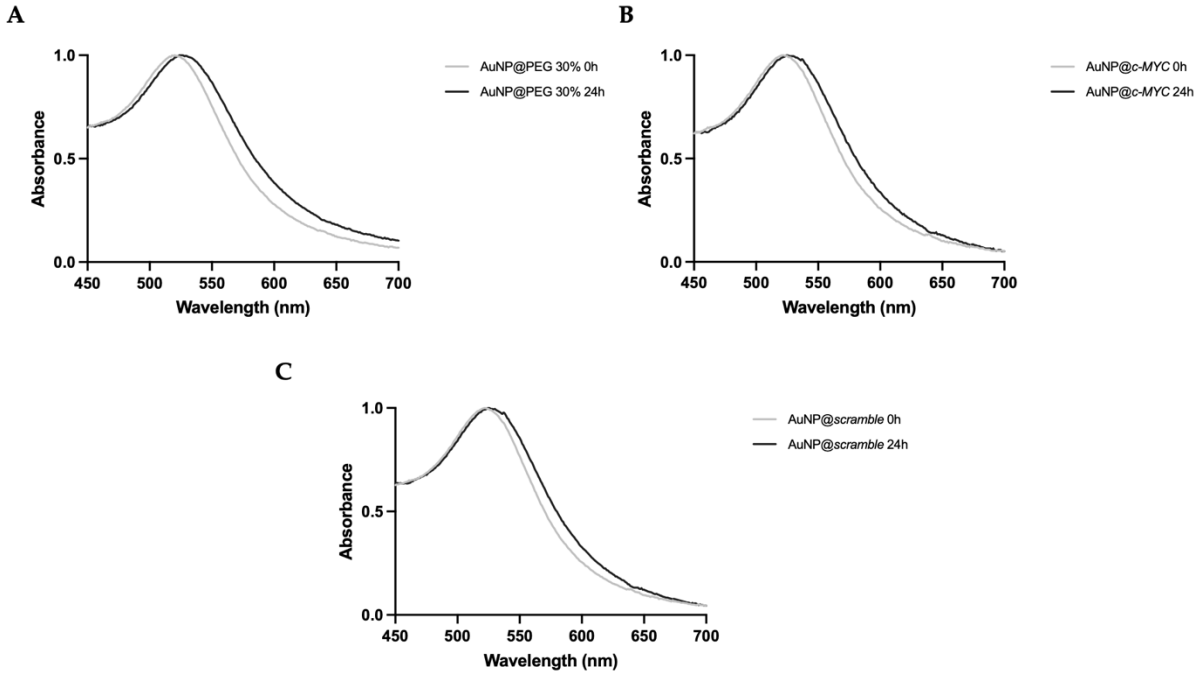

Figure 4.3 - Normalized UV-Vis spectra of Au-nanoconjugates incubated in DMEM without phenol red at 37ºC. (A) UV-Vis spectra of AuNP@PEG 30%, B) UV-Vis spectra of AuNP@*c-MYC*, and (C) UV-Vis spectra of AuNP@*scramble* in supplemented cell culture medium at 0 h and 24 h.

4.3.2 Optimization of *c-MYC* gene silencing

We evaluated the efficacy of the mild photothermy combined with AuNP@*c-MYC* in silencing the frequently overexpressed *c-MYC* oncogene. In fact, *c-MYC* is a suitable target for gene silencing concepts for eventual gene therapy approaches since this proto-oncogene is a well-known transcription factor involved in cell cycle homeostasis and often dysregulated in cancer cells [451,468], and several studies have reported its efficacious silencing by ASO vectorized by AuNPs [356,452,469,470]. All conditions tested and the amount of ASO used in silencing experiments were described in section 4.2. We first optimized the *c-MYC* silencing at different time points (6 h, 9 h, 12 h, and 24 h) in HCT116 2D cells with AuNP@*c-MYC*, using AuNP@PEG 30% and AuNP@*scramble* as controls. An effective decrease of *c-MYC* expression of approximately 70% was observed at 9 h, which was then selected for subsequent experiments (Figure 4.4).

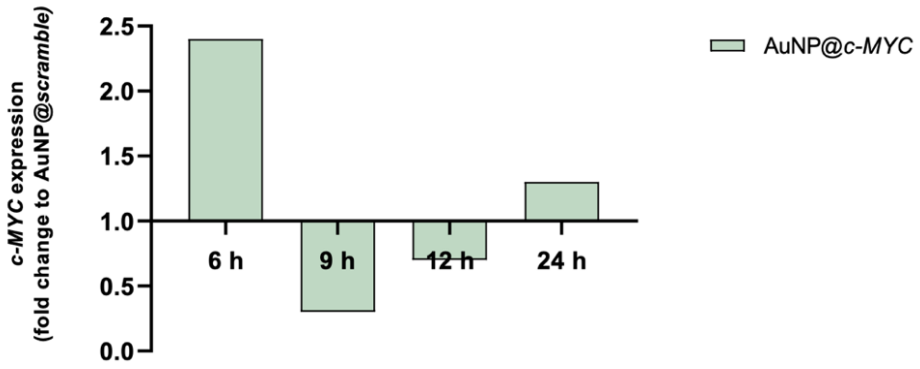

Figure 4.4 - Evaluation of *c-MYC* expression using RT-qPCR at different time points in HCT116 2D cells. HCT116 2D cells were challenged with AuNP@*c-MYC* or AuNP@*scramble* to evaluate *c-MYC* gene silencing. The fold change was calculated between AuNP@*c-MYC* and AuNP@*scramble* (ratio) with the *c-MYC* expression values normalized to the respective AuNP@PEG 30% control. AuNP@*scramble* was used as a control to analyze the effect of ASO in *c-MYC* expression. Data represent at least two biologically independent experiments with two technical replicates each.

This evaluation allowed the identification of the ideal time point for the more pronounced gene silencing. Initially, *c-MYC* expression is triggered as a response to the challenge with nanoparticles, as reported in the literature. After this moment, the silencing starts to be noticed. Cell division and consequent nanoparticles "dilution" per cell, causes a recovery of *c-MYC* expression, which usually returns to normal levels at 24 h [452].

4.3.3 Mild photothermy for *c-MYC* silencing in HCT116 2D cells

Cells were challenged for 9 h with the Au-nanoconjugates and laser irradiation was conducted 4 h post Au-nanoconjugate challenge. Cell viability was assessed by the MTS Assay, *c-MYC* gene expression was analyzed by RT-qPCR, and the c-MYC protein expression was evaluated by Immunofluorescence. The *c-MYC* silencing was compared between irradiated cells incubated with AuNP@*c-MYC* (AuNP@*c-MYC*+Laser) and non-irradiated cells incubated with AuNP@*c-MYC*. Total RNA was extracted from all conditions tested after 9 h and RT-qPCR analysis confirmed the silencing of the *c-MYC* gene in AuNP@*c-MYC* and AuNP@*c-MYC*+Laser samples.

Figure 4.5A shows the significant reduction of *c-MYC* expression (25% of gene silencing compared to untreated cells Control, $2^{\Delta\Delta Ct} = 1$). This silencing effect was higher than that obtained for AuNP@*c-MYC* alone (approximately 20%). Mild photothermy alone or combined with Au-nanoconjugates has a slight impact on cell viability. A small decrease in cell viability upon 9 h of silencing is observed when combined with mild photothermy, which might be attributed to the downregulation of *c-MYC* itself, which would have an impact on cell proliferation (Figure 4.5) [471,472].

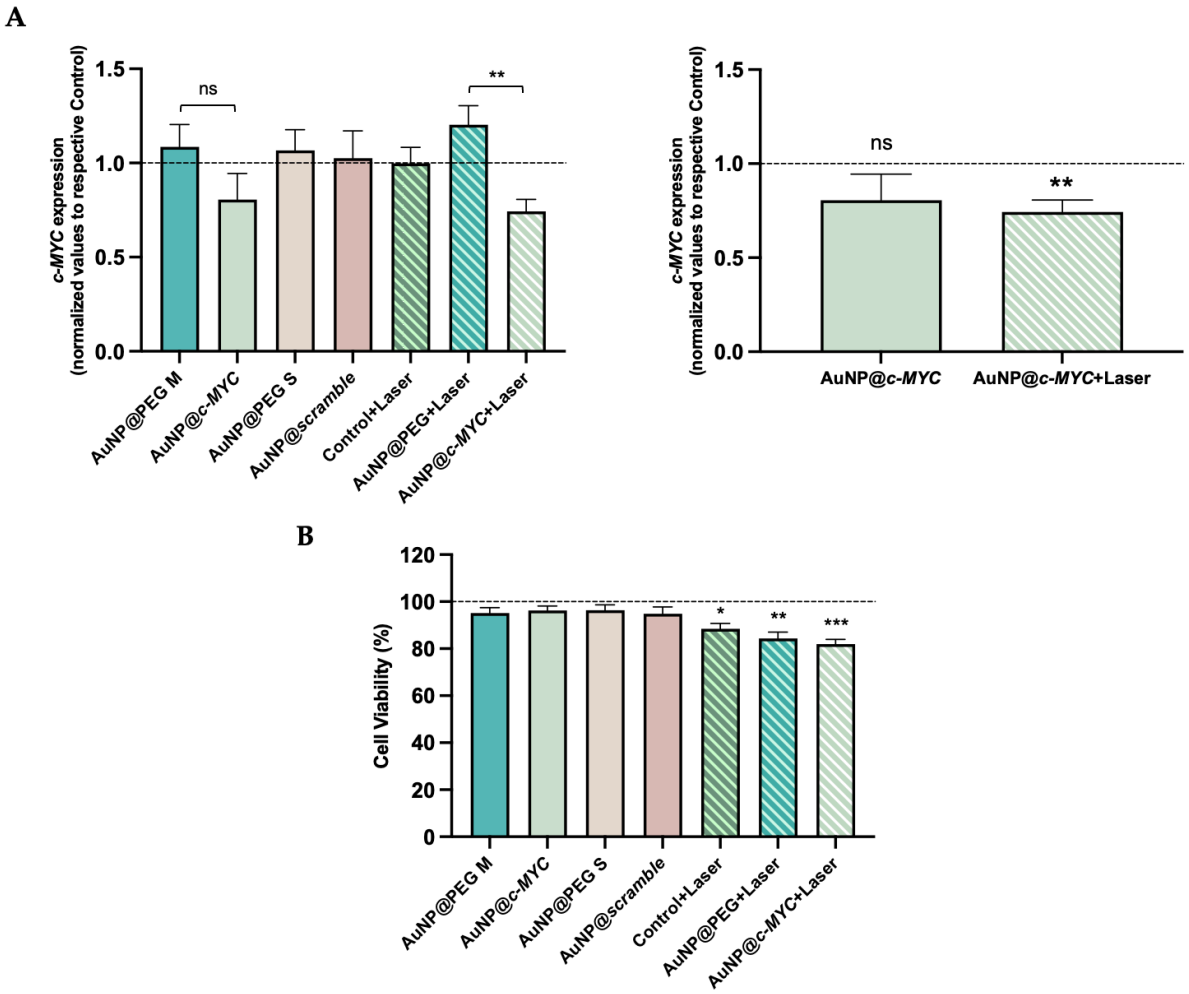

Figure 4.5 - RT-qPCR analysis and cell viability assay in HCT116 2D cells. (A) RT-qPCR to evaluate *c-MYC* gene expression at 9 h in different conditions tested. Gene expression levels were normalized to respective Controls. Black asterisks indicate statistical differences between AuNP@*c-MYC*+Laser and their respective AuNP@PEG control (left) and with Control (right) (**$p < 0.01$; ns - not statistically significant; Unpaired parametric t-test with Welch's correction). Data represent the mean value ± the standard error of the mean of at least three biologically independent experiments with two technical replicates each. (B) Cell viability analysis of the different samples tested after 9 h of *c-MYC* silencing via MTS assay. The seven conditions tested were normalized to untreated cells (Control). Statistical differences were observed between Control+Laser, AuNP@PEG+Laser, and AuNP@*c-MYC* with Control. Black asterisks indicate statistical differences between samples and the Control (*$p < 0.05$; **$p < 0.01$; ***$p < 0.001$; One-way ANOVA - Mixed-effects analysis with Tukey's multiple comparison test). Data represent the mean value ± the standard error of the mean of at least three biologically independent experiments with two technical replicates each.

The quantitative analysis of CTCF of fluorescence microscopy images shows a reduction of c-MYC protein expression corroborating the data attained for the mild photothermy using AuNP@*c-MYC* (Figure 4.5). We denoted a c-MYC protein expression 10% lower in AuNP@*c-MYC*+Laser sample compared to AuNP@*c-MYC* (Figure 4.6). Fluorescence microscopy images of all conditions tested are presented in Figure 4.7.

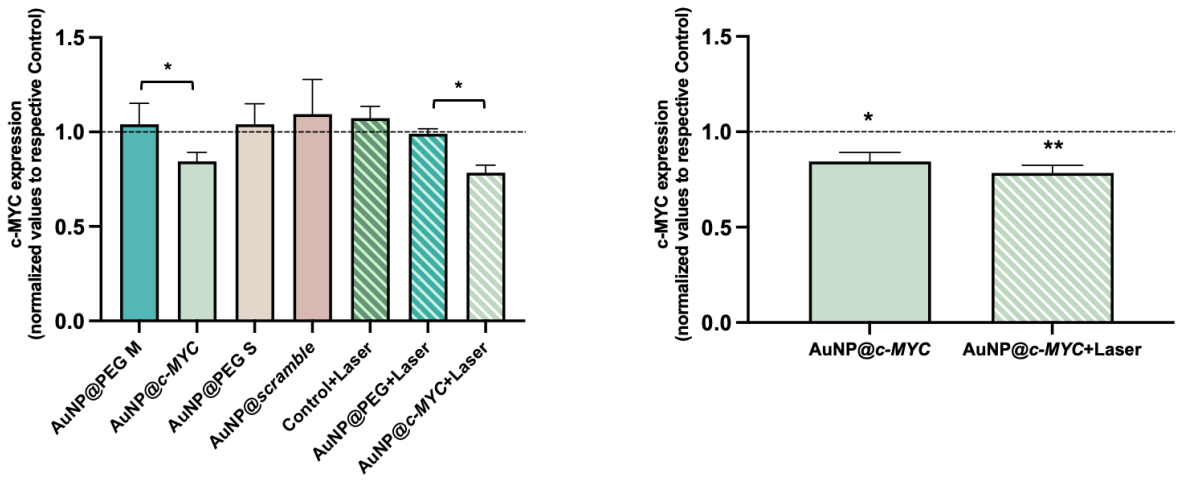

Figure 4.6 - CTCF evaluation of c-MYC protein expression by Immunofluorescence assay of HCT116 2D cells. CTCF analysis via Immunofluorescence assay to evaluate c-MYC protein expression at 9 h of gene silencing. Black asterisks indicate statistical differences between AuNP@*c-MYC* and AuNP@*c-MYC*+Laser samples with their respective AuNP@PEG control (left), and with Control (right) (*$p < 0.05$; **$p < 0.01$; Unpaired parametric t-test with Welch's correction). Data represent the mean value ± the standard error of the mean of two biologically independent experiments with three technical replicates each.

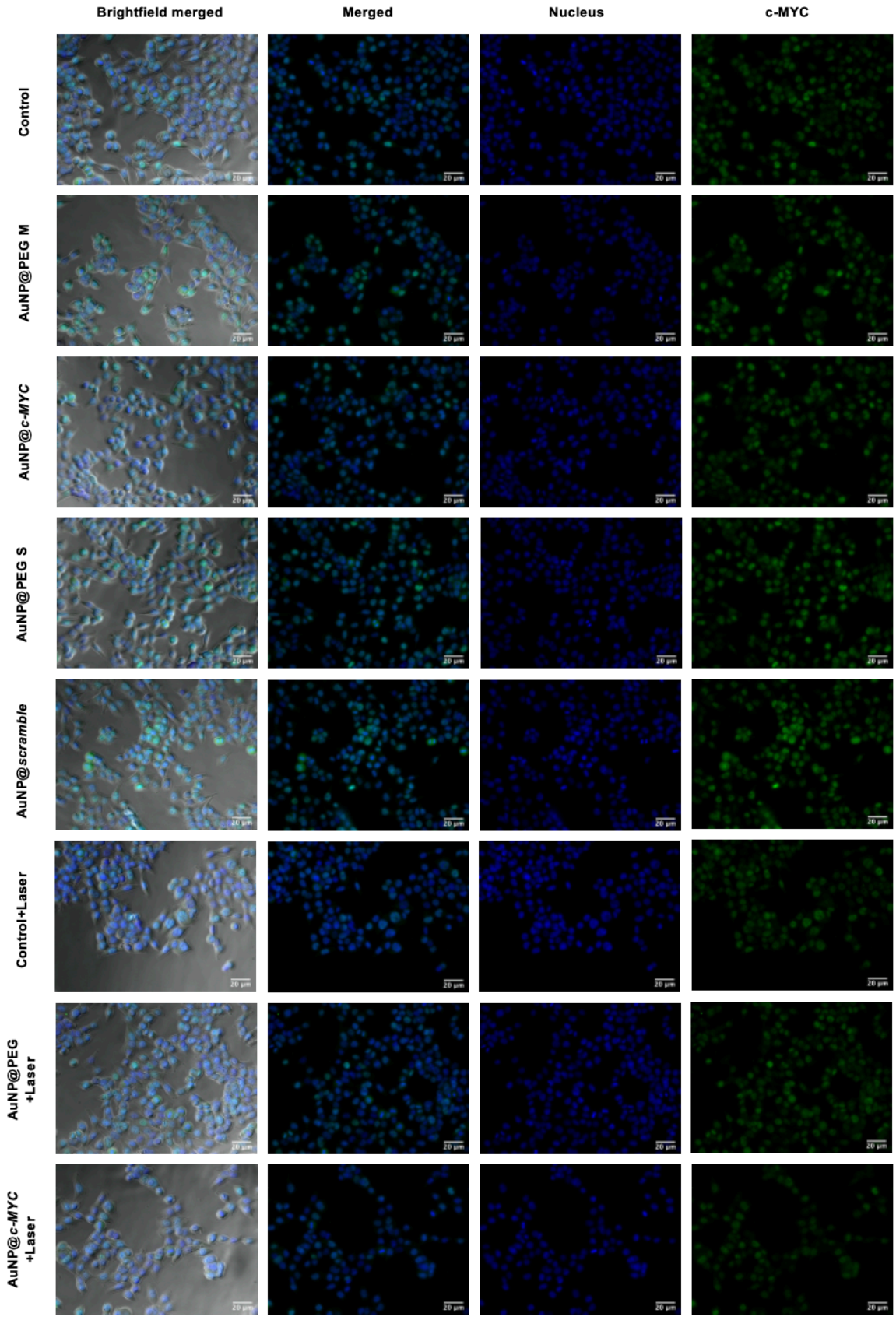

Figure 4.7 - Fluorescence microscopy images of HCT116 2D cells by Immunofluorescence assay. Seven conditions were tested after 9 h of silencing experiment in HCT116 cells. Scale bars correspond to 20 µm.

4.3.4 Mild photothermy for *c-MYC* silencing in HCT116 3D spheroids

Spheroids are 3D cell models that more closely resemble the *in vivo* behavior of cell growth than the standard 2D monolayer culture [460,473,474]. These cell models are appropriate for large-scale screening and display enhanced recapitulative potential of the *in vivo* TME, including the 3D architecture of tissues, cell-to-cell and cell-matrix interactions, cell polarization, gradient dynamics (e.g., formation of oxygen, nutrient and pH gradients), de novo ECM deposition and growth kinetics [2,475–477]. As such, we used HCT116 3D spheroids models for a final proof-of-concept for *c-MYC* silencing. We select 3- and 7-day spheroids owing to their differences in functional characteristics (e.g., size and structure, metabolic gradients, and gene and protein patterns).

The formation of three distinct cell layers with different functions and metabolic activity is expected in spheroids with more than 500 μm in diameter: a highly proliferative external layer, a quiescent intermediate layer, and an internal necrotic core [459,462,464]. Spheroids of 3 days are smaller and contain more proliferative cells in their layers than 7-day spheroids, which are larger in diameter, more compact, and might show a hypoxic or necrotic core surrounded by proliferating cells in the outer layers. Also, it was expected that 3-day spheroids would have higher cell viability than 7-day spheroids. The inner layer "core" of 7-day spheroids has limited oxygen and nutrient diffusion, which could lead to hypoxia or necrosis [459,460]. In the literature, it is reported that gene and protein expression patterns change over spheroids' growth [474]. For instance, our group reported that hypoxia-inducible factors (e.g., *HIFA* gene/HIF-1α) are more expressed after 4 days of HCT116 3D spheroid growth [459]. Overall, 3-day spheroids could be more representative of early TME and tumor formation, which are useful to study initial cell-cell and cell-ECM interactions, whereas 7-day spheroids could better mimic a complex TME and are often used to explore mechanisms of action and cellular responses, including drug internalization assays [403,459,460,478,479].

We first evaluated the number of cells in 3- and 7-day spheroids and their respective size (Figure 4.8).

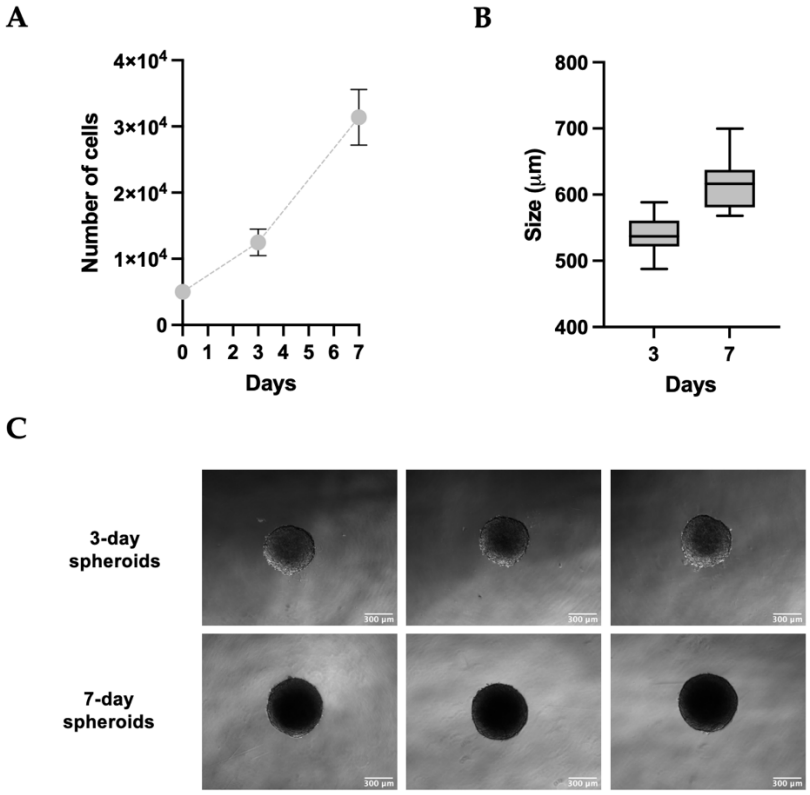

Figure 4.8 - HCT116 3D spheroids growth for 3 and 7 days. (A) Evolution of cell number for 0, 3, and 7 days of spheroids growth. Data represent the mean value ± the standard deviation of at least four independent spheroids. (B) Spheroid's size of 3 and 7 days. At least 40 independent spheroids were measured using Feret's diameter. Data represent the mean value and the min to max value for the diameter size of spheroids. (C) Brightfield microscopy images of 3- and 7-day spheroids. The scale bar corresponds to 300 μm.

As expected, the cell density increases during spheroids' growth, which is concordant with a consistent linear increase observed by Valente *et al.* [459]. The spheroid's size was measured, showing an average diameter of 540 ± 24 μm for 3-day spheroids and 616 ± 34 μm for 7-day spheroids. Our results are similar to those attained in recent reports of our group, in which compacted spheroids presented a diameter greater than 500 μm upon 2 days of growth [452,459].

Following the growth of spheroids for 3- or 7- days, they were challenged with Au-nanoconjugates and *c-MYC* silencing was evaluated as described above for 2D cell cultures, with the same ratio of ASO per cell previously selected. The impact on the viability of the spheroids was assessed using the LIVE/DEAD Viability/ Cytotoxicity assay and the LDH assay.

Figure 4.9 highlights the effective silencing of the *c-MYC* for the mild photothermy conditions in 7-day spheroids (AuNP@*c-MYC*+Laser), with a 30% reduction in the gene expression of *c-MYC*. Also, statistically significant differences between AuNP@*c-MYC*+Laser and AuNP@*c-MYC* highlight the effect of laser irradiation (photothermy) to potentiate *c-MYC* silencing - Figure 4.9B. Interestingly, our mild photothermy did not show the same pronounced reduction of *c-MYC* expression in the 3-day spheroids. This might be because 3-day

spheroids are actively proliferating, where *c-MYC* is continuously being positively induced [459,476,480]. Still, there is a reduction of 5% in AuNP@*c-MYC*+Laser samples in 3-day spheroids - Figure 4.9A.

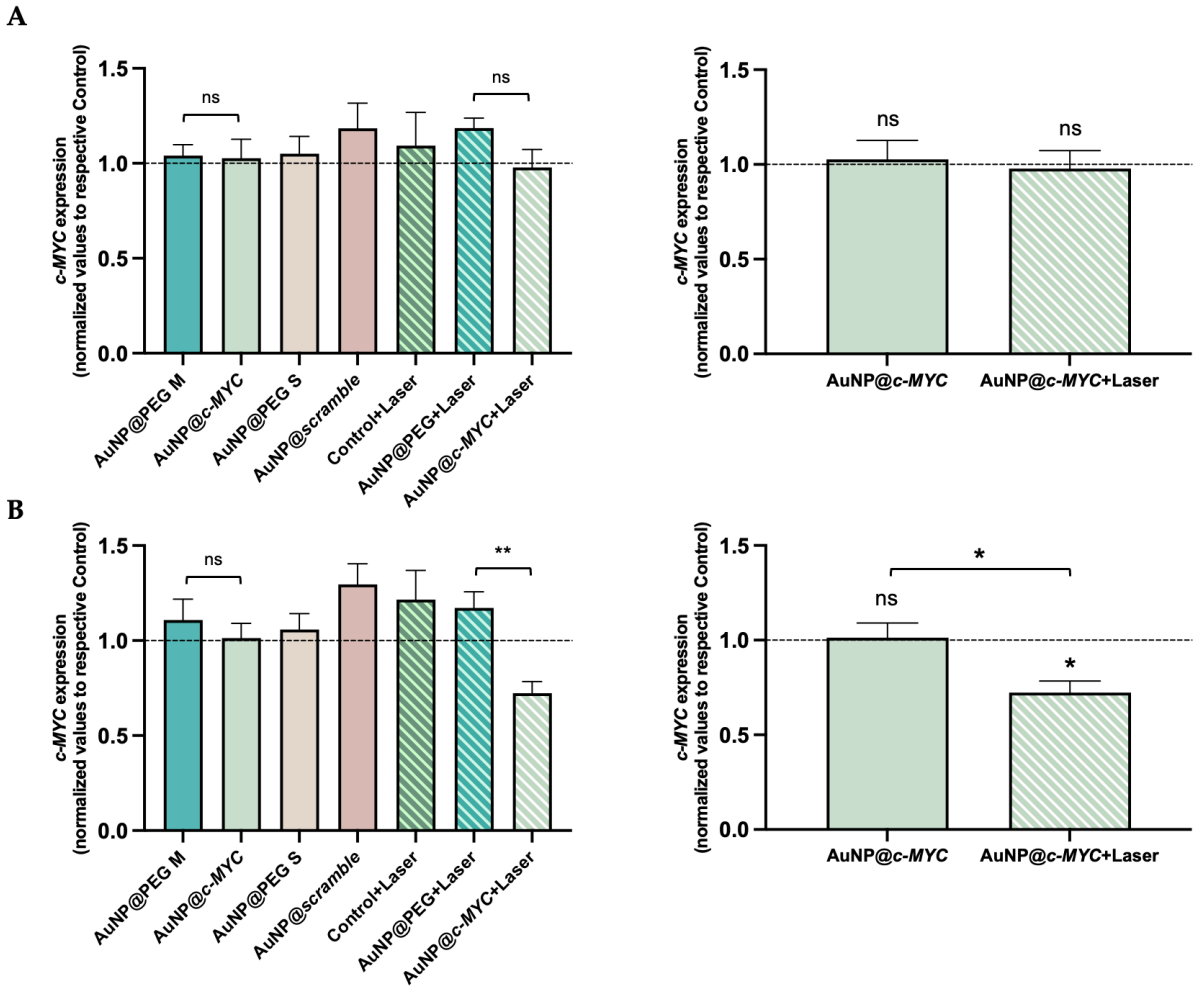

Figure 4.9 - RT-qPCR analysis of *c-MYC* gene silencing in 3- and 7-day HCT116 3D spheroids. *c-MYC* gene expression at 9 h of gene silencing in (A) 3-day spheroids and (B) 7-day spheroids. Gene expression levels were normalized to the respective Controls. Black asterisks indicate statistical differences between AuNP@*c-MYC*+Laser and their respective AuNP@PEG control (left), and with Control (right) for 7-day spheroids (*$p < 0.05$; **$p < 0.01$; ns - not statistically significant; Unpaired parametric t-test with Welch's correction). Data represent the mean value ± the standard error of the mean of at least three biologically independent experiments with two technical replicates for each.

To validate the RT-qPCR data, the quantitative analysis of CTCF by fluorescence microscopy denotes a slight decrease of c-MYC protein expression between AuNP@*c-MYC* and AuNP@*c-MYC*+Laser in 3-day spheroids (10% and 20%, respectively) - Figure 4.10A. A 20% reduction in c-MYC expression could be observed for the mild photothermy in 7-day spheroids compared to Control, which confirms the potential of mild photothermy - Figure 4.10B.

Fluorescence microscopy images of all conditions tested are presented in Figure 4.11 and Figure 4.12.

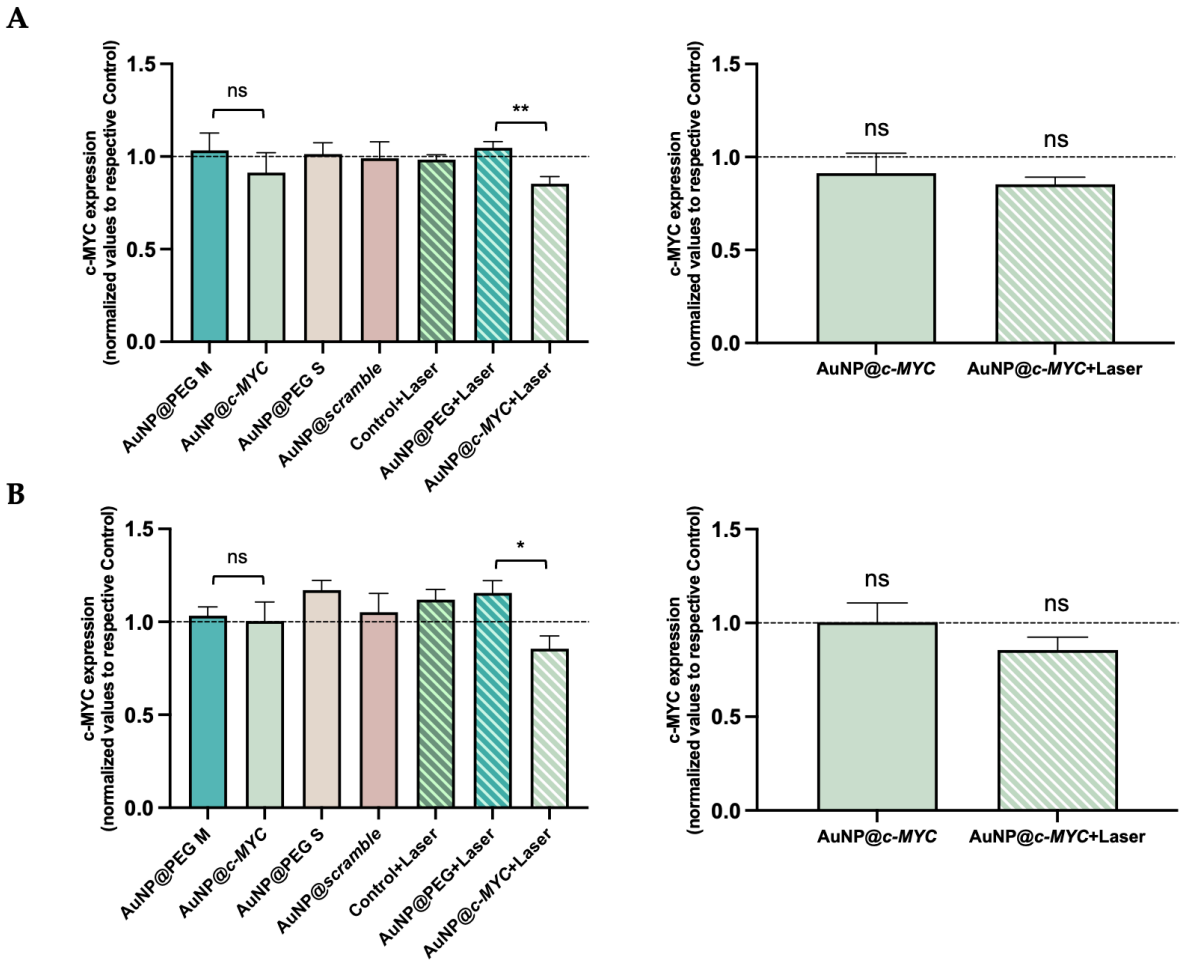

Figure 4.10 - CTCF evaluation of c-MYC protein expression in 3- and 7-day HCT116 3D spheroids. CTCF analysis of Immunofluorescence assay evaluates c-MYC protein expression at 9 h after gene silencing in (A) 3-day spheroids and (B) 7-day spheroids. Black asterisks indicate statistical differences between AuNP@*c-MYC*+Laser and their respective AuNP@PEG control (left) and were not observed with Control (right) (*p < 0.05; **p < 0.01; ns - not statistically significant; Unpaired parametric t-test with Welch's correction). Data represent the mean value ± the standard error of the mean of two biological independent experiments with three technical replicates for each.

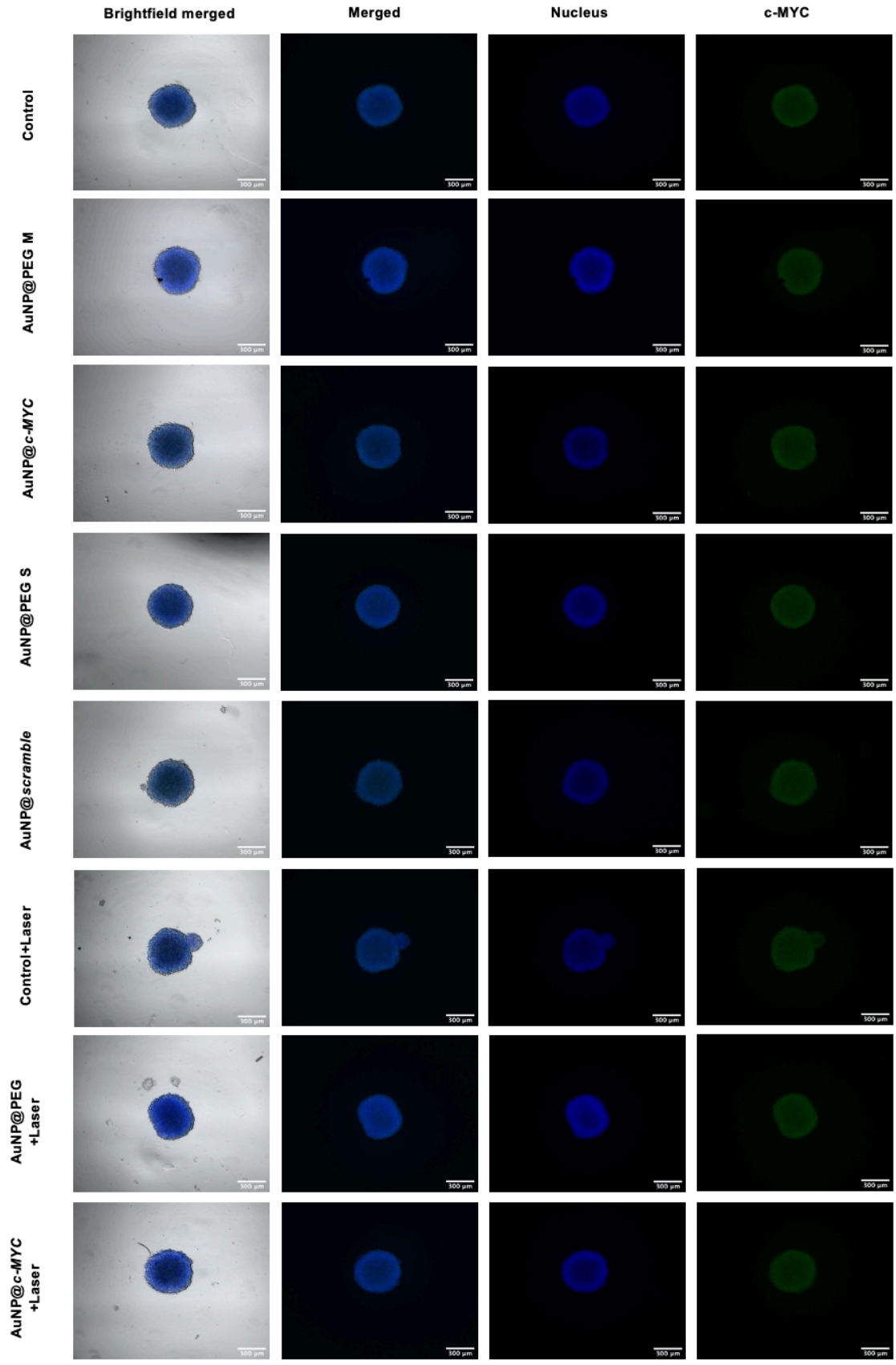

Figure 4.11 - Fluorescence microscopy images of 3-day HCT116 3D spheroids by Immunofluorescence assay. Seven conditions were tested after 9 h of silencing experiment in 3-day spheroids. Scale bars correspond to 300 μm.

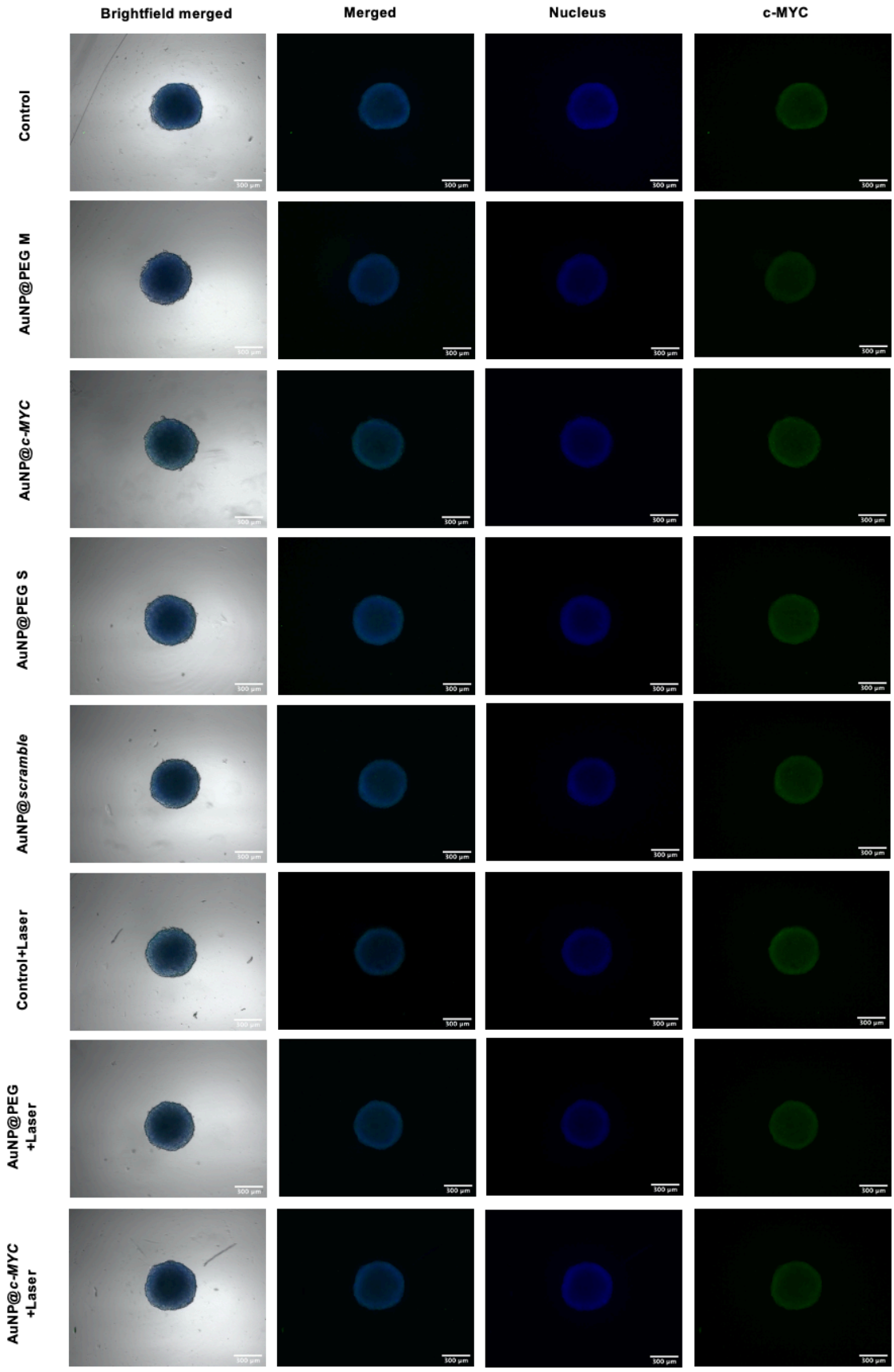

Figure 4.12 - Fluorescence microscopy images of 7-day HCT116 3D spheroids by Immunofluorescence assay. Seven conditions were tested after 9 h of silencing experiment in 7-day spheroids. Scale bars correspond to 300 μm.

The impact of *c-MYC* silencing on cell viability in non-irradiated and irradiated spheroids was assessed by LIVE/DEAD Viability/Cytotoxicity assay and LDH assay. The ratio between Calcein AM and EthD-1 was calculated since the living cells active intracellular esterase to cleavage the cell-permeant Calcein AM to intensely fluorescent Calcein (Live cells), and EthD-1 is a cell-impermeant that enters in cells with compromised membranes (Dead cells). Irradiated 3-day spheroids show a compromise cell membrane as indicated by the statistically significant decrease to the Calcein AM/EthD-1 ratio, 1.4-fold, and 2-fold for AuNP@PEG+Laser and AuNP@*c-MYC*+Laser more than Control, respectively – Figure 4.13A. In 7-day spheroids, a slight reduction to the Calcein AM/EthD-1 ratio in AuNP@PEG+Laser and AuNP@*c-MYC*+Laser (around 1.2-fold more) compared to Control is observed although without statistical significance - Figure 4.13B. Fluorescence microscopy images of all conditions tested are presented in Figure 4.14 and Figure 4.15.

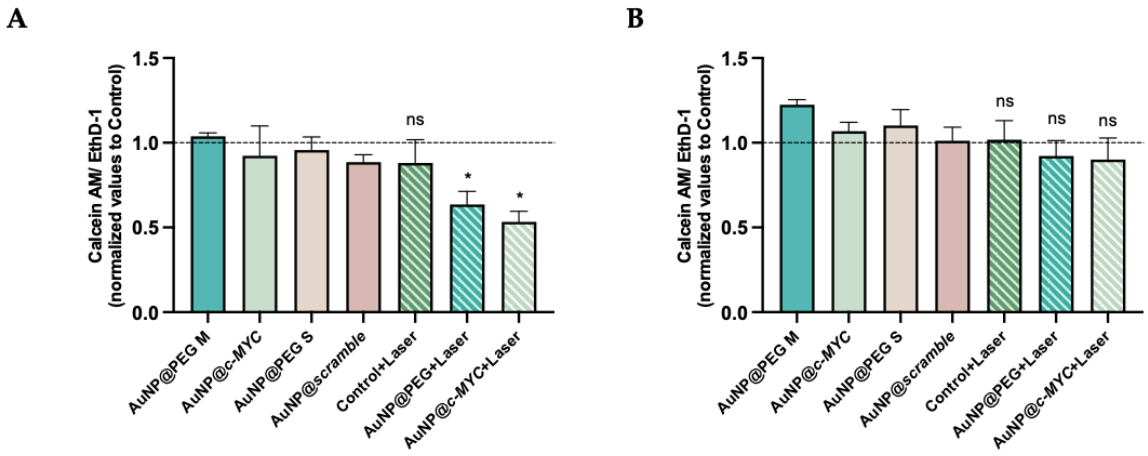

Figure 4.13 - Cell viability/cytotoxicity assay of 3- and 7-day HCT116 3D spheroids. Cell viability/cytotoxicity evaluation of the different samples tested after 9 h of *c-MYC* silencing via LIVE/DEAD Viability/ Cytotoxicity assay of (A) 3-day spheroids and (B) 7-day spheroids. Scale bars correspond to 300 mm. The seven conditions tested were normalized to untreated cells (Control). Statistical differences were observed between AuNP@PEG+Laser and AuNP@*c-MYC*+Laser with Control in 3-day spheroids. Black asterisks indicate statistical differences between samples and the Control (*$p < 0.05$; ns - not statistically significant; Unpaired parametric t-test with Welch's correction). Data represent the mean value ± the standard error of the mean of two biologically independent experiments with three technical replicates each.

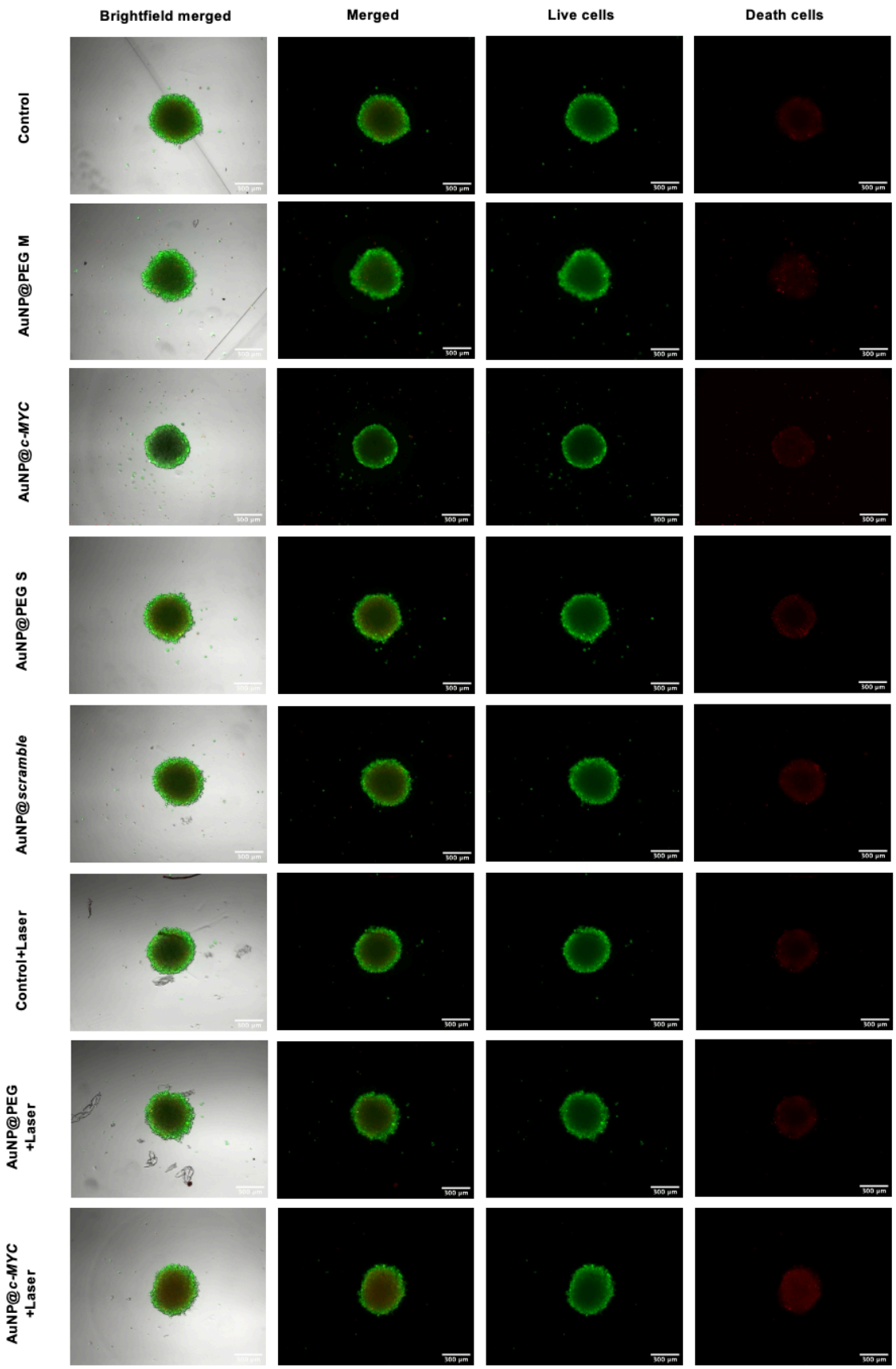

Figure 4.14 - Fluorescence microscopy images of 3-day HCT116 3D spheroids by Live/DEAD Viability/ Cytotoxicity assay. Seven conditions were tested after 9 h of silencing experiment in 3-day spheroids. Scale bars correspond to 300 μm.

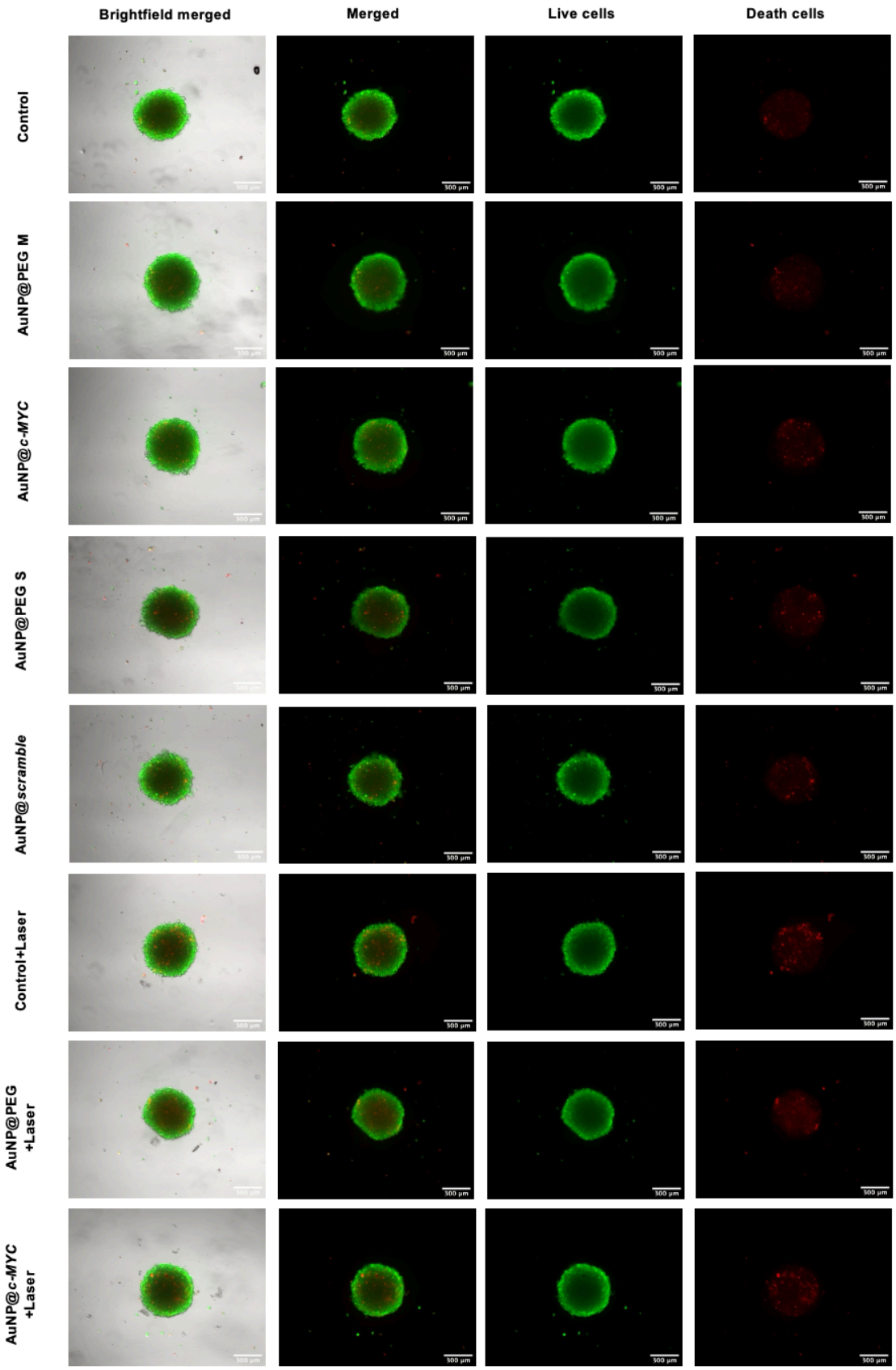

Figure 4.15 - Fluorescence microscopy images of 7-day HCT116 3D spheroids by Live/DEAD Viability/Cytotoxicity assay. Seven conditions were tested after 9 h of silencing experiment in 7-day spheroids. Scale bars correspond to 300 µm.

These observations are corroborated by those attained by the LDH assay, where 3-day spheroids showed a 3-fold and 3.3-fold higher LDH activity for AuNP@PEG+Laser and AuNP@*c-MYC*+Laser compared to Control (Figure 4.16A) and in 7-day spheroids were observed approximately 1.7-fold more than Control (Figure 4.16B). These observations are concordant with previous reports using AuNPs or other photothermal agents with laser irradiation [481–483].

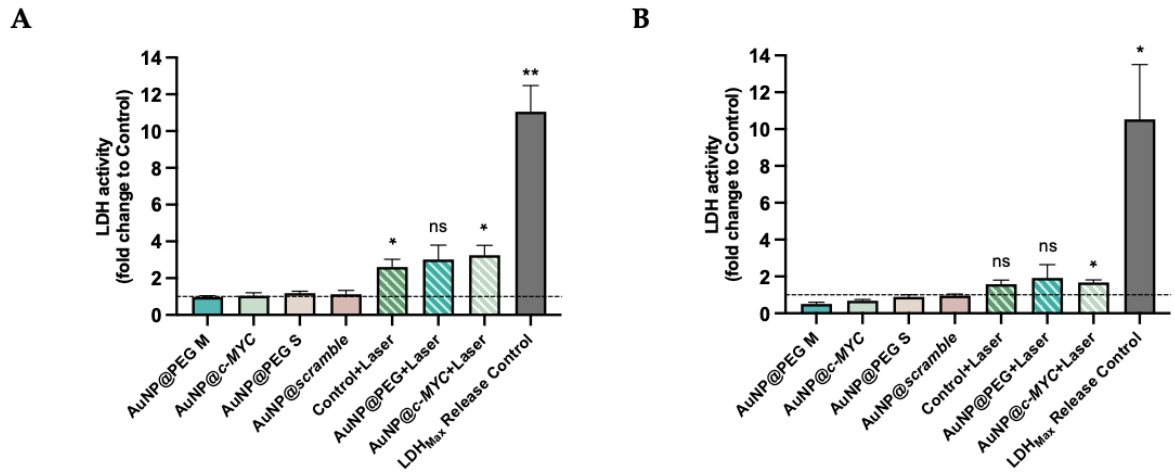

Figure 4.16 - LDH activity analysis after 9 h of *c-MYC* silencing via LDH Assay in 3- and 7-day HCT116 3D spheroids. The seven conditions tested were normalized to untreated cells (Control) and LDH maximum Release Control as Positive Control. Statistical differences were observed between Control+Laser and AuNP@*c-MYC*+Laser with Control in 3-day spheroids; AuNP@*c-MYC*+Laser with Control in 7-day spheroids. Black asterisks indicate statistical differences between samples and the Control (*$p < 0.05$; **$p < 0.01$; ns - not statistically significant; Unpaired parametric t-test with Welch's correction). Data represent the mean value ± the standard error of the mean of two biological independent experiments with three technical replicates for each.

Few studies have reported the combination of laser irradiation and AuNP for gene silencing in a 3D spheroids model [356,484]. Small gold nanoparticles seem to penetrate more than larger AuNPs, indicating that internalization into spheroids depends on the size of AuNPs [452,485]. Huang *et al*. developed a pulsed NIR light-based technique for the spatiotemporal control of gene silencing in 3D-cultured human embryonic stem cells, using siRNA covalently attached to hollow gold nanoshells [486]. Interestingly, 3-day spheroids were more sensitive to localized heat compared to 7-day spheroids, which reinforces the need for the characterization of spheroid size and structure, cells-cells contact, and TME modifications to allow comparison between gene silencing studies with AuNP@ASO combined with photo-irradiation.

4.4 Conclusions

Herein, we demonstrated for the first time the effective silencing of *c-MYC* via mild photothermy in colorectal carcinoma 3D spheroids. The AuNP@PEG were successfully functionalized with ASO, and their stability remains in biological conditions, as well as their unique optical properties. We first verified the effective gene silencing of the *c-MYC* gene at 9 h in HCT116 2D cells using Au-nanoconjugates. Then, we proved that the use of low concentrations of Au-nanoconjugates combined with an LDI 2.37 W/cm^2 for 60 s allows for enhanced cell uptake. Our results highlight the enhancement of *c-MYC* silencing in HCT116 2D cells and 7-day 3D spheroids due to the proposed mild photothermy to improve the internalization of AuNP@*c-MYC*.

The complexity of 3D cell growth showed that there is a clear difference in sensitivity of 3-day spheroids to localized heat compared to 7-day spheroids, which reinforces the relevance of correlating data of gene silencing and cell viability considering the volume of the spheroids and respective cell number/density. These outcomes are important for tailoring novel therapeutic strategies that can enhance gene silencing efficacy and provide more accurate *in vitro* models for cancer research. Overall, our findings offer an efficient approach for the delivery of nucleic acids effectors triggered by mild hyperthermia that might enable spatiotemporal control of gene modulation in 2D and 3D cancer models for gene therapy application.

5

MEMBRANE-LOCALIZED MAGNETIC HYPERTHERMIA FOR TRANSFECTION OF NUCLEIC ACIDS

Data enclosed in this chapter was originally published in the following issue, and I was responsible for the transfection of nucleic acids and gene silencing experiments, cell viability assessment, gene expression assays, and statistical analysis. Synthesis and characterization of MNPs, and optimization of the introduction of azide reporters on the surface of MCF-7 cells and SPAAC reaction with MNPs@PMAO@PEG@DBCO were performed by Javier Idiago-López from Instituto de Nanociencia y Materiales de Aragón, INMA (CSIC-Universidad de Zaragoza) and Centro de Investigación Biomédica en Red de Bioingeniería, Biomateriales y Nanomedicina (CIBER-BBN), Spain.

Idiago-López, J., **Ferreira, D.**, Asín, L., Moros, M., Armenia, I., Grazú, V., Fernandes, A. R., de la Fuente, J. M., Baptista, P. V., & Fratila, R. M. Membrane-localized magnetic hyperthermia promotes intracellular delivery of cell-impermeant probes. *Nanoscale*, *16*(32), 15176–15195 (2024). https://doi.org/10.1039/d4nr01955e

5.1 Introduction

Cell transfection is described as the incorporation of exogenous nucleic acids into target cells and as a valuable tool for the modulation of gene function or gene products with promising therapeutic prospects for many diseases linked to genetic disorders [487,488]. RNAi technology and genome and gene editing tools allow the manipulation of DNA and edit gene sequences, regulate gene expression, and reconfigure chromatin structure, thus modulating specific traits in the target cells' phenotype [102,103]. In particular, siRNA and ASO have been extensively used to target specific mRNA in the cells' cytoplasm to suppress protein translation [489]. The efficacy of target moieties depends on the capability to penetrate the cell membrane and avoid intracellular enzymatic degradation or lysosomal entrapment. Transfection of nucleic acids may be achieved via many different approaches, including viral vectors [490], physical [491,] or chemical (e.g., lipids) methods [183], but all have disadvantages (e.g., cell toxicity, loading efficiency, or cell specificity) [492]. Furthermore, transfection reproducibility and efficiency vary greatly with the cell line or the method used [493].

Advances in materials science and nanotechnology in the past decades have put forward a range of nanomaterials as tools for the transport and delivery of (therapeutic) nucleic acids [186]. This is due to the singular properties that certain nanomaterials exhibit in terms of inherent biocompatibility, easy internalization in cells, protection against nuclease degradation, or their ability to respond to external stimuli (e.g., light, magnetic field) to release the cargo [494–497]. MNPs have been widely exploited for diverse biomedical applications, including imaging, drug delivery, theranostics, separation, and therapeutic hyperthermia [498–502]. Magnetic hyperthermia is based on the ability of certain magnetic materials to generate heat when exposed to an AMF and has been extensively used mostly in cancer therapy [503], but also for controlled drug release [504] and remote control of cellular functions [505–507]. MNPs mediate the conversion of the electromagnetic energy from the AMF to thermal energy via different mechanisms such as hysteresis losses, Néel and Brownian relaxation; the heat dissipated by MNPs depends highly on their intrinsic physico-chemical properties (size, shape, composition, anisotropy), as well as on their environment (medium viscosity, aggregation effects) and on the amplitude and frequency of the AMF [508,509].

While MNPs have been widely exploited for magnetic-field guided delivery of nucleic acids, a technique known as magnetofection [256,304,310,312], the localized heating that takes place in the vicinity of the nanoparticle surface when they are exposed to an external AMF has not been used for transfection purposes. Idiago-López *et al.* recently described the covalent immobilization of MNPs on living cell membranes using SPAAC, one of the most powerful reactions in the bioorthogonal chemistry arsenal [193]. In this case, azide artificial chemical reporters are introduced on the cell membranes through metabolic glycoengineering and can react with MNPs functionalized with cyclooctyne probes to yield stable triazole adducts. Metabolic glycoengineering offers the advantage of a dose-dependent expression of chemical reporters (by

carefully tuning the concentration of the azide metabolic precursor and the incubation times) and can be applied to virtually any cell line [510].

Herein, I shall demonstrate the utility of membrane-localized magnetic hyperthermia via immobilized MNPs for nucleic acids transfection into cancer cells and compare to a standard commercial reagent.

5.2 Materials and Methods

5.2.1 MNPs synthesis and characterization

MNPs synthesis and characterization, water transfer, and functionalization with PEG-NH_2 and DBCO-NH_2 were performed as described in 2.2.2 section (Chapter 2).

5.2.2 Metabolic glycoengineering and MNPs immobilization on the cell membrane

Introduction of azide reporters on the surface of MCF-7 cells and SPAAC reaction with MNPs@PMAO@PEG@DBCO were performed following the conditions previously optimized in a previous work by Idiago-López *et al.* [193].

5.2.3 Plasmid Transfection with Lipofectamine™ LTX with Plus Reagent

The plasmid transfection in MCF-7 cells was performed as described in section 2.2.4 (Chapter 2).

5.2.4 Magnetic hyperthermia-mediated transfection in MCF-7 and MCF-7/GFP cells

MCF-7 and MCF-7/GFP cells were seeded in a 24-well plate at a density of $1.5x10^5$ cells/well and $2.5x10^4$ cells/well for 24 h, respectively. MCF-7 cells were transfected transiently with pAcGFP1 Nuc Vector (carried out as described in section 2.2.4). Subsequently, cells

were treated with 100 μM of Ac_4ManNAz for 48 h before proceeding to magnetic hyperthermia experiments. After 48 h of incubation with Ac_4ManNAz, cells were washed twice with PBS and incubated for 10 minutes with MNP@PMAO@PEG@DBCO (10 μg_{Fe}/mL) in DMEM without FBS at 37ºC. Cells were subjected to two additional washes with PBS, detached with Versene™ solution, centrifuged, and resuspended in a fresh medium. The cell suspension was introduced into an adapted glass vial of 2 mL, 12 x 32 mm in size, suitable for the magnetic hyperthermia equipment, and 20 nM *anti-AcGFP1* was added. The AMF (23.9 kA/m, 418 kHz) was applied for 30 minutes with five-minute pulses and 60-second pauses between pulses, using an magnetic hyperthermia applicator (D5 Series device). As a control for gene silencing experiments, transfection with Lipofectamine™ RNAiMAX was used, according to the manufacturer's instructions. Following transfection, cells were counted and seeded in a 96-well plate for cell viability assay and in a 24-well plate for fluorescence microscopy and RNA extraction, and grown under standard cell culture conditions.

AcGFP1 and copGFP expression was verified by fluorescence microscopy following 24 h and 48 h of gene silencing experiment. 48 h post-transfection incubation, total RNA was extracted, and the efficiency of transfection for AcGFP1 silencing was evaluated by RT-qPCR, and by RT-qPCR and fluorescence microscopy for copGFP silencing. The images were analyzed using ImageJ software and for fluorescence quantification, CTCF was determined using Equation 3.1 (Chapter 3).

5.2.5 Cells transfection with Lipofectamine™ RNAiMAX Reagent

The transfection of *anti-AcGFP1* and *anti-copGFP* in MCF-7 and MCF-7/GFP cells, respectively, was performed as described in section 2.2.5 (Chapter 2).

5.2.6 Cell viability post-transfection

Cell viability assessment via MTS assay was performed as described in section 2.2.6 (Chapter 2).

5.2.7 Gene expression analysis

The analysis of gene expression of *AcGFP1* and *copGFP* via RT-qPCR was performed as described in section 2.2.7 (Chapter 2).

5.2.8 Statistical analysis

Data were analyzed using GraphPad Prism 8.0 (GraphPad Software, San Diego, USA). Unpaired parametric t-test with Welch's correction was used to evaluate differences between groups. They were considered statistically significant at p-value < 0.05. Data are the mean value of at least three independent assays with at least two technical replicates, and the errors are calculated by the standard error of the mean.

5.3 Results and Discussion

5.3.1 MNPs functionalization with strained alkynes

The MNPs used in this work were 13 nm spherical iron oxide MNPs with carboxylic acid surface functionality, obtained following the methodology previously described and optimized by Fratila *et al.* and Moros *et al*.[192,393]. The polymer coating the MNPs - poly(maleic anhydride-*alt*-1-octadecene), PMAO - was modified using a fluorescent dye, tetramethylrhodamine 5-(6)- carboxamide (TAMRA) cadaverine, to allow MNP tracking *in vitro* by fluorescence microscopy [193,511]. The PMAO-coated MNPs, having carboxyl acid groups on their surface, were then functionalized with strained alkynes in a two-step process, by firstly introducing an amino-poly(ethylene glycol) (PEG) derivative to improve the colloidal stability of the MNPs, followed by the incorporation in a second step of a dibenzocyclooctynylamine (DBCO) derivative bearing a short ethylene glycol chain, to yield MNPs@PMAO@PEG@DBCO, as described in a previous work [192,193]. This strategy was chosen due to the hydrophobic character of the DBCO derivative, which leads to a loss of the colloidal stability of the MNPs if the functionalization is attempted directly on the MNPs@PMAO [192].

The preparation and physico-chemical characterization of these MNPs are reported in a recent work by Idiago-López *et al*. [193]; however, relevant characterization data are provided in Figure 5.1 for the specific batches employed in this work.

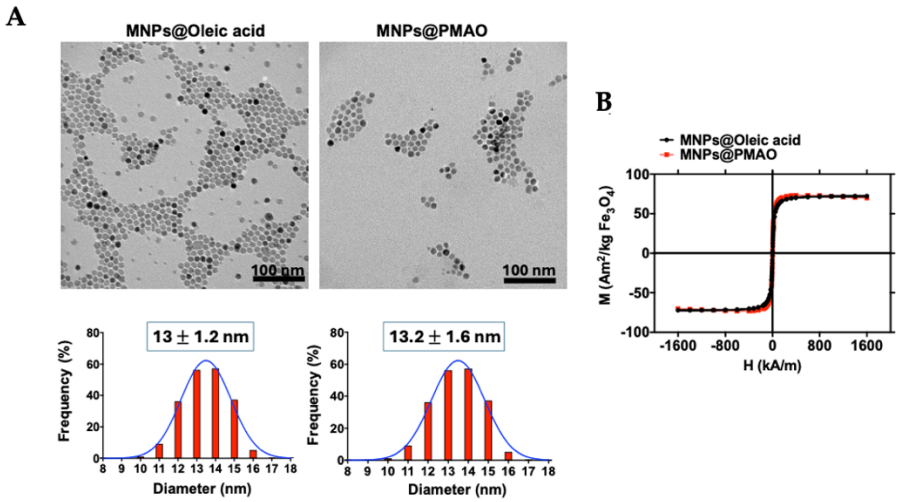

C

MNP	Hydrodynamic diameter (nm, intensity)	ζ potential (mV)
MNPs@PMAO	106 ± 5	-32.6 ± 0.8
MNPs@PMAO@PEG	91 ± 2	-21.1 ± 1.5
MNPs@PMAO@PEG@DBCO	82 ± 3	-8.4 ± 0.4

Figure 5.1 - Physico-chemical characterization of MNPs. (A) TEM images and size distribution histograms of the hydrophobic MNPs obtained by thermal decomposition (MNPs@Oleic acid) and the hydrophilic MNPs after polymer coating (MNPs@PMAO). (B) Field-dependent magnetization of the two types of MNPs. (C) Hydrodynamic diameters and ζ-potential values of the MNPs@PMAO, MNPs@PMAO@PEG and MNPs@PMAO@PEG@DBCO in water.

The heating efficiency of the MNPs@PMAO@PEG@DBCO, expressed in terms of SLP (defined as the power generated per gram of magnetic material) [512] was measured at different AMF amplitudes and frequencies (Figure 5.2), yielding a maximum value of approximately 100 W/gFe at a frequency (f) of 445 kHz and a field amplitude (H) of 16.9 kA/m (AMF conditions within the $H \times f$ safety limit of 5×10^9 A m/s established by Hergt and Dutz [513]), determined in an aqueous suspension at a concentration of 1 mg_{Fe}/mL. Noteworthy, the heating efficiency of these MNPs determined in a suspension prepared in supplemented cell culture medium was very similar to the one obtained in water, suggesting that the slightly higher viscosity of the supplemented cell culture medium had no impact on the SLP values. The SLP measurements described above were performed at a relatively high MNPs concentration, ten times higher than the one used for previous cell membrane immobilization experiments (100 μg_{Fe}/mL)[193]. At low concentrations, MNPs can continue to generate heat locally under the application of an AMF with suitable parameters, although a variation in the temperature of the medium in which they are dispersed is no longer detected.

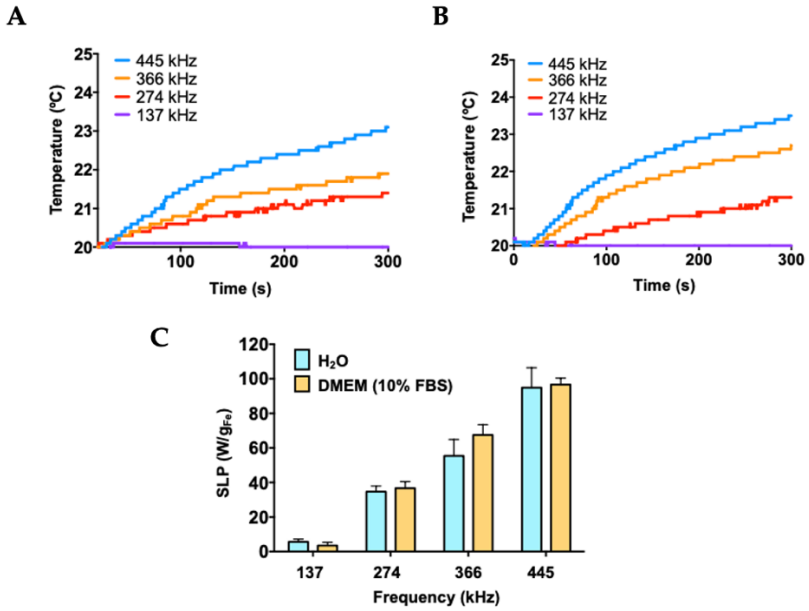

Figure 5.2 - Heating properties of MNPs. SLP measurements of MNPs@PMAO@PEG@DBCO (1 mg_{Fe}/mL) in H_2O (A) and supplemented DMEM (B) at a field amplitude of 16.9 kA/m and different frequencies. (C) Comparison of SLP values in H_2O and supplemented DMEM. Results represent the mean ± standard deviation of two different measurements.

5.3.2 Expression of azide bioorthogonal reporters on cell membranes

As mentioned in the Introduction, for the immobilization of MNPs on living cell membranes using the SPAAC reaction, cells must be engineered to express artificial azide reporters on their surface, while MNPs should be decorated with strained alkynes.

For the labeling of cell membranes with azides, we used the sialic acid metabolic pathway to incorporate these chemical reporters into the glycocalyx. Metabolic glycoengineering relies on the use of a biosynthetic precursor containing an azide functional group, typically Ac_4ManNAz. This synthetic molecule is taken up by cells and efficiently hydrolyzed to N-α-azidoacetylmannosamine (ManNAz) by cytosolic esterases. ManNAz is then converted to sialic acid via five enzymatic steps and conjugated to the end of the sugar chains, displaying end azide reporter groups [514]. It is worth mentioning that the introduction of azide reporters on cell membranes can be achieved in a controlled manner, by adjusting the concentration of the azide precursor and/or the incubation time [295,515]. Indeed, Idiago-López *et al.* demonstrated this dose-dependent expression of azide groups on the membrane of MCF-7 cells (Figure 5.3), and established the optimal conditions of 48 h of incubation with Ac_4ManNAz at a concentration of 100 μM [193].

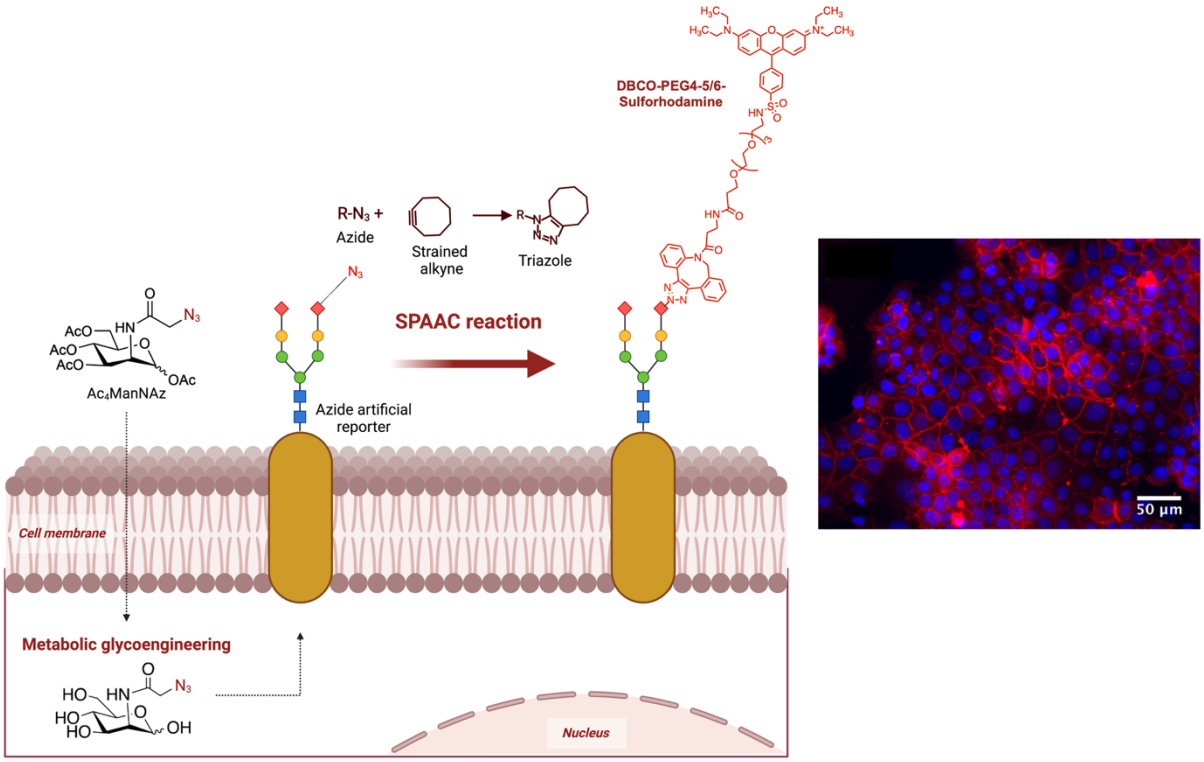

Figure 5.3 - Scheme of the metabolic engineering approach. Expression of azide bioorthogonal reporters on cell surfaces (left) and confocal fluorescence microscopy images of MCF-7 cells treated with $Ac_4ManNAz$ for 48 h, followed by 30 minutes of incubation with 20 µM of DBCO-sulforhodamine B (right). Red: DBCO-sulforhodamine B. Blue: DAPI (nuclei staining). Scale bar: 50 µm. (Created with BioRender.com)

5.3.3 Transfection of nucleic acids via membrane-localized magnetic hyperthermia

After Idiago-López *et al.* confirmed the potential of cell membrane-localized magnetic hyperthermia to induce changes in the membrane fluidity and favor the internalization of impermeant exogenous molecules (YO-PRO®-1) without detrimental effects on cell viability, we sought to extend its use to a specific biomedical application, namely cell transfection [516]. We propose the use of MNPs as "hotspots" able to induce changes in the fluidity of cell membrane and promote the transient transfection of silencing moieties in MCF-7 cells. We considered the MCF-7 cell line a relevant model for developing a novel transfection method based on localized magnetic hyperthermia and cell surface engineering through bioorthogonal chemistry [516].

Probing the effect of localized magnetic hyperthermia for the transfection of silencing moiety into azide-labeled cells requires the selection of a target protein that can be easily quantified with biomolecular techniques (e.g., fluorescence microscopy and RT-qPCR) and whose suppression does not compromise cell viability, such as GFP [517,518]. For this purpose, we demonstrated that our strategy could enhance the transfection of *anti-AcGFP1* targeting a

transiently expressed *AcGFP1* gene in MCF-7 cells and *anti-copGFP* targeting a constitutively expressed *copGFP* in MCF7/GFP cells. An overview of the general concept for cell membrane-localized magnetic hyperthermia-mediated transfection using MNPs immobilized on the cell membrane via SPAAC bioorthogonal chemistry is represented in Figure 5.4.

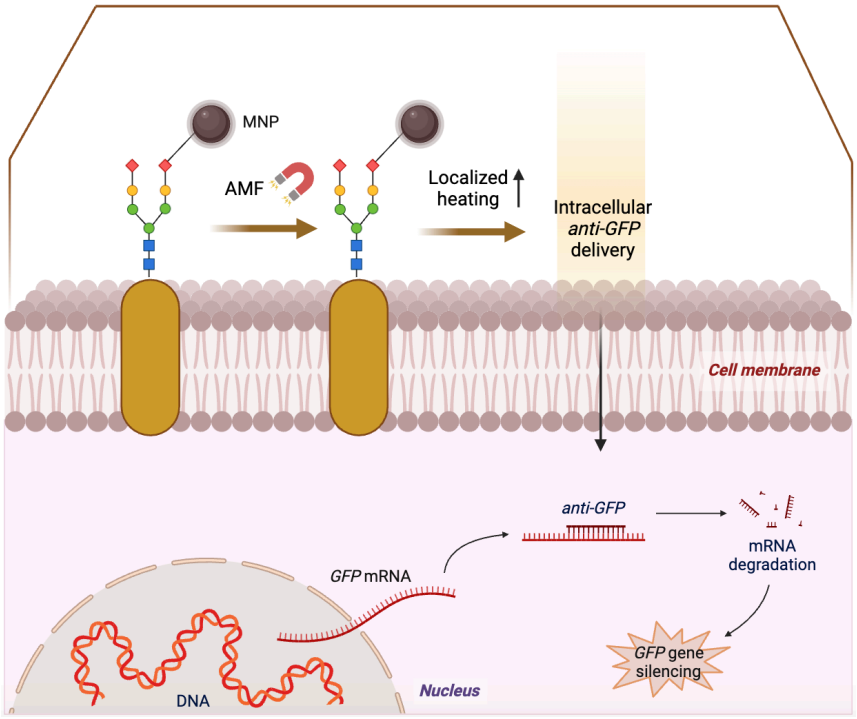

Figure 5.4 - Overview of the general concept for cell membrane-localized magnetic hyperthermia-mediated transfection of anti-*GFP* - MNPs+N_3+MH+. (Created with BioRender.com)

5.3.3.1 Membrane-localized magnetic hyperthermia for *AcGFP1* silencing in MCF-7 cells

Optimization of the conditions for cell transfection experiments was performed in MCF-7 cells co-transfected with pAcGFP1 Nuc Vector, regarding the main parameters (cells confluency, plasmid quantity) and Lipofectamine™ LTX with Plus Reagent standard protocol, as described in section 2.2.4. The analysis of AcGFP1 expression was performed by fluorescence microscopy at 24 h and 48 h post-transfection (Figure 5.5). Results revealed a minimal AcGFP1 expression using 0.25 μg of plasmid for the three time-points tested. However, by increasing the plasmid concentration to 0.5 and 1 μg, each expression rate was almost double when compared to the previous one, confirming a plasmid dose-dependent transfection efficiency. Concentrations above 1 μg of plasmid were discarded because of the inherent toxicity of the Lipofectamine™ LTX with Plus Reagent (the higher the plasmid concentration, the higher the concentration of reagent is required) and to ensure a cost-effective experiment, due to the high price of the transfection reagent.

Concerning fluorescence microscopy images, green cells were counted in four aleatory images, and we determined that using 1 μg of plasmid we could estimate the transfection efficiency of approximately 28%. These results indicate that the optimal AcGFP1 expression was reached with 1 µg of plasmid, and then we selected 48 h post-transfection to perform membrane-localized magnetic hyperthermia due to the prior incubation with azide groups for 48 h, which was previously optimized by Idiago-López *et al.* [193].

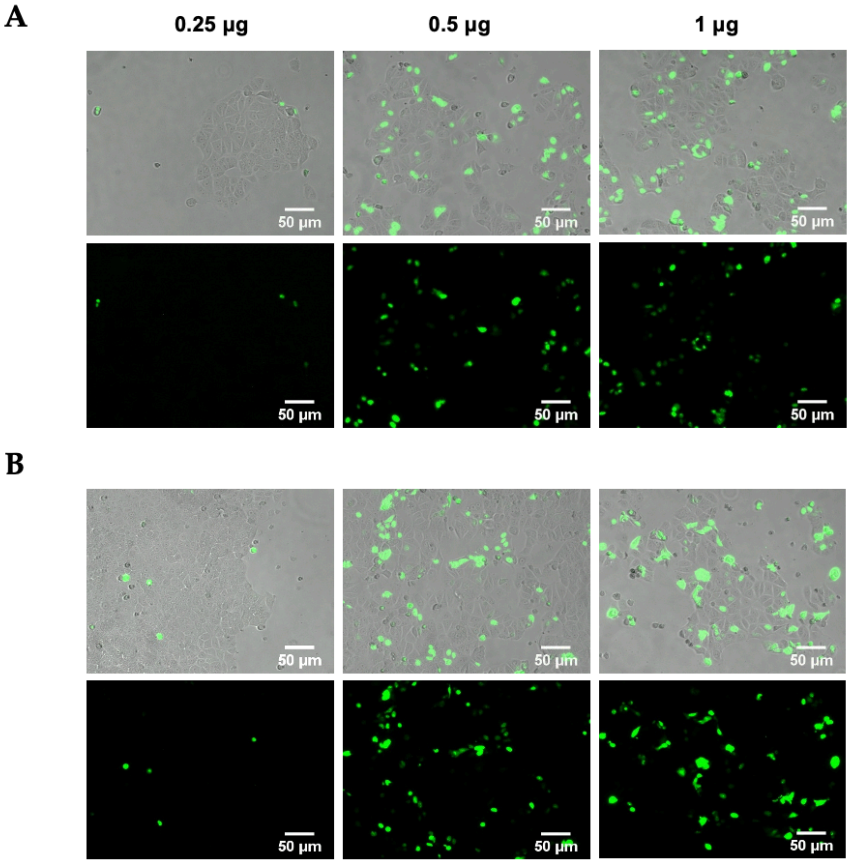

Figure 5.5 - Optimization of the quantity of pGFP (0.25, 0.5, and 1 µg) for MCF-7 cell transfection using Lipofectamine™ LTX with Plus Reagent. Fluorescence microscopy images were obtained for each amount of pAcGFP1 Nuc Vector at (A) 24 h and (B) 48 h post-transfection. Scale bars correspond to 50 µm.

For magnetic hyperthermia silencing experiments (Figure 5.6), MCF-7 cells transiently expressing AcGFP1 were incubated with Ac_4ManNAz for 48 h before magnetic hyperthermia to provide them with artificial azide reporters for the click immobilization of MNPs on the membrane, as determined by Idiago-López *et al.* [193]. Hereafter cells were incubated with MNPs@PMAO@PEG@DBCO (at 10 μg_{Fe}/mL for 10 minutes) and the AMF (23.9 kA/m and 418 kHz) was applied for 30 minutes with pulses (each pulse with a duration of five minutes, with sixty seconds pause between pulses). The transfection efficiency was compared with a positive control using LipofectamineTM RNAiMAX reagent under the same experimental conditions of magnetic hyperthermia samples. Moreover, control experiments using cells

transfected with Ac_4ManNAz treatment, and incubated with MNPs, but without magnetic hyperthermia application (MNPs+ N_3+MH-) were used to verify if the presence of MNPs could promote the intracellular *anti-AcGFP1* delivery. *AcGFP1* silencing was followed for all the conditions tested using fluorescence microscopy, 24 h and 48 h after magnetic hyperthermia-mediated transfection (Figure 5.7A, B). After 48 h, RNA was extracted and expression analysis by RT-qPCR confirmed the effectiveness of magnetic hyperthermia on the silencing of *AcGFP1* (Figure 5.7C).

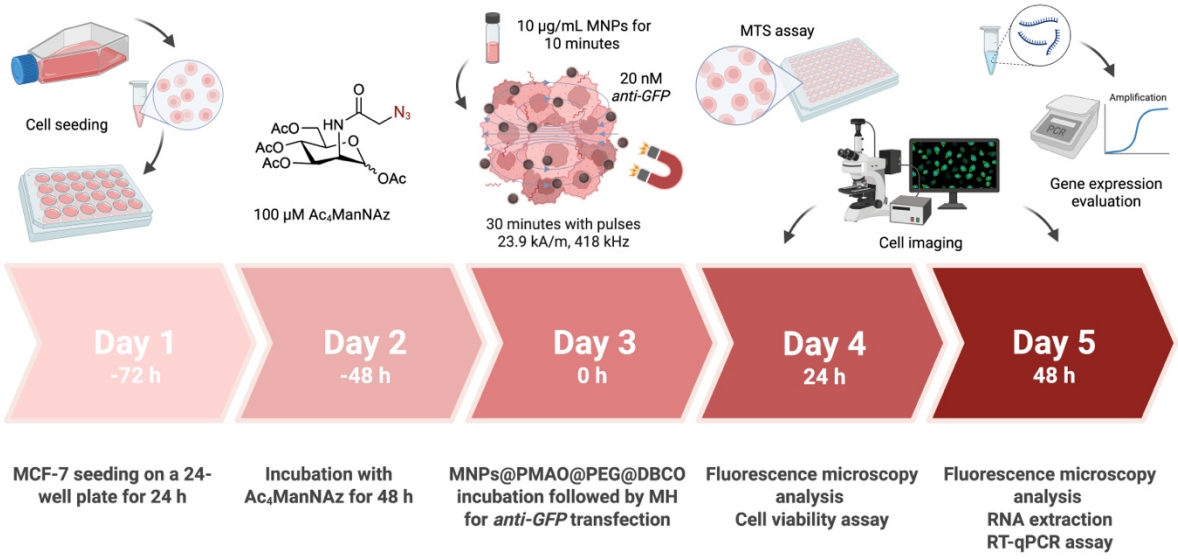

Figure 5.6 - Scheme of the experimental design used to evaluate the nucleic acids transfection via magnetic hyperthermia in MCF-7 cells expressing GFP, labeled with azide groups. (Created with BioRender.com)

The results obtained for *anti-AcGFP1* transfection via magnetic hyperthermia confirm the effect of MNPs+N_3+MH+ (50% of *AcGFP1* silencing) on the transfection of silencing oligos comparable to Lipofectamine™ RNAiMAX reagent (Figure 5.7C). In addition, MNPs+N_3+MH- sample has a slight reduction of *AcGFP1* expression compared to Control (cells without *anti-AcGFP1*), indicating the potential of localized magnetic hyperthermia for transfection. Besides, for the magnetic hyperthermia-treated cells (MH+), although there were no statistical differences in the effect observed between cells expressing azide reporters (N_3+) and cells without azides (N_3-), expression of *AcGFP1* for MNPs+N_3+MH+ was 5% lower than for MNPs+N_3-MH+. This confirms that the non-specific attachment of MNPs to cells without azide groups on the membrane also contributes to permeabilization and promotes the intracellular delivery of *anti-AcGFP1* by AMF. Finally, cells (both N_3+ and N_3-) incubated with MNPs but without magnetic hyperthermia application do not show significant inhibition of the expression of *AcGFP1*.

One of the most important limitations of the commercially available transfection methods are their impact on cell viability, with many reports describing the cytotoxicity of cationic lipid reagents [189,519] or the impact of electroporation on cell viability [520]. For this reason, once the efficiency of the transfection and the silencing of the *AcGFP1* gene was demonstrated, the impact on cell viability was assessed. Lipofectamine™ RNAiMAX was found to induce a statistically significant reduction of cell viability around 25%, which was not observed for magnetic hyperthermia-treated cells (MNPs+N_3+MH+) (Figure 5.7D).

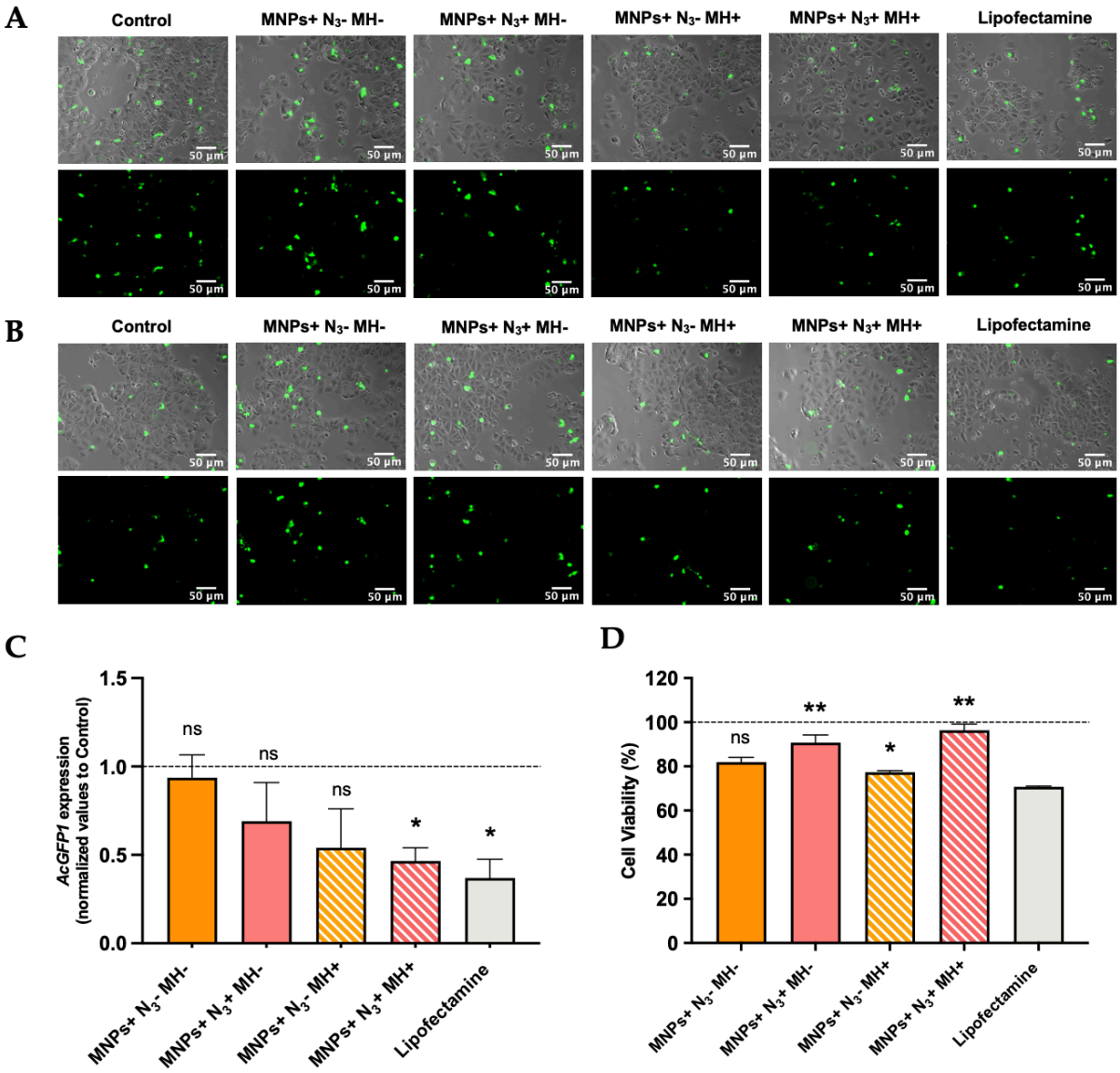

Figure 5.7 - Fluorescence microscopy images of MCF-7 cells, RT-qPCR analysis, and cell viability assessment 48 h post-transfection. Fluorescence microscopy images (A) 24 h and (B) 48 h after magnetic hyperthermia experiment for the different conditions tested. Scale bars correspond to 50 µm. (C) RT-qPCR to evaluate *AcGFP1* gene expression in different conditions tested. Expression levels were normalized to unchallenged cells (Control, $2^{-\Delta\Delta Ct}$=1). Black asterisks indicate statistical differences between MNPs+N_3+MH+ and Lipofectamine with the Control (*$p < 0.05$; unpaired parametric t-test with Welch's correction). Data represent the mean value ± the standard error of the mean of three biologically independent experiments with two technical replicates for each. (D) Cell viability

analysis of the different samples tested after magnetic hyperthermia via MTS assay. The statistical difference between Lipofectamine sample and the other conditions is represented (*p < 0.05; **p < 0.01; ns – not statistically significant; unpaired parametric t-test with Welch's correction). Data represent the mean value ± the standard error of the mean of at least three biologically independent experiments with two technical replicates each.

5.3.3.2 Membrane-localized magnetic hyperthermia for *copGFP* silencing in MCF-7/GFP cells

Afterward, we proved our magnetic hyperthermia-mediated transfection in MCF-7 cells constitutively expressing copGFP, and *copGFP* silencing was followed 24 h and 48 h after magnetic hyperthermia, by fluorescence microscopy (Figure 5.8).

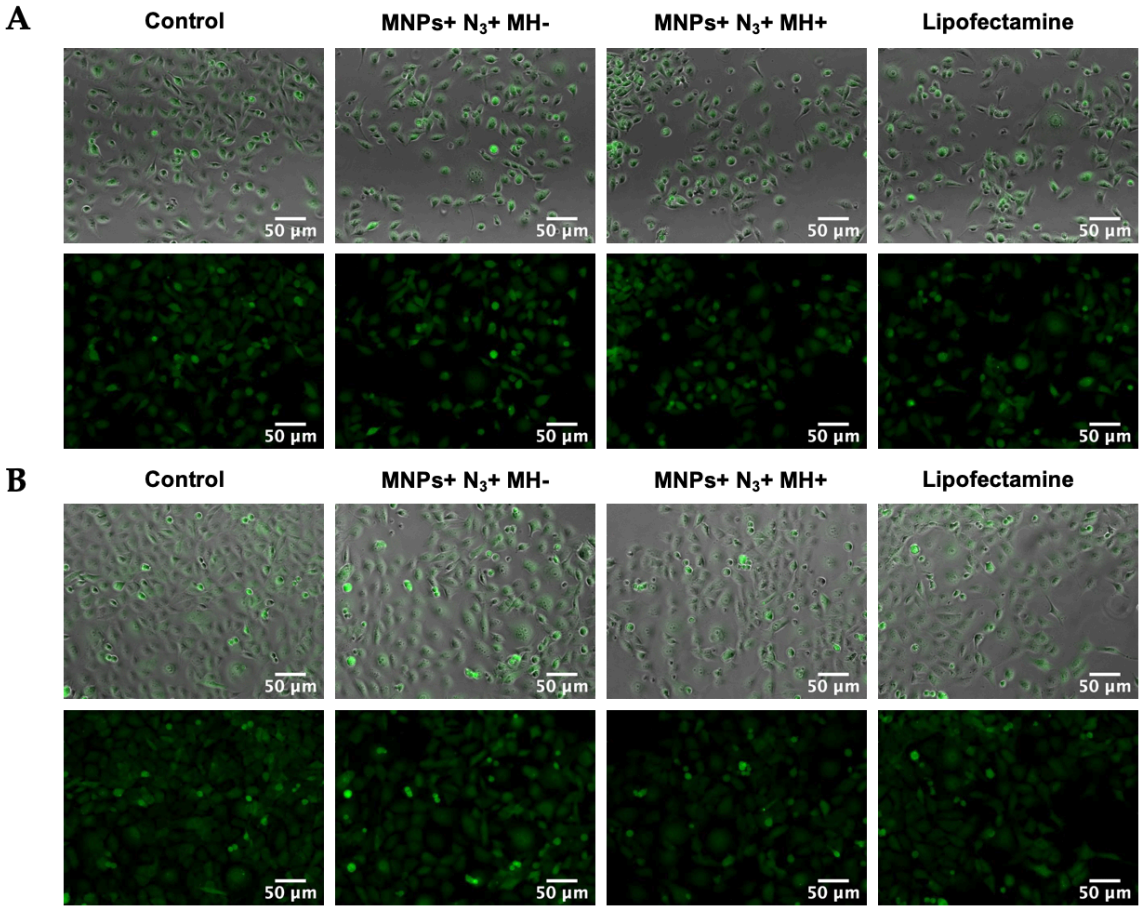

Figure 5.8 - Fluorescence microscopy images of MCF-7 cells constitutively expressing *copGFP* gene. Fluorescence microscopy images at (A) 24 h and (B) 48 h after magnetic hyperthermia experiment in the different conditions tested.

The results obtained were similar to the ones attained in MCF-7 cells transiently expressing AcGFP1 and reveal that in cells with MNPs attached to the membrane via click chemistry and exposed to AMF (MNPs+N_3+MH+), *copGFP* expression was 40% lower (Figure 5.9A).

This silencing was comparable with that obtained using the commercial Lipofectamine™ RNAiMAX, but without cytotoxicity (Figure 5.9C).

Moreover, in the absence of AMF (MNPs+N_3+MH-), no statistically significant reduction of *copGFP* expression was observed compared to Control (cells without *anti-copGFP*), indicating the potential of localized magnetic hyperthermia for transfection in MCF7/GFP cells (Figure 5.9A). The quantitative analysis of CTCF of fluorescence microscopy images from the 48h post-magnetic hyperthermia transfection, demonstrated a statistically significant difference between MNPs+N_3+MH+ and Lipofectamine samples with the Control for reduction of copGFP protein expression (Figure 5.9B), confirming the effect of gene silencing.

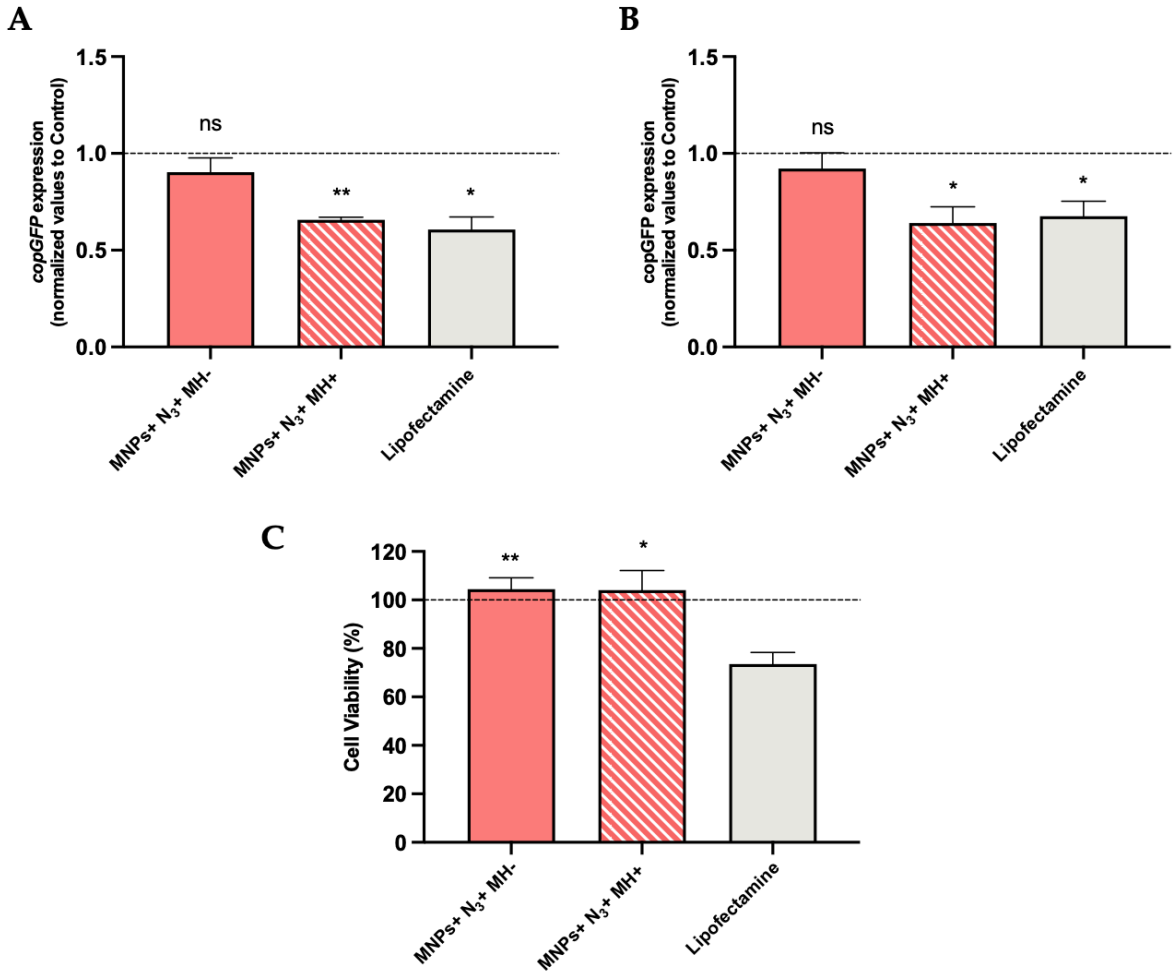

Figure 5.9 - RT-qPCR analysis, CTCF evaluation of the fluorescence microscopy images of MCF-7/GFP, and cell viability assay. (A) *copGFP* gene expression after 48 h post-transfection in the different samples tested. The gene expression levels were normalized to the Control. Black asterisks indicate statistical differences between MNPs+N_3+MH+ and Lipofectamine with the Control, $2^{-\Delta\Delta Ct}$=1; (**p < 0.01; *p < 0.05, respectively; ns – not statistically significant; unpaired parametric t-test with Welch's correction). Data represent the mean value ± the standard error of the mean of three biologically independent experiments with two technical replicates for each. (B) CTCF analysis to evaluate copGFP protein expression at 48 h post-transfection. Black asterisks indicate statistical differences between MNPs+N_3+MH+ and Lipofectamine with the Control (*p < 0.05; ns – not statistically significant; unpaired parametric t-test with Welch's correction). Data represent the mean value ± the standard error of the mean

of three biologically independent experiments with two technical replicates for each. (C) Cell viability analysis of the different samples tested after magnetic hyperthermia via MTS assay. The statistical difference between Lipofectamine sample and the other conditions is represented (*$p < 0.05$; **$p < 0.01$; ns – not statistically significant unpaired parametric t-test with Welch's correction). Data represent the mean value ± the standard error of the mean of at least three biologically independent experiments with two technical replicates each.

These results confirmed that the MNPs immobilized on the cell membrane acted as "hotspots" under an AMF, inducing localized heating and triggering an increase in the fluidity of the membrane, which enhances the transfection of exogenous molecules [516]. The effect observed might reached its maximum when the cell membrane glycocalyx was labeled with azides, as the density of "hotspots" generated on the membrane was the highest among all different conditions tested. This new transfection method can attain similar efficiencies of transfection compared to the gold standard Lipofectamine™ RNAiMAX without cellular cytotoxicity.

Overall, results suggest the modulation of the cell membrane permeability and fluidity based on the so-called "hotspot" behavior of the MNPs. These findings are supported by a recent report based on the effect of the localized increase in temperature in the immediate environment of individual MNP deposited on a model cell membrane upon the application of the AMF [521]. The use of magnetic hyperthermia as a stimulus for inducing membrane permeabilization has also been documented by Alvarez-Berríos *et al*., who proved that Caco-2 colorectal adenocarcinoma cell line subjected to magnetic fluid hyperthermia using iron oxide carboxymethyl dextran nanoparticles showed a higher sensitivity to cisplatin therapy than in the case of a similar temperature increase (41°C) induced by hot water hyperthermia, an effect attributed to an increase of cell membrane fluidity favoring the passive transport of the drug across the membrane [522]. However, in this report the MNPs were not immobilized onto the membranes of living cells but suspended in the cell culture medium. On the other hand, Hulangamuwa *et al.* found that the use of internalized MNPs in U937 pro-monocytic cell line (derived from histiocytic lymphoma) and the application of very short pulses (200 μs) of an inhomogeneous magnetic field at a frequency of 30.9 kHz favored the internalization of a model drug (doxorubicin) due to the change in membrane permeability [520,523]. Nonetheless, this phenomenon did not stem from the "hotspot" effect of the MNPs and might be caused by the transmission of ultrasonic frequency sound waves resulting from the translational motion of MNPs within the applied magnetic field.

5.4 Conclusions

In this chapter, we validated the successful transfection of nucleic acids into MCF-7 cells (transiently or stably expressing GFP) and the subsequent *GFP* silencing through the application of localized heating generated by MNPs immobilized on cell membranes, with similar

levels compared to Lipofectamine™ RNAiMAX reagent, but without affecting cell viability. This approach addresses some of the challenges associated with standard transfection methods, providing a safer method for improving the delivery and action of (therapeutic) nucleic acids, with spatiotemporal control through the application of an AMF.

This on-demand modification of cell membrane permeability will allow the magnetic hyperthermia-mediated intracellular transport of biologically relevant (bio)molecules, drugs, and nanomaterials, promoting direct intracellular delivery and thus overcoming traditional endocytosis pathways and avoiding endosomal entrapment. Moreover, cell surface engineering with artificial chemical reporters such as the azide groups and the nanoparticles immobilization via bioorthogonal chemistry could provide a universal tool for intracellular delivery, applicable practically to any cell line and nanoparticle type. Considering this, we will further explore the membrane-localized magnetic hyperthermia for transfection of a siRNA against *IDO1* gene, an immunomodulatory gene involved in TME, in cells difficult to transfect (THP-1 cell line as a DCs-model) - Chapter 6.

6

TRANSFECTION OF SIRNA AGAINST *IDO1* GENE VIA MAGNETIC HYPERTHERMIA IN THP-1-DERIVED-DCS

The work presented in this chapter is being prepared for submission (Heat up, Silence On: *IDO1* gene silencing in THP-1-derived Dendritic Cells triggered by Magnetic Hyperthermia). I was responsible for the differentiation and characterization of THP-1 cell line in DCs, characterization of cell membrane labelling, siRNA transfection and gene silencing experiments, cell viability assessment, gene expression assays and statistical analysis. The optimization of THP-1 cells differentiation in DCs and expression and characterization of azide groups were performed with the help of Laura Asín, the synthesis and characterization of MNPs@PMAO@PEG@CO were performed by Javier Idiago-López, both from Instituto de Nanociencia y Materiales de Aragón, INMA (CSIC-Universidad de Zaragoza) and Centro de Investigación Biomédica en Red de Bioingeniería, Biomateriales y Nanomedicina (CIBER-BBN), Spain.

6.1 Introduction

DCs have been used *in vitro* and *in vivo* studies, and in clinical trials as primary targets for autoimmune disorders, infectious diseases, allergy, and cancer [524]. Primary DCs are extremely difficult to manipulate *in vitro* and *in vivo* owing to the lower number of cells obtained [525]. Over the years the identification of different maturation stages and phenotypes of DCs have been explored, but their specific characteristics and functions in a specific biological system still require a better understanding [525–528]. Hence, monocytes or other bone marrow-derived stem cells, and myeloid leukemia-derived cell lines have been used as DCs precursors for isolation and differentiation *in vitro* to increase knowledge of the role of DCs in cancer immunomodulation [527–529]. DCs have been employed for the development of vaccine delivery systems, gene therapy, and cancer immunotherapy strategies. For instance, electroporation [530–532] and viral approaches [533,534] are the most common transfection methods for DCs, but still present limitations (e.g., low transfection efficiency and cytotoxicity) [535]. Since DCs are difficult to transfect, alternative non-viral nanoscale approaches, such as organic and inorganic nanoparticles, must be addressed to improve gene delivery [533,536].

IDO1 is a cytosolic heme-containing enzyme that plays a key role in the degradation of tryptophan to kynurenine and in the modulation of innate immune responses [537–539]. Recent findings suggest that IDO-expressing DCs in cancer contribute to immune tolerance by suppressing the function of effector T and NK cells, while promoting the expansion of Treg cells and MDSCs [540–542]. Nevertheless, silencing of *IDO1* gene in DCs represents a powerful novel strategy in gene therapy due to their ability to regulate T cells function and activation. For instance, immature DCs (iDCs) and mature DCs (mDCs) have an essential function in the TME, decreasing T cells activity owing to the induction of immune suppression that promotes tumor progression and survival [543,544].

The delivery of TNAs, such as siRNA, shRNA, and ASO has been reported as a proper strategy to silence specific intracellular targets to overcome tumor development and metastasis [545–547]. No single transfection approach for delivering TNAs suits all cell types and experimental goals. The optimal transfection strategy is determined by many factors, such as: i) the origin of cells; ii) the type of nucleic acids to be transfected; iii) the transfection efficiency; iv) the host-cells cytotoxicity; v) the experimental budget, and vi) the availability of required facilities [189]. Subsequently, innovative, less cytotoxic, and more effective approaches for siRNA delivery into DCs compared to commercial transfection reagents or electroporation methods are required [535,548–551].

Previously, we demonstrated that cell membrane-localized magnetic hyperthermia enhances the transfection of *anti-GFP*, effectively silencing the *GFP* gene in the MCF-7 breast adenocarcinoma cell line (Chapter 5). In this chapter, we applied this strategy in more difficult to transfect cells, such as DCs derived from THP-1 acute monocytic leukemia cell line as model, for the delivery of siRNA targeting *IDO1* that could enhance immunomodulation for cancer therapeutics. The general concept for magnetic hyperthermia-mediated transfection

using MNPs immobilized on the cell membrane of THP-1-derived DCs is represented in Figure 6.1.

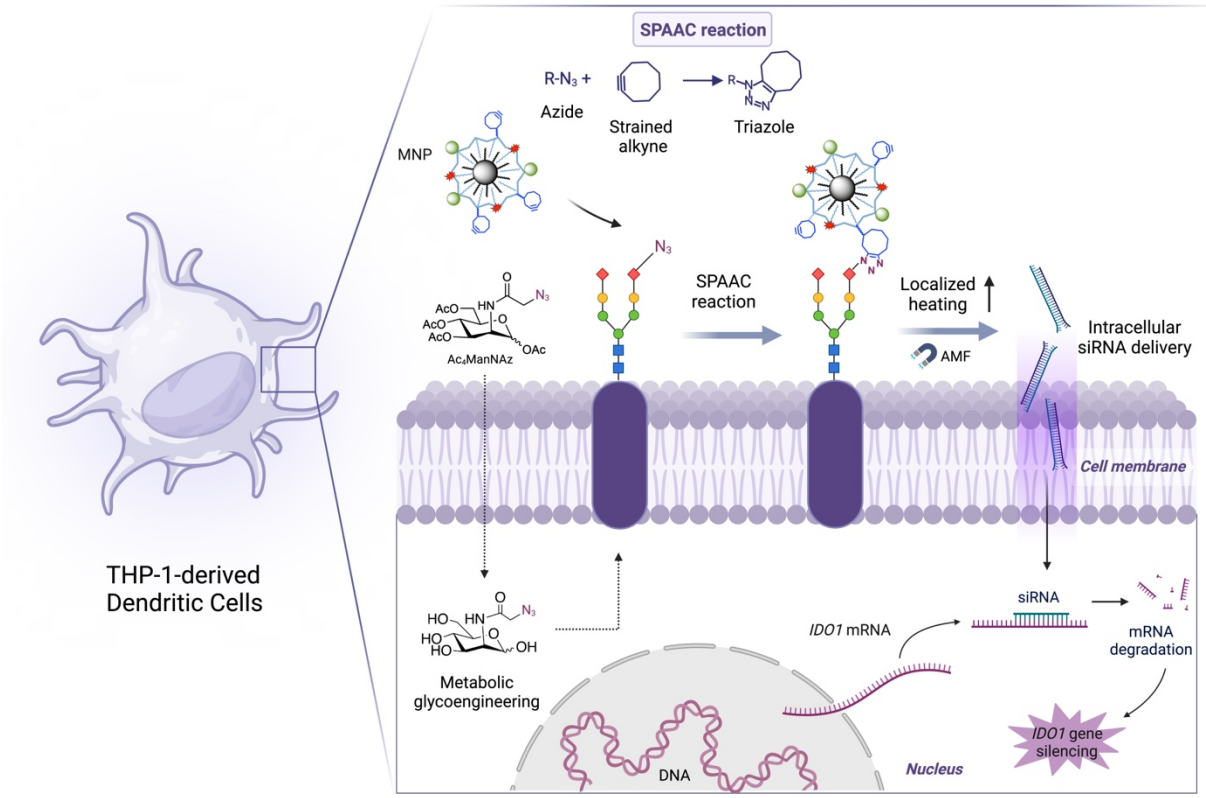

Figure 6.1 - Schematic overview of the magnetic hyperthermia-mediated siRNA transfection. The magnetic nanoheaters (MNPs functionalized with cyclooctyne) were attached to the membrane of THP-1-derived DCs previously exposed to metabolic glycoengineering to express unnatural azide bioorthogonal reporters. Upon application of the AMF, the localized changes in cell membrane fluidity were used for intracellular delivery of siRNA to silence the *IDO1* gene.

6.2 Materials and Methods

6.2.1 MNPs synthesis and characterization

MNPs synthesis and characterization, water transfer, and functionalization with PEG-NH_2 and CO-NH_2 were performed as described in 2.2.2 section (Chapter 2).

6.2.2 THP-1 acute monocytic leukemia cell line differentiation in THP-1-derived DCs

For differentiation of THP-1-derived iDCs, $2x10^5$ cells/mL of THP-1 were grown in RPMI supplemented with 25 ng/mL of recombinant human Interleukin 4 (rh IL-4) and recombinant human Granulocyte Macrophage Colony-Stimulating Factor (rh GM-CSF). Cells were incubated for five days at 37ºC, under standard cell culture conditions and the culture medium of THP-1-derived iDCs was replaced every two or three days, supplemented with 25 ng/mL of IL-4 and GM-CSF. For THP-1-derived mDCs, $2x10^5$ cells/mL of THP-1-derived iDCs were grown in culture medium without FBS, supplemented with 25 ng/mL of rh IL-4 and rh GM-CSF, 200 ng/mL of Ionomycin and 25 ng/mL of recombinant human Tumor Necrosis Factor α (rh TNF-α) for three days at 37ºC, 5% (v/v) $C0_2$ and 99% of relative humidity. After this incubation period, the THP-1-derived mDCs culture medium was replaced with RPMI supplemented with FBS and respective growth factors [552–554].

6.2.3 Characterization of the expression of cell membrane receptors

The expression of each specific membrane receptor was measured using suitable monoclonal antibodies conjugated with phycoerythrin (PE). In a microfuge tube, $2x10^5$ cells were placed with PBS supplemented with 10% FBS and the respective monoclonal antibody: Monoclonal IgG1 (Isotype Control), Monoclonal CD80 (costimulatory molecule CD24), Monoclonal CD83 (signal of maturation) and CD86 (costimulatory molecule CD24); incubated for 30 minutes at 4ºC, in a dark room. At last, cells were centrifuged to remove the supernatant, washed twice and resuspend in PBS. Flow cytometry was analyzed on an Attune® Acoustic Focusing Flow Cytometer and Attune® Cytometric software. The fluorescence of PE (λ_{abs} 488 nm/λ_{em} 575 nm) was acquired using filter BL2 (excitation and emission range wavelengths of 488 nm and 561 to 587 nm, respectively).

6.2.4 Cell membrane labeling in THP-1 cells and THP-1-derived DCs

6.2.4.1 Expression and characterization of azide groups

Cells were seeded at a density of $1.5x10^5$ cells/well on a 24-well plate in supplemented RPMI and incubated with 10, 20, 50, and 100 μM of Ac_4ManNAz for 48 h at 37°C, under standard cell culture conditions. Upon incubation, cells were washed twice with DPBS (PBS with extra Ca^{2+} and Mg^{2+}). Then, cells were incubated for 30 minutes at 37°C in serum-free RPMI containing 20 μM DBCO-PEG_4-5/6-Sulforhodamine B. Cells without Ac_4ManNAz pre-

treatment were used as control. Lastly, the cells were washed twice, resuspend in PBS and analyzed by flow cytometry. The fluorescence of Sulforhodamine B (λ_{abs} 568 nm/λ_{em} 585 nm) corresponding to red fluorescence, was acquired using filter BL2 (excitation and emission range wavelengths of 488 nm and 561 to 587 nm, respectively).

6.2.4.2 Interaction of MNPs with cells treated and non-treated with Ac_4ManNAz

6.2.4.2.1 Confocal Microscopy

Cells were seeded at a density of $1.5x10^5$ cells/well on 12 mm coverslips treated with 0.01 % (v/v) of poly-L-lysine solution inside a standard 24-well plate and incubated with 100 μM of Ac_4ManNAz for 48 h at 37°C, under 5% CO_2 and 99% relative humidity. Following 48 h, cells were washed twice with DPBS and incubated with 20 μM of DBCO-PEG_4-5/6-TAMRA as control to ensure the correct expression of azide groups on the cell membrane, and with 100 μg_{Fe}/mL of MNPs for 30 minutes; or 10 μg_{Fe}/mL of MNPs for 10 minutes, in RPMI without FBS at 37ºC. Control experiments were also performed using cells without Ac_4ManNAz pre-treatment. After this step, cells were swiftly washed twice with DPBS and fixed with 4 % (v/v) of paraformaldehyde for 20 minutes at RT and under light protection. After fixation, cells were washed twice with PBS and stained for 15 minutes at RT with 7.5 μg/mL of Hoechst 33258. Then, two more washing steps with PBS were performed and the coverslips were mounted on glass microscope slides using ProLong™ Glass Antifade Mountant. Confocal microscopy images were acquired using a Confocal Microscope Zeiss LSM 710 with a 40x oil immersion objective. TAMRA and Hoechst fluorophores were laser excited at 561 and 405 nm, respectively. Laser intensity and sensitivity values were optimized and maintained constant for each image capture for the samples with the same amount of fluorophore. Z stack images were obtained with a 1024 x 1024 resolution and analyzed with the ImageJ software.

6.2.4.2.2 Flow Cytometry

Cells were seeded at a density of $1.5x10^5$ cells/well in 24-well plates and incubated with 100 μM of Ac_4ManNAz for 48 h at 37°C, under standard cell culture conditions. After 48 h, cells were then washed twice with DPBS. Samples were incubated for 10 minutes with 10 μg_{Fe}/mL of MNPs in RPMI without FBS. Control experiments were also carried out using cells without Ac_4ManNAz pre-treatment, and as positive control cells were incubated for 30 minutes at 37ºC with 20 μM of DBCO-PEG_4-5/6-TAMRA. Cells were washed twice with PBS and resuspended in PBS and analyzed by flow cytometry. The fluorescence of TAMRA (λ_{abs} 560 nm/λ_{em} 565 nm) corresponding to red fluorescence, was acquired using filter BL2 (excitation and emission range wavelengths of 488 nm and 561 to 587 nm, respectively).

6.2.5 Magnetic hyperthermia-mediated transfection in THP-1-derived DCs

THP-1-derived DCs cells were seeded at a density of $3x10^5$ cells/well and treated with 100 μM of Ac_4ManNAz before the magnetic hyperthermia experiment for 48 h at 37ºC, under 5% CO_2 and 99% relative humidity. After 24 h, 10 ng/μl of LPS was added to cells to induce expression of *IDO1* gene. Following 48 h with Ac_4ManNAz treatment, cells were washed twice with PBS and incubated for 10 minutes with 10 μg_{Fe}/mL of MNPs in RPMI without FBS. Then, cells were washed twice with PBS, centrifuged, and resuspended in fresh supplemented medium. The cells suspension was introduced into the adapted glass vial suitable for the magnetic hyperthermia equipment, and 20 nM of siRNA complementary to *IDO1* mRNA (GenBank NM_002164.6) was added. Magnetic hyperthermia was applied for 30 minutes with pulses (each 5 minutes, 60 seconds pause), 300 Gauss, 418 kHz in a magnetic hyperthermia applicator (DM100 Series device). As control of gene silencing, 20 nM of siRNA was added with Lipofectamine™ RNAiMAX, according to manufacturer's recommendations. After transfection with the siRNA, cells were counted and seeded on 96-well plate for cell viability assessment and on a new 24-well plate for RNA extraction at 37°C, under standard cell culture conditions.

6.2.6 Cells transfection with Lipofectamine™ RNAiMAX Reagent

The transfection of siRNA against *IDO1* in THP-1-derived DCs was performed as described in section 2.2.5 (Chapter 2).

6.2.7 Cell viability assessment

The MTS assay was performed to evaluate the viability of cells incubated with Ac_4ManNAz and MNPs and the viability of THP-1-derived DCs following the transfection of siRNA mediated by magnetic hyperthermia, as described in section 2.2.6 (Chapter 2).

6.2.8 Gene expression analysis

The analysis of gene expression of *IDO1*, *IL6*, *IL10*, *TNFA*, and *IL12A* via RT-qPCR was performed as described in section 2.2.7 (Chapter 2).

6.2.9 Statistical analysis

Data were analyzed using GraphPad Prism 8.0. Two-way ANOVA with Tukey's multiple comparison test and unpaired parametric t-test with Welch's correction were used to evaluate differences between groups. They were considered statistically significant at p-value < 0.05. Data are the mean value of at least two independent assays with at least two technical replicates, and the errors are calculated by the standard error of the mean.

6.3 Results and Discussion

6.3.1 THP-1 acute monocytic leukemia cell line as DCs-model

The immunomodulation of DCs is required to overcome the immune suppression in cancer therapy. DCs can activate inflammatory cytokines such as TNF-α, IL-12 and interferon-γ, co-stimulatory molecules (e.g., CD80, CD86, CD40), necessary for cytotoxic effect; or anti-inflammatory cytokines (e.g., IL-10, IL-13), transforming growth factor β (TGF-β) and other inhibitory receptors that can mediate signaling pathways involved in cancer [528,553,555–557]. In Table 6.1, the main differences between iDCs and mDCs are presented.

Table 6.1 - Morphological and immunological characteristics of iDCs and mDCs [558].

Characteristics	iDCs	mDCs
Cell morphology	Round and smooth surface; change shape and migrate to lymph nodes induced by cytokines after phagocytosis.	Rough surface with multiple pseudopodia; migrate to lymph nodes using active movement of dendrites at higher speed than iDCs.
Cell phenotype	Lower levels of CD80, CD83, CD86 and MHC II; secrete lower levels of cytokines (IL-12, IL-10 and TNF-α); express chemokine receptors (CCR7) and are induced by chemokines (CCL19 and CCL21) after phagocytosis.	High levels of costimulatory molecules (CD80, CD83, CD86); secrete higher levels of immunostimulatory cytokines (TNF-α, IL-12 and IL-10); express increase levels of fascin-1, an actin-bundling protein.

Cell behavior	Ability to detect and phagocytize pathogens and antigens; initiate innate and adaptative immunity responses.	Ability to produce higher levels of immunostimulatory cytokines and to behave as antigen-presenting cells for T cells activation.

Some myeloid leukemia-derived cell lines (e.g., THP-1, U937, and MUTZ-3) stimulated by specific growth factors and cytokines can resemble differentiated DCs-model [552–554,559]. THP-1 have been reported as an appropriate cell model owing to their similar immunophenotype, functional characteristics, and typical morphology comparable to iDCs and mDCs when induced with IL-4, *GM-CSF*, TNF-α, and ionomycin (Figure 6.2) [560]. The differentiation stage and morphology of THP-1 cells are similar to those observed in human primary monocytes and macrophages. THP-1 cells have a large, round single-cell morphology, express specific monocytic markers, and have an advantage due to their easy manipulation *in vitro* [559].

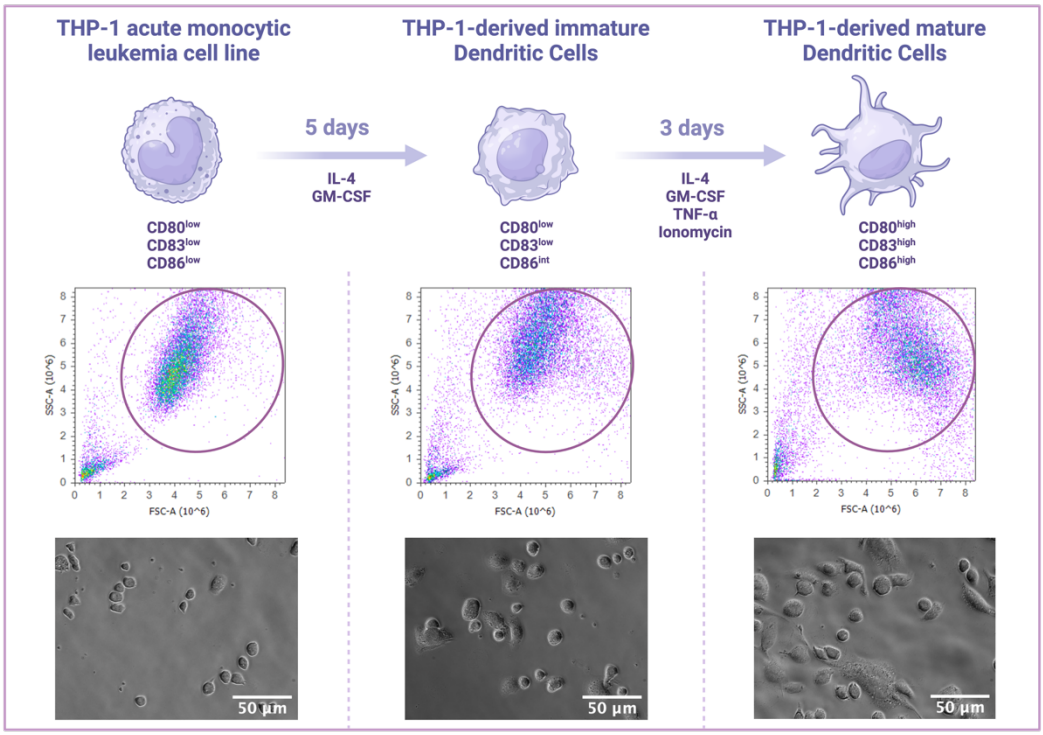

Figure 6.2 - Differentiation of THP-1 cell line in a DCs-model. THP-1 cells were incubated with IL-4 and GM-CSF for five days under standard cell culture conditions to differentiate into THP-1-derived iDCs. Then, THP-1-derived iDCs were induced with IL-4, GM-CSF, TNF-α, and ionomycin for three days in serum-free media under standard cell culture conditions to mature into THP-1-derived mDCs. A shift in the flow cytometry plots' forward scatter (size) and side scatter (complexity) was observed due to the differentiation and maturation of THP-1-derived DCs.

After finishing the incubation time necessary for cell differentiation in the presence of the respective growth factors and cytokines, the expression of THP-1-derived DCs membrane receptors was characterized by flow cytometry using monoclonal antibodies conjugated with fluorescent dye (PE). CD80 and CD86 are co-stimulatory molecules important for T cells activation and regulation, mostly expressed in mDCs [555,558]. Furthermore, the presence of CD83 is a signal of DCs maturation, whose expression can be detected in activated immune cells and antigen-presenting cells [561]. The results obtained in Figure 6.3 show a higher expression of CD80, CD83, and CD86 in THP-1-derived mDCs (see the purple rectangle in Figure 6.3A), proving that THP-1 cell line can be differentiated into mDCs in agreement with the literature. Compared to THP-1 cells, the expression of CD80 (Figure 6.3B) increases 3-fold and 16-fold in THP-1-derived iDCs and in THP-1-derived mDCs, respectively. A significant increase of CD83 expression (Figure 6.3C) around 5-fold and 25-fold was observed in THP-1-derived iDCs and in THP-1-derived mDCs compared to THP-1 cells, which confirms DCs maturation. Moreover, in Figure 6.3D a higher expression of CD86 was observed in THP-1 derived mDCs, approximately 4-fold and 2-fold compared to THP-1 derived iDCs and THP-1 cells, respectively.

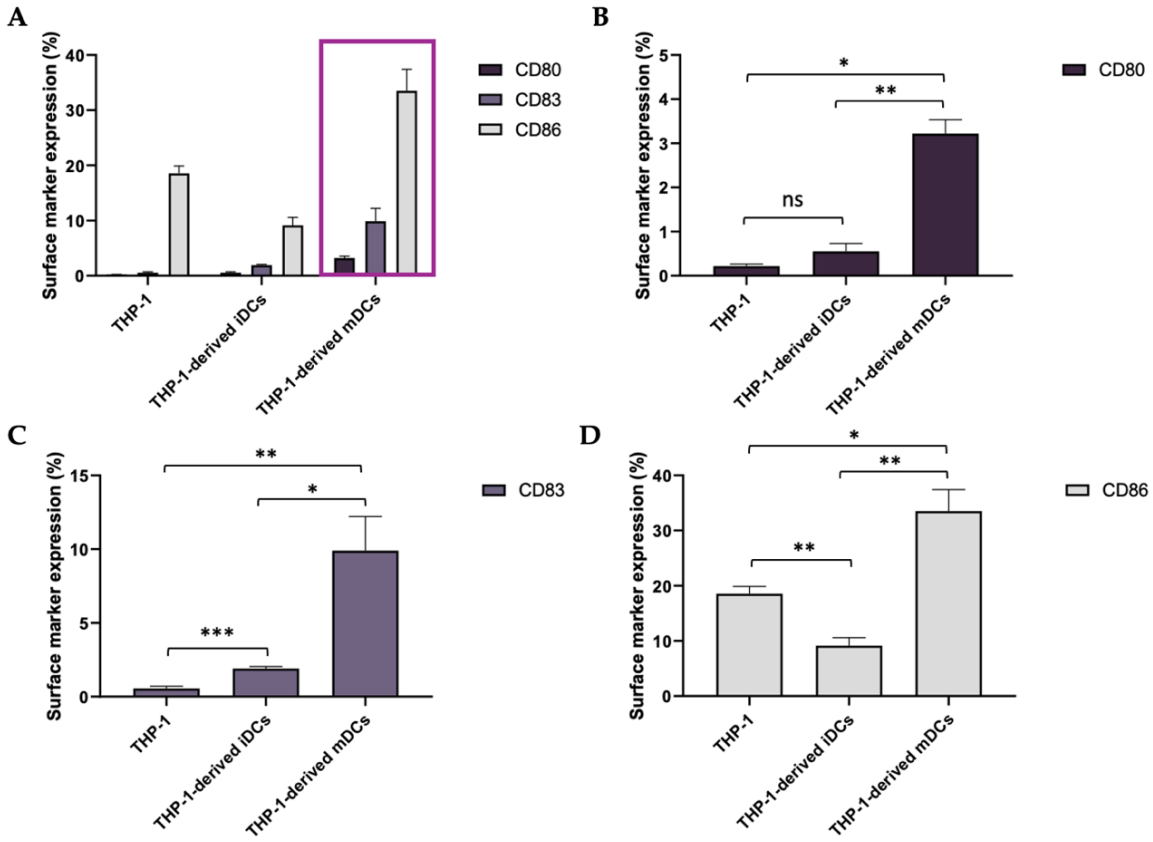

Figure 6.3 - Characterization of membrane receptors expression in THP-1 cells and in THP-1-derived DCs. (A) Surface markers expression analyzed by flow cytometry in the different stages of THP-1 cells; (B) CD80 surface marker expression; (C) CD83 surface marker expression; (D) CD86 surface marker expression. Statistical differences were observed between THP-1 and THP-1-derived DCs for the membrane receptors analyzed. (*$p < 0.05$; **$p < 0.01$; ***$p < 0.001$; ns – not statistically significant; two-way ANOVA - Mixed-effects analysis with Tukey's multiple

comparison test). Data represent the mean value ± the standard error of the mean of at least three biologically independent experiments with two technical replicates for each.

6.3.2 Preparation and characterization of cyclooctyne-functionalized MNPs

The MNPs used in this work are spherical iron oxide MNPs with a mean diameter of 13 nm, obtained as previously described [192,393]. The MNPs are coated with an amphiphilic polymer - poly(maleic anhydride-alt-1-octadecene), PMAO - modified with a fluorescent dye, tetramethylrhodamine 5-(6)- carboxamide cadaverine (TAMRA), to allow MNPs tracking *in vitro* by fluorescence microscopy and flow cytometry. The maleic anhydride moieties of the polymer were hydrolyzed under alkaline conditions to yield carboxylic groups on the MNPs surface for subsequent functionalization with an amino-poly(ethylene glycol) (PEG) and a cyclooctynylamine (CO) derivative, respectively (*vide infra*).

Bioorthogonal click reaction of MNPs on living cell membranes requires the use of strained alkynes for the SPAAC reaction with azide groups. However, most of the cyclooctynes described in the literature have a pronounced hydrophobic character; in fact, the higher their hydrophobicity, the higher the reaction rate towards azides [192,562]. This hydrophobic character can have a negative effect on the stability of nanoparticles in biological media. For this reason, the MNPs were functionalized in a two-step process (Figure 6.4), by firstly introducing an amino-poly(ethylene glycol) (PEG) derivative to improve the colloidal stability of the MNPs, followed by the incorporation in a second step of a cyclooctynylamine derivative (CO) bearing a short ethylene glycol chain, as described by Fratila *et al.* [192]. The cyclooctyne-functionalized MNPs (MNPs@PMAO@PEG@CO) had a SAR of 112 W/g, measured at a frequency of 418 kHz and a field amplitude of 23.9 kA/m. A detailed physico-chemical characterization of the MNPs is in Figure 6.5.

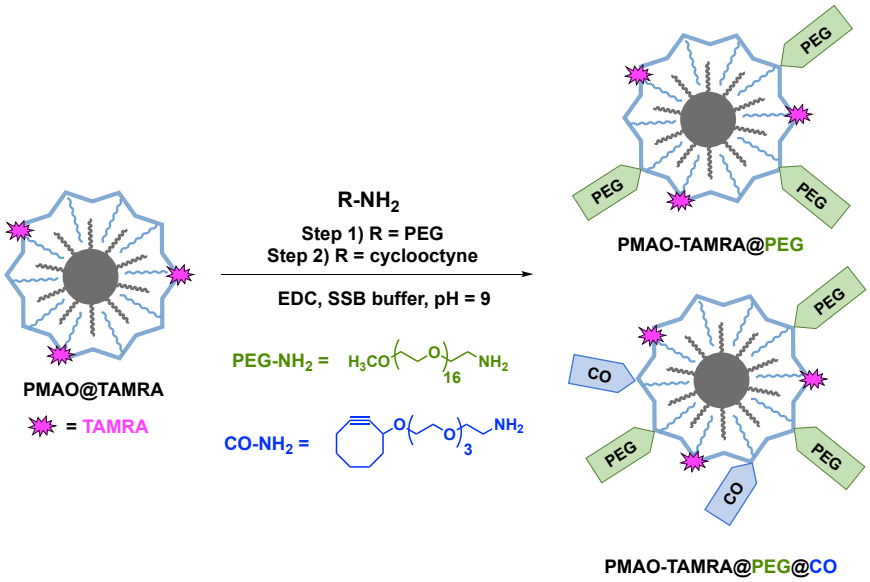

Figure 6.4 - Functionalization of MNPs with amino-poly(ethylene glycol) (PEG) and cyclooctynylamine (CO) derivatives. Scheme of MNPs functionalization with amino-poly(ethylene glycol) (PEG) and cyclooctynylamine (CO) derivatives in a two-step process.

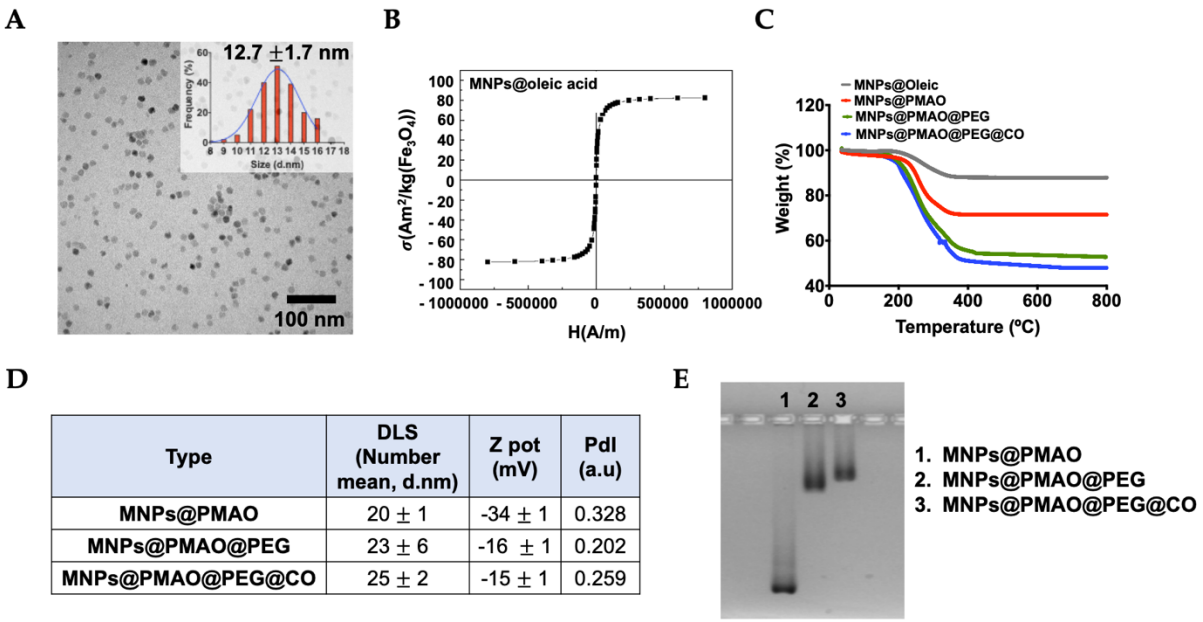

Type	DLS (Number mean, d.nm)	Z pot (mV)	PdI (a.u)
MNPs@PMAO	20 ± 1	-34 ± 1	0.328
MNPs@PMAO@PEG	23 ± 6	-16 ± 1	0.202
MNPs@PMAO@PEG@CO	25 ± 2	-15 ± 1	0.259

Figure 6.5 - Physicochemical characterization of MNPs. (A) TEM images and (B) magnetization curve of as-synthesized MNPs (MNPs@oleic acid). (C) Thermogravimetric analysis of the different types of MNPs. (D) DLS and ζ-potential measurements. (E) Electrophoresis in agarose gel (1%) for 45 minutes at 90 V. The correct functionalization was confirmed qualitatively after each step by ζ-potential measurements and electrophoresis in agarose gel. Moreover, from thermogravimetric analysis, we could obtain a quantitative estimation of the extent of functionalization: from the initial 3740 COOH groups present on each nanoparticle, 1450 were modified with PEG, while in the second step approximately 760 CO moieties were introduced per nanoparticle [192].

6.3.3 Optimization of metabolic glycoengineering and labeling of cell membrane with DBCO

The sialic acid metabolic pathway has been employed for the labeling of cell membranes, specifically for integrating azides into the glycocalyx. This process, known as metabolic glycoengineering, is initiated using a biosynthetic precursor that contains an azide functional group. For instance, in this work we used Ac_4ManNAz which is a synthetic molecule that can be absorbed by cells and effectively hydrolyzed to ManNAz by cytosolic esterases. ManNAz is subsequently converted to sialic acid via five enzymatic steps and conjugated to the end of the sugar chains, displaying end azide reporter groups [563,564]. It is noteworthy that the integration of azide reporters on cell membranes can be regulated in a dose-dependent manner, by adjusting the concentration of the azide precursor and/or the incubation time [564–566].

In a previous work conducted by Idiago-López *et al.*, the introduction of bioorthogonal azide reporters on the surface of different living cells (MCF-7, HCT116, and A549 lung adenocarcinoma) was optimized considering three different parameters: the concentration of the azide precursor, the incubation time, and the effect of the metabolic glycoengineering process on cell viability [564]. Based on these previous results, we selected for the subsequent experiments an incubation time of 48 h with Ac_4ManNAz. First, azide generation on cell surfaces was initially evaluated by flow cytometry, after SPAAC reaction with a fluorescent dibenzylcyclooctyne (DBCO-PEG_4-5/6-Sulforhodamine B). DBCO is mostly used for fluorescent labeling and detection of azide groups via SPAAC reaction between alkyne and azide groups [563,564,567,568]. Upon incubation with the presence of Ac_4ManNAz (10, 20, 50, and 100 μM) for 48 h, the amount of azide groups expressed on the cell membrane also increased (Figure 6.6), demonstrating a precursor dose-dependent generation of these artificial reporters, which is in line with previous literature reports [564,569–572].

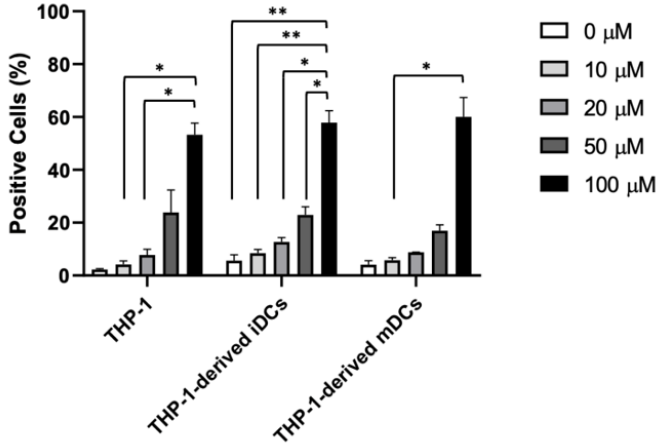

Figure 6.6 - Optimization of cell membrane labeling with azide groups in THP-1 cells and THP-1-derived DCs. Different concentrations of $Ac_4ManNAz$ (0 to 100 mM) were used to optimize cell membrane labeling and the expression of azide groups was evaluated using flow cytometry after SPAAC reaction with DBCO-PEG_4-5/6-Sulforhodamine B (20 mM). Statistical differences were observed between cell membrane labeling with DBCO (*$p < 0.05$; *$p < 0.01$; ns – not statistically significant; two-way ANOVA - Mixed-effects analysis with Tukey's multiple comparison test). Data represent the mean value ± the standard error of the mean of two biologically independent experiments with two technical replicates for each.

6.3.4 Labeling of cell membrane with MNPs

The MTS assay was used to evaluate the impact of MNPs and the metabolic glycoengineering process on cell viability. We do not observe a cytotoxic effect upon 30 minutes of incubation with 100 $\mu g_{Fe}/mL$, with or without the previous incubation with $Ac_4ManNAz$ for 48 h (Figure 6.7). These results are in concordance with a previous work conducted by Idiago-López *et al.*, since no significant cytotoxicity was observed at concentrations up to 150 $\mu g_{Fe}/mL$ using different cancer cell lines [564].

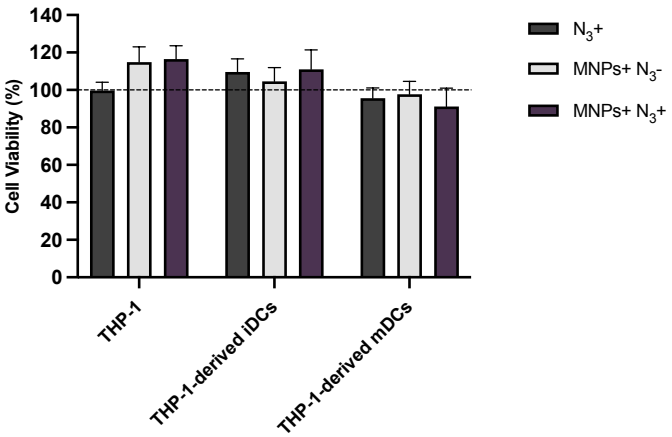

Figure 6.7 - Cell viability analysis via MTS assay in THP-1 cells and THP-1-derived DCs. The conditions tested were normalized to untreated cells. N_3+: cells treated with 100 mM of $Ac_4ManNAz$ for 48 h; MNPs+ N_3-: cells incubated for 30 minutes with 100 $\mu g_{Fe}/mL$ of MNPs; MNPs+ N_3+: cells treated with 100 mM of $Ac_4ManNAz$ for 48 h and incubated for 30 minutes with 100 $\mu g_{Fe}/mL$ of MNPs. Statistical differences were not observed between the samples

and untreated cells. Data represents the mean value ± the standard error of the mean of two biologically independent experiments with two technical replicates for each.

To perform the SPAAC bioorthogonal chemistry, THP-1 cells, and THP-1-derived DCs expressing azide groups were incubated with the MNPs functionalized with cyclooctyne. Cells were treated with 100 μM of Ac_4ManNAz for 48 h and then incubated for 30 minutes with 100 μg_{Fe}/mL of MNPs, in RPMI without FBS at 37ºC. RPMI serum-free was used to circumvent any potential adverse impact that the formation of serum protein corona on the MNPs surface might have on the click reaction due to steric hindrance between the two bioorthogonal partners [564,573]. Control experiments using cells without Ac_4ManNAz pre-treatment (N_3-) were also performed. To validate the correct expression of azide groups, a positive control was included, incubating the cells with 20 μM of DBCO-PEG_4-5/6-TAMRA for 30 minutes, under the same experimental conditions. First, confocal fluorescence microscopy was used to analyze the labeling of cell membrane with MNPs and DBCO. In the presence of previous incubation with azide groups (N_3+) for 48 h, as can be noted, cell labeling for 30 minutes with DBCO shows an increase of fluorescence signal at the cell membrane due to the covalent bonding between the alkyne and azide groups (Figure 6.8). The MNPs were functionalized as described above with a fluorescent dye, TAMRA and with a cyclooctyne to promote the click chemistry reaction. We denoted a cell membrane labeling more evident in cells treated with Ac_4ManNAz in confocal microscopy images (Figure 6.9). These results were comparable to the ones obtained in a previous work, in which prolonged MNPs incubation time seemed to enhance the click reaction but simultaneously increased non-specific interactions of the MNPs with cells lacking azide expression [564].

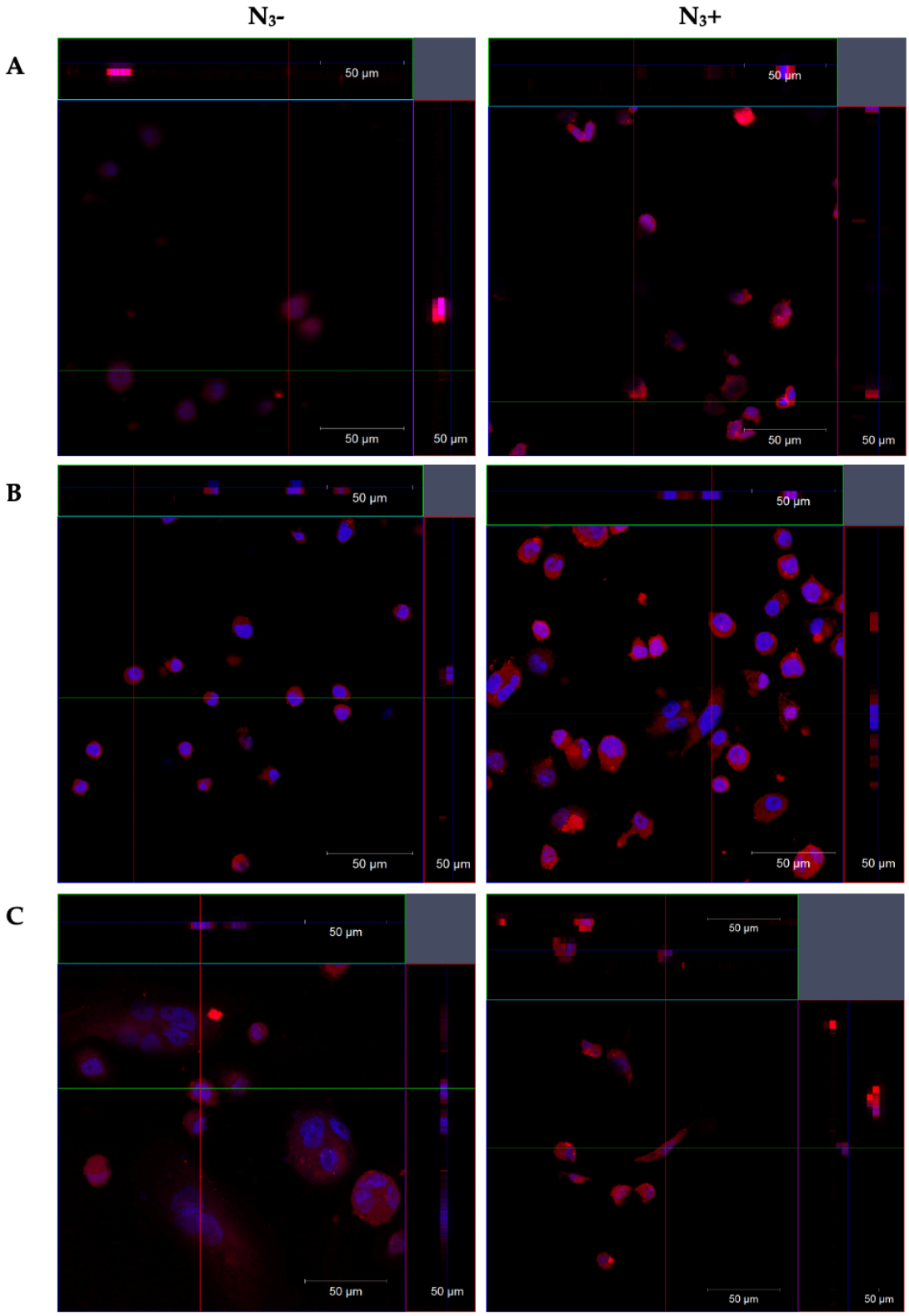

Figure 6.8 - Cell membrane labeling with DBCO for 30 minutes in THP-1 cells and THP-derived DCs. Orthogonal view of the z stack confocal microscopy images of the cell membrane labeling with 20 µM of DBCO-PEG_4-5/6-TAMRA in (A) THP-1 cells, (B) THP-1-derived iDCs and in (C) THP-1-derived DCs, with the absence (N_3-) or presence (N_3+) of azide groups.

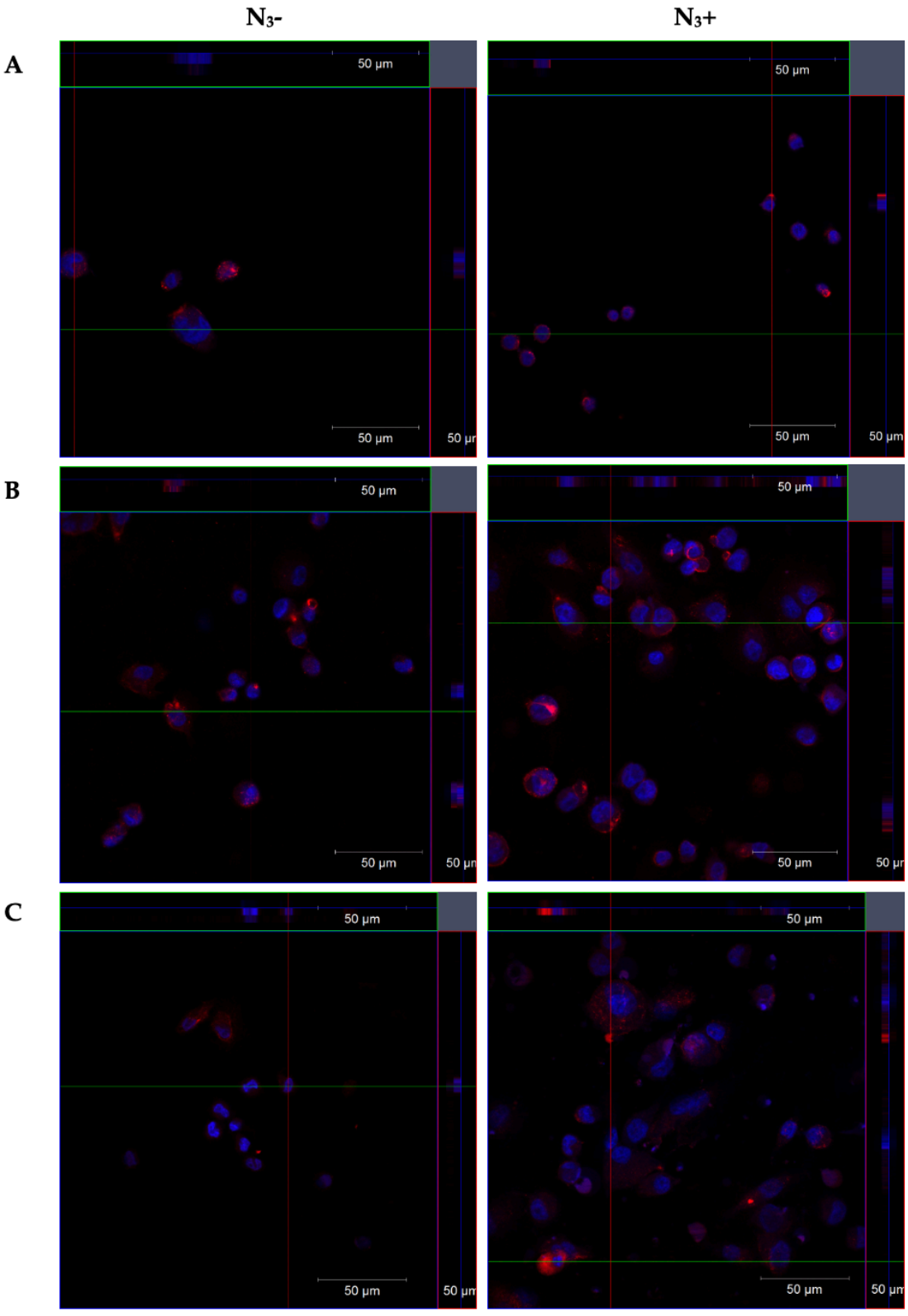

Figure 6.9 - Cell membrane labeling with MNPs for 30 minutes in THP-1 cells and THP-derived DCs. Orthogonal view of the z stack confocal microscopy images of the cell membrane labeling with 100 μg_{Fe}/mL of MNPs in (A) THP-1 cells, (B) THP-1-derived iDCs and in (C) THP-1-derived mDCs, with the absence (N_3-) or presence (N_3+) of azide groups.

Consequently, to decrease non-specific interactions of the MNPs with the cell membrane, both the concentration of MNPs (from 100 to 10 $\mu g_{Fe}/mL$) and the incubation time (30 to 10 minutes) were reduced. We therefore incubated THP-1 cells and THP-1-derived DCs with 10 $\mu g_{Fe}/mL$ of MNPs for 10 minutes, which leads to a very low fluorescence signal at the cell membrane, probably due to the dispersion of the MNPs throughout the membrane surface (Figure 6.10). This result can be attributed also to the resolution limits of fluorescence microscopy, which does not allow to discriminate 13 nm diameter MNPs on fully spread cell membranes [564,574].

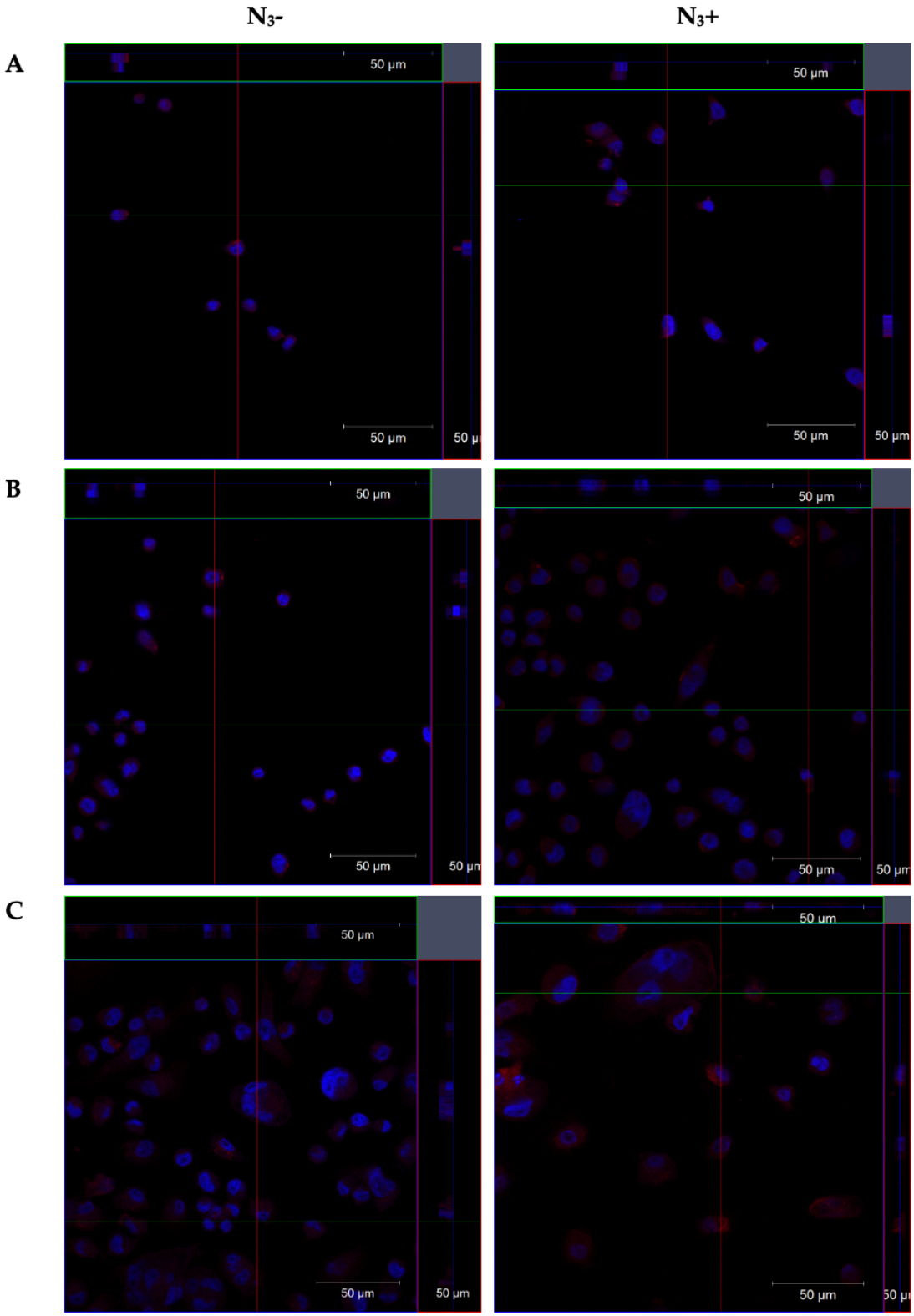

Figure 6.10 - Cell membrane labeling with MNPs for 10 minutes in THP-1 cells and THP-derived DCs. Orthogonal view of the z stack confocal microscopy images of the cell membrane labeling with 10 $\mu g_{Fe}/mL$ of MNPs in (A) THP-1 cells, (B) THP-1-derived iDCs, and in (C) THP-1-derived DCs, in the absence (N_3-) or presence (N_3+) of azide groups.

Considering these limitations, flow cytometry was used as an alternative and quantitative technique that allows to determine the total fluorescence provided by the MNPs after their interaction with cells. The bioorthogonal click reactivity of the MNPs towards azide-labeled cell membranes was evaluated by incubating THP-1 cells and THP-1-derived DCs with 10 μg_{Fe}/mL of MNPs for 10 minutes. Cells labeling for 30 minutes with 20 μM of DBCO was used as control. The results observed in Figure 6.11 were compared with the interaction of MNPs and DBCO with cells without the prior Ac_4ManNAz treatment (N_3-). The labeling of DBCO on cell membrane in samples treated with Ac_4ManNaz (N_3+) shows statistically significant differences, confirming the click chemistry reaction between DBCO fluorescent dye and azide-labeled THP-1 cells and THP-1-derived DCs (Figure 6.11A). We did not observe statistically significant differences between MNPs with (N_3+) or without (N_3-) the presence of azide groups, although a slight increase of cell membrane labeling in cells treated with Ac_4ManNAz is evident. This would allow us to maximize the effect of the localized magnetic hyperthermia on the cell membrane for siRNA transfection using a minimal amount of MNPs (Figure 6.11B). Concerning these results, we determine that cells with Ac_4ManNAz treatment show an improvement of cell membrane labeling with MNPs compared to cells without the presence of azide groups, which is important for future magnetic hyperthermia experiments.

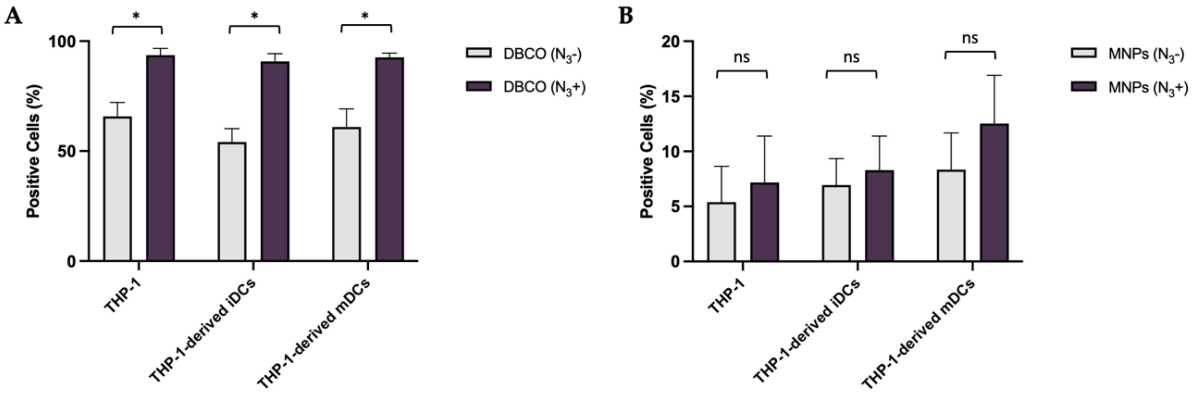

Figure 6.11 - Cell membrane labeling with DBCO and with MNPs in THP-1 and THP-1-derived DCs. Cell membrane labeling with (A) DBCO-PEG_4-5/6-TAMRA and with (B) MNPs in the absence (N_3-) or presence (N_3+) of azide groups. Statistical differences were observed between cells membrane labeling with DBCO (*$p < 0.05$; ns – not statistically significant; two-way ANOVA - Mixed-effects analysis with Tukey's multiple comparison test). Data represent the mean value ± the standard error of the mean of at least two biologically independent experiments with two technical replicates for each.

6.3.5 *IDO1* gene silencing enhanced by magnetic hyperthermia

IDO1 is a rate-limiting enzyme related with tryptophan metabolism which contributes significantly to immune suppression in the TME. The depletion of tryptophan is associated with the suppression of effector T cells activity, the differentiation of naïve T cells to Treg cells, and the recruitment of MDSCs to tumor vasculature [541,575,576]. In fact, IDO1 activity is

upregulated in many types of cancer and is associated with a poor prognosis [577]. Previous studies reported that the inhibition of IDO1 in DCs is considered a promising strategy to promote the efficacy of DC-based therapy [544]. Novel strategies to deliver TNA, such as siRNA, are required to promote transfection in DCs and other primary cells of the immune system [578–580]. DCs are difficult to transfect, and the efficiency of transfection is low using commercially available reagents or electroporation [530,531,578,581].

In this work, we used magnetic hyperthermia to transfect siRNA against *IDO1* gene in THP-1-derived DCs. To provide artificial azide reporters for the click immobilization of MNPs on the cell membrane, THP-1-derived DCs were incubated with Ac_4ManNAz for 48 h before magnetic hyperthermia, as described in section 6.2.5. To induce *IDO1* expression, cells were incubated with 10 ng/μL of LPS for 24 h before magnetic hyperthermia transfection experiment. Hereafter, cells were incubated with MNPs (at 10 μg_{Fe}/mL for 10 minutes) and the AMF (23.9 kA/m and 418 kHz) was applied for 30 minutes with pulses (each pulse with a duration of five minutes, with sixty seconds pause between pulses). Transfection efficiency was compared with the positive control (Lipofectamine), under the same experimental conditions of magnetic hyperthermia samples. Moreover, control experiments were used to verify if the presence of MNPs, with (N_3+) or without (N_3-) Ac_4ManNAz treatment and with (MH+) or without (MH-) magnetic hyperthermia application could promote the intracellular siRNA delivery. After 24 h, RNA was extracted, and RT-qPCR analysis confirmed the effectiveness of magnetic hyperthermia targeting siRNA delivery and consequently the silencing of *IDO1* gene.

The results observed in Figure 6.12 reveal that in cells with MNPs attached to the membrane via click chemistry and exposed to the AMF (MNPs+ N_3+ MH+), the *IDO1* expression decreased approximately 65% and 75% in THP-1-derived iDCs and THP-1-derived mDCs, respectively. This silencing effect was comparable to that attained by commercial Lipofectamine.

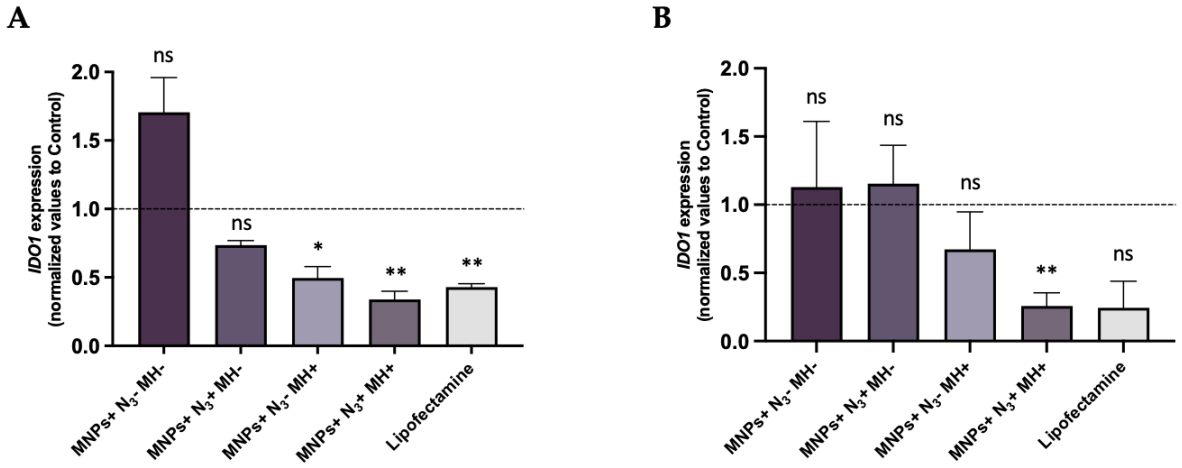

Figure 6.12 - RT-qPCR assay to evaluate *IDO1* gene expression in THP-1-derived DCs. *IDO1* silencing was observed in all samples tested except MNPs+ N_3- MH- in **(A)** THP-1-derived iDCs; except MNPs+ N_3- MH- and MNPs+ N_3+ MH- in **(B)** THP-1-derived mDCs. The gene expression levels were normalized to the cells without siRNA (Control, $2^{-\Delta\Delta Ct}$=1). Black asterisks indicate statistical differences between samples and Control (*p < 0.05; **p < 0.01; ns – not

statistically significant; Unpaired parametric t-test with Welch's correction). Data represent the mean value ± the standard error of the mean of at least three biologically independent experiments.

Our results confirmed that membrane-localized magnetic hyperthermia enhances the transfection of siRNA against the *IDO1* gene in THP-1-derived DCs, using the same strategy previously used in MCF-7 cells to silence the *GFP* gene. The contribution of IDO1 in immunomodulation in cancer has been explored since this enzyme depletes tryptophan in TME, which suppresses T cell proliferation and promotes the differentiation of Treg cells [539,582]. *IDO1* silencing can reduce this immunosuppressive effect, potentially leading to a more robust immune activation [583,584]. For example, Endo *et al.* reported *IDO1* gene silencing in DCs derived from mouse using low doses of siRNA encapsulated in lipid nanoparticles, and the silencing efficiency was compared to commercial reagents available for transfection such as Lipofectamine [544]. In other study, the role of *IDO1* silencing in the inhibition of lung cancer growth was demonstrated using an *in vitro* Lewis lung carcinoma (LLC) cell line. Moreover, T cells exhaustion during lung cancer progression was confirmed in an *in vivo* model using shRNA against *IDO1* gene [585]. Interestingly, Sioud *et al.* produced a safe IDO-silenced DC vaccine to activate allogeneic T cells in four patients with gynecological cancer to induce anti-cancer immunity [586]. For instance, *IDO1* silencing could enhance the immunogenic function of DCs *in vitro* and *in vivo*, and the silence effect did not affect the expression of the co-stimulatory molecules CD80 and CD86 [586,587]. Zheng *et al.* observed the reduction of the tumor size and the decrease of CD4+ and CD8+ apoptosis in a mouse model of breast cancer using DCs loaded with tumor antigens and siRNA targeting *IDO1* gene [588]. These findings suggest that silencing *IDO1* could potentially enhance the effectiveness of human DC vaccines [543]. Overall, those studies described *IDO1* gene as a potential target for gene therapy in cancer.

6.3.6 Effect of *IDO1* gene silencing on the gene expression of pro-inflammatory and anti-inflammatory cytokines

The expression of cytokines such as IL-6 [589,590], TNF-α [591,592], IL-12A [593,594] and IL-10 [595,596], is crucial for the role of DCs in the immune response, since those cytokines are able to modulate the balance between pro-inflammatory and anti-inflammatory status. IL-6 plays a critical role in immune responses, inflammation, and hematopoiesis [597]. The expression of this cytokine is upregulated in DCs upon activation by various stimuli (e.g., pathogen-associated molecular patterns recognized by Toll-like receptors) and is involved in the differentiation of naïve T cells into Th17 cells [589,598]. TNF-α is involved in the activation of macrophages and T cells, promotes inflammation, and enhances the maturation and antigen-presenting capabilities of DCs [591,599]. This cytokine is produced by activated DCs and their expression is induced in response to contact with T cells, cytokines, or pathogens [600]. IL-12A is generally produced by activated DCs and/or mDCs and is essential to promote the differentiation of Th1 cells and

the cytotoxic functions of NK cells and cytotoxic T cells [601,602]. The expression of IL-12A in DCs is upregulated in response to exogenous stimulus (e.g., pathogens products) and interactions with activated T cells [603,604]. Contrary to those cytokines, IL-10 regulates immune responses by suppressing the expression of pro-inflammatory cytokines (e.g., IL-6 and TNF-α) and can modulate the function of DCs while inhibits their maturation and reduces their capacity to present antigens [595,605]. IL-10 expression can be induced in response to immune regulatory signals or pathogens and is important to prevent excessive inflammatory responses [606,607].

Considering all this, we evaluated the effect of *IDO1* silencing in the expression of genes encoding pro-inflammatory cytokines IL-6, IL-12A, and TNF-α, and anti-inflammatory cytokine IL-10 in all conditions previously tested. As observed in Figure 6.13, an upregulation of mRNA levels of *IL6*, *TNFA*, and *IL12A*, and a downregulation of *IL10* expression is observed in THP-1-derived DCs transfected with MNPs+ N_3+ MH+ or Lipofectamine, which are consistent with previous reports regarding *IDO1* gene silencing (see references below).

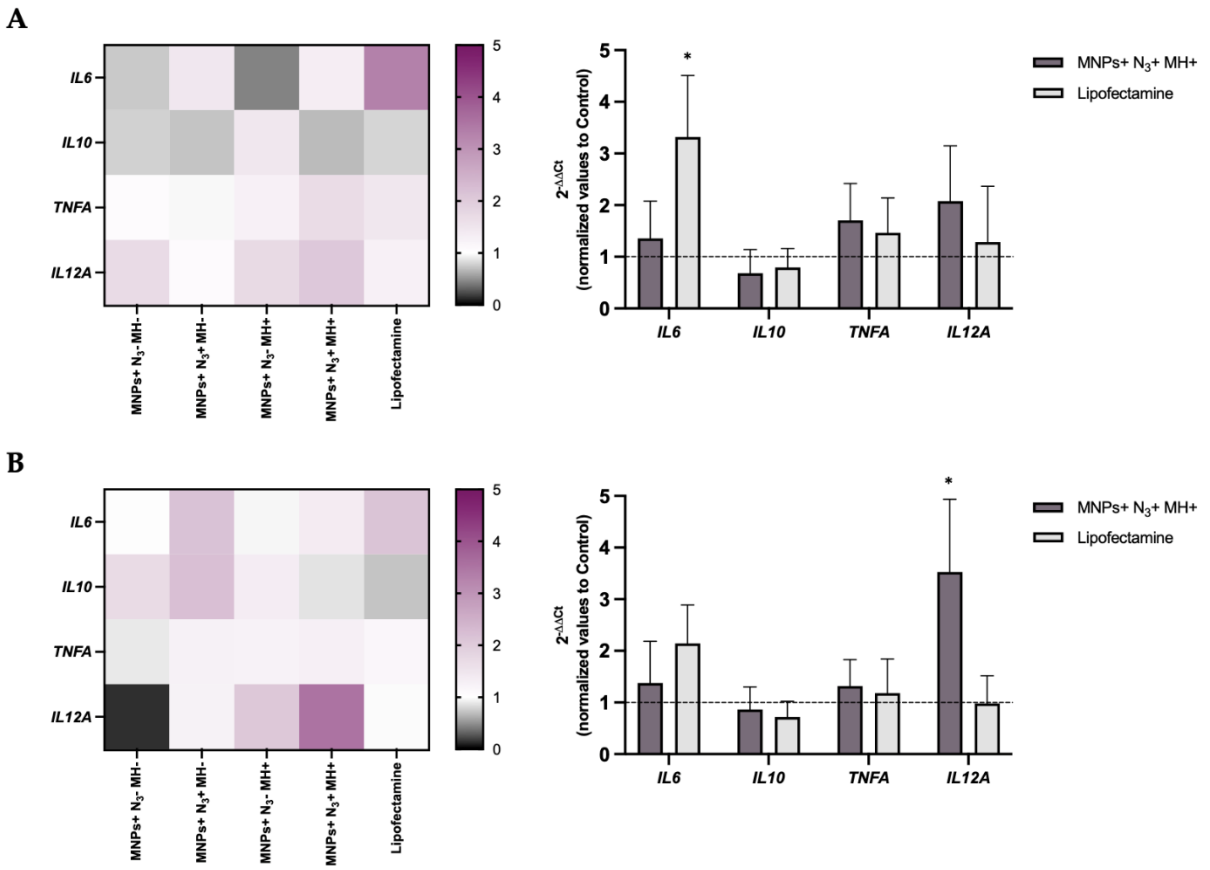

Figure 6.13 - RT-qPCR analysis of gene expression of *IL6*, *IL10*, *TNFA*, and *IL12A* after *IDO1* silencing in the different conditions tested. Heatmap of (A) THP-1-derived iDCs and (B) THP-1-derived mDCs. The gene expression was normalized to the cells without siRNA (Control, $2^{-\Delta\Delta Ct}$ =1: white color); purple represents the upregulation of gene expression, and black represents the downregulation of gene expression. Black asterisks indicate statistical differences between Lipofectamine sample and Control in (A) THP-1-derived iDCs; and between MNPs+ N_3+ MH+ and Control in (B) THP-1-derived mDCs (*p < 0.05; two-way ANOVA - Mixed-effects analysis with Tukey's multiple comparison test). Data represent the mean value ± the standard error of the mean of at least three biologically

independent experiments with two technical replicates for each. Overall, *IDO1* gene silencing promotes *IL6*, *TNFA,* and *IL12A* upregulation and *IL10* downregulation in MNPs+ N_3+ MH+ and Lipofectamine samples.

Silencing the *IDO1* gene in DCs could significantly impact their function and the expression of these cytokines[583,586,608,609]. For instance, researchers have been exploring the inhibition of IDO1 activity and its impact on the cytokine's expression. A previous study conducted in LLC-bearing mice treated with shRNA against the *IDO1* gene shows an increase in the production of pro-inflammatory cytokines TNF-α and IL-2 compared to controls, which suggests that this treatment may recover cytokine secretion in tumors *in vivo* [585]. Heidari *et al.* described the effect of IDO1 suppression on the immunomodulatory function of adipose-derived mesenchymal stem cells in cancer, which leads to a downregulation of the expression of the immunoregulatory mediators studied namely, Gal-3, HGF, TGF-β and IL-10 [610]. Several studies reported that the induction of IL-10 expression in monocytes promotes Treg cells to express IL-10 and TGF-β and consequently suppresses the activity of DCs and Th1 cells [611,612]. Ravishankar *et al.* denoted a significant reduction in IL-10 and TGF-β protein relative levels and an increase of mRNA relative levels of pro-inflammatory cytokines TNF-α, IL-6, and IL-12 in mice [613]. The literature has been recognized that DCs-secreted IL-10 promotes the development of Treg cells, while IL-12 induces the differentiation of CD4+ T cells into Th1 cells [614,615]. Thus, IDO1 activity suppresses effector T cell responses, which promotes the differentiation and activation of Treg cells and inhibits the production of IL-6 by DCs [616]. Recently, the impact of IDO1 on the production of secreted cytokines was studied using stable DCs lines with both gain and reduction of IDO1 function, established by recombinant DNA technique. The reduction of IDO1 function improves the secretion of Th1 cell polarizing IL-12 and decreases Treg cell polarizing IL-10 from DCs, which is important to understand the tolerogenic regulation of DCs-mediated T cells differentiation by IDO1 [609]. These data confirm that tryptophane depletion facilitates the production of anti-inflammatory cytokines by IDO-expressing DCs, which promotes the recruitment of Treg cells, and suppresses T cell activation and proliferation [586,609]. Additionally, it has been widely reported that DCs with elevated kynurenine levels (tolerogenic stage) drive T cells differentiation to Treg cells and induce apoptosis in effector T cells. In contrast, DCs with low IDO expression (immunogenic stage) hamper Treg cells development and reduce T cells apoptosis [609,617].

6.3.7 Cells viability assessment post-transfection of siRNA

Many of the commercially available transfection methods are known for their high impact on cell viability. Several studies have described the cytotoxicity of cationic lipid reagents and the impact of electroporation on cell survival [189,618,619]. Therefore, the impact on cell viability was assessed in THP-1-derived DCs upon the transfection of siRNA against *IDO1* gene in all conditions tested. Figure 6.14 reveals that Lipofectamine induces a statistically significant

reduction of cell viability of approximately 40% in THP-1-derived DCs, not observed for MNPs+ N_3+ MH+ (cell viability of 80%).

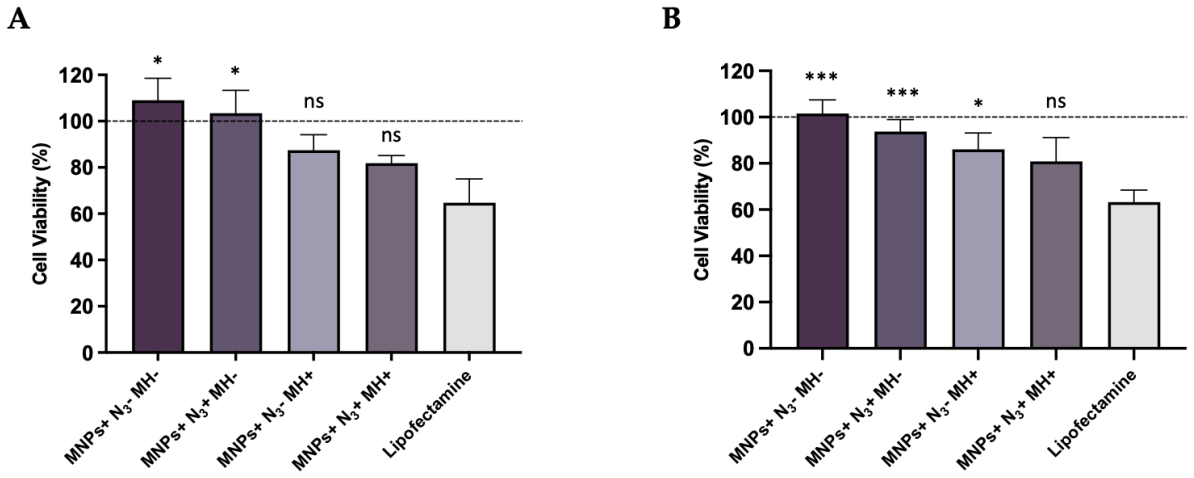

Figure 6.14 - Cell viability analysis post-magnetic hyperthermia experiment via MTS assay in THP-1-derived DCs. The conditions tested were normalized to cells without siRNA (Control). Statistical differences were observed between Control, MNPs+ N_3- MH- and MNPs+ N_3+ MH- samples with Lipofectamine in **(A)** THP-1-derived iDCs; between Control, MNPs+ N_3- MH-, MNPs+ N_3+ MH- and MNPs+ N_3- MH- samples with Lipofectamine in **(B)** THP-1-derived mDCs (*$p < 0.05$; ***$p < 0.001$; ns – not statistically significant; Unpaired parametric t-test with Welch's correction). Data represent the mean value ± the standard error of the mean of at least three biologically independent experiments with two technical replicates for each.

As observed in Figure 6.14, when compared to our magnetic hyperthermia strategy, Lipofectamine has a more cytotoxic effect in THP-1-derived DCs. Indeed, using our magnetic hyperthermia transfection strategy, a lower impact on cell viability was observed (81% of cell viability), which might be related to the *IDO1* silencing effect. IDO1 is an enzyme involved in immune regulation and modulation of metabolic pathways, such as the catabolism of tryptophan through the kynurenine pathway [537]. Silencing of the *IDO1* gene results in higher levels of tryptophan and reduces the production of kynurenine and its downstream metabolites, leading to shifts in cellular respiration and energy production that potentially can affect cell proliferation. For instance, the kynurenine pathway contributes to NAD+ synthesis and reduced activity of this pathway which can impact NAD+ levels, influencing metabolic processes like glycolysis, oxidative phosphorylation, and DNA repair mechanisms [620,621]. In some contexts, the silencing of the *IDO1* gene can promote cell death through various mechanisms, such as increasing pro-apoptotic factors, enhancing the activity of effector T cells and NK cells in the TME, and altering signaling pathways that regulate cell survival [537,539,584]. Taken together, these findings suggest that this novel transfection approach can attain comparable transfection compared to the commercially available reagent Lipofectamine, with less cytotoxic effect. Nonetheless, it is important to consider that part of the observed viability reduction may stem

from the biological effects of the *IDO1* gene silencing itself. Further research on metabolic assessments will be important to clarify the potential contribution of IDO1 inhibition in cell proliferation and survival.

6.4 Conclusions

IDO1 plays a critical role in modulating tryptophan metabolism, immune responses, and cell survival pathways. Silencing the *IDO1* gene impacts these processes, leading to altered metabolic states and increased cell death, particularly in contexts where *IDO1* is upregulated, such as in many cancers (e.g., CRC, melanoma), due to its contribution to the immunosuppressive TME.

Our results indicated an effective *IDO1* gene silencing in THP-1-derived DCs after magnetic hyperthermia-mediated transfection of siRNA against *IDO1* gene via SPAAC reaction of cyclooctyne-MNPs with azide groups expressed on the cell membrane via metabolic glycoengineering. Our approach has the same silencing efficiency as Lipofectamine and shows a lower impact on cell viability due to the silencing of the *IDO1* gene when compared to this commercially available lipid cationic reagent. The MNPs act as cell membrane localized heating sources due to their immobilization at the time of AMF application, increasing membrane fluidity and permeability, which in turn promotes the delivery of silencing moieties. Moreover, we proved that *IDO1* silencing in THP-1-derived DCs possibly leads to a shift towards a pro-inflammatory state (more immunogenic) characterized by the increase of gene expression of *IL6*, *TNFA*, and *IL12*, and the decrease of *IL10* mRNA levels. The reduction of the immunosuppressive effects of IDO1 might lead to enhanced effector T cells activation and proliferation and the specific outcomes will depend on the context in which *IDO1* is silenced (e.g., TME).

Overall, our findings highlight the potential of IDO1 as a therapeutic target and the employment of magnetic hyperthermia-mediated transfection for TNA, or other molecules for targeted therapy in cancer.

7

Conclusions and Future Perspectives

7.1 Conclusions

The delivery of nucleic acids effectors (e.g., siRNA and ASO) into cells is widely used in gene therapy. Several nanocarriers, including polymeric, lipid and inorganic nanoparticles, have been developed to improve TNAs delivery, avoiding nucleases degradation and off-target effects [162]. Since conventional transfection methods (e.g., cationic lipid vesicles) often display cytotoxicity [163,622], there is a demand for the development of novel therapeutic approaches to deliver silencing moieties with maximal transfection efficiency and minimal toxicity.

Metallic nanoparticles, such as AuNPs and MNPs, have received attention as promising alternatives to lipid-based nanocarriers and viral vectors for TNAs delivery owing to their unique physico-chemical properties (e.g., ease of synthesis and functionalization, high surface area, and biocompatibility) [185,623]. AuNPs have proved to be effective in delivering silencing moieties with high efficacy [214,452]. Due to their unique optical characteristics, AuNPs provide additional features, such as the possibility for spatiotemporal triggering of cell uptake and internalization through light irradiation [185,216]. The ability of MNPs for magnetic-field guided delivery of nucleic acids (magnetofection) has been explored [257,375], while the localized heat generated in MNPs' surface when exposed to an AMF has not been used for nucleic acids transfection. This thesis was focused on novel methodologies based on mild hyperthermia mediated by nanoheaters to promote the delivery of nucleic acids to cancer cells.

In chapter 3, spherical AuNPs were used as photothermal agents upon irradiation with a visible light laser. This approach was used to attain mild hyperthermia conditions in cells. The major challenge of using visible light irradiation (CW 532 nm laser) is that it does not penetrate as deeply as NIR light irradiation [159,216]. However, this mild photothermy system aims to irradiate peripheral tissues (e.g., skin, eye) or specific sites using a laser coupled with a probe that can be inserted through a body cavity (e.g., rectum and colon). Irradiation of cells previously incubated with AuNPs promoted their cellular uptake compared to non-irradiated cells, without cytotoxicity. The obtained results suggested that the localized heat produced by irradiated AuNP@PEG could increase the cells' membrane permeability, which was in line with the observed by LDH release and in accordance with previous literature results [366,430,432]. As a proof-of-concept, transfection of *anti-GFP* was performed in HCT116 and MCF-7 cells, and transfection efficiency was compared with a commercial Lipofectamine™ reagent. Results revealed an efficient *GFP* gene silencing, similar to that attained with Lipofectamine™ reagent but without cell toxicity. Still, other transfection methods could be performed to reinforce the safety and non-cytotoxicity of this approach [189].

Spherical AuNPs have been described as more suitable for ASO vectorization than Au-nanorods, which have been widely exploited in PTT [216,345]. In chapter 4, mild photothermy was used to improve the internalization of AuNPs functionalized with ASO against *c-MYC* oncogene in HCT116 2D cells and 3D tumor spheroids. 3D tumor models have been demonstrated as cancer models that better resemble the *in vivo* TME [2]. Considering this, 3- and 7-day spheroids were selected due to their differences in size and structure, metabolic and oxygen

gradients, and molecular patterns [465,474]. Results showed that *c-MYC* gene silencing was more pronounced in HCT116 2D cells and 7-day 3D spheroids when the internalization of AuNP@*c-MYC* was improved by mild photothermy. Therefore, quantifying the number of AuNP@*c-MYC* internalized in irradiated and non-irradiated cells/spheroids is required to corroborate those data, considering that there is no correlation between the quantity of AuNP@*c-MYC* internalized with gene silencing efficacy as described by Oliveira *et al.* [452]. Interestingly, 3-day spheroids (only 5% of *c-MYC* silencing) were more sensitive to localized heat compared to 7-day spheroids, which reinforces the need for further studies concerning the complexity of 3D cell growth [474].

In chapter 5, the immobilization of MNPs through bioorthogonal chemistry and cell surface engineering with azide groups via SPAAC reaction [193] was explored as an intracellular delivery tool mediated by magnetic hyperthermia. Membrane-localized magnetic hyperthermia mediated by immobilized MNPs on the cell membrane was used to promote *anti-GFP* transfection in MCF-7 cells. The transfection efficiency and cell viability were compared with Lipofectamine™ reagent, and similar gene silencing effect was observed, with less cytotoxicity. While further research into the cell plasma membrane thermal disruption with localized magnetic hyperthermia and the mechanism of internalization of nucleic acids is needed, this strategy might lead to the development of a more efficient procedure for the "opening and closing" of cells membrane with minimal disturbance of cellular integrity, which are concordant with previous findings [521].

In the last chapter, the membrane-localized magnetic hyperthermia mediated transfection was used to deliver siRNA against *IDO1* gene in cells difficult to transfect, such as DCs. An acute monocytic leukemia cell line (THP-1) was selected and successfully differentiated in THP-1-derived DCs. Then, the SPAAC reaction was observed between the azide groups of the cell membrane and the MNPs functionalized with a cyclooctyne derivative. An effective *IDO1* gene silencing was achieved comparable to Lipofectamine™ reagent, but with less impact on cell viability. Furthermore, the increase of expression of pro-inflammatory cytokines genes *IL6*, *TNFA*, and *IL12* and the decrease of the anti-inflammatory *IL10* gene might contribute to a more immunogenic state. IDO1 inhibition has been explored as a therapeutic strategy in cancer [624] since it may enhance anti-tumor immunity by boosting the activity of DCs and other immune cells, and shifting DCs to a pro-inflammatory state might potentiate immune responses [609]. Still, additional studies would be important to confirm the immunogenic state of DCs in a TME context.

7.2 Future perspectives

From the outset of this work, it was evident that we aimed to develop a novel, universal, and efficient methodology for precisely delivering (therapeutic) nucleic acids; however, some questions remain to be answered and explored. This section provides recommendations for future work based on the presented results.

Thermal adaptation of cancer cells to mild hyperthermia

Results showed that these nanoparticles-mediated mild hyperthermia approaches enhanced cellular uptake and delivery of (therapeutic) nucleic acids without cytotoxicity. To increase my knowledge about the thermal adaptation of the cellular membrane of mild photothermy by AuNPs, further research on cell membrane fluidity would be necessary. For instance, time-resolved fluorescent polarization measurements with TMA-DPH (1-(4-Trimethylammoniumphenyl)-6-Phenyl-1,3,5-Hexatriene p-Toluenesulfonate) hydrophobic fluorescent membrane probe [24] could be used to assess membrane dynamics alterations [519]. Mild photothermy conditions were optimized (temperature measurements, LDH release and cell viability assessment) to maintain cell membrane integrity and to avoid global heating that could trigger the activation of cell death mechanism. Still, other techniques such as apoptosis/necrosis, ROS generation and cell cycle arrest by flow cytometry, the expression of HSPs, and the BAX/BCL-2 ratio would allow a better understanding of the thermal adaptation profile of cancer cells to mild photothermy [333,516]. Regarding the cell membrane-localized magnetic hyperthermia, Idiago-López *et al.* demonstrated that this approach can act as a disruptive agent of cell membrane fluidity and permeability, leading to the internalization of cell-impermeant probes (YO-PRO®-1) without impairing cell viability [516]. Before cell transfection with nucleic acids, cell viability post-magnetic hyperthermia was analyzed by Idiago-López using flow cytometry (apoptosis/necrosis with Annexin V-FITC and propidium iodide, ROS generation, and cell cycle analysis). Moreover, a molecular study of the localized hyperthermia effect (HSPs activation) was performed.

Transfection and vectorization of nucleic acids

Regarding the transfection of nucleic acids, it would be beneficial to fluorescently label the nucleic acid effectors to enable real-time tracking of their internalization and cellular trafficking[625]. In the case of AuNPs, it would be important to study the precise intracellular mechanism in irradiated cells by conjugating the AuNPs with suitable fluorophores for effective cell tracking. Other stabilizing agents, such as PEG-NH_2 or PEI, have been described for gene delivery [292,626]. AuNPs functionalized with PEG-NH_2 or PEI should enhance transfection of *anti-GFP*, as these polymers provide a positive charge to the nanoparticles. However, selecting an alternative functionalization strategy might alter the nanoparticle-cell interactions,

including the internalization mechanism of AuNPs, instability of Au-nanoconjugates, and negatively impact cell viability. Additionally, real-time internalization of AuNPs functionalized with ASO labeled with a fluorophore could be observed through confocal microscopy. Other methodologies, such as ICP-AES, TEM, and dark-field microscopy, could be employed to demonstrate that mild photothermy enhances AuNP@*c-MYC* internalization into cells and spheroids [452,469,627].

Active versus passive targeting of the nanoheaters

This thesis explored the use of SPAAC reaction to immobilize alkyne strained-MNPs on the azide-modified living cell membrane, that upon the application of an AMF act as "hotspots", which might induce changes in the fluidity of cell membranes and promote transfection of silencing moieties. This methodology explores the active targeting of immobilized MNPs as nanoheaters via biorthogonal chemistry, whereas mild photothermy exploits passive targeting of Au-nanoconjugates triggered by green laser irradiation. This poses the question: if AuNPs were used to promote precise and localized heat in the cell membrane via SPAAC reaction, could it enhance cell transfection without cytotoxicity when irradiated using the same laser settings previously optimized? Further studies comparing these two approaches would be valuable, concerning the advantages and limitations of passive and active targeting [148].

Complex cancer models

Testing the performance of green photo-irradiation combined with silencing moieties vectorized by AuNPs in multicellular spheroids and patient-derived organoids would clarify the feasibility of this approach for gene therapy in cancer research [2]. Therefore, exploring magnetic hyperthermia-mediated transfection via SPAAC biorthogonal chemistry in other cells that play a crucial role in TME and are difficult to transfect (e.g., CAFs and tumor-associated macrophages) and adapting for more advanced cancer cell models are highly relevant [19,571]. Regarding their immunogenic state when the *IDO1* gene is silenced, it would be interesting to evaluate if DCs could activate T cell effectors and suppress Tregs and MDSCs functions in a TME context using *in vitro*/*ex vivo* cancer cell models, such as multicellular 2D cells and 3D spheroids, and patient-derived organoids [2,25]. Furthermore, combining the *IDO1* gene silencing with immune checkpoint inhibitors (e.g., anti-PD-1/PD-L1) would be useful to enhance the antitumor immune response [26,609]. The next step would be combining both nanoparticles-mediated mild hyperthermia approaches into a single platform to deliver silencing moieties in advanced cancer cell models.

Taken together, the findings of this thesis, along with all these future *in vitro* results, have the potential to drive clinical translation, paving the way to a new era of TNA delivery in cancer therapy.

8

REFERENCES

1. Ferreira D, Fontinha D, Martins C, Pires D, Fernandes AR, Baptista P V. Gold nanoparticles for vectorization of nucleic acids for cancer therapeutics. *Molecules*. 2020;25(15). doi:10.3390/molecules25153489
2. Cordeiro S, Oliveira BB, Valente R, et al. Breaking the mold: 3D cell cultures reshaping the future of cancer research. *Front Cell Dev Biol*. 2024;12. doi:10.3389/fcell.2024.1507388
3. Bray F, Laversanne M, Sung H, et al. Global cancer statistics 2022: GLOBOCAN estimates of incidence and mortality worldwide for 36 cancers in 185 countries. *CA Cancer J Clin*. 2024;74(3):229-263. doi:10.3322/caac.21834
4. World Health Organization. The top 10 causes of death. 2024. Accessed September 26, 2024. https://www.who.int/news-room/fact-sheets/detail/the-top-10-causes-of-death
5. Ferlay J. et al. Globocan 2022. Global Cancer Observatory: Cancer Today. Lyon, France: International Agency for Research on Cancer. 2024. Accessed September 26, 2024. https://gco.iarc.who.int/today
6. Ferlay J, Colombet M, Soerjomataram I, et al. Cancer statistics for the year 2020: An overview. *Int J Cancer*. 2021;149(4):778-789. doi:10.1002/ijc.33588
7. Hanahan D, Weinberg RA. Hallmarks of Cancer: The Next Generation. *Cell*. 2011;144(5):646-674. doi:10.1016/j.cell.2011.02.013
8. Hanahan D. Hallmarks of Cancer: New Dimensions. *Cancer Discov*. 2022;12(1):31-46. doi:10.1158/2159-8290.CD-21-1059
9. Roma-Rodrigues C, Mendes R, Baptista P V., Fernandes AR. Targeting Tumor Microenvironment for Cancer Therapy. *Int J Mol Sci*. 2019;20(4):840. doi:10.3390/ijms20040840
10. Belli C, Trapani D, Viale G, et al. Targeting the microenvironment in solid tumors. *Cancer Treat Rev*. 2018;65:22-32. doi:10.1016/j.ctrv.2018.02.004
11. Baghy K, Ladányi A, Reszegi A, Kovalszky I. Insights into the Tumor Microenvironment—Components, Functions and Therapeutics. *Int J Mol Sci*. 2023;24(24):17536. doi:10.3390/ijms242417536
12. Li W, Zhou Z, Zhou X, et al. 3D Biomimetic Models to Reconstitute Tumor Microenvironment In Vitro: Spheroids, Organoids, and Tumor-on-a-Chip. *Adv Healthc Mater*. 2023;12(18). doi:10.1002/adhm.202202609
13. Manduca N, Maccafeo E, De Maria R, Sistigu A, Musella M. 3D cancer models: One step closer to in vitro human studies. *Front Immunol*. 2023;14. doi:10.3389/fimmu.2023.1175503
14. de Winde CM, Munday C, Acton SE. Molecular mechanisms of dendritic cell migration in immunity and cancer. *Med Microbiol Immunol*. 2020;209(4):515-529. doi:10.1007/s00430-020-00680-4
15. Del Prete A, Salvi V, Soriani A, et al. Dendritic cell subsets in cancer immunity and tumor antigen sensing. *Cell Mol Immunol*. 2023;20(5):432-447. doi:10.1038/s41423-023-00990-6

16. Fu C, Jiang A. Dendritic Cells and CD8 T Cell Immunity in Tumor Microenvironment. *Front Immunol*. 2018;9. doi:10.3389/fimmu.2018.03059
17. van Helden SFG, van Leeuwen FN, Figdor CG. Human and murine model cell lines for dendritic cell biology evaluated. *Immunol Lett*. 2008;117(2):191-197. doi:10.1016/j.imlet.2008.02.003
18. Hornyák L, Dobos N, Koncz G, et al. The Role of Indoleamine-2,3-Dioxygenase in Cancer Development, Diagnostics, and Therapy. *Front Immunol*. 2018;9. doi:10.3389/fimmu.2018.00151
19. Liu M, Wang X, Wang L, et al. Targeting the IDO1 pathway in cancer: from bench to bedside. *J Hematol Oncol*. 2018;11(1):100. doi:10.1186/s13045-018-0644-y
20. Fucikova J, Palova-Jelinkova L, Bartunkova J, Spisek R. Induction of Tolerance and Immunity by Dendritic Cells: Mechanisms and Clinical Applications. *Front Immunol*. 2019;10. doi:10.3389/fimmu.2019.02393
21. Meireson A, Devos M, Brochez L. IDO Expression in Cancer: Different Compartment, Different Functionality? *Front Immunol*. 2020;11. doi:10.3389/fimmu.2020.531491
22. Pallotta MT, Rossini S, Suvieri C, et al. Indoleamine 2,3-dioxygenase 1 (IDO1): an up-to-date overview of an eclectic immunoregulatory enzyme. *FEBS J*. 2022;289(20):6099-6118. doi:10.1111/febs.16086
23. Song X, Si Q, Qi R, et al. Indoleamine 2,3-Dioxygenase 1: A Promising Therapeutic Target in Malignant Tumor. *Front Immunol*. 2021;12. doi:10.3389/fimmu.2021.800630
24. de Visser KE, Joyce JA. The evolving tumor microenvironment: From cancer initiation to metastatic outgrowth. *Cancer Cell*. 2023;41(3):374-403. doi:10.1016/j.ccell.2023.02.016
25. Huang X, Zhang F, Wang X, Liu K. The Role of Indoleamine 2, 3-Dioxygenase 1 in Regulating Tumor Microenvironment. *Cancers (Basel)*. 2022;14(11):2756. doi:10.3390/cancers14112756
26. Jiang X, Wang J, Deng X, et al. Role of the tumor microenvironment in PD-L1/PD-1-mediated tumor immune escape. *Mol Cancer*. 2019;18(1):10. doi:10.1186/s12943-018-0928-4
27. Choi Y, Seok SH, Yoon HY, Ryu JH, Kwon IC. Advancing cancer immunotherapy through siRNA-based gene silencing for immune checkpoint blockade. *Adv Drug Deliv Rev*. 2024;209:115306. doi:10.1016/j.addr.2024.115306
28. Endo R, Nakamura T, Kawakami K, Sato Y, Harashima H. The silencing of indoleamine 2,3-dioxygenase 1 (IDO1) in dendritic cells by siRNA-loaded lipid nanoparticles enhances cell-based cancer immunotherapy. *Sci Rep*. 2019;9(1):11335. doi:10.1038/s41598-019-47799-w
29. Zhang Y, Feng Y, Huang Y, et al. Tumor-Targeted Gene Silencing IDO Synergizes PTT-Induced Apoptosis and Enhances Anti-tumor Immunity. *Front Immunol*. 2020;11. doi:10.3389/fimmu.2020.00968
30. Bol KF, Schreibelt G, Rabold K, et al. The clinical application of cancer immunotherapy based on naturally circulating dendritic cells. *J Immunother Cancer*. 2019;7(1):109. doi:10.1186/s40425-019-0580-6

31. Cifuentes-Rius A, Desai A, Yuen D, Johnston APR, Voelcker NH. Inducing immune tolerance with dendritic cell-targeting nanomedicines. *Nat Nanotechnol*. 2021;16(1):37-46. doi:10.1038/s41565-020-00810-2
32. Liu YH, Yeh IJ, Lai MD, Liu KT, Kuo PL, Yen MC. Cancer Immunotherapy: Silencing Intracellular Negative Immune Regulators of Dendritic Cells. *Cancers (Basel)*. 2019;11(1):108. doi:10.3390/cancers11010108
33. Xiao Z, Wang R, Wang X, et al. Impaired function of dendritic cells within the tumor microenvironment. *Front Immunol*. 2023;14. doi:10.3389/fimmu.2023.1213629
34. Abedizadeh R, Majidi F, Khorasani HR, Abedi H, Sabour D. Colorectal cancer: a comprehensive review of carcinogenesis, diagnosis, and novel strategies for classified treatments. *Cancer and Metastasis Reviews*. 2024;43(2):729-753. doi:10.1007/s10555-023-10158-3
35. Burgos-Panadero R, Lucantoni F, Gamero-Sandemetrio E, Cruz-Merino L de la, Álvaro T, Noguera R. The tumour microenvironment as an integrated framework to understand cancer biology. *Cancer Lett*. 2019;461:112-122. doi:10.1016/j.canlet.2019.07.010
36. Babar Q, Saeed A, Tabish TA, Sarwar M, Thorat ND. Targeting the tumor microenvironment: Potential strategy for cancer therapeutics. *Biochimica et Biophysica Acta (BBA) - Molecular Basis of Disease*. 2023;1869(6):166746. doi:10.1016/j.bbadis.2023.166746
37. Abd Elkodous M, El-Sayyad GS, Abdelrahman IY, et al. Therapeutic and diagnostic potential of nanomaterials for enhanced biomedical applications. *Colloids Surf B Biointerfaces*. 2019;180:411-428. doi:10.1016/j.colsurfb.2019.05.008
38. Hossain MdS, Karuniawati H, Jairoun AA, et al. Colorectal Cancer: A Review of Carcinogenesis, Global Epidemiology, Current Challenges, Risk Factors, Preventive and Treatment Strategies. *Cancers (Basel)*. 2022;14(7):1732. doi:10.3390/cancers14071732
39. Ciardiello D, Vitiello PP, Cardone C, et al. Immunotherapy of colorectal cancer: Challenges for therapeutic efficacy. *Cancer Treat Rev*. 2019;76:22-32. doi:10.1016/j.ctrv.2019.04.003
40. Edwards BK, Ward E, Kohler BA, et al. Annual report to the nation on the status of cancer, 1975-2006, featuring colorectal cancer trends and impact of interventions (risk factors, screening, and treatment) to reduce future rates. *Cancer*. 2010;116(3):544-573. doi:10.1002/cncr.24760
41. Xie Y, Shi L, He X, Luo Y. Gastrointestinal cancers in China, the USA, and Europe. *Gastroenterol Rep (Oxf)*. 2021;9(2):91-104. doi:10.1093/gastro/goab010
42. Xiong Y, Wang Y, Tiruthani K. Tumor immune microenvironment and nano-immunotherapeutics in colorectal cancer. *Nanomedicine*. 2019;21:102034. doi:10.1016/j.nano.2019.102034
43. Sillo TO, Beggs AD, Morton DG, Middleton G. Mechanisms of immunogenicity in colorectal cancer. *British Journal of Surgery*. 2019;106(10):1283-1297. doi:10.1002/bjs.11204
44. Triantafillidis JK, Nasioulas G, Kosmidis PA. Colorectal cancer and inflammatory bowel disease: epidemiology, risk factors, mechanisms of carcinogenesis and prevention strategies. *Anticancer Res*. 2009;29(7):2727-2737.

45. Hanna Jr, MG, Hoover Jr, HC, Pinedo HM, Finer M. Active Specific Immunotherapy with Autologous Tumor cell vaccines for Stage II Colon Cancer: Logistics, Efficacy, Safety and Immunological Pharmacodynamics. *Hum Vaccin*. 2006;2(4):185-191. doi:10.4161/hv.2.4.3196
46. Abakushina E V., Gelm Yu V., Pasova IA, Bazhin A V. Immunotherapeutic Approaches for the Treatment of Colorectal Cancer. *Biochemistry (Moscow)*. 2019;84(7):720-728. doi:10.1134/S0006297919070046
47. Chen S, Parmigiani G. Meta-Analysis of BRCA1 and BRCA2 Penetrance. *Journal of Clinical Oncology*. 2007;25(11):1329-1333. doi:10.1200/JCO.2006.09.1066
48. Nolan E, Lindeman GJ, Visvader JE. Deciphering breast cancer: from biology to the clinic. *Cell*. 2023;186(8):1708-1728. doi:10.1016/j.cell.2023.01.040
49. Sung H, Ferlay J, Siegel RL, et al. Global Cancer Statistics 2020: GLOBOCAN Estimates of Incidence and Mortality Worldwide for 36 Cancers in 185 Countries. *CA Cancer J Clin*. 2021;71(3):209-249. doi:10.3322/caac.21660
50. Hong R, Xu B. Breast cancer: an up-to-date review and future perspectives. *Cancer Commun*. 2022;42(10):913-936. doi:10.1002/cac2.12358
51. Hereditary Cancer Syndromes and Risk Assessment. *Obstetrics & Gynecology*. 2019;134(6):1366-1367. doi:10.1097/AOG.0000000000003563
52. Danaei G, Vander Hoorn S, Lopez AD, Murray CJ, Ezzati M. Causes of cancer in the world: comparative risk assessment of nine behavioural and environmental risk factors. *The Lancet*. 2005;366(9499):1784-1793. doi:10.1016/S0140-6736(05)67725-2
53. Hankinson SE, Colditz GA, Willett WC. Towards an integrated model for breast cancer etiology: The lifelong interplay of genes, lifestyle, and hormones. *Breast Cancer Research*. 2004;6(5):213. doi:10.1186/bcr921
54. Smolarz B, Nowak AZ, Romanowicz H. Breast Cancer—Epidemiology, Classification, Pathogenesis and Treatment (Review of Literature). *Cancers (Basel)*. 2022;14(10):2569. doi:10.3390/cancers14102569
55. Curigliano G, Burstein HJ, Winer EP, et al. De-escalating and escalating treatments for early-stage breast cancer: the St. Gallen International Expert Consensus Conference on the Primary Therapy of Early Breast Cancer 2017. *Annals of Oncology*. 2017;28(8):1700-1712. doi:10.1093/annonc/mdx308
56. Hashim D, Boffetta P, La Vecchia C, et al. The global decrease in cancer mortality: trends and disparities. *Annals of Oncology*. 2016;27(5):926-933. doi:10.1093/annonc/mdw027
57. Liu B, Zhou H, Tan L, Siu KTH, Guan XY. Exploring treatment options in cancer: tumor treatment strategies. *Signal Transduct Target Ther*. 2024;9(1):175. doi:10.1038/s41392-024-01856-7
58. Frankel RI. Centennial of Röntgen's discovery of x-rays. *West J Med*. 1996;164(6):497-501.
59. Steinberg FM, Raso J. Biotech pharmaceuticals and biotherapy: an overview. *J Pharm Pharm Sci*. 1998;1(2):48-59.

60. Kalia M. Biomarkers for personalized oncology: recent advances and future challenges. *Metabolism*. 2015;64(3):S16-S21. doi:10.1016/j.metabol.2014.10.027
61. Henry NL, Hayes DF. Cancer biomarkers. *Mol Oncol*. 2012;6(2):140-146. doi:10.1016/j.molonc.2012.01.010
62. Qu Z. Investigating Conventional and Novel Methods for Treatment of Cancer. In: *Proceedings of the 12th International Conference on Bioscience, Biochemistry and Bioinformatics*. ACM; 2023:103-111. doi:10.1145/3586139.3586154
63. Holland JF. *Cancer Medicine 6*. Vol 2. 6th ed. (Kufe DW, HJF, FEmil, ed.). BC Decker; 2003.
64. Miles WE. A Method of Performing Abdomino-Perineal Excision for Carcinoma of the Rectum and of the Terminal Portion of the Pelvic Colon (1908). *CA Cancer J Clin*. 1971;21(6):361-364. doi:10.3322/canjclin.21.6.361
65. Naef AP. Hugh Morriston Davies: First dissection lobectomy in 1912. *Ann Thorac Surg*. 1993;56(4):988-989. doi:10.1016/0003-4975(93)90377-T
66. Dursun P, Gultekin M, Ayhan A. The History of Radical Hysterectomy. *J Low Genit Tract Dis*. 2011;15(3):235-245. doi:10.1097/LGT.0b013e31820eb038
67. Phillips EH, Franklin M, Carroll BJ, Fallas MJ, Ramos R, Rosenthal D. Laparoscopie Colectomy. *Ann Surg*. 1992;216(6):703-710. doi:10.1097/00000658-199212000-00015
68. Sherwood JT, Brock M V. Lung cancer: New surgical approaches. *Respirology*. 2007;12(3):326-332. doi:10.1111/j.1440-1843.2007.01083.x
69. Singletary SE. Minimally invasive techniques in breast cancer treatment. *Semin Surg Oncol*. 2001;20(3):246-250. doi:10.1002/ssu.1040
70. Genden EM, Ferlito A, Silver CE, et al. Evolution of the management of laryngeal cancer. *Oral Oncol*. 2007;43(5):431-439. doi:10.1016/j.oraloncology.2006.08.007
71. Hashizume M. MRI-guided laparoscopic and robotic surgery for malignancies. *Int J Clin Oncol*. 2007;12(2):94-98. doi:10.1007/s10147-007-0664-z
72. Arruebo M, Vilaboa N, Sáez-Gutierrez B, et al. Assessment of the Evolution of Cancer Treatment Therapies. *Cancers (Basel)*. 2011;3(3):3279-3330. doi:10.3390/cancers3033279
73. Tohme S, Simmons RL, Tsung A. Surgery for Cancer: A Trigger for Metastases. *Cancer Res*. 2017;77(7):1548-1552. doi:10.1158/0008-5472.CAN-16-1536
74. Cavalcanti IDLima, SJCSantos. *Advances in Cancer Treatment: From Systemic Chemotherapy to Targeted Therap*. Springer International Publishing; 2021.
75. Begg AC, Stewart FA, Vens C. Strategies to improve radiotherapy with targeted drugs. *Nat Rev Cancer*. 2011;11(4):239-253. doi:10.1038/nrc3007
76. Henríquez-Hernández LA, Bordón E, Pinar B, Lloret M, Rodríguez-Gallego C, Lara PC. Prediction of normal tissue toxicity as part of the individualized treatment with radiotherapy in oncology patients. *Surg Oncol*. 2012;21(3):201-206. doi:10.1016/j.suronc.2011.12.002
77. Wittig A, Engenhart-Cabillic R. Cardiac side effects of conventional and particle radiotherapy in cancer patients. *Herz*. 2011;36(4):311-324. doi:10.1007/s00059-011-3471-2

78. Joiner M, Van Der Kogel A, Steel G. *Basic Clinical Radiobiology*. 4th ed. CRC Press; 2009. doi:10.1201/b13224-2
79. Jassem J. The role of radiotherapy in lung cancer: Where is the evidence? *Radiotherapy and Oncology*. 2007;83(2):203-213. doi:10.1016/j.radonc.2007.04.004
80. Baskar R, Lee KA, Yeo R, Yeoh KW. Cancer and Radiation Therapy: Current Advances and Future Directions. *Int J Med Sci*. 2012;9(3):193-199. doi:10.7150/ijms.3635
81. Chen HHW, Kuo MT. Improving radiotherapy in cancer treatment: Promises and challenges. *Oncotarget*. 2017;8(37):62742-62758. doi:10.18632/oncotarget.18409
82. Cooper GM, HRE. *The Cell: A Molecular Approach*. 3rd ed. ASM Press; 2004.
83. Liang XJ, Chen C, Zhao Y, Wang PC. Circumventing Tumor Resistance to Chemotherapy by Nanotechnology. In: ; 2010:467-488. doi:10.1007/978-1-60761-416-6_21
84. Skeel R and KS,. *Handbook of Cancer Chemotherapy*. Philadelphia: Wolters Kluwer. ; 2015.
85. Saevarsdottir T, Fridriksdottir N, Gunnarsdottir S. Quality of Life and Symptoms of Anxiety and Depression of Patients Receiving Cancer Chemotherapy. *Cancer Nurs*. 2010;33(1):E1-E10. doi:10.1097/NCC.0b013e3181b4adb5
86. Tilsed CM, Fisher SA, Nowak AK, Lake RA, Lesterhuis WJ. Cancer chemotherapy: insights into cellular and tumor microenvironmental mechanisms of action. *Front Oncol*. 2022;12. doi:10.3389/fonc.2022.960317
87. Schmidt E V., Chisamore MJ, Chaney MF, et al. Assessment of Clinical Activity of PD-1 Checkpoint Inhibitor Combination Therapies Reported in Clinical Trials. *JAMA Netw Open*. 2020;3(2):e1920833. doi:10.1001/jamanetworkopen.2019.20833
88. van Hagen P, Hulshof MCCM, van Lanschot JJB, et al. Preoperative Chemoradiotherapy for Esophageal or Junctional Cancer. *New England Journal of Medicine*. 2012;366(22):2074-2084. doi:10.1056/NEJMoa1112088
89. Achilli P, Crippa J, Grass F, et al. Survival impact of adjuvant chemotherapy in patients with stage IIA colon cancer: Analysis of the National Cancer Database. *Int J Cancer*. 2021;148(1):161-169. doi:10.1002/ijc.33203
90. Anand U, Dey A, Chandel AKS, et al. Cancer chemotherapy and beyond: Current status, drug candidates, associated risks and progress in targeted therapeutics. *Genes Dis*. 2023;10(4):1367-1401. doi:10.1016/j.gendis.2022.02.007
91. Dewanjee S, Vallamkondu J, Kalra RS, et al. The Emerging Role of HDACs: Pathology and Therapeutic Targets in Diabetes Mellitus. *Cells*. 2021;10(6):1340. doi:10.3390/cells10061340
92. Waldman AD, Fritz JM, Lenardo MJ. A guide to cancer immunotherapy: from T cell basic science to clinical practice. *Nat Rev Immunol*. 2020;20(11):651-668. doi:10.1038/s41577-020-0306-5
93. Esfahani K, Roudaia L, Buhlaiga N, Del Rincon SV, Papneja N, Miller WH. A Review of Cancer Immunotherapy: From the Past, to the Present, to the Future. *Current Oncology*. 2020;27(12):87-97. doi:10.3747/co.27.5223

94. Fife BT, Bluestone JA. Control of peripheral T-cell tolerance and autoimmunity via the CTLA-4 and PD-1 pathways. *Immunol Rev*. 2008;224(1):166-182. doi:10.1111/j.1600-065X.2008.00662.x
95. Roy R, Singh S, Misra S. Advancements in Cancer Immunotherapies. *Vaccines (Basel)*. 2022;11(1):59. doi:10.3390/vaccines11010059
96. Sun Q, Hong Z, Zhang C, Wang L, Han Z, Ma D. Immune checkpoint therapy for solid tumours: clinical dilemmas and future trends. *Signal Transduct Target Ther*. 2023;8(1):320. doi:10.1038/s41392-023-01522-4
97. Twomey JD, Zhang B. Cancer Immunotherapy Update: FDA-Approved Checkpoint Inhibitors and Companion Diagnostics. *AAPS J*. 2021;23(2):39. doi:10.1208/s12248-021-00574-0
98. Egloff H, Kidwell KM, Schott A. Ado-Trastuzumab Emtansine-Induced Pulmonary Toxicity: A Single-Institution Retrospective Review. *Case Rep Oncol*. 2018;11(2):527-533. doi:10.1159/000491574
99. Debela DT, Muzazu SGY, Heraro KD, et al. New approaches and procedures for cancer treatment: Current perspectives. *SAGE Open Med*. 2021;9. doi:10.1177/20503121211034366
100. Mokhtari RB, Homayouni TS, Baluch N, et al. Combination therapy in combating cancer. *Oncotarget*. 2017;8(23):38022-38043. doi:10.18632/oncotarget.16723
101. Hurwitz H, Fehrenbacher L, Novotny W, et al. Bevacizumab plus Irinotecan, Fluorouracil, and Leucovorin for Metastatic Colorectal Cancer. *New England Journal of Medicine*. 2004;350(23):2335-2342. doi:10.1056/NEJMoa032691
102. Waryah CB, Moses C, Arooj M, Blancafort P. Zinc Fingers, TALEs, and CRISPR Systems: A Comparison of Tools for Epigenome Editing. In: ; 2018:19-63. doi:10.1007/978-1-4939-7774-1_2
103. Gupta SK, Shukla P. Gene editing for cell engineering: trends and applications. *Crit Rev Biotechnol*. 2017;37(5):672-684. doi:10.1080/07388551.2016.1214557
104. Carroll D. Genome Editing: Past, Present, and Future. *Yale J Biol Med*. 2017;90(4):653-659.
105. Cring MR, Sheffield VC. Gene therapy and gene correction: targets, progress, and challenges for treating human diseases. *Gene Ther*. 2022;29(1-2):3-12. doi:10.1038/s41434-020-00197-8
106. Roma-Rodrigues C, Rivas-García L, Baptista P V., Fernandes AR. Gene Therapy in Cancer Treatment: Why Go Nano? *Pharmaceutics*. 2020;12(3):233. doi:10.3390/pharmaceutics12030233
107. Karimian A, Azizian K, Parsian H, et al. CRISPR/Cas9 technology as a potent molecular tool for gene therapy. *J Cell Physiol*. 2019;234(8):12267-12277. doi:10.1002/jcp.27972
108. Moon S Bin, Kim DY, Ko JH, Kim YS. Recent advances in the CRISPR genome editing tool set. *Exp Mol Med*. 2019;51(11):1-11. doi:10.1038/s12276-019-0339-7

109. Biagioni A, Laurenzana A, Margheri F, Chillà A, Fibbi G, Del Rosso M. Delivery systems of CRISPR/Cas9-based cancer gene therapy. *J Biol Eng*. 2018;12(1):33. doi:10.1186/s13036-018-0127-2
110. Li T, Yang Y, Qi H, et al. CRISPR/Cas9 therapeutics: progress and prospects. *Signal Transduct Target Ther*. 2023;8(1):36. doi:10.1038/s41392-023-01309-7
111. Jinek M, Chylinski K, Fonfara I, Hauer M, Doudna JA, Charpentier E. A Programmable Dual-RNA–Guided DNA Endonuclease in Adaptive Bacterial Immunity. *Science (1979)*. 2012;337(6096):816-821. doi:10.1126/science.1225829
112. Makarova KS, Wolf YI, Alkhnbashi OS, et al. An updated evolutionary classification of CRISPR–Cas systems. *Nat Rev Microbiol*. 2015;13(11):722-736. doi:10.1038/nrmicro3569
113. Ran FA, Hsu PD, Wright J, Agarwala V, Scott DA, Zhang F. Genome engineering using the CRISPR-Cas9 system. *Nat Protoc*. 2013;8(11):2281-2308. doi:10.1038/nprot.2013.143
114. Jiang W, Bikard D, Cox D, Zhang F, Marraffini LA. RNA-guided editing of bacterial genomes using CRISPR-Cas systems. *Nat Biotechnol*. 2013;31(3):233-239. doi:10.1038/nbt.2508
115. Liu C, Zhang L, Liu H, Cheng K. Delivery strategies of the CRISPR-Cas9 gene-editing system for therapeutic applications. *Journal of Controlled Release*. 2017;266:17-26. doi:10.1016/j.jconrel.2017.09.012
116. Givens BE, Naguib YW, Geary SM, Devor EJ, Salem AK. Nanoparticle-Based Delivery of CRISPR/Cas9 Genome-Editing Therapeutics. *AAPS J*. 2018;20(6):108. doi:10.1208/s12248-018-0267-9
117. Li H, Yang Y, Hong W, Huang M, Wu M, Zhao X. Applications of genome editing technology in the targeted therapy of human diseases: mechanisms, advances and prospects. *Signal Transduct Target Ther*. 2020;5(1):1. doi:10.1038/s41392-019-0089-y
118. Stadtmauer EA, Fraietta JA, Davis MM, et al. CRISPR-engineered T cells in patients with refractory cancer. *Science (1979)*. 2020;367(6481). doi:10.1126/science.aba7365
119. Khoshandam M, Soltaninejad H, Mousazadeh M, Hamidieh AA, Hosseinkhani S. Clinical applications of the CRISPR/Cas9 genome-editing system: Delivery options and challenges in precision medicine. *Genes Dis*. 2024;11(1):268-282. doi:10.1016/j.gendis.2023.02.027
120. Kamaliyan Z, Clarke TL. Zinc finger proteins: guardians of genome stability. *Front Cell Dev Biol*. 2024;12. doi:10.3389/fcell.2024.1448789
121. Rots MG, Jeltsch A. Editing the Epigenome: Overview, Open Questions, and Directions of Future Development. In: ; 2018:3-18. doi:10.1007/978-1-4939-7774-1_1
122. Guo J, Gaj T, Barbas CF. Directed Evolution of an Enhanced and Highly Efficient FokI Cleavage Domain for Zinc Finger Nucleases. *J Mol Biol*. 2010;400(1):96-107. doi:10.1016/j.jmb.2010.04.060
123. Paschon DE, Lussier S, Wangzor T, et al. Diversifying the structure of zinc finger nucleases for high-precision genome editing. *Nat Commun*. 2019;10(1):1133. doi:10.1038/s41467-019-08867-x

124. Zheng N, Li L, Wang X. Molecular mechanisms, off-target activities, and clinical potentials of genome editing systems. *Clin Transl Med*. 2020;10(1):412-426. doi:10.1002/ctm2.34
125. Bogdanove AJ, Voytas DF. TAL Effectors: Customizable Proteins for DNA Targeting. *Science (1979)*. 2011;333(6051):1843-1846. doi:10.1126/science.1204094
126. Cermak T, Doyle EL, Christian M, et al. Efficient design and assembly of custom TALEN and other TAL effector-based constructs for DNA targeting. *Nucleic Acids Res*. 2011;39(12):e82-e82. doi:10.1093/nar/gkr218
127. Schmid-Burgk JL, Schmidt T, Kaiser V, Höning K, Hornung V. A ligation-independent cloning technique for high-throughput assembly of transcription activator–like effector genes. *Nat Biotechnol*. 2013;31(1):76-81. doi:10.1038/nbt.2460
128. Reyon D, Tsai SQ, Khayter C, Foden JA, Sander JD, Joung JK. FLASH assembly of TALENs for high-throughput genome editing. *Nat Biotechnol*. 2012;30(5):460-465. doi:10.1038/nbt.2170
129. Eshka SFA, Bahador M, Gordan MM, Karbasi S, Tabar ZM, Basiri M. A systematic review of gene editing clinical trials. Published online November 25, 2022. doi:10.1101/2022.11.24.22282599
130. Silva G, Poirot L, Galetto R, et al. Meganucleases and Other Tools for Targeted Genome Engineering: Perspectives and Challenges for Gene Therapy. *Curr Gene Ther*. 2011;11(1):11-27. doi:10.2174/156652311794520111
131. Khan SH. Genome-Editing Technologies: Concept, Pros, and Cons of Various Genome-Editing Techniques and Bioethical Concerns for Clinical Application. *Mol Ther Nucleic Acids*. 2019;16:326-334. doi:10.1016/j.omtn.2019.02.027
132. Serganov A, Patel DJ. Ribozymes, riboswitches and beyond: regulation of gene expression without proteins. *Nat Rev Genet*. 2007;8(10):776-790. doi:10.1038/nrg2172
133. Mahmoodi Chalbatani G, Dana H, Gharagouzloo E, et al. Small interfering RNAs (siRNAs) in cancer therapy: a nano-based approach. *Int J Nanomedicine*. 2019;Volume 14:3111-3128. doi:10.2147/IJN.S200253
134. Fernandes AR, Baptista P V. Gene Silencing Using Multifunctionalized Gold Nanoparticles for Cancer Therapy. In: ; 2017:319-336. doi:10.1007/978-1-4939-6646-2_19
135. Kim DH, Rossi JJ. RNAi Mechanisms and Applications. *Biotechniques*. 2008;44(5):613-616. doi:10.2144/000112792
136. Chery J. RNA therapeutics: RNAi and antisense mechanisms and clinical applications. *Postdoc Journal*. 2016;4(7). doi:10.14304/SURYA.JPR.V4N7.5
137. Kumar S, Gonzalez EA, Rameshwar P, Etchegaray JP. Non-Coding RNAs as Mediators of Epigenetic Changes in Malignancies. *Cancers (Basel)*. 2020;12(12):3657. doi:10.3390/cancers12123657
138. Senapati D, Patra BC, Kar A, et al. Promising approaches of small interfering RNAs (siRNAs) mediated cancer gene therapy. *Gene*. 2019;719:144071. doi:10.1016/j.gene.2019.144071

139. Lou W, Zhang L, Wang J. Current status of nucleic acid therapy and its new progress in cancer treatment. *Int Immunopharmacol*. 2024;142:113157. doi:10.1016/j.intimp.2024.113157
140. Mansoor M, Melendez AJ. Advances in Antisense Oligonucleotide Development for Target Identification, Validation, and as Novel Therapeutics. *Gene Regul Syst Bio*. 2008;2. doi:10.4137/GRSB.S418
141. Younis HS, Templin M, Whiteley LO, Kornbrust D, Kim TW, Henry SP. Overview of the Nonclinical Development Strategies and Class-Effects of Oligonucleotide-Based Therapeutics. In: *A Comprehensive Guide to Toxicology in Nonclinical Drug Development*. Elsevier; 2017:737-754. doi:10.1016/B978-0-12-803620-4.00028-1
142. Kher G, Trehan S, Misra A. Antisense Oligonucleotides and RNA Interference. In: *Challenges in Delivery of Therapeutic Genomics and Proteomics*. Elsevier; 2011:325-386. doi:10.1016/B978-0-12-384964-9.00007-4
143. Calin GA, Dumitru CD, Shimizu M, et al. Frequent deletions and down-regulation of micro- RNA genes *miR15* and *miR16* at 13q14 in chronic lymphocytic leukemia. *Proceedings of the National Academy of Sciences*. 2002;99(24):15524-15529. doi:10.1073/pnas.242606799
144. Jebelli A, Baradaran B, Mosafer J, Baghbanzadeh A, Mokhtarzadeh A, Tayebi L. Recent developments in targeting genes and pathways by RNAi-based approaches in colorectal cancer. *Med Res Rev*. 2021;41(1):395-434. doi:10.1002/med.21735
145. Chandramohan K, Balan DJ, Devi KP, et al. Short interfering RNA in colorectal cancer: is it wise to shoot the messenger? *Eur J Pharmacol*. 2023;949:175699. doi:10.1016/j.ejphar.2023.175699
146. Weber LI, Hartl M. Strategies to target the cancer driver MYC in tumor cells. *Front Oncol*. 2023;13. doi:10.3389/fonc.2023.1142111
147. Ozcan G, Ozpolat B, Coleman RL, Sood AK, Lopez-Berestein G. Preclinical and clinical development of siRNA-based therapeutics. *Adv Drug Deliv Rev*. 2015;87:108-119. doi:10.1016/j.addr.2015.01.007
148. Walia S, Mehta MJ. Recent progress on nanosystems for nucleic acid delivery. *RSC Pharmaceutics*. 2024;1(4):645-674. doi:10.1039/D4PM00009A
149. Stephenson ML, Zamecnik PC. Inhibition of Rous sarcoma viral RNA translation by a specific oligodeoxyribonucleotide. *Proceedings of the National Academy of Sciences*. 1978;75(1):285-288. doi:10.1073/pnas.75.1.285
150. Verma A. Recent advances in antisense oligonucleotide therapy in genetic neuromuscular diseases. *Ann Indian Acad Neurol*. 2018;21(1):3. doi:10.4103/aian.AIAN_298_17
151. Goyenvalle A, Leumann C, Garcia L. Therapeutic Potential of Tricyclo-DNA antisense oligonucleotides. *J Neuromuscul Dis*. 2016;3(2):157-167. doi:10.3233/JND-160146
152. Chi X, Gatti P, Papoian T. Safety of antisense oligonucleotide and siRNA-based therapeutics. *Drug Discov Today*. 2017;22(5):823-833. doi:10.1016/j.drudis.2017.01.013
153. Farrar MA, Park SB, Vucic S, et al. Emerging therapies and challenges in spinal muscular atrophy. *Ann Neurol*. 2017;81(3):355-368. doi:10.1002/ana.24864

154. Kole R, Krainer AR, Altman S. RNA therapeutics: beyond RNA interference and antisense oligonucleotides. *Nat Rev Drug Discov*. 2012;11(2):125-140. doi:10.1038/nrd3625
155. Crooke ST. *Antisense Drug Technology : Principles: Strategies, and Applications*. CRC Press; 2001.
156. Sridharan K, Gogtay NJ. Therapeutic nucleic acids: current clinical status. *Br J Clin Pharmacol*. 2016;82(3):659-672. doi:10.1111/bcp.12987
157. Rader DJ, Kastelein JJP. Lomitapide and Mipomersen. *Circulation*. 2014;129(9):1022-1032. doi:10.1161/CIRCULATIONAHA.113.001292
158. Wicki A, Witzigmann D, Balasubramanian V, Huwyler J. Nanomedicine in cancer therapy: Challenges, opportunities, and clinical applications. *Journal of Controlled Release*. 2015;200:138-157. doi:10.1016/j.jconrel.2014.12.030
159. Oliveira BB, Ferreira D, Fernandes AR, Baptista PV. Engineering gold nanoparticles for molecular diagnostics and biosensing. *WIREs Nanomedicine and Nanobiotechnology*. 2023;15(1). doi:10.1002/wnan.1836
160. Roma-Rodrigues C, Pombo I, Raposo L, Pedrosa P, Fernandes AR, Baptista P V. Nanotheranostics targeting the tumor microenvironment. *Front Bioeng Biotechnol*. 2019;7(AUG). doi:10.3389/fbioe.2019.00197
161. He H, Liu L, Morin EE, Liu M, Schwendeman A. Survey of Clinical Translation of Cancer Nanomedicines—Lessons Learned from Successes and Failures. *Acc Chem Res*. 2019;52(9):2445-2461. doi:10.1021/acs.accounts.9b00228
162. Attia MS, Kijanka G, Nguyen NT, Zhang J, An H. Advances and prospects of RNA delivery nanoplatforms for cancer therapy. *Acta Pharm Sin B*. 2025;15(1):52-96. doi:10.1016/j.apsb.2024.09.009
163. Dastgerdi NK, Dastgerdi NK, Bayraktutan H, et al. Enhancing siRNA cancer therapy: Multifaceted strategies with lipid and polymer-based carrier systems. *Int J Pharm*. 2024;663:124545. doi:10.1016/j.ijpharm.2024.124545
164. Ferrari M. Cancer nanotechnology: opportunities and challenges. *Nat Rev Cancer*. 2005;5(3):161-171. doi:10.1038/nrc1566
165. Peer D, Karp JM, Hong S, Farokhzad OC, Margalit R, Langer R. Nanocarriers as an emerging platform for cancer therapy. *Nat Nanotechnol*. 2007;2(12):751-760. doi:10.1038/nnano.2007.387
166. Sumer B, Gao J. Theranostic Nanomedicine for Cancer. *Nanomedicine*. 2008;3(2):137-140. doi:10.2217/17435889.3.2.137
167. Patel S, Kim J, Herrera M, Mukherjee A, Kabanov A V., Sahay G. Brief update on endocytosis of nanomedicines. *Adv Drug Deliv Rev*. 2019;144:90-111. doi:10.1016/j.addr.2019.08.004
168. Kesharwani P, Iyer AK. Recent advances in dendrimer-based nanovectors for tumor-targeted drug and gene delivery. *Drug Discov Today*. 2015;20(5):536-547. doi:10.1016/j.drudis.2014.12.012
169. Hu CM, Zhang L. Therapeutic Nanoparticles to Combat Cancer Drug Resistance. *Curr Drug Metab*. 2009;10(8):836-841. doi:10.2174/138920009790274540

170. Idiago-López J, Moreno-Antolín E, de la Fuente JM, Fratila RM. Nanoparticles and bioorthogonal chemistry joining forces for improved biomedical applications. *Nanoscale Adv*. 2021;3(5):1261-1292. doi:10.1039/D0NA00873G
171. Kumar S, Diwan A, Singh P, et al. Functionalized gold nanostructures: promising gene delivery vehicles in cancer treatment. *RSC Adv*. 2019;9(41):23894-23907. doi:10.1039/C9RA03608C
172. Kaestner L, Scholz A, Lipp P. Conceptual and technical aspects of transfection and gene delivery. *Bioorg Med Chem Lett*. 2015;25(6):1171-1176. doi:10.1016/j.bmcl.2015.01.018
173. Karimi S, Fouani MH, Moshaii A, Nikkhah M, Hosseinkhani S, Sheikhnejad R. Development of Dual Functional Nucleic Acid Delivery Nanosystem for DNA Induced Silencing of Bcl-2 Oncogene. *Int J Nanomedicine*. 2020;Volume 15:1693-1708. doi:10.2147/IJN.S236217
174. Bessis N, GarciaCozar FJ, Boissier MC. Immune responses to gene therapy vectors: influence on vector function and effector mechanisms. *Gene Ther*. 2004;11(S1):S10-S17. doi:10.1038/sj.gt.3302364
175. Ramamoorth M. Non Viral Vectors in Gene Therapy- An Overview. *Journal of Clinical and Diagnostic Research*. Published online 2015. doi:10.7860/JCDR/2015/10443.5394
176. Lu C, Stewart DJ, Lee JJ, et al. Phase I Clinical Trial of Systemically Administered TUSC2(FUS1)-Nanoparticles Mediating Functional Gene Transfer in Humans. *PLoS One*. 2012;7(4):e34833. doi:10.1371/journal.pone.0034833
177. Schultheis B, Strumberg D, Santel A, et al. First-in-Human Phase I Study of the Liposomal RNA Interference Therapeutic Atu027 in Patients With Advanced Solid Tumors. *Journal of Clinical Oncology*. 2014;32(36):4141-4148. doi:10.1200/JCO.2013.55.0376
178. Wang JH, Gessler DJ, Zhan W, Gallagher TL, Gao G. Adeno-associated virus as a delivery vector for gene therapy of human diseases. *Signal Transduct Target Ther*. 2024;9(1):78. doi:10.1038/s41392-024-01780-w
179. Zhang WW, Li L, Li D, et al. The First Approved Gene Therapy Product for Cancer Ad-*p53* (Gendicine): 12 Years in the Clinic. *Hum Gene Ther*. 2018;29(2):160-179. doi:10.1089/hum.2017.218
180. Mukai H, Ogawa K, Kato N, Kawakami S. Recent advances in lipid nanoparticles for delivery of nucleic acid, mRNA, and gene editing-based therapeutics. *Drug Metab Pharmacokinet*. 2022;44:100450. doi:10.1016/j.dmpk.2022.100450
181. Ozpolat B, Sood AK, Lopez-Berestein G. Nanomedicine based approaches for the delivery of siRNA in cancer. *J Intern Med*. 2010;267(1):44-53. doi:10.1111/j.1365-2796.2009.02191.x
182. Singh A, Trivedi P, Jain NK. Advances in siRNA delivery in cancer therapy. *Artif Cells Nanomed Biotechnol*. 2018;46(2):274-283. doi:10.1080/21691401.2017.1307210
183. Cardarelli F, Digiacomo L, Marchini C, et al. The intracellular trafficking mechanism of Lipofectamine-based transfection reagents and its implication for gene delivery. *Sci Rep*. 2016;6(1):25879. doi:10.1038/srep25879

184. Wu FG, Zhang X, Chen X, et al. Quantum Dots for Cancer Therapy and Bioimaging. In: ; 2018:89-135. doi:10.1007/978-3-319-89878-0_3
185. Singh P, Pandit S, Balusamy SR, et al. Advanced Nanomaterials for Cancer Therapy: Gold, Silver, and Iron Oxide Nanoparticles in Oncological Applications. *Adv Healthc Mater*. 2025;14(4). doi:10.1002/adhm.202403059
186. Sokolova V, Epple M. Inorganic Nanoparticles as Carriers of Nucleic Acids into Cells. *Angewandte Chemie International Edition*. 2008;47(8):1382-1395. doi:10.1002/anie.200703039
187. Mainini F, Eccles MR. Lipid and Polymer-Based Nanoparticle siRNA Delivery Systems for Cancer Therapy. *Molecules*. 2020;25(11):2692. doi:10.3390/molecules25112692
188. Jin JO, Kim G, Hwang J, Han KH, Kwak M, Lee PCW. Nucleic acid nanotechnology for cancer treatment. *Biochimica et Biophysica Acta (BBA) - Reviews on Cancer*. 2020;1874(1):188377. doi:10.1016/j.bbcan.2020.188377
189. Chong ZX, Yeap SK, Ho WY. Transfection types, methods and strategies: a technical review. *PeerJ*. 2021;9:e11165. doi:10.7717/peerj.11165
190. Dulińska-Litewka J, Łazarczyk A, Hałubiec P, Szafrański O, Karnas K, Karewicz A. Superparamagnetic Iron Oxide Nanoparticles—Current and Prospective Medical Applications. *Materials*. 2019;12(4):617. doi:10.3390/ma12040617
191. Revia RA, Stephen ZR, Zhang M. Theranostic Nanoparticles for RNA-Based Cancer Treatment. *Acc Chem Res*. 2019;52(6):1496-1506. doi:10.1021/acs.accounts.9b00101
192. Fratila RM, Navascuez M, Idiago-López J, et al. Covalent immobilisation of magnetic nanoparticles on surfaces via strain-promoted azide–alkyne click chemistry. *New Journal of Chemistry*. 2017;41(19):10835-10840. doi:10.1039/C7NJ01822C
193. Idiago-López J, Moreno-Antolín E, Eceiza M, et al. From Bench to Cell: A Roadmap for Assessing the Bioorthogonal "Click" Reactivity of Magnetic Nanoparticles for Cell Surface Engineering. *Bioconjug Chem*. 2022;33(9):1620-1633. doi:10.1021/acs.bioconjchem.2c00230
194. Farokhzad OC, Karp JM, Langer R. Nanoparticle–aptamer bioconjugates for cancer targeting. *Expert Opin Drug Deliv*. 2006;3(3):311-324. doi:10.1517/17425247.3.3.311
195. Thomsen T, Klok HA. Chemical Cell Surface Modification and Analysis of Nanoparticle-Modified Living Cells. *ACS Appl Bio Mater*. 2021;4(3):2293-2306. doi:10.1021/acsabm.0c01619
196. Stephan MT, Irvine DJ. Enhancing cell therapies from the outside in: Cell surface engineering using synthetic nanomaterials. *Nano Today*. 2011;6(3):309-325. doi:10.1016/j.nantod.2011.04.001
197. Algar WR, Prasuhn DE, Stewart MH, et al. The Controlled Display of Biomolecules on Nanoparticles: A Challenge Suited to Bioorthogonal Chemistry. *Bioconjug Chem*. 2011;22(5):825-858. doi:10.1021/bc200065z
198. Lamoot A, Uvyn A, Kasmi S, De Geest BG. Covalent Cell Surface Conjugation of Nanoparticles by a Combination of Metabolic Labeling and Click Chemistry. *Angewandte Chemie International Edition*. 2021;60(12):6320-6325. doi:10.1002/anie.202015625

199. Lim S, Kim W, Song S, et al. Intracellular Uptake Mechanism of Bioorthogonally Conjugated Nanoparticles on Metabolically Engineered Mesenchymal Stem Cells. *Bioconjug Chem*. 2021;32(1):199-214. doi:10.1021/acs.bioconjchem.0c00640
200. Agard NJ, Prescher JA, Bertozzi CR. A Strain-Promoted [3 + 2] Azide−Alkyne Cycloaddition for Covalent Modification of Biomolecules in Living Systems. *J Am Chem Soc*. 2004;126(46):15046-15047. doi:10.1021/ja044996f
201. Maeda H. Toward a full understanding of the EPR effect in primary and metastatic tumors as well as issues related to its heterogeneity. *Adv Drug Deliv Rev*. 2015;91:3-6. doi:10.1016/j.addr.2015.01.002
202. Vines JB, Yoon JH, Ryu NE, Lim DJ, Park H. Gold Nanoparticles for Photothermal Cancer Therapy. *Front Chem*. 2019;7. doi:10.3389/fchem.2019.00167
203. Kritika, Roy I. Therapeutic applications of magnetic nanoparticles: recent advances. *Mater Adv*. 2022;3(20):7425-7444. doi:10.1039/D2MA00444E
204. X. The Bakerian Lecture. —Experimental relations of gold (and other metals) to light. *Philos Trans R Soc Lond*. 1857;147:145-181. doi:10.1098/rstl.1857.0011
205. Turkevich J, Stevenson PC, Hillier J. A study of the nucleation and growth processes in the synthesis of colloidal gold. *Discuss Faraday Soc*. 1951;11:55. doi:10.1039/df9511100055
206. Chandra P, Singh J, Singh A, Srivastava A, Goyal RN, Shim YB. Gold Nanoparticles and Nanocomposites in Clinical Diagnostics Using Electrochemical Methods. *Journal of Nanoparticles*. 2013;2013:1-12. doi:10.1155/2013/535901
207. Mandal R, Baranwal A, Srivastava A, Chandra P. Evolving trends in bio/chemical sensor fabrication incorporating bimetallic nanoparticles. *Biosens Bioelectron*. 2018;117:546-561. doi:10.1016/j.bios.2018.06.039
208. Brust M, Walker M, Bethell D, Schiffrin DJ, Whyman R. Synthesis of thiol-derivatised gold nanoparticles in a two-phase Liquid–Liquid system. *J Chem Soc, Chem Commun*. 1994;0(7):801-802. doi:10.1039/C39940000801
209. Hinman JG, Stork AJ, Varnell JA, Gewirth AA, Murphy CJ. Seed mediated growth of gold nanorods: towards nanorod matryoshkas. *Faraday Discuss*. 2016;191:9-33. doi:10.1039/C6FD00145A
210. Sahu P, Prasad BL V. Time and Temperature Effects on the Digestive Ripening of Gold Nanoparticles: Is There a Crossover from Digestive Ripening to Ostwald Ripening? *Langmuir*. 2014;30(34):10143-10150. doi:10.1021/la500914j
211. Baranwal A, Mahato K, Srivastava A, Maurya PK, Chandra P. Phytofabricated metallic nanoparticles and their clinical applications. *RSC Adv*. 2016;6(107):105996-106010. doi:10.1039/C6RA23411A
212. Mahato K, Nagpal S, Shah MA, et al. Gold nanoparticle surface engineering strategies and their applications in biomedicine and diagnostics. *3 Biotech*. 2019;9(2):57. doi:10.1007/s13205-019-1577-z

213. Thiruppathi R, Mishra S, Ganapathy M, Padmanabhan P, Gulyás B. Nanoparticle Functionalization and Its Potentials for Molecular Imaging. *Advanced Science*. 2017;4(3). doi:10.1002/advs.201600279
214. Shamim, Ali S, Ali T, Sharma H, Kishor BN, Jha SK. Recent Advances in Monodisperse Gold Nanoparticle Delivery, Synthesis, and Emerging Applications in Cancer Therapy. *Plasmonics*. Published online January 21, 2025. doi:10.1007/s11468-024-02732-4
215. Naahidi S, Jafari M, Edalat F, Raymond K, Khademhosseini A, Chen P. Biocompatibility of engineered nanoparticles for drug delivery. *Journal of Controlled Release*. 2013;166(2):182-194. doi:10.1016/j.jconrel.2012.12.013
216. Badir A, Refki S, Sekkat Z. Utilizing gold nanoparticles in plasmonic photothermal therapy for cancer treatment. *Heliyon*. 2025;11(4):e42738. doi:10.1016/j.heliyon.2025.e42738
217. Cole LE, Ross RD, Tilley JM, Vargo-Gogola T, Roeder RK. Gold Nanoparticles as Contrast Agents in x-ray Imaging and Computed Tomography. *Nanomedicine*. 2015;10(2):321-341. doi:10.2217/nnm.14.171
218. Li W, Chen X. Gold Nanoparticles for Photoacoustic Imaging. *Nanomedicine*. 2015;10(2):299-320. doi:10.2217/nnm.14.169
219. Wu Y, Ali MRK, Chen K, Fang N, El-Sayed MA. Gold nanoparticles in biological optical imaging. *Nano Today*. 2019;24:120-140. doi:10.1016/j.nantod.2018.12.006
220. Astruc D. *Nanoparticles and Catalysis*. (Astruc D, ed.). Wiley; 2007. doi:10.1002/9783527621323
221. Moore TL, Rodriguez-Lorenzo L, Hirsch V, et al. Nanoparticle colloidal stability in cell culture media and impact on cellular interactions. *Chem Soc Rev*. 2015;44(17):6287-6305. doi:10.1039/C4CS00487F
222. Nicol JR, Dixon D, Coulter JA. Gold Nanoparticle Surface Functionalization: A Necessary Requirement in the Development of Novel Nanotherapeutics. *Nanomedicine*. 2015;10(8):1315-1326. doi:10.2217/nnm.14.219
223. Hao Y, Yang X, Song S, et al. Exploring the cell uptake mechanism of phospholipid and polyethylene glycol coated gold nanoparticles. *Nanotechnology*. 2012;23(4):045103. doi:10.1088/0957-4484/23/4/045103
224. Yeh YC, Creran B, Rotello VM. Gold nanoparticles: preparation, properties, and applications in bionanotechnology. *Nanoscale*. 2012;4(6):1871-1880. doi:10.1039/C1NR11188D
225. Bahadur K.C. R, Thapa B, Bhattarai N. Gold nanoparticle-based gene delivery: promises and challenges. *Nanotechnol Rev*. 2014;3(3). doi:10.1515/ntrev-2013-0026
226. Thomas M, Klibanov AM. Conjugation to gold nanoparticles enhances polyethylenimine's transfer of plasmid DNA into mammalian cells. *Proceedings of the National Academy of Sciences*. 2003;100(16):9138-9143. doi:10.1073/pnas.1233634100
227. Hu C, Peng Q, Chen F, Zhong Z, Zhuo R. Low Molecular Weight Polyethylenimine Conjugated Gold Nanoparticles as Efficient Gene Vectors. *Bioconjug Chem*. 2010;21(5):836-843. doi:10.1021/bc900374d

228. Kong WH, Bae KH, Jo SD, Kim JS, Park TG. Cationic Lipid-Coated Gold Nanoparticles as Efficient and Non-Cytotoxic Intracellular siRNA Delivery Vehicles. *Pharm Res*. 2012;29(2):362-374. doi:10.1007/s11095-011-0554-y
229. Li P, Li D, Zhang L, Li G, Wang E. Cationic lipid bilayer coated gold nanoparticles-mediated transfection of mammalian cells. *Biomaterials*. 2008;29(26):3617-3624. doi:10.1016/j.biomaterials.2008.05.020
230. Kawano T, Yamagata M, Takahashi H, et al. Stabilizing of plasmid DNA in vivo by PEG-modified cationic gold nanoparticles and the gene expression assisted with electrical pulses. *Journal of Controlled Release*. 2006;111(3):382-389. doi:10.1016/j.jconrel.2005.12.022
231. Lee SH, Bae KH, Kim SH, Lee KR, Park TG. Amine-functionalized gold nanoparticles as non-cytotoxic and efficient intracellular siRNA delivery carriers. *Int J Pharm*. 2008;364(1):94-101. doi:10.1016/j.ijpharm.2008.07.027
232. Baptista PV. Gold Nanobeacons: A Potential Nanotheranostics Platform. *Nanomedicine*. 2014;9(15):2247-2250. doi:10.2217/nnm.14.143
233. Ding Y, Jiang Z, Saha K, et al. Gold Nanoparticles for Nucleic Acid Delivery. *Molecular Therapy*. 2014;22(6):1075-1083. doi:10.1038/mt.2014.30
234. Rosi NL, Giljohann DA, Thaxton CS, Lytton-Jean AKR, Han MS, Mirkin CA. Oligonucleotide-Modified Gold Nanoparticles for Intracellular Gene Regulation. *Science (1979)*. 2006;312(5776):1027-1030. doi:10.1126/science.1125559
235. Carnerero JM, Jimenez-Ruiz A, Castillo PM, Prado-Gotor R. Covalent and Non-Covalent DNA–Gold-Nanoparticle Interactions: New Avenues of Research. *ChemPhysChem*. 2017;18(1):17-33. doi:10.1002/cphc.201601077
236. Ghosh PS, Kim CK, Han G, Forbes NS, Rotello VM. Efficient Gene Delivery Vectors by Tuning the Surface Charge Density of Amino Acid-Functionalized Gold Nanoparticles. *ACS Nano*. 2008;2(11):2213-2218. doi:10.1021/nn800507t
237. McIntosh CM, Esposito EA, Boal AK, Simard JM, Martin CT, Rotello VM. Inhibition of DNA Transcription Using Cationic Mixed Monolayer Protected Gold Clusters. *J Am Chem Soc*. 2001;123(31):7626-7629. doi:10.1021/ja015556g
238. Elbakry A, Zaky A, Liebl R, Rachel R, Goepferich A, Breunig M. Layer-by-Layer Assembled Gold Nanoparticles for siRNA Delivery. *Nano Lett*. 2009;9(5):2059-2064. doi:10.1021/nl9003865
239. Conde J, Rosa J, de la Fuente JM, Baptista P V. Gold-nanobeacons for simultaneous gene specific silencing and intracellular tracking of the silencing events. *Biomaterials*. 2013;34(10):2516-2523. doi:10.1016/j.biomaterials.2012.12.015
240. Pedrosa P, Corvo ML, Ferreira-Silva M, et al. Targeting Cancer Resistance via Multifunctional Gold Nanoparticles. *Int J Mol Sci*. 2019;20(21):5510. doi:10.3390/ijms20215510
241. Mendes R, Fernandes AR, Baptista P V. Gold nanoparticle approach to the selective delivery of gene silencing in cancer-The case for combined delivery? *Genes (Basel)*. 2017;8(3). doi:10.3390/genes8030094

242. Barnaby SN, Lee A, Mirkin CA. Probing the inherent stability of siRNA immobilized on nanoparticle constructs. *Proceedings of the National Academy of Sciences*. 2014;111(27):9739-9744. doi:10.1073/pnas.1409431111
243. Sousa de Almeida M, Susnik E, Drasler B, Taladriz-Blanco P, Petri-Fink A, Rothen-Rutishauser B. Understanding nanoparticle endocytosis to improve targeting strategies in nanomedicine. *Chem Soc Rev*. 2021;50(9):5397-5434. doi:10.1039/D0CS01127D
244. Foroozandeh P, Aziz AA. Insight into Cellular Uptake and Intracellular Trafficking of Nanoparticles. *Nanoscale Res Lett*. 2018;13(1):339. doi:10.1186/s11671-018-2728-6
245. McCully M, Hernandez Y, Conde J, et al. Significance of the balance between intracellular glutathione and polyethylene glycol for successful release of small interfering RNA from gold nanoparticles. *Nano Res*. 2015;8(10):3281-3292. doi:10.1007/s12274-015-0828-5
246. Conde J, Tian F, Hernández Y, et al. In vivo tumor targeting via nanoparticle-mediated therapeutic siRNA coupled to inflammatory response in lung cancer mouse models. *Biomaterials*. 2013;34(31):7744-7753. doi:10.1016/j.biomaterials.2013.06.041
247. Vinhas R, Fernandes AR, Baptista P V. Gold Nanoparticles for BCR-ABL1 Gene Silencing: Improving Tyrosine Kinase Inhibitor Efficacy in Chronic Myeloid Leukemia. *Mol Ther Nucleic Acids*. 2017;7:408-416. doi:10.1016/j.omtn.2017.05.003
248. Ali A, Shah T, Ullah R, et al. Review on Recent Progress in Magnetic Nanoparticles: Synthesis, Characterization, and Diverse Applications. *Front Chem*. 2021;9. doi:10.3389/fchem.2021.629054
249. Shen B, Sun S. Chemical Synthesis of Magnetic Nanoparticles for Permanent Magnet Applications. *Chemistry – A European Journal*. 2020;26(30):6757-6766. doi:10.1002/chem.201902916
250. Dave S, Dave S, Mathur A, Das J. Biological synthesis of magnetic nanoparticles. In: *Nanobiotechnology*. Elsevier; 2021:225-234. doi:10.1016/B978-0-12-822878-4.00014-6
251. Majidi S, Zeinali Sehrig F, Farkhani SM, Soleymani Goloujeh M, Akbarzadeh A. Current methods for synthesis of magnetic nanoparticles. *Artif Cells Nanomed Biotechnol*. 2016;44(2):722-734. doi:10.3109/21691401.2014.982802
252. Stiufiuc GF, Stiufiuc RI. Magnetic Nanoparticles: Synthesis, Characterization, and Their Use in Biomedical Field. *Applied Sciences*. 2024;14(4):1623. doi:10.3390/app14041623
253. Tiefenauer LX, Kuehne G, Andres RY. Antibody-magnetite nanoparticles: In vitro characterization of a potential tumor-specific contrast agent for magnetic resonance imaging. *Bioconjug Chem*. 1993;4(5):347-352. doi:10.1021/bc00023a007
254. Jordan A, Wust P, Scholz R, Faehling H, Krause J, Felix R. Magnetic Fluid Hyperthermia (MFH). In: *Scientific and Clinical Applications of Magnetic Carriers*. Springer US; 1997:569-595. doi:10.1007/978-1-4757-6482-6_43
255. Banerjee SS, Chen DH. Magnetic Nanoparticles Grafted with Cyclodextrin for Hydrophobic Drug Delivery. *Chemistry of Materials*. 2007;19(25):6345-6349. doi:10.1021/cm702278u

256. Schillinger U, Brill T, Rudolph C, et al. Advances in magnetofection—magnetically guided nucleic acid delivery. *J Magn Magn Mater*. 2005;293(1):501-508. doi:10.1016/j.jmmm.2005.01.032
257. Albukhaty S, Sulaiman GM, Al-Karagoly H, et al. Iron oxide nanoparticles: The versatility of the magnetic and functionalized nanomaterials in targeting drugs, and gene deliveries with effectual magnetofection. *J Drug Deliv Sci Technol*. 2024;99:105838. doi:10.1016/j.jddst.2024.105838
258. Wang H, Shrestha TB, Basel MT, et al. Magnetic-Fe/Fe 3 O 4 -nanoparticle-bound SN38 as carboxylesterase-cleavable prodrug for the delivery to tumors within monocytes/macrophages. *Beilstein Journal of Nanotechnology*. 2012;3:444-455. doi:10.3762/bjnano.3.51
259. Purushotham S, Chang PEJ, Rumpel H, et al. Thermoresponsive core–shell magnetic nanoparticles for combined modalities of cancer therapy. *Nanotechnology*. 2009;20(30):305101. doi:10.1088/0957-4484/20/30/305101
260. Hervault A, Thanh NTK. Magnetic nanoparticle-based therapeutic agents for thermo-chemotherapy treatment of cancer. *Nanoscale*. 2014;6(20):11553-11573. doi:10.1039/C4NR03482A
261. Veiseh O, Gunn JW, Zhang M. Design and fabrication of magnetic nanoparticles for targeted drug delivery and imaging. *Adv Drug Deliv Rev*. 2010;62(3):284-304. doi:10.1016/j.addr.2009.11.002
262. Sanson C, Diou O, Thévenot J, et al. Doxorubicin Loaded Magnetic Polymersomes: Theranostic Nanocarriers for MR Imaging and Magneto-Chemotherapy. *ACS Nano*. 2011;5(2):1122-1140. doi:10.1021/nn102762f
263. Gobbo OL, Sjaastad K, Radomski MW, Volkov Y, Prina-Mello A. Magnetic Nanoparticles in Cancer Theranostics. *Theranostics*. 2015;5(11):1249-1263. doi:10.7150/thno.11544
264. Belyanina I, Kolovskaya O, Zamay S, Gargaun A, Zamay T, Kichkailo A. Targeted Magnetic Nanotheranostics of Cancer. *Molecules*. 2017;22(6):975. doi:10.3390/molecules22060975
265. Thuy TTMS, TNT. *Magnetic Nanoparticles: From Fabrication to Clinical Applications*. 1st ed. (Thanh NT, ed.). CRC Press; 2012. doi:10.1201/b11760
266. Jahan S, Alias YB, Abu Bakar AF Bin, Yusoff I Bin. Ionic release behavior of polymer-coated and uncoated metal nanoparticles (MNPs) in various conditions: effects of particle shape, size, and natural media reactivity. *Colloid Polym Sci*. 2017;295(10):1961-1971. doi:10.1007/s00396-017-4155-0
267. Mamontova E, Favier I, Pla D, Gómez M. Organometallic interactions between metal nanoparticles and carbon-based molecules: A surface reactivity rationale. In: ; 2022:43-103. doi:10.1016/bs.adomc.2022.01.004
268. Zahraei M, Marciello M, Lazaro-Carrillo A, et al. Versatile theranostics agents designed by coating ferrite nanoparticles with biocompatible polymers. *Nanotechnology*. 2016;27(25):255702. doi:10.1088/0957-4484/27/25/255702

269. LaConte L, Nitin N, Bao G. Magnetic nanoparticle probes. *Materials Today*. 2005;8(5):32-38. doi:10.1016/S1369-7021(05)00893-X
270. Nordin A, Ahmad Z, Husna S, et al. The State of the Art of Natural Polymer Functionalized Fe3O4 Magnetic Nanoparticle Composites for Drug Delivery Applications: A Review. *Gels*. 2023;9(2):121. doi:10.3390/gels9020121
271. Gómez-Lopera SA, Plaza RC, Delgado AV. Synthesis and Characterization of Spherical Magnetite/Biodegradable Polymer Composite Particles. *J Colloid Interface Sci*. 2001;240(1):40-47. doi:10.1006/jcis.2001.7579
272. Fratila RM, Mitchell SG, del Pino P, Grazu V, de la Fuente JM. Strategies for the Biofunctionalization of Gold and Iron Oxide Nanoparticles. *Langmuir*. 2014;30(50):15057-15071. doi:10.1021/la5015658
273. Bertrand N, Wu J, Xu X, Kamaly N, Farokhzad OC. Cancer nanotechnology: The impact of passive and active targeting in the era of modern cancer biology. *Adv Drug Deliv Rev*. 2014;66:2-25. doi:10.1016/j.addr.2013.11.009
274. Scheinberg DA, Grimm J, Heller DA, Stater EP, Bradbury M, McDevitt MR. Advances in the clinical translation of nanotechnology. *Curr Opin Biotechnol*. 2017;46:66-73. doi:10.1016/j.copbio.2017.01.002
275. Arsiwala A, Castro A, Frey S, Stathos M, Kane RS. Designing Multivalent Ligands to Control Biological Interactions: From Vaccines and Cellular Effectors to Targeted Drug Delivery. *Chem Asian J*. 2019;14(2):244-255. doi:10.1002/asia.201801677
276. Fabris F, Lima E, De Biasi E, et al. Controlling the dominant magnetic relaxation mechanisms for magnetic hyperthermia in bimagnetic core–shell nanoparticles. *Nanoscale*. 2019;11(7):3164-3172. doi:10.1039/C8NR07834C
277. Saville SL, Stone RC, Qi B, Mefford OT. Investigation of the stability of magnetite nanoparticles functionalized with catechol based ligands in biological media. *J Mater Chem*. 2012;22(47):24909. doi:10.1039/c2jm34902g
278. Sandler SE, Fellows B, Mefford OT. Best Practices for Characterization of Magnetic Nanoparticles for Biomedical Applications. *Anal Chem*. 2019;91(22):14159-14169. doi:10.1021/acs.analchem.9b03518
279. Babu A, Muralidharan R, Amreddy N, Mehta M, Munshi A, Ramesh R. Nanoparticles for siRNA-Based Gene Silencing in Tumor Therapy. *IEEE Trans Nanobioscience*. 2016;15(8):849-863. doi:10.1109/TNB.2016.2621730
280. Reddy AN, Anjaneyulu K, Basak P, Rao NM, Manorama S V. A Simple Approach to the Design and Functionalization of Fe 3 O 4 –Au Nanoparticles for Biomedical Applications. *Chempluschem*. 2012;77(4):284-292. doi:10.1002/cplu.201100032
281. Narsireddy A, Vijayashree K, Irudayaraj J, Manorama S V., Rao NM. Targeted in vivo photodynamic therapy with epidermal growth factor receptor-specific peptide linked nanoparticles. *Int J Pharm*. 2014;471(1-2):421-429. doi:10.1016/j.ijpharm.2014.05.063
282. Mohammadi MR, Malkovskiy A V., Jothimuthu P, et al. PEG/Dextran Double Layer Influences Fe Ion Release and Colloidal Stability of Iron Oxide Nanoparticles. *Sci Rep*. 2018;8(1):4286. doi:10.1038/s41598-018-22644-8

283. Zhang T, Li F, Xu Q, et al. Ferrimagnetic Nanochains-Based Mesenchymal Stem Cell Engineering for Highly Efficient Post-Stroke Recovery. *Adv Funct Mater*. 2019;29(24). doi:10.1002/adfm.201900603
284. Xu Q, Zhang T, Wang Q, et al. Uniformly sized iron oxide nanoparticles for efficient gene delivery to mesenchymal stem cells. *Int J Pharm*. 2018;552(1-2):443-452. doi:10.1016/j.ijpharm.2018.10.023
285. Saber Braim F, Noor Ashikin Nik Ab Razak N, Abdul Aziz A, Qasim Ismael L, Kayode Sodipo B. Ultrasound assisted chitosan coated iron oxide nanoparticles: Influence of ultrasonic irradiation on the crystallinity, stability, toxicity and magnetization of the functionalized nanoparticles. *Ultrason Sonochem*. 2022;88:106072. doi:10.1016/j.ultsonch.2022.106072
286. Min KA, Cho JH, Song YK, Kim CK. Iron casein succinylate-chitosan coacervate for the liquid oral delivery of iron with bioavailability and stability enhancement. *Arch Pharm Res*. 2016;39(1):94-102. doi:10.1007/s12272-015-0684-6
287. Yin H, Kauffman KJ, Anderson DG. Delivery technologies for genome editing. *Nat Rev Drug Discov*. 2017;16(6):387-399. doi:10.1038/nrd.2016.280
288. Zhang J, Zhang T, Gao J. Biocompatible Iron Oxide Nanoparticles for Targeted Cancer Gene Therapy: A Review. *Nanomaterials*. 2022;12(19):3323. doi:10.3390/nano12193323
289. Liu G, Xie J, Zhang F, et al. N-Alkyl-PEI-Functionalized Iron Oxide Nanoclusters for Efficient siRNA Delivery. *Small*. 2011;7(19):2742-2749. doi:10.1002/smll.201100825
290. Wang K, Kievit FM, Sham JG, et al. Iron-Oxide-Based Nanovector for Tumor Targeted siRNA Delivery in an Orthotopic Hepatocellular Carcinoma Xenograft Mouse Model. *Small*. 2016;12(4):477-487. doi:10.1002/smll.201501985
291. Shim MS, Kwon YJ. Acid-Responsive Linear Polyethylenimine for Efficient, Specific, and Biocompatible siRNA Delivery. *Bioconjug Chem*. 2009;20(3):488-499. doi:10.1021/bc800436v
292. Casper J, Schenk SH, Parhizkar E, Detampel P, Dehshahri A, Huwyler J. Polyethylenimine (PEI) in gene therapy: Current status and clinical applications. *Journal of Controlled Release*. 2023;362:667-691. doi:10.1016/j.jconrel.2023.09.001
293. Yoon HY, Koo H, Kim K, Kwon IC. Molecular imaging based on metabolic glycoengineering and bioorthogonal click chemistry. *Biomaterials*. 2017;132:28-36. doi:10.1016/j.biomaterials.2017.04.003
294. Lim S, Yoon HY, Jang HJ, et al. Dual-Modal Imaging-Guided Precise Tracking of Bioorthogonally Labeled Mesenchymal Stem Cells in Mouse Brain Stroke. *ACS Nano*. 2019;13(10):10991-11007. doi:10.1021/acsnano.9b02173
295. Koo H, Lee S, Na JH, et al. Bioorthogonal Copper-Free Click Chemistry In Vivo for Tumor-Targeted Delivery of Nanoparticles. *Angewandte Chemie International Edition*. 2012;51(47):11836-11840. doi:10.1002/anie.201206703
296. Shang L, Nienhaus K, Nienhaus GU. Engineered nanoparticles interacting with cells: size matters. *J Nanobiotechnology*. 2014;12(1):5. doi:10.1186/1477-3155-12-5

297. Jiang W, Kim BYS, Rutka JT, Chan WCW. Nanoparticle-mediated cellular response is size-dependent. *Nat Nanotechnol*. 2008;3(3):145-150. doi:10.1038/nnano.2008.30
298. Mirshafiee V, Mahmoudi M, Lou K, Cheng J, Kraft ML. Protein corona significantly reduces active targeting yield. *Chemical Communications*. 2013;49(25):2557. doi:10.1039/c3cc37307j
299. Kami D, Takeda S, Itakura Y, Gojo S, Watanabe M, Toyoda M. Application of Magnetic Nanoparticles to Gene Delivery. *Int J Mol Sci*. 2011;12(6):3705-3722. doi:10.3390/ijms12063705
300. Majidi S, Zeinali Sehrig F, Samiei M, et al. Magnetic nanoparticles: Applications in gene delivery and gene therapy. *Artif Cells Nanomed Biotechnol*. Published online March 2, 2015:1-8. doi:10.3109/21691401.2015.1014093
301. Mah C, Fraites TJ, Zolotukhin I, et al. Improved Method of Recombinant AAV2 Delivery for Systemic Targeted Gene Therapy. *Molecular Therapy*. 2002;6(1):106-112. doi:10.1006/mthe.2001.0636
302. Akinc A, Thomas M, Klibanov AM, Langer R. Exploring polyethylenimine-mediated DNA transfection and the proton sponge hypothesis. *J Gene Med*. 2005;7(5):657-663. doi:10.1002/jgm.696
303. McBain SC, Yiu HHP, El Haj A, Dobson J. Polyethyleneimine functionalized iron oxide nanoparticles as agents for DNA delivery and transfection. *J Mater Chem*. 2007;17(24):2561. doi:10.1039/b617402g
304. Scherer F, Anton M, Schillinger U, et al. Magnetofection: enhancing and targeting gene delivery by magnetic force in vitro and in vivo. *Gene Ther*. 2002;9(2):102-109. doi:10.1038/sj.gt.3301624
305. Boyer C, Priyanto P, Davis TP, et al. Anti-fouling magnetic nanoparticles for siRNA delivery. *J Mater Chem*. 2010;20(2):255-265. doi:10.1039/B914063H
306. Ebrahimi N, Manavi MS, Nazari A, et al. Nano-scale delivery systems for siRNA delivery in cancer therapy: New era of gene therapy empowered by nanotechnology. *Environ Res*. 2023;239:117263. doi:10.1016/j.envres.2023.117263
307. Miao L, Liu C, Ge J, et al. Antitumor Effect of TRAIL on Oral Squamous Cell Carcinoma using Magnetic Nanoparticle-Mediated Gene Expression. *Cell Biochem Biophys*. 2014;69(3):663-672. doi:10.1007/s12013-014-9849-z
308. Wang X, Zhu L, Hou X, Wang L, Yin S. Polyethylenimine mediated magnetic nanoparticles for combined intracellular imaging, siRNA delivery and anti-tumor therapy. *RSC Adv*. 2015;5(123):101569-101581. doi:10.1039/C5RA18464A
309. Cruz-Acuña M, Halman JR, Afonin KA, Dobson J, Rinaldi C. Magnetic nanoparticles loaded with functional RNA nanoparticles. *Nanoscale*. 2018;10(37):17761-17770. doi:10.1039/C8NR04254C
310. Sizikov AA, Nikitin PI, Nikitin MP. Magnetofection In Vivo by Nanomagnetic Carriers Systemically Administered into the Bloodstream. *Pharmaceutics*. 2021;13(11):1927. doi:10.3390/pharmaceutics13111927

311. Stein R, Pfister F, Friedrich B, et al. Plasmid-DNA Delivery by Covalently Functionalized PEI-SPIONs as a Potential 'Magnetofection' Agent. *Molecules*. 2022;27(21):7416. doi:10.3390/molecules27217416
312. Farooq N, Ather L, Shafiq M, et al. Magnetofection approach for the transformation of okra using green iron nanoparticles. *Sci Rep*. 2022;12(1):16568. doi:10.1038/s41598-022-20569-x
313. Chung S, Sugimoto Y, Huang J, Zhang M. Iron Oxide Nanoparticles Decorated with Functional Peptides for a Targeted siRNA Delivery to Glioma Cells. *ACS Appl Mater Interfaces*. 2023;15(1):106-119. doi:10.1021/acsami.2c17802
314. Karpinska K, Li L, Wang T. Dual conjugation of magnetic nanoparticles with antibodies and siRNA for cell-specific gene silencing in vascular cells. *Frontiers in Drug Delivery*. 2024;4. doi:10.3389/fddev.2024.1416737
315. Kaur P, Aliru ML, Chadha AS, Asea A, Krishnan S. Hyperthermia using nanoparticles – Promises and pitfalls. *International Journal of Hyperthermia*. 2016;32(1):76-88. doi:10.3109/02656736.2015.1120889
316. Hoption Cann SA, van Netten JP, van Netten C. Dr William Coley and tumour regression: a place in history or in the future. *Postgrad Med J*. 2003;79(938):672-680.
317. Hannon G, Tansi FL, Hilger I, Prina-Mello A. The Effects of Localized Heat on the Hallmarks of Cancer. *Adv Ther (Weinh)*. 2021;4(7). doi:10.1002/adtp.202000267
318. Behrouzkia Z, Joveini Z, Keshavarzi B, Eyvazzadeh N, Aghdam RZ. Hyperthermia: How Can It Be Used? *Oman Med J*. 2016;31(2):89-97. doi:10.5001/omj.2016.19
319. Bravo M, Fortuni B, Mulvaney P, et al. Nanoparticle-mediated thermal Cancer therapies: Strategies to improve clinical translatability. *Journal of Controlled Release*. 2024;372:751-777. doi:10.1016/j.jconrel.2024.06.055
320. Cordeiro S, Roma-Rodrigues C, Baptista P V., Fernandes AR. Gold Nanoparticles as a Tool for Combinatorial Nanomedicine. In: ; 2024:315-370. doi:10.1142/9789811283208_0010
321. Han HS, Choi KY. Advances in Nanomaterial-Mediated Photothermal Cancer Therapies: Toward Clinical Applications. *Biomedicines*. 2021;9(3):305. doi:10.3390/biomedicines9030305
322. Kok HP, Cressman ENK, Ceelen W, et al. Heating technology for malignant tumors: a review. *International Journal of Hyperthermia*. 2020;37(1):711-741. doi:10.1080/02656736.2020.1779357
323. Stauffer PR, Goldberg SN. Introduction: Thermal ablation therapy. *International Journal of Hyperthermia*. 2004;20(7):671-677. doi:10.1080/02656730400007220
324. Rajan A, Sahu NK. Review on magnetic nanoparticle-mediated hyperthermia for cancer therapy. *Journal of Nanoparticle Research*. 2020;22(11):319. doi:10.1007/s11051-020-05045-9
325. Chatterjee DK, Diagaradjane P, Krishnan S. Nanoparticle-mediated Hyperthermia in Cancer Therapy. *Ther Deliv*. 2011;2(8):1001-1014. doi:10.4155/tde.11.72

326. Elming P, Sørensen B, Oei A, et al. Hyperthermia: The Optimal Treatment to Overcome Radiation Resistant Hypoxia. *Cancers (Basel)*. 2019;11(1):60. doi:10.3390/cancers11010060
327. Phung DC, Nguyen HT, Phuong Tran TT, et al. Combined hyperthermia and chemotherapy as a synergistic anticancer treatment. *J Pharm Investig*. 2019;49(5):519-526. doi:10.1007/s40005-019-00431-5
328. Stephen ZR, Zhang M. Recent Progress in the Synergistic Combination of Nanoparticle-Mediated Hyperthermia and Immunotherapy for Treatment of Cancer. *Adv Healthc Mater*. 2021;10(2). doi:10.1002/adhm.202001415
329. Graham K, Unger E. Overcoming tumor hypoxia as a barrier to radiotherapy, chemotherapy and immunotherapy in cancer treatment. *Int J Nanomedicine*. 2018;Volume 13:6049-6058. doi:10.2147/IJN.S140462
330. Kumari S, Sharma N, Sahi S V. Advances in Cancer Therapeutics: Conventional Thermal Therapy to Nanotechnology-Based Photothermal Therapy. *Pharmaceutics*. 2021;13(8):1174. doi:10.3390/pharmaceutics13081174
331. Fernandes S, Fernandez T, Metze S, et al. Magnetic Nanoparticle-Based Hyperthermia Mediates Drug Delivery and Impairs the Tumorigenic Capacity of Quiescent Colorectal Cancer Stem Cells. *ACS Appl Mater Interfaces*. 2021;13(14):15959-15972. doi:10.1021/acsami.0c21349
332. Khafaji M, Zamani M, Golizadeh M, Bavi O. Inorganic nanomaterials for chemo/photothermal therapy: a promising horizon on effective cancer treatment. *Biophys Rev*. 2019;11(3):335-352. doi:10.1007/s12551-019-00532-3
333. Yi GY, Kim MJ, Kim HI, Park J, Baek SH. Hyperthermia Treatment as a Promising Anti-Cancer Strategy: Therapeutic Targets, Perspective Mechanisms and Synergistic Combinations in Experimental Approaches. *Antioxidants*. 2022;11(4):625. doi:10.3390/antiox11040625
334. Das P, Colombo M, Prosperi D. Recent advances in magnetic fluid hyperthermia for cancer therapy. *Colloids Surf B Biointerfaces*. 2019;174:42-55. doi:10.1016/j.colsurfb.2018.10.051
335. Kumar AVP, Dubey SK, Tiwari S, et al. Recent advances in nanoparticles mediated photothermal therapy induced tumor regression. *Int J Pharm*. 2021;606:120848. doi:10.1016/j.ijpharm.2021.120848
336. Ackroyd R, Kelty C, Brown N, Reed M. The History of Photodetection and Photodynamic Therapy. *Photochem Photobiol*. 2001;74(5):656. doi:10.1562/0031-8655(2001)074<0656:THOPAP>2.0.CO;2
337. Pérez-Hernández M, del Pino P, Mitchell SG, et al. Dissecting the Molecular Mechanism of Apoptosis during Photothermal Therapy Using Gold Nanoprisms. *ACS Nano*. 2015;9(1):52-61. doi:10.1021/nn505468v
338. Yamamoto N, Homma S, Sery TW, Donoso LA, Kenneth Hoober J. Photodynamic immunopotentiation: in vitro activation of macrophages by treatment of mouse peritoneal

cells with haematoporphyrin derivative and light. *Eur J Cancer Clin Oncol*. 1991;27(4):467-471. doi:10.1016/0277-5379(91)90388-T

339. Agarwal ML, Larkin HE, Zaidi SI, Mukhtar H, Oleinick NL. Phospholipase activation triggers apoptosis in photosensitized mouse lymphoma cells. *Cancer Res*. 1993;53(24):5897-5902.
340. Gollnick SO, Vaughan L, Henderson BW. Generation of effective antitumor vaccines using photodynamic therapy. *Cancer Res*. 2002;62(6):1604-1608.
341. Jaque D, Martínez Maestro L, del Rosal B, et al. Nanoparticles for photothermal therapies. *Nanoscale*. 2014;6(16):9494-9530. doi:10.1039/C4NR00708E
342. Kumar PPP, Lim DK. Photothermal Effect of Gold Nanoparticles as a Nanomedicine for Diagnosis and Therapeutics. *Pharmaceutics*. 2023;15(9):2349. doi:10.3390/pharmaceutics15092349
343. Li X, Lovell JF, Yoon J, Chen X. Clinical development and potential of photothermal and photodynamic therapies for cancer. *Nat Rev Clin Oncol*. 2020;17(11):657-674. doi:10.1038/s41571-020-0410-2
344. Hao Y, Chung CK, Yu Z, et al. Combinatorial Therapeutic Approaches with Nanomaterial-Based Photodynamic Cancer Therapy. *Pharmaceutics*. 2022;14(1):120. doi:10.3390/pharmaceutics14010120
345. Yang W, Liang H, Ma S, Wang D, Huang J. Gold nanoparticle based photothermal therapy: Development and application for effective cancer treatment. *Sustainable Materials and Technologies*. 2019;22:e00109. doi:10.1016/j.susmat.2019.e00109
346. Cabral RM, Baptista P V. Anti-cancer precision theranostics: A focus on multifunctional gold nanoparticles. *Expert Rev Mol Diagn*. 2014;14(8):1041-1052. doi:10.1586/14737159.2014.965683
347. Huang X, El-Sayed MA. Gold nanoparticles: Optical properties and implementations in cancer diagnosis and photothermal therapy. *J Adv Res*. 2010;1(1):13-28. doi:10.1016/j.jare.2010.02.002
348. Cabral RM, Baptista P V. The chemistry and biology of gold nanoparticle-mediated photothermal therapy: promises and challenges. *Nano Life*. 2013;03(03):1330001. doi:10.1142/S179398441330001X
349. El-Sayed I, Huang X, El-Sayed M. Selective laser photo-thermal therapy of epithelial carcinoma using anti-EGFR antibody conjugated gold nanoparticles. *Cancer Lett*. 2006;239(1):129-135. doi:10.1016/j.canlet.2005.07.035
350. Kim J, Kim J, Jeong C, Kim WJ. Synergistic nanomedicine by combined gene and photothermal therapy. *Adv Drug Deliv Rev*. 2016;98:99-112. doi:10.1016/j.addr.2015.12.018
351. Shen J, Kim H, Mu C, et al. Multifunctional Gold Nanorods for siRNA Gene Silencing and Photothermal Therapy. *Adv Healthc Mater*. 2014;3(10):1629-1637. doi:10.1002/adhm.201400103
352. Yang Z, Liu T, Xie Y, et al. Chitosan layered gold nanorods as synergistic therapeutics for photothermal ablation and gene silencing in triple-negative breast cancer. *Acta Biomater*. 2015;25:194-204. doi:10.1016/j.actbio.2015.07.026

353. Wang BK, Yu XF, Wang JH, et al. Gold-nanorods-siRNA nanoplex for improved photothermal therapy by gene silencing. *Biomaterials*. 2016;78:27-39. doi:10.1016/j.biomaterials.2015.11.025
354. Liu B, Cao W, Qiao G, et al. Effects of gold nanoprism-assisted human PD-L1 siRNA on both gene down-regulation and photothermal therapy on lung cancer. *Acta Biomater*. 2019;99:307-319. doi:10.1016/j.actbio.2019.08.046
355. Wei P, Chen J, Hu Y, et al. Dendrimer-Stabilized Gold Nanostars as a Multifunctional Theranostic Nanoplatform for CT Imaging, Photothermal Therapy, and Gene Silencing of Tumors. *Adv Healthc Mater*. 2016;5(24):3203-3213. doi:10.1002/adhm.201600923
356. Huo S, Gong N, Jiang Y, et al. Gold-DNA nanosunflowers for efficient gene silencing with controllable transformation. *Sci Adv*. 2019;5(10). doi:10.1126/sciadv.aaw6264
357. Huang S, Duan S, Wang J, et al. Folic-Acid-Mediated Functionalized Gold Nanocages for Targeted Delivery of Anti-miR-181b in Combination of Gene Therapy and Photothermal Therapy against Hepatocellular Carcinoma. *Adv Funct Mater*. 2016;26(15):2532-2544. doi:10.1002/adfm.201504912
358. Huschka R, Barhoumi A, Liu Q, Roth JA, Ji L, Halas NJ. Gene Silencing by Gold Nanoshell-Mediated Delivery and Laser-Triggered Release of Antisense Oligonucleotide and siRNA. *ACS Nano*. 2012;6(9):7681-7691. doi:10.1021/nn301135w
359. Kim BS, Kumar D, Park CH, Kim CS. HSPA1A-siRNA nucleated gold nanorods for stimulated photothermal therapy through strategic heat shock to HSP70. *Mater Chem Front*. 2021;5(17):6461-6470. doi:10.1039/D1QM00630D
360. Son S, Kim N, You DG, et al. Antitumor therapeutic application of self-assembled RNAi-AuNP nanoconstructs: Combination of VEGF-RNAi and photothermal ablation. *Theranostics*. 2017;7(1):9-22. doi:10.7150/thno.16042
361. Heinemann D, Schomaker M, Kalies S, et al. Gold Nanoparticle Mediated Laser Transfection for Efficient siRNA Mediated Gene Knock Down. *PLoS One*. 2013;8(3):e58604. doi:10.1371/journal.pone.0058604
362. Shasha C, Krishnan KM. Nonequilibrium Dynamics of Magnetic Nanoparticles with Applications in Biomedicine. *Advanced Materials*. 2021;33(23). doi:10.1002/adma.201904131
363. Soetaert F, Korangath P, Serantes D, Fiering S, Ivkov R. Cancer therapy with iron oxide nanoparticles: Agents of thermal and immune therapies. *Adv Drug Deliv Rev*. 2020;163-164:65-83. doi:10.1016/j.addr.2020.06.025
364. Peiravi M, Eslami H, Ansari M, Zare-Zardini H. Magnetic hyperthermia: Potentials and limitations. *Journal of the Indian Chemical Society*. 2022;99(1):100269. doi:10.1016/j.jics.2021.100269
365. Liu J, Su D, Wu K, Wang JP. High-moment magnetic nanoparticles. *Journal of Nanoparticle Research*. 2020;22(3):66. doi:10.1007/s11051-020-4758-0
366. Beola L, Asín L, Fratila RM, et al. Dual Role of Magnetic Nanoparticles as Intracellular Hotspots and Extracellular Matrix Disruptors Triggered by Magnetic Hyperthermia in

3D Cell Culture Models. *ACS Appl Mater Interfaces*. 2018;10(51):44301-44313. doi:10.1021/acsami.8b18270

367. Cazares-Cortes E, Cabana S, Boitard C, et al. Recent insights in magnetic hyperthermia: From the "hot-spot" effect for local delivery to combined magneto-photo-thermia using magneto-plasmonic hybrids. *Adv Drug Deliv Rev*. 2019;138:233-246. doi:10.1016/j.addr.2018.10.016
368. de Andrade Mello P, Bian S, Savio LEB, et al. Hyperthermia and associated changes in membrane fluidity potentiate P2X7 activation to promote tumor cell death. *Oncotarget*. 2017;8(40):67254-67268. doi:10.18632/oncotarget.18595
369. Garanina AS, Naumenko VA, Nikitin AA, et al. Temperature-controlled magnetic nanoparticles hyperthermia inhibits primary tumor growth and metastases dissemination. *Nanomedicine*. 2020;25:102171. doi:10.1016/j.nano.2020.102171
370. Freitas M, Nouws HPA, Keating E, Delerue-Matos C. High-performance electrochemical immunomagnetic assay for breast cancer analysis. *Sens Actuators B Chem*. 2020;308:127667. doi:10.1016/j.snb.2020.127667
371. Gilchrist RK, Medal R, Shorey WD, Hanselman RC, Parrott JC, Taylor CB. Selective Inductive Heating of Lymph Nodes. *Ann Surg*. 1957;146(4):596-606. doi:10.1097/00000658-195710000-00007
372. Kumar CSSR, Mohammad F. Magnetic nanomaterials for hyperthermia-based therapy and controlled drug delivery. *Adv Drug Deliv Rev*. 2011;63(9):789-808. doi:10.1016/j.addr.2011.03.008
373. Monzel C, Vicario C, Piehler J, Coppey M, Dahan M. Magnetic control of cellular processes using biofunctional nanoparticles. *Chem Sci*. 2017;8(11):7330-7338. doi:10.1039/C7SC01462G
374. Laurent S, Dutz S, Häfeli UO, Mahmoudi M. Magnetic fluid hyperthermia: Focus on superparamagnetic iron oxide nanoparticles. *Adv Colloid Interface Sci*. 2011;166(1-2):8-23. doi:10.1016/j.cis.2011.04.003
375. Szwed M, Marczak A. Application of Nanoparticles for Magnetic Hyperthermia for Cancer Treatment—The Current State of Knowledge. *Cancers (Basel)*. 2024;16(6):1156. doi:10.3390/cancers16061156
376. Denkbaş EB, Çelik E, Erdal E, et al. Magnetically based nanocarriers in drug delivery. In: *Nanobiomaterials in Drug Delivery*. Elsevier; 2016:285-331. doi:10.1016/B978-0-323-42866-8.00009-5
377. Saini J, Sharma PK. Clinical, Prognostic and Therapeutic Significance of Heat Shock Proteins in Cancer. *Curr Drug Targets*. 2018;19(13):1478-1490. doi:10.2174/1389450118666170823121248
378. Ortner V, Kaspar C, Halter C, et al. Magnetic field-controlled gene expression in encapsulated cells. *Journal of Controlled Release*. 2012;158(3):424-432. doi:10.1016/j.jconrel.2011.12.006

379. de Sousa ME, Carrea A, Mendoza Zélis P, et al. Stress-Induced Gene Expression Sensing Intracellular Heating Triggered by Magnetic Hyperthermia. *The Journal of Physical Chemistry C*. 2016;120(13):7339-7348. doi:10.1021/acs.jpcc.5b12330
380. Moros M, Idiago-López J, Asín L, et al. Triggering antitumoural drug release and gene expression by magnetic hyperthermia. *Adv Drug Deliv Rev*. 2019;138:326-343. doi:10.1016/j.addr.2018.10.004
381. Ito A, Shinkai M, Honda H, Kobayashi T. Heat-inducible TNF-α gene therapy combined with hyperthermia using magnetic nanoparticles as a novel tumor-targeted therapy. *Cancer Gene Ther*. 2001;8(9):649-654. doi:10.1038/sj.cgt.7700357
382. Li Z, Guo T, Zhao S, Lin M. The Therapeutic Effects of MUC1-C shRNA@Fe3O4 Magnetic Nanoparticles in Alternating Magnetic Fields on Triple-Negative Breast Cancer. *Int J Nanomedicine*. 2023;Volume 18:5651-5670. doi:10.2147/IJN.S426849
383. Kang MA, Fang J, Paragodaarachchi A, et al. Magnetically Induced Brownian Motion of Iron Oxide Nanocages in Alternating Magnetic Fields and Their Application for Efficient siRNA Delivery. *Nano Lett*. 2022;22(22):8852-8859. doi:10.1021/acs.nanolett.2c02691
384. Kang MA, Rao PP, Matsui H, Mahajan SS. Delivery of mGluR5 siRNAs by Iron Oxide Nanocages by Alternating Magnetic Fields for Blocking Proliferation of Metastatic Osteosarcoma Cells. *Int J Mol Sci*. 2022;23(14):7944. doi:10.3390/ijms23147944
385. Chen Z, Peng Y, Li Y, et al. Aptamer-Dendrimer Functionalized Magnetic Nano-Octahedrons: Theranostic Drug/Gene Delivery Platform for Near-Infrared/Magnetic Resonance Imaging-Guided Magnetochemotherapy. *ACS Nano*. 2021;15(10):16683-16696. doi:10.1021/acsnano.1c06667
386. Park JK, Jung J, Subramaniam P, et al. Graphite-Coated Magnetic Nanoparticles as Multimodal Imaging Probes and Cooperative Therapeutic Agents for Tumor Cells. *Small*. 2011;7(12):1647-1652. doi:10.1002/smll.201100012
387. Cheng L, Ke Y, Yu S, Jing J. Co-delivery of doxorubicin and recombinant plasmid pHSP70-Plk1-shRNA by bacterial magnetosomes for osteosarcoma therapy. *Int J Nanomedicine*. 2016;Volume 11:5277-5286. doi:10.2147/IJN.S115364
388. Yang Z, Guo X, Meng M, et al. A single magnetic nanoplatform-mediated combination therapy of immune checkpoint silencing and magnetic hyperthermia for enhanced anticancer immunity. *Nano Res*. 2023;16(8):11206-11215. doi:10.1007/s12274-023-5839-z
389. Lee PC, Meisel D. Adsorption and surface-enhanced Raman of dyes on silver and gold sols. *J Phys Chem*. 1982;86(17):3391-3395. doi:10.1021/j100214a025
390. Baptista P, Conde J, Rosa J, Baptista P. Gold-Nanobeacons as a theranostic system for the detection and inhibition of specific genes. *Protoc Exch*. Published online November 27, 2013. doi:10.1038/protex.2013.088
391. Dolinnyi AI. Extinction coefficients of gold nanoparticles and their dimers. Dependence of optical factor on particle size. *Colloid Journal*. 2017;79(5):611-620. doi:10.1134/S1061933X17050052

392. Jain PK, Lee KS, El-Sayed IH, El-Sayed MA. Calculated Absorption and Scattering Properties of Gold Nanoparticles of Different Size, Shape, and Composition: Applications in Biological Imaging and Biomedicine. *J Phys Chem B*. 2006;110(14):7238-7248. doi:10.1021/jp057170o
393. Moros M, Pelaz B, López-Larrubia P, García-Martin ML, Grazú V, De La Fuente JM. Engineering biofunctional magnetic nanoparticles for biotechnological applications. *Nanoscale*. 2010;2(9):1746-1755. doi:10.1039/c0nr00104j
394. Livak KJ, Schmittgen TD. Analysis of Relative Gene Expression Data Using Real-Time Quantitative PCR and the 2−ΔΔCT Method. *Methods*. 2001;25(4):402-408. doi:10.1006/meth.2001.1262
395. Nouizi F, Algarawi M, Erkol H, Gulsen G. Gold nanoparticle-mediated photothermal therapy guidance with multi-wavelength photomagnetic imaging. *Photodiagnosis Photodyn Ther*. 2024;45:103956. doi:10.1016/j.pdpdt.2023.103956
396. Mendes R, Pedrosa P, Lima JC, Fernandes AR, Baptista P V. Photothermal enhancement of chemotherapy in breast cancer by visible irradiation of Gold Nanoparticles. *Sci Rep*. 2017;7(1):10872. doi:10.1038/s41598-017-11491-8
397. Wang P, Chen B, Zhan Y, et al. Enhancing the Efficiency of Mild-Temperature Photothermal Therapy for Cancer Assisting with Various Strategies. *Pharmaceutics*. 2022;14(11):2279. doi:10.3390/pharmaceutics14112279
398. Riley RS, Day ES. Gold nanoparticle-mediated photothermal therapy: applications and opportunities for multimodal cancer treatment. *WIREs Nanomedicine and Nanobiotechnology*. 2017;9(4). doi:10.1002/wnan.1449
399. Zhao L, Zhang X, Wang X, Guan X, Zhang W, Ma J. Recent advances in selective photothermal therapy of tumor. *J Nanobiotechnology*. 2021;19(1):335. doi:10.1186/s12951-021-01080-3
400. Amendoeira A, García LR, Fernandes AR, Baptista P V. Light Irradiation of Gold Nanoparticles Toward Advanced Cancer Therapeutics. *Adv Ther (Weinh)*. 2020;3(1). doi:10.1002/adtp.201900153
401. Krajczewski J, Kołątaj K, Kudelski A. Plasmonic nanoparticles in chemical analysis. *RSC Adv*. 2017;7(28):17559-17576. doi:10.1039/C7RA01034F
402. Overchuk M, Weersink RA, Wilson BC, Zheng G. Photodynamic and Photothermal Therapies: Synergy Opportunities for Nanomedicine. *ACS Nano*. 2023;17(9):7979-8003. doi:10.1021/acsnano.3c00891
403. Roma-Rodrigues C, Pombo I, Fernandes AR, Baptista P V. Hyperthermia Induced by Gold Nanoparticles and Visible Light Photothermy Combined with Chemotherapy to Tackle Doxorubicin Sensitive and Resistant Colorectal Tumor 3D Spheroids. *Int J Mol Sci*. 2020;21(21):8017. doi:10.3390/ijms21218017
404. Pedrosa P, Heuer-Jungemann A, Kanaras AG, Fernandes AR, Baptista P V. Potentiating angiogenesis arrest in vivo via laser irradiation of peptide functionalised gold nanoparticles. *J Nanobiotechnology*. 2017;15(1):85. doi:10.1186/s12951-017-0321-2

405. Sharma AR, Lee YH, Bat-Ulzii A, Bhattacharya M, Chakraborty C, Lee SS. Recent advances of metal-based nanoparticles in nucleic acid delivery for therapeutic applications. *J Nanobiotechnology*. 2022;20(1):501. doi:10.1186/s12951-022-01650-z
406. Hu X, Zhang Y, Ding T, Liu J, Zhao H. Multifunctional Gold Nanoparticles: A Novel Nanomaterial for Various Medical Applications and Biological Activities. *Front Bioeng Biotechnol*. 2020;8. doi:10.3389/fbioe.2020.00990
407. Hosseini SA, Kardani A, Yaghoobi H. A comprehensive review of cancer therapies mediated by conjugated gold nanoparticles with nucleic acid. *Int J Biol Macromol*. 2023;253:127184. doi:10.1016/j.ijbiomac.2023.127184
408. Kanu GA, Parambath JBM, Abu Odeh RO, Mohamed AA. Gold Nanoparticle-Mediated Gene Therapy. *Cancers (Basel)*. 2022;14(21):5366. doi:10.3390/cancers14215366
409. Graczyk A, Pawlowska R, Chworos A. Gold Nanoparticles as Carriers for Functional RNA Nanostructures. *Bioconjug Chem*. 2021;32(8):1667-1674. doi:10.1021/acs.bioconjchem.1c00211
410. Deng H yue, Wang L, Tang D, Zhang Y, Zhang L. Review on the laser-induced performance of photothermal materials for ignition application. *Energetic Materials Frontiers*. 2021;2(3):201-217. doi:10.1016/j.enmf.2021.08.001
411. Pedrosa P, Mendes R, Cabral R, Martins LMDRS, Baptista P V., Fernandes AR. Combination of chemotherapy and Au-nanoparticle photothermy in the visible light to tackle doxorubicin resistance in cancer cells. *Sci Rep*. 2018;8(1):11429. doi:10.1038/s41598-018-29870-0
412. Rueden CT, Schindelin J, Hiner MC, et al. ImageJ2: ImageJ for the next generation of scientific image data. *BMC Bioinformatics*. 2017;18(1):529. doi:10.1186/s12859-017-1934-z
413. McCully M, Conde J, V. Baptista P, Mullin M, Dalby MJ, Berry CC. Nanoparticle-antagomiR based targeting of miR-31 to induce osterix and osteocalcin expression in mesenchymal stem cells. *PLoS One*. 2018;13(2):e0192562. doi:10.1371/journal.pone.0192562
414. Rappon M, Syvitski RT. Kinetics of photobleaching of Aberchrome 540 in various solvents: solvent effects. *J Photochem Photobiol A Chem*. 1996;94(2-3):243-247. doi:10.1016/1010-6030(95)04216-4
415. Kim D, Paik J, Kim H. Effect of gold nanoparticles distribution radius on photothermal therapy efficacy. *Sci Rep*. 2023;13(1):12135. doi:10.1038/s41598-023-39040-6
416. Jiang K, Smith DA, Pinchuk A. Size-Dependent Photothermal Conversion Efficiencies of Plasmonically Heated Gold Nanoparticles. *The Journal of Physical Chemistry C*. 2013;117(51):27073-27080. doi:10.1021/jp409067h
417. Cui X, Ruan Q, Zhuo X, et al. Photothermal Nanomaterials: A Powerful Light-to-Heat Converter. *Chem Rev*. 2023;123(11):6891-6952. doi:10.1021/acs.chemrev.3c00159
418. Roti Roti JL. Cellular responses to hyperthermia (40–46 ° C): Cell killing and molecular events. *International Journal of Hyperthermia*. 2008;24(1):3-15. doi:10.1080/02656730701769841

419. Paściak A, Marin R, Abiven L, et al. Quantitative Comparison of the Light-to-Heat Conversion Efficiency in Nanomaterials Suitable for Photothermal Therapy. *ACS Appl Mater Interfaces*. 2022;14(29):33555-33566. doi:10.1021/acsami.2c08013
420. Kim M, Lee J, Nam J. Plasmonic Photothermal Nanoparticles for Biomedical Applications. *Advanced Science*. 2019;6(17). doi:10.1002/advs.201900471
421. Pamies R, Cifre JGH, Espín VF, Collado-González M, Baños FGD, de la Torre JG. Aggregation behaviour of gold nanoparticles in saline aqueous media. *Journal of Nanoparticle Research*. 2014;16(4):2376. doi:10.1007/s11051-014-2376-4
422. Comenge J, Puntes VF. The role of PEG conformation in mixed layers: from protein corona substrate to steric stabilization avoiding protein adsorption. *ScienceOpen Res*. 2015;0(0). doi:10.14293/S2199-1006.1.SOR-MATSCI.A0Z6OM.v1
423. Dunne M, Regenold M, Allen C. Hyperthermia can alter tumor physiology and improve chemo- and radio-therapy efficacy. *Adv Drug Deliv Rev*. 2020;163-164:98-124. doi:10.1016/j.addr.2020.07.007
424. Strober W. Trypan Blue Exclusion Test of Cell Viability. *Curr Protoc Immunol*. 2015;111(1). doi:10.1002/0471142735.ima03bs111
425. Cory AH, Owen TC, Barltrop JA, Cory JG. Use of an Aqueous Soluble Tetrazolium/Formazan Assay for Cell Growth Assays in Culture. *Cancer Commun*. 1991;3(7):207-212. doi:10.3727/095535491820873191
426. Stoddart MJ. Cell Viability Assays: Introduction. In: ; 2011:1-6. doi:10.1007/978-1-61779-108-6_1
427. Decker T, Lohmann-Matthes ML. A quick and simple method for the quantitation of lactate dehydrogenase release in measurements of cellular cytotoxicity and tumor necrosis factor (TNF) activity. *J Immunol Methods*. 1988;115(1):61-69. doi:10.1016/0022-1759(88)90310-9
428. Janic B, Liu F, R Bobbitt K, et al. Cellular Uptake and Radio-sensitization Effect of Small Gold Nanoparticles in MCF-7 Breast Cancer Cells. *J Nanomed Nanotechnol*. 2018;09(03). doi:10.4172/2157-7439.1000499
429. Carnovale C, Bryant G, Shukla R, Bansal V. Identifying Trends in Gold Nanoparticle Toxicity and Uptake: Size, Shape, Capping Ligand, and Biological Corona. *ACS Omega*. 2019;4(1):242-256. doi:10.1021/acsomega.8b03227
430. Madrid M. Plasmonic Intracellular Delivery. In: *Plasmonics*. IntechOpen; 2018. doi:10.5772/intechopen.79384
431. Beola L, Asín L, Roma-Rodrigues C, et al. The Intracellular Number of Magnetic Nanoparticles Modulates the Apoptotic Death Pathway after Magnetic Hyperthermia Treatment. *ACS Appl Mater Interfaces*. 2020;12(39):43474-43487. doi:10.1021/acsami.0c12900
432. Kang P, Li X, Liu Y, et al. Transient Photoinactivation of Cell Membrane Protein Activity without Genetic Modification by Molecular Hyperthermia. *ACS Nano*. 2019;13(11):12487-12499. doi:10.1021/acsnano.9b01993

433. Durymanov M, Reineke J. Non-viral Delivery of Nucleic Acids: Insight Into Mechanisms of Overcoming Intracellular Barriers. *Front Pharmacol*. 2018;9. doi:10.3389/fphar.2018.00971
434. Gillard M, Jia Z, Hou J, et al. Intracellular trafficking pathways for plasmid DNA complexed with highly efficient endosome escape polymers. *BMC Proc*. 2015;9(S9):P69. doi:10.1186/1753-6561-9-S9-P69
435. Vermeulen LMP, Fraire JC, Raes L, et al. Photothermally Triggered Endosomal Escape and Its Influence on Transfection Efficiency of Gold-Functionalized JetPEI/pDNA Nanoparticles. *Int J Mol Sci*. 2018;19(8):2400. doi:10.3390/ijms19082400
436. Xiong R, Raemdonck K, Peynshaert K, et al. Comparison of Gold Nanoparticle Mediated Photoporation: Vapor Nanobubbles Outperform Direct Heating for Delivering Macromolecules in Live Cells. *ACS Nano*. 2014;8(6):6288-6296. doi:10.1021/nn5017742
437. Han S, Zal T, Sokolov K V. Fate of Antibody-Targeted Ultrasmall Gold Nanoparticles in Cancer Cells after Receptor-Mediated Uptake. *ACS Nano*. 2021;15(6):9495-9508. doi:10.1021/acsnano.0c08128
438. Fraire JC, Houthaeve G, Liu J, et al. Vapor nanobubble is the more reliable photothermal mechanism for inducing endosomal escape of siRNA without disturbing cell homeostasis. *Journal of Controlled Release*. 2020;319:262-275. doi:10.1016/j.jconrel.2019.12.050
439. Elsner M. Single-stranded siRNAs for in vivo gene silencing. *Nat Biotechnol*. 2012;30(11):1063-1063. doi:10.1038/nbt.2413
440. Stewart MP, Langer R, Jensen KF. Intracellular Delivery by Membrane Disruption: Mechanisms, Strategies, and Concepts. *Chem Rev*. 2018;118(16):7409-7531. doi:10.1021/acs.chemrev.7b00678
441. Mokhtary P, Javan B, Sharbatkhari M, Soltani A, Erfani-Moghadam V. Cationic vesicles for efficient shRNA transfection in the MCF-7 breast cancer cell line. *Int J Nanomedicine*. 2018;Volume 13:7107-7121. doi:10.2147/IJN.S177674
442. Yu X, Liang X, Xie H, et al. Improved delivery of Cas9 protein/gRNA complexes using lipofectamine CRISPRMAX. *Biotechnol Lett*. 2016;38(6):919-929. doi:10.1007/s10529-016-2064-9
443. Raval GN, Bharadwaj S, Levine EA, et al. Loss of expression of tropomyosin-1, a novel class II tumor suppressor that induces anoikis, in primary breast tumors. *Oncogene*. 2003;22(40):6194-6203. doi:10.1038/sj.onc.1206719
444. Nugoli M, Chuchana P, Vendrell J, et al. Genetic variability in MCF-7 sublines: evidence of rapid genomic and RNA expression profile modifications. *BMC Cancer*. 2003;3(1):13. doi:10.1186/1471-2407-3-13
445. Kasai H, Inoue K, Imamura K, Yuvienco C, Montclare JK, Yamano S. Efficient siRNA delivery and gene silencing using a lipopolypeptide hybrid vector mediated by a caveolae-mediated and temperature-dependent endocytic pathway. *J Nanobiotechnology*. 2019;17(1):11. doi:10.1186/s12951-019-0444-8

446. Tenchov B, Sugimoto Y, Koynova R, Brueggemeier RW, Lee RJ. Highly efficient cationic ethylphosphatidylcholine siRNA carrier for GFP suppression in modified breast cancer cells. *Anticancer Res*. 2012;32(7):2563-2566.
447. Du X, Zhao M, Jiang L, et al. A mini-review on gene delivery technique using nanoparticles-mediated photoporation induced by nanosecond pulsed laser. *Drug Deliv*. 2024;31(1). doi:10.1080/10717544.2024.2306231
448. Stevenson DJ, Gunn-Moore FJ, Campbell P, Dholakia K. Single cell optical transfection. *J R Soc Interface*. 2010;7(47):863-871. doi:10.1098/rsif.2009.0463
449. Schneckenburger H, Hendinger A, Sailer R, Strauss WSL, Schmitt M. Laser-assisted optoporation of single cells. *J Biomed Opt*. 2002;7(3):410. doi:10.1117/1.1485758
450. Schneckenburger H. Laser-assisted optoporation of cells and tissues – a mini-review. *Biomed Opt Express*. 2019;10(6):2883. doi:10.1364/BOE.10.002883
451. Duffy MJ, O'Grady S, Tang M, Crown J. MYC as a target for cancer treatment. *Cancer Treat Rev*. 2021;94:102154. doi:10.1016/j.ctrv.2021.102154
452. Oliveira BB, Fernandes AR, Baptista PV. Assessing the gene silencing potential of AuNP-based approaches on conventional 2D cell culture versus 3D tumor spheroid. *Front Bioeng Biotechnol*. 2024;12. doi:10.3389/fbioe.2024.1320729
453. Wang C, Pan C, Yong H, et al. Emerging non-viral vectors for gene delivery. *J Nanobiotechnology*. 2023;21(1):272. doi:10.1186/s12951-023-02044-5
454. Fus-Kujawa A, Prus P, Bajdak-Rusinek K, et al. An Overview of Methods and Tools for Transfection of Eukaryotic Cells in vitro. *Front Bioeng Biotechnol*. 2021;9. doi:10.3389/fbioe.2021.701031
455. Carballo-Pedrares N, Ponti F, Lopez-Seijas J, et al. Non-viral gene delivery to human mesenchymal stem cells: a practical guide towards cell engineering. *J Biol Eng*. 2023;17(1):49. doi:10.1186/s13036-023-00363-7
456. Braun GB, Pallaoro A, Wu G, et al. Laser-Activated Gene Silencing *via* Gold Nanoshell−siRNA Conjugates. *ACS Nano*. 2009;3(7):2007-2015. doi:10.1021/nn900469q
457. Tang XY, Wu S, Wang D, et al. Human organoids in basic research and clinical applications. *Signal Transduct Target Ther*. 2022;7(1):168. doi:10.1038/s41392-022-01024-9
458. Kim J, Koo BK, Knoblich JA. Human organoids: model systems for human biology and medicine. *Nat Rev Mol Cell Biol*. 2020;21(10):571-584. doi:10.1038/s41580-020-0259-3
459. Valente R, Cordeiro S, Luz A, et al. Doxorubicin-sensitive and -resistant colorectal cancer spheroid models: assessing tumor microenvironment features for therapeutic modulation. *Front Cell Dev Biol*. 2023;11. doi:10.3389/fcell.2023.1310397
460. Pinto B, Henriques AC, Silva PMA, Bousbaa H. Three-Dimensional Spheroids as In Vitro Preclinical Models for Cancer Research. *Pharmaceutics*. 2020;12(12):1186. doi:10.3390/pharmaceutics12121186
461. Jensen C, Teng Y. Is It Time to Start Transitioning From 2D to 3D Cell Culture? *Front Mol Biosci*. 2020;7. doi:10.3389/fmolb.2020.00033

462. Zanoni M, Cortesi M, Zamagni A, Arienti C, Pignatta S, Tesei A. Modeling neoplastic disease with spheroids and organoids. *J Hematol Oncol*. 2020;13(1):97. doi:10.1186/s13045-020-00931-0
463. Xin X, Yang H, Zhang F, Yang ST. 3D cell coculture tumor model: A promising approach for future cancer drug discovery. *Process Biochemistry*. 2019;78:148-160. doi:10.1016/j.procbio.2018.12.028
464. Hoarau-Véchot J, Rafii A, Touboul C, Pasquier J. Halfway between 2D and Animal Models: Are 3D Cultures the Ideal Tool to Study Cancer-Microenvironment Interactions? *Int J Mol Sci*. 2018;19(1):181. doi:10.3390/ijms19010181
465. Arutyunyan I V., Soboleva AG, Kovtunov EA, et al. Gene Expression Profile of 3D Spheroids in Comparison with 2D Cell Cultures and Tissue Strains of Diffuse High-Grade Gliomas. *Bull Exp Biol Med*. 2023;175(4):576-584. doi:10.1007/s10517-023-05906-y
466. Miller CP, Fung M, Jaeger-Ruckstuhl CA, et al. Therapeutic targeting of tumor spheroids in a 3D microphysiological renal cell carcinoma-on-a-chip system. *Neoplasia*. 2023;46:100948. doi:10.1016/j.neo.2023.100948
467. Al-Thyabat S, Miles NJ. An improved estimation of size distribution from particle profile measurements. *Powder Technol*. 2006;166(3):152-160. doi:10.1016/j.powtec.2006.05.008
468. Strippoli A, Cocomazzi A, Basso M, et al. c-MYC Expression Is a Possible Keystone in the Colorectal Cancer Resistance to EGFR Inhibitors. *Cancers (Basel)*. 2020;12(3):638. doi:10.3390/cancers12030638
469. Susnik E, Bazzoni A, Taladriz-Blanco P, et al. Epidermal growth factor alters silica nanoparticle uptake and improves gold-nanoparticle-mediated gene silencing in A549 cells. *Frontiers in Nanotechnology*. 2023;5. doi:10.3389/fnano.2023.1220514
470. Conde J, Ambrosone A, Sanz V, et al. Design of Multifunctional Gold Nanoparticles for In Vitro and In Vivo Gene Silencing. *ACS Nano*. 2012;6(9):8316-8324. doi:10.1021/nn3030223
471. Santo D, Mendonça P V., Serra AC, Coelho JFJ, Faneca H. Targeted downregulation of MYC mediated by a highly efficient lactobionic acid-based glycoplex to enhance chemosensitivity in human hepatocellular carcinoma cells. *Int J Pharm*. 2023;637:122865. doi:10.1016/j.ijpharm.2023.122865
472. Russo P, Arzani D, Trombino S, Falugi C. c-myc Down-Regulation Induces Apoptosis in Human Cancer Cell Lines Exposed to RPR-115135 (C31H29NO4), a Non-Peptidomimetic Farnesyltransferase Inhibitor. *J Pharmacol Exp Ther*. 2003;304(1):37-47. doi:10.1124/jpet.102.042952
473. Jubelin C, Muñoz-Garcia J, Griscom L, et al. Three-dimensional in vitro culture models in oncology research. *Cell Biosci*. 2022;12(1):155. doi:10.1186/s13578-022-00887-3
474. Abbas ZN, Al-Saffar AZ, Jasim SM, Sulaiman GM. Comparative analysis between 2D and 3D colorectal cancer culture models for insights into cellular morphological and transcriptomic variations. *Sci Rep*. 2023;13(1):18380. doi:10.1038/s41598-023-45144-w

475. Brooks A, Zhang Y, Chen J, Zhao C. Cancer Metastasis-on-a-Chip for Modeling Metastatic Cascade and Drug Screening. *Adv Healthc Mater*. 2024;13(21). doi:10.1002/adhm.202302436
476. Nayak P, Bentivoglio V, Varani M, Signore A. Three-Dimensional In Vitro Tumor Spheroid Models for Evaluation of Anticancer Therapy: Recent Updates. *Cancers (Basel)*. 2023;15(19):4846. doi:10.3390/cancers15194846
477. Barbosa MAG, Xavier CPR, Pereira RF, Petrikaitė V, Vasconcelos MH. 3D Cell Culture Models as Recapitulators of the Tumor Microenvironment for the Screening of Anti-Cancer Drugs. *Cancers (Basel)*. 2021;14(1):190. doi:10.3390/cancers14010190
478. Vakhshiteh F, Bagheri Z, Soleimani M, et al. Heterotypic tumor spheroids: a platform for nanomedicine evaluation. *J Nanobiotechnology*. 2023;21(1):249. doi:10.1186/s12951-023-02021-y
479. Tchoryk A, Taresco V, Argent RH, et al. Penetration and Uptake of Nanoparticles in 3D Tumor Spheroids. *Bioconjug Chem*. 2019;30(5):1371-1384. doi:10.1021/acs.bioconjchem.9b00136
480. Białkowska K, Komorowski P, Bryszewska M, Miłowska K. Spheroids as a Type of Three-Dimensional Cell Cultures—Examples of Methods of Preparation and the Most Important Application. *Int J Mol Sci*. 2020;21(17):6225. doi:10.3390/ijms21176225
481. Pereira PMR, Berisha N, Bhupathiraju NVSDK, Fernandes R, Tomé JPC, Drain CM. Cancer cell spheroids are a better screen for the photodynamic efficiency of glycosylated photosensitizers. *PLoS One*. 2017;12(5):e0177737. doi:10.1371/journal.pone.0177737
482. Camarero P, Haro-González P, Quintanilla M. Near infrared laser irradiation on single multicellular spheroids. *Opt Mater (Amst)*. 2023;142:114055. doi:10.1016/j.optmat.2023.114055
483. Bromma K, Beckham W, Chithrani DB. Utilizing two-dimensional monolayer and three-dimensional spheroids to enhance radiotherapeutic potential by combining gold nanoparticles and docetaxel. *Cancer Nanotechnol*. 2023;14(1):80. doi:10.1186/s12645-023-00231-5
484. Lazzari G, Couvreur P, Mura S. Multicellular tumor spheroids: a relevant 3D model for the in vitro preclinical investigation of polymer nanomedicines. *Polym Chem*. 2017;8(34):4947-4969. doi:10.1039/C7PY00559H
485. Huang K, Ma H, Liu J, et al. Size-Dependent Localization and Penetration of Ultrasmall Gold Nanoparticles in Cancer Cells, Multicellular Spheroids, and Tumors *in Vivo*. *ACS Nano*. 2012;6(5):4483-4493. doi:10.1021/nn301282m
486. Huang X, Hu Q, Lai Y, Morales DP, Clegg DO, Reich NO. Light-Patterned RNA Interference of 3D-Cultured Human Embryonic Stem Cells. *Advanced Materials*. 2016;28(48):10732-10737. doi:10.1002/adma.201603318
487. Moradian H, Roch T, Anthofer L, Lendlein A, Gossen M. Chemical modification of uridine modulates mRNA-mediated proinflammatory and antiviral response in primary human macrophages. *Mol Ther Nucleic Acids*. 2022;27:854-869. doi:10.1016/j.omtn.2022.01.004

488. Guo ZS, Li Q, Bartlett DL, Yang JY, Fang B. Gene transfer: the challenge of regulated gene expression. *Trends Mol Med*. 2008;14(9):410-418. doi:10.1016/j.molmed.2008.07.003
489. Dana H, Chalbatani GM, Mahmoodzadeh H, et al. Molecular Mechanisms and Biological Functions of siRNA. *Int J Biomed Sci*. 2017;13(2):48-57.
490. Howarth JL, Lee YB, Uney JB. Using viral vectors as gene transfer tools (Cell Biology and Toxicology Special Issue: ETCS-UK 1 day meeting on genetic manipulation of cells). *Cell Biol Toxicol*. 2010;26(1):1-20. doi:10.1007/s10565-009-9139-5
491. Lee M, Chea K, Pyda R, Chua M, Dominguez I. Comparative Analysis of Non-viral Transfection Methods in Mouse Embryonic Fibroblast Cells. *J Biomol Tech*. 2017;28(2):67-74. doi:10.7171/jbt.17-2802-003
492. Kim TK, Eberwine JH. Mammalian cell transfection: the present and the future. *Anal Bioanal Chem*. 2010;397(8):3173-3178. doi:10.1007/s00216-010-3821-6
493. Neuhaus B, Tosun B, Rotan O, Frede A, Westendorf AM, Epple M. Nanoparticles as transfection agents: a comprehensive study with ten different cell lines. *RSC Adv*. 2016;6(22):18102-18112. doi:10.1039/C5RA25333K
494. Huang RY, Liu ZH, Weng WH, Chang CW. Magnetic nanocomplexes for gene delivery applications. *J Mater Chem B*. 2021;9(21):4267-4286. doi:10.1039/D0TB02713H
495. Chernousova S, Epple M. Live-cell imaging to compare the transfection and gene silencing efficiency of calcium phosphate nanoparticles and a liposomal transfection agent. *Gene Ther*. 2017;24(5):282-289. doi:10.1038/gt.2017.13
496. Magro M, Martinello T, Bonaiuto E, et al. Covalently bound DNA on naked iron oxide nanoparticles: Intelligent colloidal nano-vector for cell transfection. *Biochimica et Biophysica Acta (BBA) - General Subjects*. 2017;1861(11):2802-2810. doi:10.1016/j.bbagen.2017.07.025
497. Sandhu KK, McIntosh CM, Simard JM, Smith SW, Rotello VM. Gold Nanoparticle-Mediated Transfection of Mammalian Cells. *Bioconjug Chem*. 2002;13(1):3-6. doi:10.1021/bc015545c
498. Hao R, Xing R, Xu Z, Hou Y, Gao S, Sun S. Synthesis, Functionalization, and Biomedical Applications of Multifunctional Magnetic Nanoparticles. *Advanced Materials*. 2010;22(25):2729-2742. doi:10.1002/adma.201000260
499. Laurent S, Saei AA, Behzadi S, Panahifar A, Mahmoudi M. Superparamagnetic iron oxide nanoparticles for delivery of therapeutic agents: opportunities and challenges. *Expert Opin Drug Deliv*. 2014;11(9):1449-1470. doi:10.1517/17425247.2014.924501
500. Mosayebi J, Kiyasatfar M, Laurent S. Synthesis, Functionalization, and Design of Magnetic Nanoparticles for Theranostic Applications. *Adv Healthc Mater*. 2017;6(23):1700306. doi:10.1002/adhm.201700306
501. Dadfar SM, Roemhild K, Drude NI, et al. Iron oxide nanoparticles: Diagnostic, therapeutic and theranostic applications. *Adv Drug Deliv Rev*. 2019;138:302-325. doi:10.1016/j.addr.2019.01.005

502. Farzin A, Etesami SA, Quint J, Memic A, Tamayol A. Magnetic Nanoparticles in Cancer Therapy and Diagnosis. *Adv Healthc Mater*. 2020;9(9):1901058. doi:10.1002/adhm.201901058
503. Das P, Colombo M, Prosperi D. Recent advances in magnetic fluid hyperthermia for cancer therapy. *Colloids Surf B Biointerfaces*. 2019;174(July 2018):42-55. doi:10.1016/j.colsurfb.2018.10.051
504. Moros M, Idiago-López J, Asín L, et al. Triggering antitumoural drug release and gene expression by magnetic hyperthermia. *Adv Drug Deliv Rev*. 2019;138:326-343. doi:10.1016/j.addr.2018.10.004
505. Huang H, Delikanli S, Zeng H, Ferkey DM, Pralle A. Remote control of ion channels and neurons through magnetic-field heating of nanoparticles. *Nat Nanotechnol*. 2010;5(8):602-606. doi:10.1038/nnano.2010.125
506. Munshi R, Qadri SM, Zhang Q, Castellanos Rubio I, del Pino P, Pralle A. Magnetothermal genetic deep brain stimulation of motor behaviors in awake, freely moving mice. *Elife*. 2017;6. doi:10.7554/eLife.27069
507. Munshi R, Qadri SM, Pralle A. Transient Magnetothermal Neuronal Silencing Using the Chloride Channel Anoctamin 1 (TMEM16A). *Front Neurosci*. 2018;12. doi:10.3389/fnins.2018.00560
508. Chiu-Lam A, Rinaldi C. Nanoscale Thermal Phenomena in the Vicinity of Magnetic Nanoparticles in Alternating Magnetic Fields. *Adv Funct Mater*. 2016;26(22):3933-3941. doi:10.1002/adfm.201505256
509. Noh S hyun, Moon SH, Shin TH, Lim Y, Cheon J. Recent advances of magneto-thermal capabilities of nanoparticles: From design principles to biomedical applications. *Nano Today*. 2017;13:61-76. doi:10.1016/j.nantod.2017.02.006
510. Yoon HY, Koo H, Kim K, Kwon IC. Molecular imaging based on metabolic glycoengineering and bioorthogonal click chemistry. *Biomaterials*. 2017;132:28-36. doi:10.1016/j.biomaterials.2017.04.003
511. Moros M, Hernáez B, Garet E, et al. Monosaccharides versus PEG-Functionalized NPs: Influence in the Cellular Uptake. *ACS Nano*. 2012;6(2):1565-1577. doi:10.1021/nn204543c
512. Makridis A, Curto S, van Rhoon GC, Samaras T, Angelakeris M. A standardisation protocol for accurate evaluation of specific loss power in magnetic hyperthermia. *J Phys D Appl Phys*. 2019;52(25):255001. doi:10.1088/1361-6463/ab140c
513. Hergt R, Dutz S. Magnetic particle hyperthermia—biophysical limitations of a visionary tumour therapy. *J Magn Magn Mater*. 2007;311(1):187-192. doi:10.1016/j.jmmm.2006.10.1156
514. Du J, Meledeo MA, Wang Z, Khanna HS, Paruchuri VDP, Yarema KJ. Metabolic glycoengineering: Sialic acid and beyond. *Glycobiology*. 2009;19(12):1382-1401. doi:10.1093/glycob/cwp115
515. Lee S, Koo H, Na JH, et al. Chemical tumor-targeting of nanoparticles based on metabolic glycoengineering and click chemistry. *ACS Nano*. 2014;8(3):2048-2063. doi:10.1021/nn406584y

516. Idiago-López J, Ferreira D, Asín L, et al. Membrane-localized magnetic hyperthermia promotes intracellular delivery of cell-impermeant probes. *Nanoscale*. 2024;16(32):15176-15195. doi:10.1039/D4NR01955E
517. Li C, Liu Z, Yang F, et al. siRNAs with decreased off-target effect facilitate the identification of essential genes in cancer cells. *Oncotarget*. 2015;6(25):21603-21613. doi:10.18632/oncotarget.4269
518. Tschaharganeh D, Ehemann V, Nussbaum T, Schirmacher P, Breuhahn K. Non-specific effects of siRNAs on tumor cells with implications on therapeutic applicability using RNA interference. *Pathology & Oncology Research*. 2007;13(2):84-90. doi:10.1007/BF02893482
519. Torres-Lugo M, Castillo, Mendez J, Rinaldi C, Soto O, Alvarez-Berrios MP. Hyperthermic potentiation of cisplatin by magnetic nanoparticle heaters is correlated with an increase in cell membrane fluidity. *Int J Nanomedicine*. Published online March 2013:1003. doi:10.2147/IJN.S38842
520. Hulangamuwa W, Acharya B, Chikan V, Rafferty RJ. Triggering Passive Molecular Transport into Cells with a Combination of Inhomogeneous Magnetic Fields and Magnetic Nanoparticles. *ACS Appl Nano Mater*. 2020;3(3):2414-2420. doi:10.1021/acsanm.9b02537
521. Ruiz-Rincón S, González-Orive A, Grazú V, Fratila RM, Fuente JM de la, Cea P. Altering model cell membranes by means of localized magnetic heating. *Colloids Surf B Biointerfaces*. 2020;196:111315. doi:10.1016/j.colsurfb.2020.111315
522. Wang T, Larcher LM, Ma L, Veedu RN. Systematic Screening of Commonly Used Commercial Transfection Reagents towards Efficient Transfection of Single-Stranded Oligonucleotides. *Molecules*. 2018;23(10):2564. doi:10.3390/molecules23102564
523. Batista Napotnik T, Polajžer T, Miklavčič D. Cell death due to electroporation – A review. *Bioelectrochemistry*. 2021;141:107871. doi:10.1016/j.bioelechem.2021.107871
524. Liu J, Zhang X, Cheng Y, Cao X. Dendritic cell migration in inflammation and immunity. *Cellular & Molecular Immunology 2021 18:11*. 2021;18(11):2461-2471. doi:10.1038/s41423-021-00726-4
525. Richter C, Thieme S, Bandoła J, Laugsch M, Anastassiadis K, Brenner S. Generation of Inducible Immortalized Dendritic Cells with Proper Immune Function In Vitro and In Vivo. *PLoS One*. 2013;8(4):62621. doi:10.1371/journal.pone.0062621
526. Hasegawa H, Matsumoto T. Mechanisms of tolerance induction by dendritic cells in vivo. *Front Immunol*. 2018;9(FEB):318281. doi:10.3389/FIMMU.2018.00350/BIBTEX
527. Wculek SK, Cueto FJ, Mujal AM, Melero I, Krummel MF, Sancho D. Dendritic cells in cancer immunology and immunotherapy. *Nat Rev Immunol*. 2020;20(1):7-24. doi:10.1038/s41577-019-0210-z
528. Cabeza-Cabrerizo M, Cardoso A, Minutti CM, Pereira da Costa M, Reis e Sousa C. Dendritic Cells Revisited. *Annu Rev Immunol*. 2021;39(1):131-166. doi:10.1146/annurev-immunol-061020-053707

529. Patente TA, Pinho MP, Oliveira AA, Evangelista GCM, Bergami-Santos PC, Barbuto JAM. Human dendritic cells: Their heterogeneity and clinical application potential in cancer immunotherapy. *Front Immunol*. 2019;10(JAN):422571. doi:10.3389/fimmu.2018.03176
530. Lenz P, Bacot SM, Frazier-Jessen MR, Feldman GM. Nucleoporation of dendritic cells: Efficient gene transfer by electroporation into human monocyte-derived dendritic cells. *FEBS Lett*. 2003;538(1-3):149-154. doi:10.1016/S0014-5793(03)00169-8
531. Bowle R, Patil S, Pincas H, Sealfon SC. Optimized protocol for efficient transfection of dendritic cells without cell maturation. *Journal of Visualized Experiments*. 2011;(53):53. doi:10.3791/2766
532. Ahmed R, Sayegh N, Graciotti M, Kandalaft LE. Electroporation as a method of choice to generate genetically modified dendritic cell cancer vaccines. *Curr Opin Biotechnol*. 2020;65:142-155. doi:10.1016/j.copbio.2020.02.009
533. Chen YZ, Yao XL, Tabata Y, Nakagawa S, Gao JQ. Gene Carriers and Transfection Systems Used in the Recombination of Dendritic Cells for Effective Cancer Immunotherapy. *J Immunol Res*. 2010;2010(1). doi:10.1155/2010/565643
534. Goyvaerts C, Breckpot K. The Journey of in vivo Virus Engineered Dendritic Cells From Bench to Bedside: A Bumpy Road. *Front Immunol*. 2018;9. doi:10.3389/fimmu.2018.02052
535. Bolhassani A, Khavari A, Oraf Z. Electroporation – Advantages and Drawbacks for Delivery of Drug, Gene and Vaccine. In: *Application of Nanotechnology in Drug Delivery*. IntechOpen; 2014. doi:10.5772/58376
536. Saengruengrit C, Rodponthukwaji K, Sucharitakul J, et al. Effective gene delivery into primary dendritic cells using synthesized PDMAEMA-iron oxide nanocubes. *Mater Today Chem*. 2021;20:100481. doi:10.1016/j.mtchem.2021.100481
537. Song X, Si Q, Qi R, et al. Indoleamine 2,3-Dioxygenase 1: A Promising Therapeutic Target in Malignant Tumor. *Front Immunol*. 2021;12:800630. doi:10.3389/fimmu.2021.800630
538. Pallotta MT, Rossini S, Suvieri C, et al. Indoleamine 2,3-dioxygenase 1 (IDO1): an up-to-date overview of an eclectic immunoregulatory enzyme. *FEBS J*. 2022;289(20):6099. doi:10.1111/FEBS.16086
539. Meireson A, Devos M, Brochez L. IDO Expression in Cancer: Different Compartment, Different Functionality? *Front Immunol*. 2020;11. doi:10.3389/FIMMU.2020.531491
540. Del Prete A, Salvi V, Soriani A, et al. Dendritic cell subsets in cancer immunity and tumor antigen sensing. *Cellular & Molecular Immunology 2023 20:5*. 2023;20(5):432-447. doi:10.1038/s41423-023-00990-6
541. Liu M, Wang X, Wang L, et al. Targeting the IDO1 pathway in cancer: from bench to bedside. *J Hematol Oncol*. 2018;11(1). doi:10.1186/S13045-018-0644-Y
542. Fucikova J, Palova-Jelinkova L, Bartunkova J, Spisek R. Induction of tolerance and immunity by dendritic cells: Mechanisms and clinical applications. *Front Immunol*. 2019;10(OCT):485788. doi:10.3389/FIMMU.2019.02393/BIBTEX

543. Liu YH, Yeh IJ, Lai MD, Liu KT, Kuo PL, Yen MC. Cancer Immunotherapy: Silencing Intracellular Negative Immune Regulators of Dendritic Cells. *Cancers (Basel)*. 2019;11(1). doi:10.3390/CANCERS11010108
544. Endo R, Nakamura T, Kawakami K, Sato Y, Harashima H. The silencing of indoleamine 2,3-dioxygenase 1 (IDO1) in dendritic cells by siRNA-loaded lipid nanoparticles enhances cell-based cancer immunotherapy. *Sci Rep*. 2019;9(1):11335. doi:10.1038/s41598-019-47799-w
545. Ferreira D, Fernandes AR, Baptista P V. Mild hyperthermia via gold nanoparticles and visible light irradiation for enhanced siRNA and ASO delivery in 2D and 3D tumour spheroids. *Cancer Nanotechnol*. 2024;15(1):1-22. doi:10.1186/s12645-024-00256-4
546. Zhang J, Chen B, Gan C, Sun H, Zhang J, Feng L. A Comprehensive Review of Small Interfering RNAs (siRNAs): Mechanism, Therapeutic Targets, and Delivery Strategies for Cancer Therapy. *Int J Nanomedicine*. 2023;18:7605-7635. doi:10.2147/IJN.S436038
547. Khorkova O, Stahl J, Joji A, Volmar CH, Wahlestedt C. Amplifying gene expression with RNA-targeted therapeutics. *Nature Reviews Drug Discovery 2023 22:7*. 2023;22(7):539-561. doi:10.1038/s41573-023-00704-7
548. Zhou H, He Y, Xiong W, et al. MSC based gene delivery methods and strategies improve the therapeutic efficacy of neurological diseases. *Bioact Mater*. 2023;23:409-437. doi:10.1016/J.BIOACTMAT.2022.11.007
549. Jensen K, Anderson JA, Glass EJ. Comparison of small interfering RNA (siRNA) delivery into bovine monocyte-derived macrophages by transfection and electroporation. *Vet Immunol Immunopathol*. 2014;158(3-4):224-232. doi:10.1016/j.vetimm.2014.02.002
550. Alawar N, Schirra C, Hohmann M, Becherer U. A solution for highly efficient electroporation of primary cytotoxic T lymphocytes. *BMC Biotechnol*. 2024;24(1):1-14. doi:10.1186/s12896-024-00839-4
551. Prechtel AT, Turza NM, Theodoridis AA, Kummer M, Steinkasserer A. Small interfering RNA (siRNA) delivery into monocyte-derived dendritic cells by electroporation. *J Immunol Methods*. 2006;311(1-2):139-152. doi:10.1016/j.jim.2006.01.021
552. Berges C, Naujokat C, Tinapp S, et al. A cell line model for the differentiation of human dendritic cells. *Biochem Biophys Res Commun*. 2005;333(3):896-907. doi:10.1016/j.bbrc.2005.05.171
553. van Helden SFG, van Leeuwen FN, Figdor CG. Human and murine model cell lines for dendritic cell biology evaluated. *Immunol Lett*. 2008;117(2):191-197. doi:10.1016/J.IMLET.2008.02.003
554. Santegoets SJAM, van den Eertwegh AJM, van de Loosdrecht AA, Scheper RJ, de Gruijl TD. Human dendritic cell line models for DC differentiation and clinical DC vaccination studies. *J Leukoc Biol*. 2008;84(6):1364-1373. doi:10.1189/jlb.0208092
555. Schmidt S V., Nino-Castro AC, Schultze JL. Regulatory dendritic cells: there is more than just immune activation. *Front Immunol*. 2012;3(SEP). doi:10.3389/FIMMU.2012.00274

556. Medrano RFV, Hunger A, Mendonça SA, et al. Immunomodulatory and antitumor effects of type I interferons and their application in cancer therapy. *Oncotarget*. 2017;8(41):71249-71284. doi:10.18632/ONCOTARGET.19531
557. Lapteva N, Seethammagari MR, Hanks BA, et al. Enhanced activation of human dendritic cells by inducible CD40 and toll-like receptor-4 ligation. *Cancer Res*. 2007;67(21):10528-10537. doi:10.1158/0008-5472.CAN-07-0833
558. Kim MK, Kim J. Properties of immature and mature dendritic cells: phenotype, morphology, phagocytosis, and migration. *RSC Adv*. 2019;9(20):11230-11238. doi:10.1039/C9RA00818G
559. Chanput W, Peters V, Wichers H. THP-1 and U937 cells. In: *The Impact of Food Bioactives on Health: In Vitro and Ex Vivo Models*. Springer International Publishing; 2015:147-159. doi:10.1007/978-3-319-16104-4_14
560. Hölken JM, Teusch N. The Monocytic Cell Line THP-1 as a Validated and Robust Surrogate Model for Human Dendritic Cells. *Int J Mol Sci*. 2023;24(2):1452. doi:10.3390/ijms24021452
561. Li Z, Ju X, Silveira PA, et al. CD83: Activation marker for antigen presenting cells and its therapeutic potential. *Front Immunol*. 2019;10(JUN):460131. doi:10.3389/FIMMU.2019.01312/BIBTEX
562. Debets MF, Van Hest JCM, Rutjes FPJT. Bioorthogonal labelling of biomolecules: new functional handles and ligation methods. *Org Biomol Chem*. 2013;11(38):6439-6455. doi:10.1039/C3OB41329B
563. Du J, Meledeo MA, Wang Z, Khanna HS, Paruchuri VDP, Yarema KJ. Metabolic glycoengineering: Sialic acid and beyond. *Glycobiology*. 2009;19(12):1382-1401. doi:10.1093/glycob/cwp115
564. Idiago-López J, Moreno-Antolín E, Eceiza M, et al. From Bench to Cell: A Roadmap for Assessing the Bioorthogonal "click" Reactivity of Magnetic Nanoparticles for Cell Surface Engineering. *Bioconjug Chem*. 2022;33(9):1620-1633. doi:10.1021/acs.bioconjchem.2c00230
565. Koo H, Lee S, Na JH, et al. Bioorthogonal copper-free click chemistry inVivo for tumor-targeted delivery of nanoparticles. *Angewandte Chemie - International Edition*. 2012;51(47):11836-11840. doi:10.1002/anie.201206703
566. Lee S, Koo H, Na JH, et al. Chemical tumor-targeting of nanoparticles based on metabolic glycoengineering and click chemistry. *ACS Nano*. 2014;8(3):2048-2063. doi:10.1021/nn406584y
567. Lauehlin ST, Bertozzi CR. Metabolic labeling of glycans with azido sugars and subsequent glycan-profiling and visualization via staudinger ligation. *Nat Protoc*. 2007;2(11):2930-2944. doi:10.1038/nprot.2007.422
568. Han SS, Shim HE, Park SJ, et al. Safety and Optimization of Metabolic Labeling of Endothelial Progenitor Cells for Tracking. *Sci Rep*. 2018;8(1):1-13. doi:10.1038/s41598-018-31594-0

569. Meghani NM, Amin HH, Park C, et al. Design and evaluation of clickable gelatin-oleic nanoparticles using fattigation-platform for cancer therapy. *Int J Pharm*. 2018;545(1-2):101-112. doi:10.1016/j.ijpharm.2018.04.047
570. Zhang P, Jiang T, Li Y, et al. Bio-orthogonal AIE Dots Based on Polyyne-Bridged Red-emissive AIEgen for Tumor Metabolic Labeling and Targeted Imaging. *Chem Asian J*. 2019;14(6):770-774. doi:10.1002/asia.201801609
571. Han J, Bhatta R, Liu Y, Bo Y, Elosegui-Artola A, Wang H. Metabolic glycan labeling immobilizes dendritic cell membrane and enhances antitumor efficacy of dendritic cell vaccine. *Nat Commun*. 2023;14(1):5049. doi:10.1038/s41467-023-40886-7
572. Wang H, Sobral MC, Zhang DKY, et al. Metabolic labeling and targeted modulation of dendritic cells. *Nat Mater*. 2020;19(11):1244-1252. doi:10.1038/s41563-020-0680-1
573. Mirshafiee V, Mahmoudi M, Lou K, Cheng J, Kraft ML. Protein corona significantly reduces active targeting yield. *Chemical Communications*. 2013;49(25):2557-2559. doi:10.1039/c3cc37307j
574. Idiago-López J, Ferreira D, Asín L, et al. Membrane-localized magnetic hyperthermia promotes intracellular delivery of cell-impermeant probes. *Nanoscale*. 2024;16(32):15176-15195. doi:10.1039/D4NR01955E
575. Chen W, Liang X, Peterson AJ, Munn DH, Blazar BR. The Indoleamine 2,3-Dioxygenase Pathway Is Essential for Human Plasmacytoid Dendritic Cell-Induced Adaptive T Regulatory Cell Generation. *The Journal of Immunology*. 2008;181(8):5396-5404. doi:10.4049/jimmunol.181.8.5396
576. Prendergast GC, Malachowski WP, DuHadaway JB, Muller AJ. Discovery of IDO1 Inhibitors: From Bench to Bedside. *Cancer Res*. 2017;77(24):6795-6811. doi:10.1158/0008-5472.CAN-17-2285
577. Godin-Ethier J, Hanafi LA, Piccirillo CA, Lapointe R. Indoleamine 2,3-dioxygenase expression in human cancers: clinical and immunologic perspectives. *Clin Cancer Res*. 2011;17(22):6985-6991. doi:10.1158/1078-0432.CCR-11-1331
578. Wang S, Tian D. High transfection efficiency and cell viability of immune cells with nanomaterials-based transfection reagent. *Biotechniques*. 2022;72(5):219-224. doi:10.2144/btn-2022-0024
579. Landi A, Babiuk LA, van Drunen Littel-van den Hurk S. High transfection efficiency, gene expression, and viability of monocyte-derived human dendritic cells after nonviral gene transfer. *J Leukoc Biol*. 2007;82(4):849-860. doi:10.1189/jlb.0906561
580. Tan PH, Beutelspacher SC, Wang YH, et al. Immunolipoplexes: An efficient, nonviral alternative for transfection of human dendritic cells with potential for clinical vaccination. *Molecular Therapy*. 2005;11(5):790-800. doi:10.1016/j.ymthe.2004.12.009
581. Zhao M, Yang H, Jiang X, et al. Lipofectamine RNAiMAX: An efficient siRNA transfection reagent in human embryonic stem cells. *Mol Biotechnol*. 2008;40(1):19-26. doi:10.1007/s12033-008-9043-x
582. Wu H, Gong J, Liu Y. Indoleamine 2, 3-dioxygenase regulation of immune response (Review). *Mol Med Rep*. 2018;17(4):4867-4873. doi:10.3892/mmr.2018.8537

583. Huang X, Zhang F, Wang X, Liu K. The Role of Indoleamine 2, 3-Dioxygenase 1 in Regulating Tumor Microenvironment. *Cancers (Basel)*. 2022;14(11). doi:10.3390/cancers14112756
584. Zhai L, Bell A, Ladomersky E, et al. Immunosuppressive IDO in Cancer: Mechanisms of Action, Animal Models, and Targeting Strategies. *Front Immunol*. 2020;11:1185. doi:10.3389/FIMMU.2020.01185
585. Shang K, Wang Z, Hu Y, Huang Y, Yuan K, Yu Y. Gene silencing of indoleamine 2,3-dioxygenase 1 inhibits lung cancer growth by suppressing T-cell exhaustion. *Oncol Lett*. 2020;19(6):3827-3838. doi:10.3892/ol.2020.11477
586. Sioud M, Sæbøe-Larssen S, Hetland TE, Kærn J, Mobergslien A, Kvalheim G. Silencing of indoleamine 2,3-dioxygenaseenhances dendritic cell immunogenicity and antitumour immunity in cancer patients. *Int J Oncol*. 2013;43(1):280-288. doi:10.3892/ijo.2013.1922
587. Flatekval GF, Sioud M. Modulation of dendritic cell maturation and function with mono- and bifunctional small interfering RNAs targeting indoleamine 2,3-dioxygenase. *Immunology*. 2009;128(1 PART 2):e837-e848. doi:10.1111/j.1365-2567.2009.03093.x
588. Zheng X, Koropatnick J, Chen D, et al. Silencing IDO in dendritic cells: A novel approach to enhance cancer immunotherapy in a murine breast cancer model. *Int J Cancer*. 2012;132(4):967-977. doi:10.1002/ijc.27710
589. Xu YD, Cheng M, Shang PP, Yang YQ. Role of IL-6 in dendritic cell functions. *J Leukoc Biol*. 2022;111(3):695-709. doi:10.1002/JLB.3MR0621-616RR
590. Al-Qahtani AA, Alhamlan FS, Al-Qahtani AA. Pro-Inflammatory and Anti-Inflammatory Interleukins in Infectious Diseases: A Comprehensive Review. *Trop Med Infect Dis*. 2024;9(1). doi:10.3390/tropicalmed9010013
591. Laha D, Grant R, Mishra P, Nilubol N. The Role of Tumor Necrosis Factor in Manipulating the Immunological Response of Tumor Microenvironment. *Front Immunol*. 2021;12. doi:10.3389/fimmu.2021.656908
592. Trevejo JM, Marino MW, Philpott N, et al. TNF-α-dependent maturation of local dendritic cells is critical for activating the adaptive immune response to virus infection. *Proceedings of the National Academy of Sciences*. 2001;98(21):12162-12167. doi:10.1073/pnas.211423598
593. Tait Wojno ED, Hunter CA, Stumhofer JS. The Immunobiology of the Interleukin-12 Family: Room for Discovery. *Immunity*. 2019;50(4):851-870. doi:10.1016/j.immuni.2019.03.011
594. Heufler C, Koch F, Stanzl U, et al. Interleukin-12 is produced by dendritic cells and mediates T helper 1 development as well as interferon-γ production by T helper 1 cells. *Eur J Immunol*. 1996;26(3):659-668. doi:10.1002/eji.1830260323
595. Schülke S. Induction of interleukin-10 producing dendritic cells as a tool to suppress allergen-specific T helper 2 responses. *Front Immunol*. 2018;9(MAR). doi:10.3389/fimmu.2018.00455

596. de Smedt T, van Mechelen M, De Becker G, Urbain J, Leo O, Moser M. Effect of interleukin-10 on dendritic cell maturation and function. *Eur J Immunol*. 1997;27(5):1229-1235. doi:10.1002/eji.1830270526
597. Hirano T. IL-6 in inflammation, autoimmunity and cancer. *Int Immunol*. 2021;33(3):127-148. doi:10.1093/intimm/dxaa078
598. Jin B, Sun T, Yu XH, Yang YX, Yeo AET. The effects of TLR activation on T-cell development and differentiation. *Clin Dev Immunol*. 2012;2012. doi:10.1155/2012/836485
599. Zhao H, Wu L, Yan G, et al. Inflammation and tumor progression: signaling pathways and targeted intervention. *Signal Transduct Target Ther*. 2021;6(1). doi:10.1038/s41392-021-00658-5
600. Jang DI, Lee AH, Shin HY, et al. The role of tumor necrosis factor alpha (Tnf-α) in autoimmune disease and current tnf-α inhibitors in therapeutics. *Int J Mol Sci*. 2021;22(5):1-16. doi:10.3390/ijms22052719
601. Zwirner NW, Ziblat A. Regulation of NK cell activation and effector functions by the IL-12 family of cytokines: The case of IL-27. *Front Immunol*. 2017;8(JAN). doi:10.3389/fimmu.2017.00025
602. Hamza T, Barnett JB, Li B. Interleukin 12 a key immunoregulatory cytokine in infection applications. *Int J Mol Sci*. 2010;11(3):789-806. doi:10.3390/ijms11030789
603. Sabado RL, Balan S, Bhardwaj N. Dendritic cell-based immunotherapy. *Cell Res*. 2017;27(1):74-95. doi:10.1038/cr.2016.157
604. Liu J, Cao S, Kim S, et al. Interleukin-12: An Update on its Immunological Activities, Signaling and Regulation of Gene Expression. *Curr Immunol Rev*. 2005;1(2):119-137. doi:10.2174/1573395054065115
605. Carlini V, Noonan DM, Abdalalem E, et al. The multifaceted nature of IL-10: regulation, role in immunological homeostasis and its relevance to cancer, COVID-19 and post-COVID conditions. *Front Immunol*. 2023;14. doi:10.3389/fimmu.2023.1161067
606. Ouyang W, O'Garra A. IL-10 Family Cytokines IL-10 and IL-22: from Basic Science to Clinical Translation. *Immunity*. 2019;50(4):871-891. doi:10.1016/j.immuni.2019.03.020
607. Iyer SS, Cheng G. Role of Interleukin 10 Transcriptional Regulation in Inflammation and Autoimmune Disease. *Crit Rev Immunol*. 2012;32(1):23-63. doi:10.1615/CritRevImmunol.v32.i1.30
608. Salminen A. Role of indoleamine 2,3-dioxygenase 1 (IDO1) and kynurenine pathway in the regulation of the aging process. *Ageing Res Rev*. 2022;75. doi:10.1016/j.arr.2022.101573
609. Wang F, Liu L, Wang J, et al. Gain-of-function of IDO in DCs inhibits T cell immunity by metabolically regulating surface molecules and cytokines. *Exp Ther Med*. 2023;25(5). doi:10.3892/etm.2023.11933
610. Heidari F, Razmkhah M, Razban V, Erfani N. Effects of indoleamine 2, 3-dioxygenase (IDO) silencing on immunomodulatory function and cancer-promoting characteristic of adipose-derived mesenchymal stem cells (ASCs). *Cell Biol Int*. 2021;45(12):2544-2556. doi:10.1002/cbin.11698

611. Jiang W, Xu J. Immune modulation by mesenchymal stem cells. *Cell Prolif*. 2020;53(1). doi:10.1111/cpr.12712
612. Sakaguchi S. Naturally arising CD4+ regulatory T cells for immunologic self-tolerance and negative control of immune responses. *Annu Rev Immunol*. 2004;22:531-562. doi:10.1146/annurev.immunol.21.120601.141122
613. Ravishankar B, Liu H, Shinde R, et al. Tolerance to apoptotic cells is regulated by indoleamine 2,3-dioxygenase. *Proc Natl Acad Sci U S A*. 2012;109(10):3909-3914. doi:10.1073/pnas.1117736109
614. Macatonia SE, Hosken NA, Litton M, et al. Dendritic cells produce IL-12 and direct the development of Th1 cells from naive CD4+ T cells. *The Journal of Immunology*. 1995;154(10):5071-5079. doi:10.4049/jimmunol.154.10.5071
615. Xu H, Jia Y, Li Y, et al. IL-10 Dampens the Th1 and Tc Activation through Modulating DC Functions in BCG Vaccination. *Mediators Inflamm*. 2019;2019:1-10. doi:10.1155/2019/8616154
616. Wachowska M, Stachura J, Tonecka K, et al. Inhibition of IDO leads to IL-6-dependent systemic inflammation in mice when combined with photodynamic therapy. *Cancer Immunology, Immunotherapy*. 2020;69(6):1101-1112. doi:10.1007/s00262-020-02528-5
617. Chen D, Koropatnick J, Jiang N, et al. Targeted siRNA Silencing of Indoleamine 2, 3-Dioxygenase in Antigen-presenting Cells Using Mannose-conjugated Liposomes. *Journal of Immunotherapy*. 2014;37(2):123-134. doi:10.1097/CJI.0000000000000022
618. Wang T, Larcher LM, Ma L, Veedu RN. Systematic screening of commonly used commercial transfection reagents towards efficient transfection of single-stranded oligonucleotides. *Molecules*. 2018;23(10). doi:10.3390/molecules23102564
619. Batista Napotnik T, Polajžer T, Miklavčič D. Cell death due to electroporation - A review. *Bioelectrochemistry*. 2021;141. doi:10.1016/J.BIOELECHEM.2021.107871
620. Pamart G, Gosset P, Le Rouzic O, Pichavant M, Poulain-Godefroy O. Kynurenine Pathway in Respiratory Diseases. *Int J Tryptophan Res*. 2024;17. doi:10.1177/11786469241232871
621. Pathak S, Nadar R, Kim S, et al. The Influence of Kynurenine Metabolites on Neurodegenerative Pathologies. *International Journal of Molecular Sciences 2024, Vol 25, Page 853*. 2024;25(2):853. doi:10.3390/IJMS25020853
622. Li X, Qin Z, Wang S, Zhang L, Jiang X. Microfluidics-Assembled Nanovesicles for Nucleic Acid Delivery. *Acc Chem Res*. 2025;58(4):570-582. doi:10.1021/acs.accounts.4c00738
623. Shahalaei M, Azad AK, Sulaiman WMAW, et al. A review of metallic nanoparticles: present issues and prospects focused on the preparation methods, characterization techniques, and their theranostic applications. *Front Chem*. 2024;12. doi:10.3389/fchem.2024.1398979
624. Prendergast GC, Malachowski WP, DuHadaway JB, Muller AJ. Discovery of IDO1 Inhibitors: From Bench to Bedside. *Cancer Res*. 2017;77(24):6795-6811. doi:10.1158/0008-5472.CAN-17-2285

625. Boutorine A, Novopashina D, Krasheninina O, Nozeret K, Venyaminova A. Fluorescent Probes for Nucleic Acid Visualization in Fixed and Live Cells. *Molecules*. 2013;18(12):15357-15397. doi:10.3390/molecules181215357
626. Zamora-Justo JA, Abrica-González P, Vázquez-Martínez GR, Muñoz-Diosdado A, Balderas-López JA, Ibáñez-Hernández M. Polyethylene Glycol-Coated Gold Nanoparticles as DNA and Atorvastatin Delivery Systems and Cytotoxicity Evaluation. *J Nanomater*. 2019;2019:1-11. doi:10.1155/2019/5982047
627. Drasler B, Vanhecke D, Rodriguez-Lorenzo L, Petri-Fink A, Rothen-Rutishauser B. Quantifying Nanoparticle Cellular Uptake: Which Method is Best? *Nanomedicine*. 2017;12(10):1095-1099. doi:10.2217/nnm-2017-0071

2025

DANIELA FILIPA CARDOSO FERREIRA

NANOHEATERS – LOCALIZED HYPERTHERMIA FOR PRECISE GENE DELIVERY